Thomas M. Klapötke

CHEMISTRY OF HIGH-ENERGY MATERIALS

2ND EDITION

Klapötke

Chemistry of High-Energy Materials
2nd Edition

"We will not waver; we will not tire; we will not falter; and we will not fail. Peace and freedom will prevail."

G. W. Bush,
Presidential Address to the Nation,
October 7th 2001

Thomas M. Klapötke

Chemistry of High-Energy Materials

2nd Edition

DE GRUYTER

Prof. Dr. Thomas M. Klapötke
Professor of Inorganic Chemistry in the
Department of Chemistry
Ludwig-Maximilians University Munich
Butenandtstr. 5–13 (Haus D)
81377 Munich (Germany)
tmk@cup.uni-muenchen.de

and

Visiting Professor of Mechanical Engineering and Chemistry
Center of Energetic Concepts Development (CECD)
University of Maryland
College Park, MD 20742 (U.S.A.)

This book contains 154 figures and 74 tables.

Preface to this 2nd English edition

Everything said in the preface to the first German and first English editions still holds and essentially does not need any addition or correction. In this revised second edition in English we have up-dated the manuscript and added some recent aspects of energetic materials:

(i) We have tried to correct some mistakes which can not be avoided in a first edition and also updated the references where appropriate.
(ii) The chapters on Ionic Liquids, Primary Explosives, NIR formulations, Smoke Compositions and High-Nitrogen Compounds were updated.
(iii) Two new short chapters on Co-Crystallization (9.5) and Future Energetic Materials (9.6) have been added.

In addition to the people thanked in the German and first English edition, the author would like to thank Dr. Jesse Sabatini and Dr. Karl Oyler (ARDEC, Picatinny Arsenal, NJ) for many inspired discussions concerning pyrotechnics.

Munich, May 2012   *Thomas M. Klapötke*

Preface to the first English edition

Everything said in the preface to the first German edition remains valid and essentially does not need any addition or correction. There are several reasons for translating this book into English:

- The corresponding lecture series at LMU is now given in English in the postgraduate M.Sc. classes, to account for the growing number of foreign students and also to familiarize German students with the English technical terms.
- To make the book available to a larger readership world-wide.
- To provide a basis for the author's lecture series at the University of Maryland, College Park.

We have tried to correct some omissions and errors which can not be avoided in a first edition and have also updated the references where appropriate. In addition, five new chapters on Combustion (Ch. 1.4), NIR formulations (Ch. 2.5.5), the Gurney Model (Ch. 7.3), dinitroguanidine chemistry (Ch. 9.4) and nanothermites (Ch. 13.3) have been included in the English edition. The chapter on calculated combustion parameters (Ch. 4.2.3) has been extended.

In addition to the people thanked in the German edition, the author would like to thank Dr. Ernst-Christian Koch (NATO, MSIAC, Brussels) for pointing out various mistakes and inconsistencies in the first German edition. For inspired discussions concerning the Gurney model special thanks goes to Joe Backofen (BRIGS Co., Oak Hill). Dr. Anthony Bellamy, Dr. Michael Cartwright (Cranfield University), Neha Mehta, Dr. Reddy Damavarapu and Gary Chen (ARDEC) and Dr. Jörg Stierstorfer (LMU) are thanked for ongoing discussions concerning secondary and primary explosives.

The author also thanks Mr. Davin Piercey, B.Sc. for corrections and for writing the new chapter on nanothermites, Dr. Christiane Rotter for her help preparing the English figures and Dr. Xaver Steemann for his help with the chapter on detonation theory and the new combustion chapter. The author thanks the staff of de Gruyter for the good collaboration preparing the final manuscript.

Munich, January 2011   *Thomas M. Klapötke*

Preface to the first German edition

This book is based on a lecture course which has been given by the author for more than 10 years at the Ludwig-Maximilian University Munich (LMU) in the post-graduate Master lecture series, to introduce the reader to the chemistry of highly energetic materials. This book also reflects the research interests of the author. It was decided to entitle the book "Chemistry of High-Energy Materials" and not simply "Chemistry of Explosives" because we also wanted to include pyrotechnics, propellant charges and rocket propellants into the discussion. On purpose we do not give a comprehensive historical overview and we also refrained from extensive mathematical deductions. Instead we want to focus on the basics of chemical explosives and we want to provide an overview of recent developments in the research of energetic materials.

This book is concerned with both the civil applications of high-energy materials (e.g. propellants for carrier or satellite launch rockets and satellite propulsion systems) as well as the many military aspects. In the latter area there have been many challenges for energetic materials scientists in recent days some of which are listed below:

- In contrast to classical targets, in the on-going global war on terror (GWT), new targets such as tunnels, caves and remote desert or mountain areas have become important.
- The efficient and immediate response to time critical targets (targets that move) has become increasingly important for an effective defense strategy.
- Particularly important is the increased precision ("we want to hit and not to miss the target", Adam Cumming, DSTL, Sevenoaks, U.K.), in order to avoid collateral damage as much as possible. In this context, an effective coupling with the target is essential. This is particularly important since some evil regimes often purposely co-localize military targets with civilian centers (e.g. military bases near hospitals or settlements).
- The interest in insensitive munitions (IM) is still one of the biggest and most important challenges in the research of new highly energetic materials.
- The large area of increasing the survivability (for example by introducing smokeless propellants and propellant charges, reduced signatures of rocket motors and last but not least, by increasing the energy density) is another vast area of huge challenge for modern synthetic chemistry.
- Last but not least, ecological aspects have become more and more important. For example, on-going research is trying to find suitable lead-free primary explosives in order to replace lead azide and lead styphnate in primary composi-

tions. Moreover, RDX shows significant eco- and human-toxicity and research is underway to find suitable alternatives for this widely used high explosive. Finally, in the area of rocket propulsion and pyrotechnical compositions, replacements for toxic ammonium perchlorate (replaces iodide in the thyroid gland) which is currently used as an oxidizer are urgently needed. Despite all this, the performance and sensitivity of a high-energy material are almost always the key-factors that determine the application of such materials − and exactly this makes research in this area a great challenge for synthetically oriented chemists.

The most important aspect of this book and the corresponding lecture series at LMU Munich, is to prevent and stop the already on-going loss of experience, knowledge and know-how in the area of the synthesis and safe handling of highly energetic compounds. There is an on-going demand in society for safe and reliable propellants, propellant charges, pyrotechnics and explosives in both the military and civilian sector. And there is no one better suited to provide this expertise than well trained and educated preparative chemists.

Last but not least, the author wants to thank those who have helped to make this book project a success. For many inspired discussions and suggestions the authors wants to thank the following colleagues and friends: Dr. Betsy M. Rice, Dr. Brad Forch and Dr. Ed Byrd (US Army Research Laboratory, Aberdeen, MD), Prof. Dr. Manfred Held (EADS, TDW, Schrobenhausen), Dr. Ernst-Christian Koch (NATO MSIAC, Brussels), Dr. Miloslav Krupka (OZM, Czech Republic), Dr. Muhamed Sucesca (Brodarski Institute, Zagreb, Croatia), Prof. Dr. Konstantin Karaghiosoff (LMU Munich), Prof. Dr. Jürgen Evers (LMU Munich), as well as many of the past and present co-workers of the authors research group in Munich without their help this project could not have been completed.

The author is also indebted to and thanks Dipl.-Chem. Norbert Mayr (LMU Munich) for his support with many hard- and soft-ware problems, Ms. Carmen Nowak and Ms. Irene S. Scheckenbach (LMU Munich) for generating many figures and for reading a difficult manuscript. The author particularly wants to thank Dr. Stephanie Dawson (de Gruyter) for the excellent and efficient collaboration.

Munich, July 2009   *Thomas M. Klapötke*

Contents

1 Introduction

1.1 Historical Overview

In this chapter we do not want to be exhaustive in scope, but rather to focus on some of the most important milestones in the chemistry of explosives (Tab. 1.1). The development of energetic materials began with the accidental discovery of **blackpowder** in China ($\sim$ 220 BC). In Europe this important discovery remained dormant until the 13th and 14th centuries, when the English monk Roger Bacon (1249) and the German monk Berthold Schwarz (1320) started to research the properties of blackpowder. At the end of the 13th century, blackpowder was finally introduced into the military world. However, it was not until 1425 that Corning greatly improved the production methods and blackpowder (or gunpowder) was then introduced as a propellant charge for smaller and later also for large calibre guns.

The next milestone was the first small-scale synthesis of **nitroglycerine (NG)** by the Italian chemist Ascanio Sobrero (1846). Later, in 1863 Imanuel Nobel and his son Alfred commercialized NG production in a small factory near Stockholm (Tab. 1.1). NG is produced by running highly concentrated, almost anhydrous, and nearly chemically pure glycerine into a highly concentrated mixture of nitric and sulfuric acids (HNO_3 / H_2SO_4), while cooling and stirring the mixture efficiently. At the end of the reaction, the nitroglycerine and acid mixture is transferred into a separator, where the NG is separated by gravity. Afterwards, washing processes using water and alkaline soda solution remove any residual acid.

Initially NG was very difficult to handle because of its high impact sensitivity and unreliable initation by blackpowder. Among many other accidents, one explosion in 1864 destroyed the Nobel factory completely, killing Alfred's brother Emil. In the same year, Alfred Nobel invented the metal blasting cap detonator, and replaced blackpowder with **mercury fulminate (MF)**, $Hg(CNO)_2$. Although the Swedish-German Scientist Johann Kunkel von Löwenstern had described $Hg(CNO)_2$ as far back as in the 17th century, it did not have any practical application prior to Alfred Nobel's blasting caps. It is interesting to mention that it was not until the year 2007 that the molecular structure of $Hg(CNO)_2$ was elucidated by the LMU research team (Fig. 1.1) [1, 2]. Literature also reports the thermal transformation of MF, which, according to the below equation, forms a new mercury containing explosive product which is reported to be stable up to 120 °C.

$$3 \, Hg(CNO)_2 \rightarrow Hg_3(C_2N_2O_2)_3$$
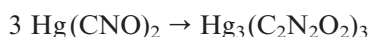
Tab. 1.1 Historical overview of some important secondary explosives.

substance	acronym	development	application	density/g cm^{-3}	explosive power[a]
blackpowder	BP	1250−1320	1425−1900	ca. 1.0	
nitroglycerine	NG	1863	in propellant charges	1.60	170
dynamite	Dy	1867	civil/commercial only	varies	varies
picric acid	PA	1885−1888	WW I	1.77	100
nitroguanidine	NQ	1877	most in TLPs	1.71	99
trinitrotoluene	TNT	1880	WW I	1.64	116
nitropenta	PETN	1894	WW II	1.77	167
hexogen	RDX	1920−1940	WW II	1.81	169
octogen	HMX	1943	WW II	1.91 (β polymorph)	169
hexanitrostilbene	HNS	1913	1966	1.74	
triaminotrinitro-benzene	TATB	1888	1978	1.93	
HNIW	CL-20	1987	under evaluation	2.1 (ε polymorph)	

[a] rel. to PA
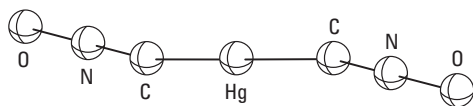
Fig. 1.1 Molecular structure of mercury fulminate, $Hg(CNO)_2$.

After another devastating explosion in 1866 which completely destroyed the NG factory, Alfred Nobel focused on the safe handling of NG explosives. In order to reduce the sensitivity, Nobel mixed NG (75%) with an absorbent clay called "Kieselguhr" (25%). This mixture called "Guhr Dynamite" was patented in 1867. Despite the great success of dynamite in the civil sector, this formulation has never found significant application or use in the military sector.

One of the great advantages of NG (Fig. 1.2) in comparison to blackpowder (75% KNO_3, 10% S_8, 15% charcoal) is that it contains both the fuel and oxidizer
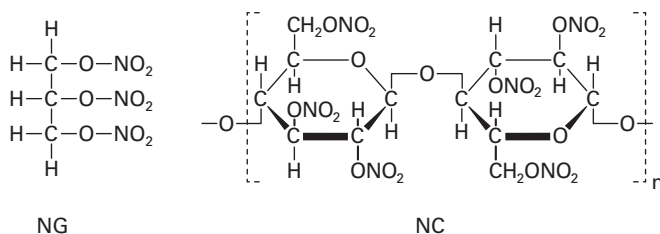
Fig. 1.2 Molecular structures of nitroglycerine (NG) and nitrocellulose (NC).

in the same molecule which guarantees optimal contact between both components, whereas in blackpowder, the oxidizer (KNO_3) and the fuel (S_8, charcoal) have to be physically mixed.

At the same time as NG was being researched and formulated several other research groups (Schönbein, Basel and Böttger, Frankfurt-am-Main) worked on the nitration of cellulose to produce **nitrocellulose (NC)**. In 1875 Alfred Nobel discovered that when NC is formulated with NG, they form a gel. This gel was further refined to produce blasting gelatine, gelatine dynamite and later in 1888 ballistite (49% NC, 49% NG, 2% benzene and camphor), which was the first smokeless powder. (Cordite which was developed in 1889 in Britain, had a very similar composition.) In 1867 it was proven that mixtures of NG or dynamite and ammonium nitrate (AN) showed enhanced performance. Such mixtures were used in the civil sector. In 1950 manufacturers started to develop explosives which were waterproof and solely contained the less hazardous AN. The most prominent formulation was ANFO (Ammonium Nitrate Fuel Oil) which found extensive use in commercial areas (mining, quarries etc.). Since the 1970s aluminium and mono-methylamine were added to such formulations to produce gelled explosives which could detonate more easily. More recent developments include production of emulsion explosives which contain suspended droplets of a solution of AN in oil. Such emulsions are water proof, yet readily detonate because the AN and oil are in direct contact. Generally, emulsion explosives are safer than dynamite and are simple and cheap to produce.

Picric acid (PA) was first reported in 1742 by Glauber, however it was not used as an explosive until the late 19th century (1885−1888), when it replaced black-powder in nearly all military operations world-wide (Fig. 1.3). PA is prepared best by dissolving phenol in sulfuric acid and the subsequent nitration of the resulting of phenol-2,4-disulfonic acid with nitric acid. The direct nitration of phenol with nitric acid is not possible because the oxidizing HNO_3 decomposes the phenol molecule. Since the sulfonation is reversible, the $-SO_3H$ groups can then be replaced with $-NO_2$ groups by refluxing the disulfonic acid in concentrated nitric acid. In this step the third nitro group is introduced as well. Although pure PA can be handled safely, a disadvantage of PA is its tendency to form impact sensitive metal salts (picrates, primary explosives) when in direct contact with shell walls. PA was used as a grenade and as mine filling.

Tetryl was developed at the end of the 19th century (Fig. 1.3) and represents the first explosive of the nitroamino (short: nitramino) type. Tetryl is best obtained by dissolving monomethylaniline in sulfuric acid and then pouring the solution intro nitric acid, while cooling the process.

The above mentioned disadvantages of PA are overcome by the introduction of **trinitrotoluene (TNT)**. Pure 2,4,6-TNT was first prepared by Hepp (Fig. 1.3) and its structure was determined by Claus and Becker in 1883. In the early 20th century TNT almost completely replaced PA and became the standard explosive during WW I. TNT is produced by the nitration of toluene with mixed nitric and sulfuric acid. For military purposes TNT must be free of any isomer other than the 2,4,6-
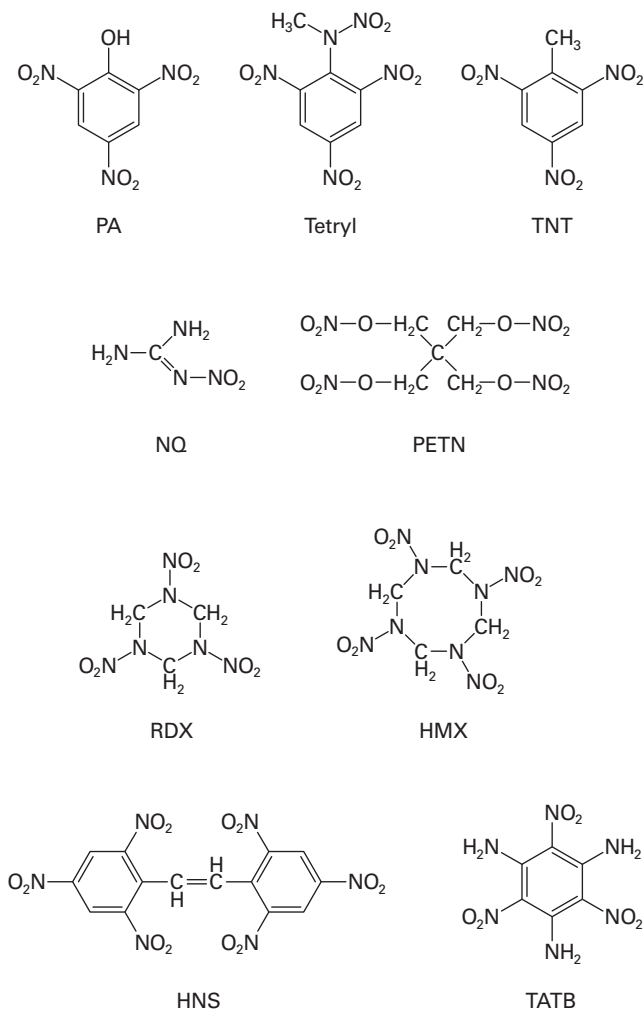
Fig. 1.3 Molecular structures of picric acid (PA), tetryl, trinitrotoluene (TNT), Nitrogua-nidine (NQ), pentaerythritol tetranitrate (PETN), hexogen (RDX), octogen (HMX), hexani-trostilbene (HNS) and triaminotrinitrobenzene (TATB).

isomer. This is achieved by recrystallization from organic solvents or from 62 % nitric acid. TNT is still one of the most important explosives for blasting charges today. Charges are produced through casting and pressing. However, cast charges of TNT often show sensitivity issues and do not comply with the modern insensitive munition requirements (IM). For this reason alternatives to TNT have been suggested. One of these replacements for TNT is NTO (filler) combined with 2,4-dinitroanisole (DNAN, binder).

   Nitroguanidine (NQ) was first prepared by Jousselin in 1887 (Fig. 1.3). However, during WW I and WW II it only found limited use, for example in formulations

with AN in grenades for mortars. In more recent days NQ has been used as a component in triple-base propellants together with NC and NG. One advantage of the triple-base propellants is that unlike double-base propellants the muzzle flash is reduced. The introduction of about 50 % of NQ to a propellant composition also results in a reduction of the combustion temperature and consequently reduced erosion and increased lifetime of the gun. NQ can be prepared from dicyandiamide and ammonium nitrate via guanidinium nitrate which is dehydrated with sulfuric acid under the formation of NQ:

$$\underset{H_2N}{\overset{H_2N}{>}}C-C\underset{N}{\overset{N}{<}} \xrightarrow[-H_2N-CN]{NH_4NO_3} C(NH_2)_3^{\oplus}NO_3^{\ominus} \xrightarrow[-H_2O]{H_2SO_4} H_2N-C\underset{N-NO_2}{\overset{NH_2}{<}}$$
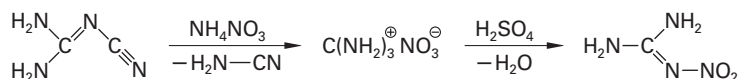
The most widely used explosives in WW II other than TNT were hexogen (RDX) and pentaerythritol tetranitrate (nitropenta, PETN) (Fig. 1.3). Since PETN is more sensitive and chemically less stable than RDX, RDX was (and is) the most commonly used high explosive. PETN is a powerful high explosive and has a great shattering effect (brisance). It is used in grenades, blasting caps, detonation cords and boosters. PETN is not used in its pure form because it is too sensitive. A formulation of 50 % TNT and 50 % PETN is known as "pentolite". In combination with plasticized nitrocellulose PETN is used to form polymer bonded explosives (PBX). The military application of PETN has largely been replaced by RDX. PETN is prepared by introducing pentaerythritol into concentrated nitric acid while cooling and stirring the mixture efficiently. The then formed bulk of PETN crystallizes out of the acid solution. The solution is then diluted to about 70 % HNO_3 in order to precipitate the remaining product. The washed crude product is purified by recrystallization from acetone.

   Hexogen (RDX) was first prepared in 1899 by Henning for medicinal use. (*N. B.* NG and PETN are also used in medicine to treat angina pectoris. The principal action of these nitrate esters is vasodilation (i.e. widening of the blood vessels). This effect arises because in the body the nitrate esters are converted to nitric oxide (NO) by mitochondrial aldehyde dehydrogenase, and nitric oxide is a natural vasodilator.) In 1920 Herz prepared RDX for the first time by the direct nitration of hexamethylene tetramine. Shortly afterwards Hale (Picatinny Arsenal, NJ) developed a process that formed RDX in 68 % yield. The two processes most widely used in WW II were

1. the Bachmann process (KA process) in which hexamethylene tetramine dinitrate reacts with AN and a small amount of nitric acid in an acetic anhydride medium to form RDX (type B RDX). The yields are high, however, 8−12 % of HMX form as a side product.
2. the Brockman process (type A RDX) essentially produces pure RDX.

After WW II **octogen (HMX)** started to become available. Until today, most high explosive compositions for military use are based on TNT, RDX and HMX (Tab. 1.2).

Tab. 1.2   Composition of some high explosive formulations.

name	composition
Composition A	88.3% RDX, 11.7% non-energetic plasticizers
Composition B	60% RDX, 39% TNT, 1% binder (wax)
Composition C4	90% RDX, 10% polyisobutylene
octol	75% HMX, 25% RDX
torpex[a]	42% RDX, 40% TNT, 18% aluminum
PBXN-109	64% RDX, 20% aluminum, 16% binder
OKFOL	96.5% HMX, 3.5% wax

[a] An Australian improved development of torpex is known under the name H6 and also contains hexogen (RDX), trinitrotoluene (TNT) and aluminum. H6 was used as a high explosive formulation in the MOAB bomb (Massive Ordnance Air Blast bomb). MOAB (also known as GBU-43/B) is with a load of approx. 9500 kg high explosive formulation one of the largest conventional bombs ever used.

Since 1966 **hexanitrostilbene (HNS)** and since 1978 **triaminotrinitrobenzene (TATB)** are produced commercially (Fig. 1.3). Both secondary explosives show excellent thermal stabilities and are therefore of great interest for the NAVY (fuel fires) and for hot deep oil drilling applications (Fig. 1.3). Especially HNS is known as a heat- and radiation-resistant explosive which is used in heat-resistant explosives in the oil industry. The brisance of HNS is lower than that of RDX, but the melting point of approx. 320 °C is much higher. HNS can directly be prepared from trinitrotoluene through oxidation with sodium hypochlorite in a methanol/THF solution:

$$2\ C_6H_2(NO_2)_3CH_3 + 2\ NaOCl \rightarrow C_6H_2(NO_2)_3\!-\!CH\!=\!CH\!-\!C_6H_2(NO_2)_3 \\ + 2\ H_2O + 2\ NaCl$$
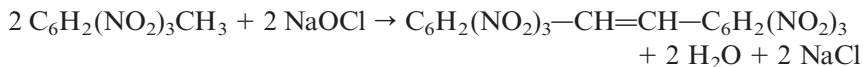
TATB is obtained from trichloro benzene by nitration followed by a reaction of the formed trichlorotrinitro benzene with ammonia gas in benzene or xylene solution.

As shown above, the number of chemical compounds which have been used for high explosive formulations until after WW II is relatively small (Tab. 1.1 and 1.2). As we can also see from Table 1.1 and 1.2 the best performing high explosives (RDX and HMX; TNT is only used because of its melt-cast applications) possess relatively high densities and contain oxidizer (nitro and nitrato groups) and fuel (C—H back bone) combined in one and the same molecule. One of the most powerful new high explosive is **CL-20** which was first synthesized in 1987 by the Naval Air Warfare Center (NAWF) China Lake (Fig. 1.7, Tab. 1.1). CL-20 is a cage compound with significant cage strain which also contains nitramine groups as oxidizers and possesses a density of about 2 g cm^{-3}. This already explains the better performance in comparison with RDX and HMX. However, due to the relatively high sensitivity of the (desirable) ε polymorph as well as possible phase transition problems and high production costs so far CL-20's wide and general application has not been established.

1.2 New Developments

1.2.1 Polymer-Bonded Explosives

Since about 1950 polymer-bonded (or plastic-bonded) explosives (PBX) have been developed in order to reduce sensivity and to facilitate safe and easy handling. PBX also show improved processibility and mechanical properties. In such materials the crystalline explosive is embedded in a rubber-like polymeric matrix. One of the most prominent examples of a PBX is **Semtex**. Semtex was invented in 1966 by Stanislav Brebera, a chemist who worked for VCHZ Synthesia in Semtin (hence the name Semtex), a suburb of Pardubice in the Czech Republic. Semtex consists of varying ratios of PETN and RDX. Usually polyisobutylene is used for the polymeric matrix, and phthalic acid n-octylester is the plasticizer. Other polymer matrices which have been introduced are polyurethane, polyvinyl alcohol, PTFE (teflon), Viton, Kel-F and various polyesters.

   Often, however, problems can arise when combining the polar explosive (RDX) with the non-polar polymeric binder (*e.g.* polybutadiene or polypropylene). In order to overcome such problems, additives are used to facilitate mixing and intermolecular interactions. One of such polar additives is dantacol (DHE) (Fig. 1.4).
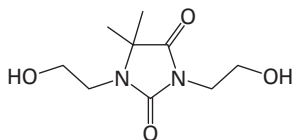
Fig. 1.4   Structure of Dantacol (DHE).

   One disadvantage of the polymer-bonded explosives of the first generation, is that the non-energetic binder (polymer) and plasticizer lessened the performance. To overcome this problem energetic binders and plasticizers have been developed. The most prominent examples for **energetic binders** are (Fig. 1.5, a):

− poly-GLYN, poly(glycidyl)nitrate
− poly-NIMMO, poly(3-nitratomethyl-3-methyl-oxetane)
− GAP, glycidylazide polymer
− poly-AMMO, poly(3-azidomethyl-3-methyl-oxetane),
− poly-BAMO, poly(3,3-bis-azidomethyl-oxetane).

Examples for **energetic plasticizers** are (Fig. 1.5, b):

− NENA derivatives, alkylnitratoethylnitramine,
− EGDN, ethyleneglycoldinitrate,
− MTN, metrioltrinitrate,
− BTTN, butane-1,2,4-trioltrinitrate.

(a)

poly-GLYN   poly-NIMMO   GAP

poly-AMMO   poly-BAMO

(b)

NENA   MTN

BTTN   EGDN

(c)

Fig. 1.5 Energetic binders (a) and energetic plasticizers (b). Synthesis of the NENA compound, ANTTO (c).

1.2.2 New High (Secondary) Explosives

New secondary explosives which are currently under research, development or testing include 5-nitro-1,2,4-triazol-3-one (NTO), 1,3,3-trinitroazetidine (TNAZ), hexanitrohexaazaisowurtzitane (HNIW, CL-20) and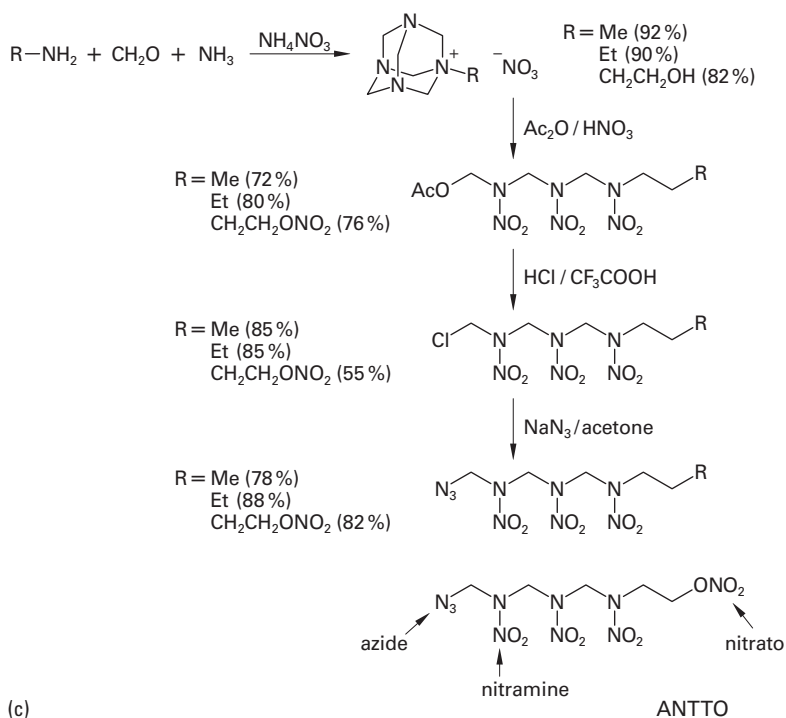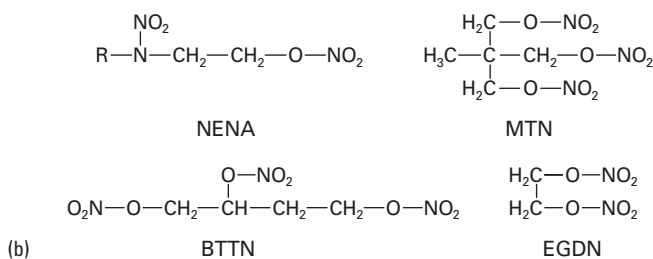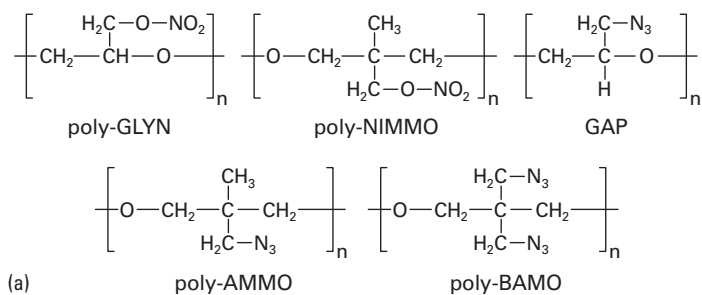 octanitrocubane (ONC) (Fig. 1.7). **NTO** has already found application as a very insensitive compound in gas generators for automobile inflatable air bags and in some polymer-bonded explosive formulations. (*N.B.* Initially NaN_3 was used in air bag systems, however, nowadays guanidinium nitrate is often used in combination with oxidizers such as AN in some non-azide automotive inflators. It is used to enhance burning at low flame temperatures. Low flame temperatures are desired in order to reduce the formation of NO_x gasses in inflators.) NTO is usually produced in a two-step process from semicarbazide hydrochloride with formic acid via the intermediate formation of 1,2,4-triazol-5-one (TO) and subsequent nitration with 70 % nitric acid:
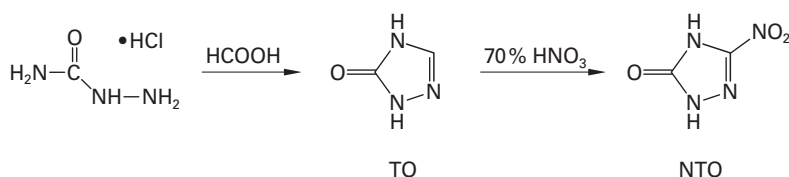
TNAZ was first synthesized in 1983 and has a strained four-membered ring backbone with both C-nitro and nitramine ($N-NO_2$) functionalities. There are various routes that yield TNAZ all of which consist of several reaction steps. One possible synthesis of TNAZ is shown in Figure 1.6. It starts from epichlorohydrine and ^tBu-amine. As far as the author of this book is aware, there has been no widespread use for TNAZ so far.

  CL-20 (1987, A. Nielsen) and ONC (1997, Eaton) are without doubt the most prominent recent explosives based on molecules with considerable cage-strain.
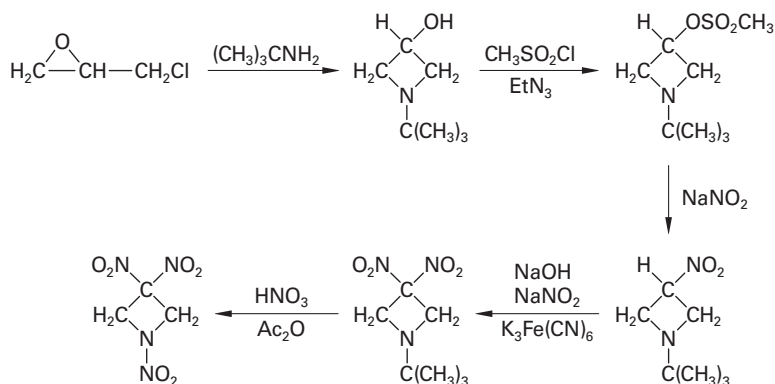
Fig. 1.6 Synthesis of 1,3,3-trinitroazetidine (TNAZ).
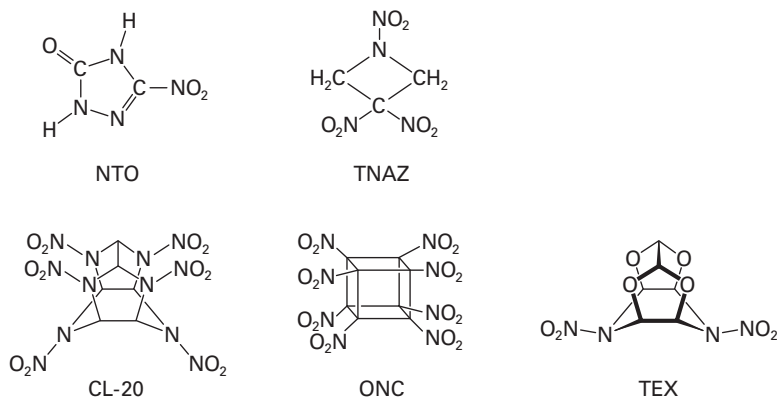
Fig. 1.7 Molecular structures of 5-nitro-1,2,4-triazol-3-one (NTO), 1,3,3-trinitroazetidine (TNAZ), hexanitrohexaazaisowurtzitane (CL-20), octanitrocubane (ONC) and 4,10-dinitro-2,6,8,12-tetraoxa-4,10-diazaisowurtzitane (TEX).
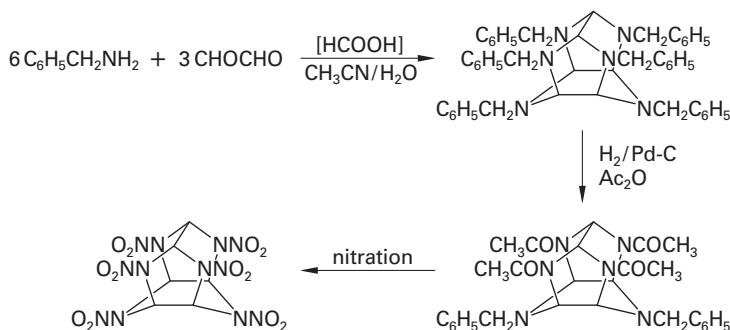
Fig. 1.8 Synthesis of hexanitrohexaazaisowurtzitane (CL-20).

While CL-20 is now already produced in 100 kg quantities (e.g. by SNPE, France or Thiokol, USA) on industrial pilot scale plants, ONC is only available on a mg to g scale because of its very difficult synthesis. Despite the great enthusiasm for CL-20 since its discovery over 20 years ago it has to be mentioned that even today most of the high explosive formulations are based on RDX (see Tab. 1.2). There are several reasons why CL-20 despite its great performance has not yet been introduced successfully:

− CL-20 is much more expensive than the relatively cheap RDX.
− CL-20 has some sensitivity issues (see insentitive munitions).
− CL-20 exists in several polymorphic forms and the desired ε polymorph (because of its high density and detonation velocity) is thermodynamically not the most stable one.

Interconversion of the ε form into a more stable but perhaps also more sensitive other polymorph would result in a loss of performance and an increase in sentitivity.
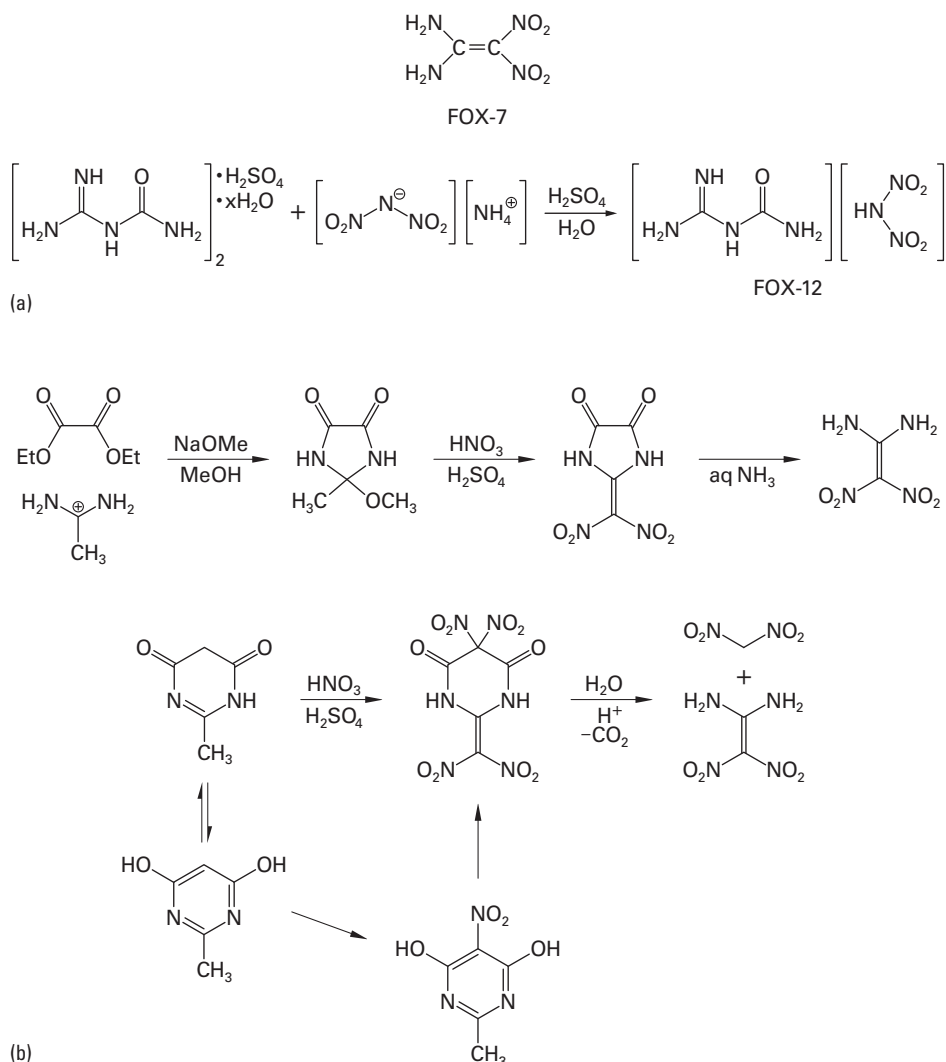
Fig. 1.9 Molecular structures of FOX-7 and FOX-12 (a). Two alternative synthetic routes for the synthesis of FOX-7 (b).

CL-20 is obtained by the condensation of glyoxal with benzylamine in an acid catalyzed reaction to yield hexabenzylhexaaxaisowurtzitane (Fig. 1.8). Afterwards the benzyl groups are replaced under reducing conditions (Pd-C catalyst) by easily removable acetyl substituents. Nitration to form CL-20 takes place in the final reaction step.

Another very insensitive high explosive which is structurally closely related to CL-20 is 4,10-dinitro-2,6,8,12-tetraoxa-4,10-diazaisowurtzitane (**TEX**, see Fig. 1.7), which was first described by Ramakrishnan and his co-workers in 1990. It displays one of the highest densities of all nitramines (2.008 g cm^{-3}) [1c].

Tab. 1.3 Characteristic performance and sensitivity data of FOX-7 and FOX-12 in comparison with RDX.

	FOX-7	FOX-12	RDX
detonation pressure, p_{C-J} / kbar	340	260	347
detonation velocity, D / m s^{-1}	8870	7900	8750
impact sensitivity / J	25	> 90	7.5
friction sensitivity / N	> 350	> 352	120
ESD / J	ca. 4.5	> 3	0.2
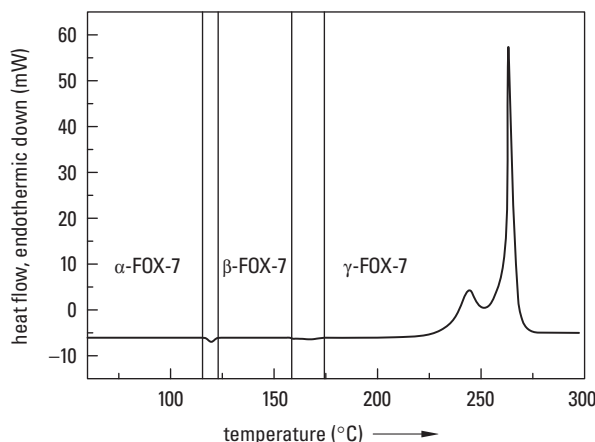
Fig. 1.10 DSC-Plot of FOX-7.

The chemist N. Latypov of the Swedish defense agency FOI developed and synthesized two other new energetic materials. These two compounds have become known as **FOX-7** and **FOX-12** (Fig. 1.9, a). FOX-7 or DADNE (diamino dinitro ethene) is the covalent molecule 1,1-diamino-2,2-dinitro ethene: $(O_2N)_2C{=}C(NH_2)_2$. The synthesis of FOX-7 always includes several reaction steps. Two alternative ways to prepare FOX-7 are shown in Figure 1.9 (b). FOX-12 or GUDN (guanylurea dinitramide) is the dinitramide of guanylurea: $[H_2N{-}C({=}NH_2){-}NH{-}C(O){-}NH_2]^+[N(NO_2)_2]^-$.

It is interesting that FOX-7 has the same C/H/N/O ratio as RDX or HMX. Although neither FOX-7 nor (and in particular not) FOX-12 meet RDX in terms of performance (detonation velocity and detonation pressure). Both compounds are much less sensitive than RDX and might be of interest due to their insensitive munition (IM) properties. Table 1.3 shows the most characteristic performance and sensitivity data of FOX-7 and FOX-12 in comparison with RDX.

FOX-7 exists in at least three different polymorphic forms (α, β and γ). The α modification converts reversibly into the β form at 389 K (Fig. 1.10) [2]. At 435 K the β polymorph converts into the γ phase and this interconversion is not reversible. The γ form can be quenched at 200 K. When heated the γ form decomposes at
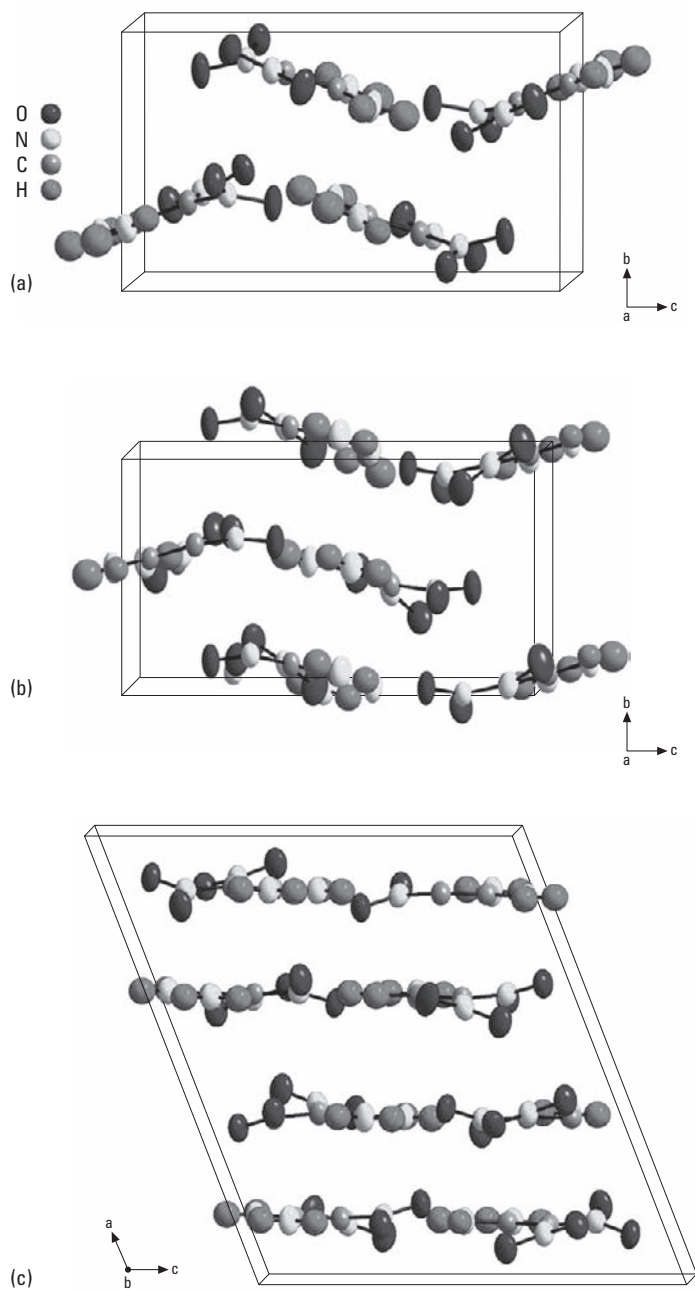
Fig. 1.11 Crystalline packing of α- FOX-7 (a), β- FOX-7 (b) and γ-FOX-7 (c).
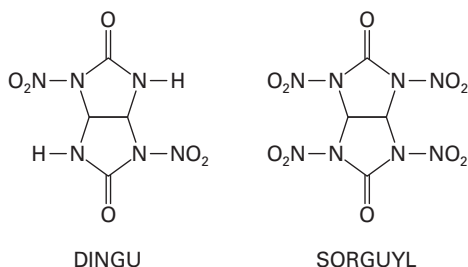
Fig. 1.12 Molecular structures of dinitroglycoluril (DINGU) and the corresponding tetramine (SORGUYL).
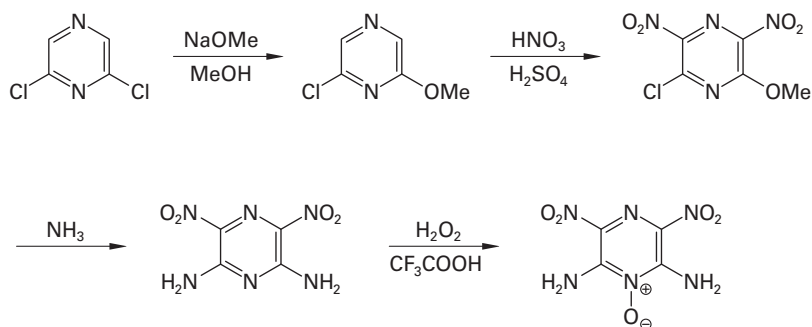
Fig. 1.13 Synthesis of LLM-105 starting from 2,6-dichloropyrazine. 3,5-dinitro-2,6-diaminopyrazine is oxidized to 3,5-dinitro-2,6-pyrazinediamine 1-oxide (LLM-105) in the final step.

504 K. Structurally, the three polymorphs are closely related and quite similar, with the planarity of the individual FOX-7 layers increasing from α via β to γ (i.e. γ posesses the most planar layers) (Fig. 1.11).

Another member of the family of nitramine explosives is the compound dinitroglycoluril (DINGU) which was first reported as early as 1888. The reaction between glyoxal (O=CH—CH=O) and urea yields glycoluril which can be nitrated with 100 % nitric acid to produce DINGU. Further nitration with a mixture of HNO_3/N_2O_5 yields the corresponding tetramine SORGUYL. The latter compound is of interest because of its high density (2.01 g cm^{-3}) and its high detonation velocity (9150 m s^{-1}) (Fig. 1.12). SORGUYL belongs to the class of cyclic dinitroureas. These compounds generally show a higher hydrolytic activity and may therefore be of interest as "self-remediating" energetic materials.

A new neutral nitrimino-functionalized high explosive which was first mentioned in 1951 (*J. Am. Chem. Soc.* **1951**, *73*, 4443) and which was recently suggested as a RDX replacement in C4 and Comp.B by Damavarapu (ARDEC) is bisnitraminotriazinone (DNAM). This compound has a melting point of 228 °C and a remarkably high density of 1.998 g/cc. Due to the high density and the not too negative enthalpy of formation ($\Delta H_f^\circ = -111$ kJ mol^{-1}) DNAM has a detonation velocity
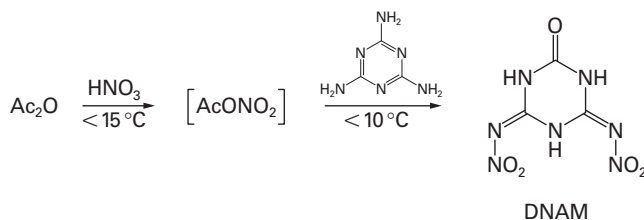
Fig. 1.13a Synthesis of DNAM.

of 9200 m s^{-1} but still desirably low sensitivities (IS = 82.5 cm, FS = 216 N, ESD = 0.25 J). The synthesis of DNAM can be achieved in 50−60 % yield by nitration of melamine using in-situ generated AcONO$_2$ as the effective nitrating agent (Fig. 1.13a) or by direct nitration of melamine. One possible concern about DNAM is that the compound hydrolyzes rapidly at 80° with liberation of nitrous oxide. At room temperature, the hydrolysis requires one to two days and is acid catalyzed.

The reaction of DNAM with NaHCO$_3$, CsOH and Sr(OH)$_2$ · 8 H$_2$O yields the corresponding mono-deprotonated salts NaDNAM, CsDNAM and Sr (DNAM)$_2$, respectively.

Pyrazine derivatives are six-membered heterocyclic compounds containing two nitrogen atoms in the ring system. As high-nitrogen heterocylic compounds, they have an ideal structure for energetic materials (EMs). Some of them have a high formation enthalpy, fine thermal stability and good safety characteristics. The basic structure of energetic pyrazine compounds is that of 3,5-dinitro-2,6-diaminopyrazine (**I** in Fig. 1.13). One of the most prominent members in this family is the 1-oxide 3,5-dinitro-2,6-pyrazinediamine 1-oxide (also known as **LLM-105**, Fig. 1.13). LLM-105 has a high density of 1.92 g cm^{-3} and it shows a detonation velocity of 8730 m s^{-1} and a detonation pressure of 359 kbar which are comparable to those of RDX (density = 1.80 g cm^{-3}, exptl. values: VoD = 8750, P$_{C-J}$ = 347 kbar). LLM-105 is a lot less impact sensitive than RDX and is not sensitive towards electrostatics and friction [1d].

Another N-oxide which has recently been suggested by Chavez et al. (LANL) as an insensitive high explosive is 3,3′ diaminoazoxy furazan (DAAF). Though the detonation velocity and detonation pressure of DAAF are rather low (7930 m s^{-1}, 306 kbar @ 1.685 g/cc), the low sensitivity (IS > 320 cm, FS > 360 N) and a critical diameter of < 3 mm make this compound promising. The synthesis of DAAF is shown in Fig 1.13b.

There are various methods to prepare LLM-105. Most methods start from commercially available 2,6-dichloropyrazine (Fig. 1.13) and oxidize dinitropyrazinediamine in the final step to the 1-oxide (LLM-105).

Organic peroxides are another class of explosives which has been researched recently. This class of explosives (organic, covalent peroxides) includes the following compounds:
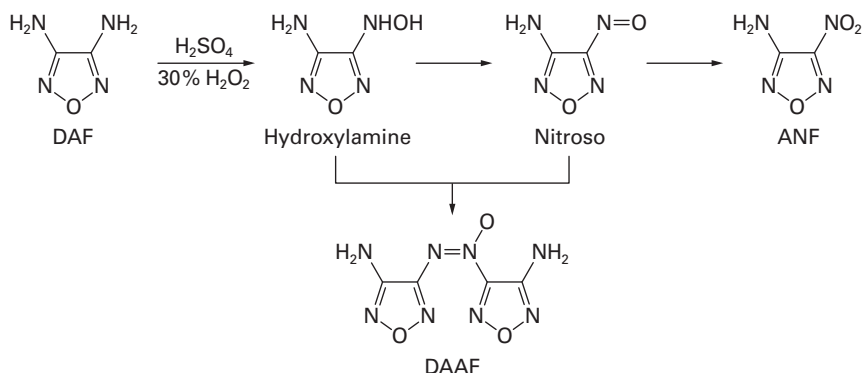
Fig. 1.13b Synthesis of DAAF.

- H$_2$O$_2$
- peracids, R—C(O)—OOH
- peresters, R—C(O)—OO—R′
- perethers, R—O—O−R′
- peracetals, R$_2'$C—(OOR)$_2$

Triacetone triperoxide (TATP, Fig. 1.14) is formed from acetone in sulfuric acid solution when acted upon by 45 % (or lower concentration) hydrogen peroxide (the acid acts as a catalyst). Like most other organic peroxides TATP has a very high impact (0.3 J), friction (0.1 N) and thermal sensitivity. TATP has the characteristics of a primary explosive. For this reason and because of its tendency to sublime (high volatility) it is not used in practice (apart from terrorist and suicide bomber activities).

Because of the use of TATP by terrorists, a reliable and fast detection of this material is desirable. In addition to conventional analytical methods such as mass spectrometry and UV (ultra violet) spectroscopy specially trained explosive detection dogs (EDD) play an important role in the detection of organic peroxides. Although the high vapor pressure helps the dogs to detect the material, it is also a disadvantage because of the limited time-span in which the dog is able to find it (traces may sublime and disappear forever). Matrices in which the compounds can
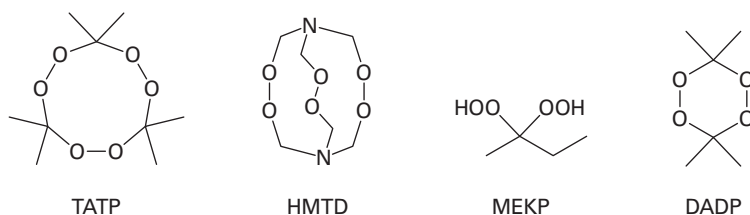
Fig. 1.14 Molecular structures of triacetone triperoxide (TATP), hexamethylene triperoxide diamine (HMTD), methyl ethyl ketone peroxide (MEKP) and diacetone diperoxide (DADP).
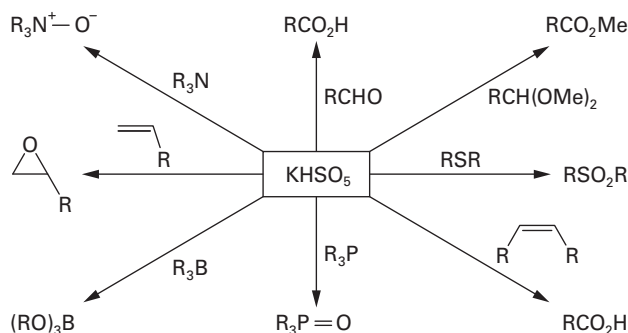
Fig. 1.15 Oxidation reactions with Oxone® as the oxidant (see for example: B. R. Travis, M. Sivakumar, G. O. Hollist, B. Borhan, Org. Lett. **2003**, 5, 1031−1034).
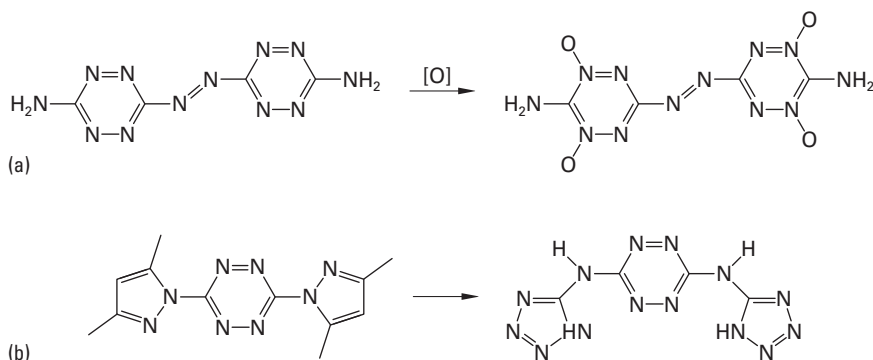
Fig. 1.16 Synthesis of an N-oxide (a) and preparation of 3,6-bis(1H-1,2,3,4-tetrazole-5-ylamino)-s-tetrazine (b).

be imbedded are sought after for safe training of explosive detection dogs. These matrices should not have any volatility or any characteristic smell for the dogs. In this respect zeolites may be of interest [1e, f]. The ongoing problem with zeolites is that they need to be loaded with solutions and the solvents (e.g. acetone) may not completely vaporize before the peroxide.

Typical organic peroxides, which have been or may be used by terrorists are so-called homemade explosives (HMEs): triacetone triperoxide (TATP), hexamethylene triperoxide diamine (HMTD), methyl ethyl ketone peroxide (MEKP) and diacetone diperoxide (DADP) (Fig. 1.14).

The following class of N-oxide compounds is considerably more stable than the above mentioned peroxides. For example, the oxidation of 3,3′-azobis(6-amino-1,2,4,5-tetrazine) in H_2O_2/CH_2Cl_2 in the presence of trifluoroacetic acid anhydride yields the corresponding N-oxide (Fig. 1.16). This compound has a desirable high density and only modest impact and friction sensitivity.

Another oxidizing reagent that has proven useful at introducing N-oxides is commercially available Oxone® ($2 KHSO_5 \cdot KHSO_4 \cdot K_2SO_4$). The active ingredient in this oxidizing agent is potassium peroxomonosulfate, $KHSO_5$, which is a salt of Caro's acid, H_2SO_5. Examples of oxidation reactions involving Oxone® are shown in Figure 1.15, including the interconversion of an amine (R_3N) into an N-oxide. (*N.B.* Sometimes, mCPBA [meta-chloro perbenzoic acid] or CF_3COOH are also used as an oxidizing agent for form N-oxides.)

Another tetrazine derivative, 3,6-bis(1H-1,2,3,4-tetrazole-5-ylamino)-s-tetrazine, has recently been prepared from (bis(pyrazolyl)tetrazine (Fig. 1.16). It is interesting to note that the tetrazine derivatives potentially form strong intermolecular interactions via π-stacking. This can influence many of the physical properties in a positive way, for example by reducing the electrostatic sensitivity.

1.2.3 New Primary Explosives

In early days Alfred Nobel already replaced mercury fulminate (MF, see above), which he had introduced into blasting caps, with the safer to handle primary explosives lead azide (LA) and lead styphnate (LS) (Fig. 1.17). However, the long-term use of LA and LS has caused considerable lead contamination in military training grounds which has stimulated world-wide activities in the search for replacements that are heavy-metal free. In 2006 Huynh und Hiskey published a paper proposing iron and copper complexes of the type $[cat]_2^+[M^{II}(NT)_4(H_2O)_2]$ ($[cat]^+ = NH_4^+$, Na^+; M = Fe, Cu; NT = 5-nitrotetrazolate) as environmentally friendly, "green" primary explosives (Fig. 1.17) [3].

In 2007 the LMU Munich research group reported on the compound copper *bis*(1-methyl-5-nitriminotetrazolate) with similarly promising properties (Fig. 1.17) [4]. Because they have only been discovered recently, none of the above mentioned complexes has found application yet, but they appear to have substantial potential as lead-free primary explosives.

Another environmentally compatible primary explosive is copper(I) 5-nitrotetrazolate (Fig. 1.17). This compound has been developed under the name of **DBX-1** by Pacific Scientific EMC and is a suitable replacement for lead azide. DBX-1 is thermally stable up to 325 °C (DSC). The impact sensitivity of DBX-1 is 0.04 J (ball-drop instrument) compared with 0.05 J for LA. The compound is stable at 180 °C for 24 hrs in air and for 2 months at 70 °C. DBX-1 can be obtained from NaNT and Cu(I)Cl in HCl/H_2O solution at a higher temperature. However, the best preparation for DBX-1 in a yield of 80−90 % is shown in the following equation where sodium ascorbate, $NaC_6H_7O_6$, is used as the reducing agent:

$$CuCl_2 + NaNT \xrightarrow{\text{reducing agent, } H_2O, \text{ 15 min, } \Delta T} DBX\text{-}1$$
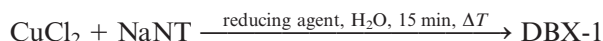
A possible replacement for lead styphnate is potassium-7-hydroxy-6-dinitrobenzofuroxane (**KDNP**) (Fig. 1.17). KDNP is a furoxane ring containing explosive and
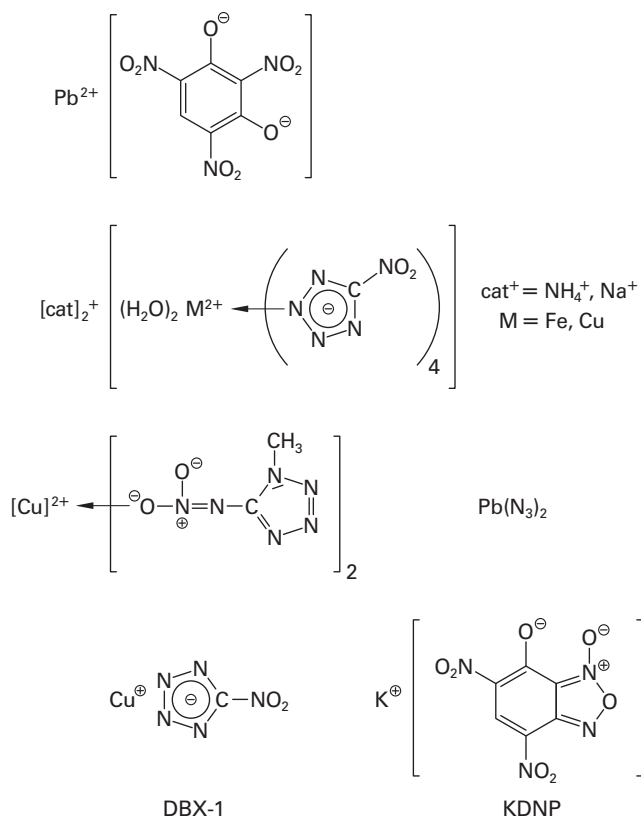
Fig. 1.17 Molecular structures of lead styphnate (LS), lead azide (LA), an iron and copper nitrotetrazolate complexes as well as copper(I) 5-nitrotetrazolate (DBX-1) and potassium-7-hydroxy-6-dinitrobenzofuroxane (KDNP).

can best be prepared from commercially available bromo anisol according to the following equation. The KN_3 substitutes the Br atom in the final reaction step and also removes the methyl group:
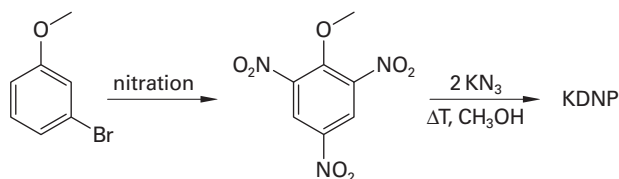
A typical stab detonator (Fig. 1.18) consists of three main components:

1. initiating mixture or initiating charge (initiated by a bridgewire),
2. transfer charge: primary explosive (usually LA),
3. output charge: secondary explosive (usually RDX).

A typical composition for the initiating charge is:

20 %   LA,
40 %   LS (basic),
 5 %   tetrazene,
20 %   barium nitrate,
15 %   antimony sulfide, Sb_2S_3.

It is therefore desirable, to find suitable heavy metal-free replacements for both lead azide and lead styphnate. Current research is addressing this problem. The following replacements in stab detonators are presently being researched:

1. initiating charge   LA   →   DBX-1
                       LS   →   KDNP
2. transfer charge: LA   →   triazine triazide (TTA) or APX
3. output charge: RDX   →   PETN or BTAT
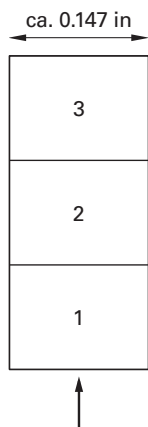
Fig. 1.18   Typical design of a stab detonator; 1: initiating charge, stab mix, e.g. NOL −130 (LA, LS, tetrazene, Sb_2S_3, $Ba(NO_3)_2$); 2: transfer charge (LA); 3: output charge (RDX).

Another promising and thermally stable (Tab. 1.3a) lead-free primary explosive is copper(II) 5-chlorotetrazolate (Cu ClT, PSI & LMU). The synthesis is achieved in a one-step reaction (Fig. 1.18a) starting from commercially available aminotetrazole. Cu ClT can then be further converted into the synthetically useful compounds sodium chlorotatrazolate and chlorotetrazole (Fig. 1.18a).
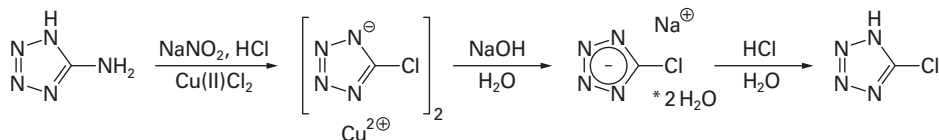
Fig. 1.18a   Synthesis of copper(II) chlorotetrazolate (Cu ClT).
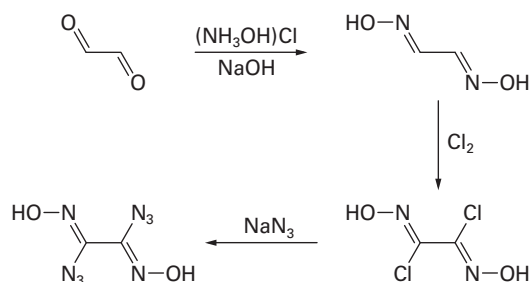
Fig. 1.18b   Synthesis of diazidoglyoxime (DAGL).

Tab. 1.3a   Energetic properties of copper(II) chlorotetrazolate (CuClT).

	CuClT
formula	$C_2Cl_2CuN_8$
molecular mass [g mol^{-1}]	270.53
impact sensitivity [J]	1
friction sensitivity [N]	< 5
ESD-test [J]	0.025
N [%]	41.42
$T_{dec.}$ [°C]	289

Tab. 1.3b   Energetic properties of TTA and DAGL in comparison with LA.

	TTA	DAGL	LA
formula	C_3N_{12}	$C_2H_2N_8O_2$	N_6Pb
molecular mass [g mol^{-1}]	204.1	170.1	291.3
impact sensitivity [J]	1.3	1.5	2.5 − 4
friction sensitivity [N]	< 0.5	< 5	0.1 − 1
ESD [J]	< 0.36 (?)	0.007	0.005
$T_{dec.}$ [°C]	187 (m.p. 94)	170	315

In the area of metal-free primary explosives, covalently bound azides are often advantageous. Although these compound soften do not show the high thermal stability of metal complexes, some may have an application as LA replacements in transfer charges (see Fig. 1.18). Two of the most promising candidates are triazido triazine (triazine triazide, TTA, ARDEC, see above) and diazidoglyoxime (DAGL, LMU). The latter one can be prepared according to Fig. 1.18b.

1.2.4 New Oxidizers for Solid Rocket Motors

Solid propellants of essentially all solid rocket boosters are based on a mixture of aluminum (Al, fuel) and ammonium perchlorate (AP, oxidizer).

$$NH_4^{\oplus} \quad {}^{\ominus}N{\overset{\displaystyle NO_2}{\underset{\displaystyle NO_2}{\Big<}}} \qquad\qquad ADN$$

$$N_2H_5^{\oplus} \quad C(NO_2)_3^{\ominus} \qquad\qquad HNF$$

$$C(NH-NH_2)_3^{\oplus} \quad C(NO_2)_3^{\ominus} \qquad TAGNF$$

Fig. 1.19 Molecular structures of ammonium dinitramide (ADN), hydrazinium nitroformate (HNF) and triaminoguanidinium nitroformate (TAGNF).

Ammonium perchlorate (AP) has applications in munitions, primarily as an oxidizer for solid rocket and missile propellants. It is also used as an air bag inflator in the automotive industry, in fireworks, and appears as a contaminant of agricultural fertilizers. As a result of these uses and ammonium perchlorate's high solubility, chemical stability, and persistence, it has become widely distributed in surface and ground water systems. There is little information about the effects of perchlorate on the aquatic life, but it is known that perchlorate is an endocrine disrupting chemical that interferes with normal thyroid function which impacts both growth and development in vertebrates. Because perchlorate competes for iod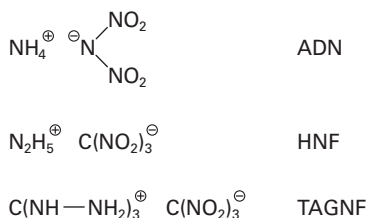ine binding sites in thyroids, adding iodine to culture water has been examined in order to determine if perchlorate effects can be mitigated. Finally, perchlorate is known to affect normal pigmentation of amphibian embryos. In the US alone the cost for remediation is estimated to be several billion dollars. That money that is urgently needed in other defense areas [5−7].

The currently most promising chlorine-free oxidizers which are being researched at present are ammonium dinitramide (ADN), which was first developed in Russia (Nikolaj Latypov) and is being commercialized today by EURENCO, as well as the nitroformate salts hydrazinium nitroformate (HNF, APP, Netherlands) and triaminoguanidinium nitroformate (Germany) (Fig. 1.19) [8]. The salt hydroxyl ammonium nitrate, $HO-NH_3^+ \ NO_3^-$ (HAN) is also of interest. However, all four compounds possess relatively low decomposition temperatures and TAGNF only has a positive oxygen balance with respect to CO (not to CO_2).

While ADN has the best oxygen balance ($\Omega_{CO_2} = 25.8\%$, *cf.* AP 34.0 %) of all presently discussed AP replacements it still has some stability issues with respect to binder compatibility and thermal stability ($T_{dec.} = 127\,°C$). Thermal decomposition of ADN is observed at 127 °C after complete melting at 91.5 °C. The main decomposition pathway is based on the formation of NH_4NO_3 and N_2O followed by the thermal decomposition of NH_4NO_3 to N_2O and H_2O at higher temperatures. Side reactions forming NO_2, NO, NH_3, N_2 and O_2 are described and a mechanism for the acid-catalyzed decomposition of hydrogen dinitramide, dissociation product of ADN, is proposed.

Alternatively, ammonium nitrate (AN, $\Omega_{CO_2} = 20.0\%$, begins decomposition at m.p. $= 169.9\,°C$, complete decomposition at 210 °C) has been discussed, however

this compound has severe burn rate issues. Furthermore, AN is hygroscopic and shows phase transitions from one polymorph to another at 125.2 °C, 84.2 °C, 32.3 °C and −16.9 °C. Phase stabilized ammonium nitrate (PSAN) and spray crystallized AN (SCAN) are special qualities provided by ICT.

Another recently suggested organic oxidizer is TNC-NO_2 which has an oxygen balance of $\Omega_{CO2} = 14.9\%$ and a thermal stability of up to 153 °C. TNC-NO_2 can be synthesized by direct nitration of TNC (2,2,2-trinitroethyl carbamate) using mixed acid:
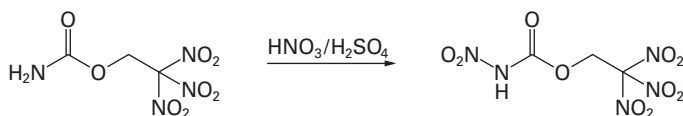
The further new nitroethyl compounds based on boron esters are tris-(2-nitroethyl) borate and tris-(2,2,2-trinitroethyl) borate. Especially the trinitroethyl derivative is a suitable candidate for high energy density oxidizers and for smoke-free, green coloring agents in pyrotechnic compositions. Tris-(2-nitroethyl) borate and tris-(2,2,2-trinitroethyl) borate can be obtained from boron oxide with 2-nitroethanol and 2,2,2-trinitroethanol, respectively:
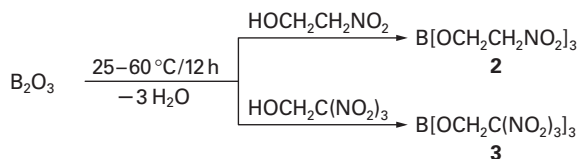
The oxygen balance of **2** is −59.70 % and of **3** is +13.07 %. The density for **3** was determined to 1.982 g cm^{-3}, which is a quite high value. DSC measurements revealed an exothermic decomposition at 216 °C for **2** and 161 °C for **3**.

The starting material 2,2,2-trinitroethanol (**1**) was prepared from the reaction of trinitromethane with formaldehyde (see Fig. 9.18).

Sensitivity data for **3**.

grain size	< 100 μm
impact sensitivity	15 J
friction sensitivity	144 N
electrostatic sensitivity	0.5 J

In general, elemental boron and boron compounds have been the subject of many studies involving propulsion systems due to the very high heats of combustion. However, due to some combustion problems, the theoretical benefits of boron and its compounds have rarely been delivered. The main limitations for boron combustion are (i) ignition delay due to the presence of an oxide layer on the surface of

the boron particle (only for elemental boron) and (ii) the energy release during the combustion process in hydrogen containing gases is significantly lowered due to the formation of HBO_2 or "HOBO" as commonly referred to. The slow oxidation of "HOBO" to the preferred product of combustion B_2O_3 often results in the particles leaving the propulsion-system prior to releasing all of their energy thus resulting in less than expected performance.

In short, there is a reason why AP has been used as the most important oxidizer for composite propellants for decades. It has the advantage of being completely convertible to gaseous reaction products and has an oxygen balance of $\Omega_{CO_2} = 34\%$. It can easily be prepared by neutralizing ammonia with perchloric acid and is purified by crystallization. AP is stable at room temperature but decomposes at measurable rates at temperatures greater than about 150 °C. At decomposition temperatures below approximately 300 °C, AP undergoes an autocatalytic reaction which ceases after about 30% decomposition. This is usually called the low-temperature reaction. The residue is quite stable at these temperatures unless rejuvenated by sublimation, recrystallization, or mechanical disturbance. At temperatures above 350 °C, the high-temperature decomposition occurs; this reaction is not autocatalytic and decomposition is complete. Concurrently with these decomposition reactions, AP also undergoes dissociative sublimation.

1.3 Definitions

In accordance to the ASTM international definition (American Society for Testing and Materials: http://www.astm.org/), an **energetic material** is defined as a compound or mixture of substances which contains both the fuel and the oxidizer and reacts readily with the release of energy and gas. Examples of energetic materials are

- primary explosives
- secondary explosives
- gun propellant charges
- rocket fuels
- pyrotechnics, e.g. signal torches und illuminants, smoke and fog generators, decoys, incendiary devices, gas generators (air bags) and delay compositions.

Energetic materials can be initiated using thermal, mechanical or electrostatic ignition sources and do not need atmospheric oxygen to maintain the exothermic reaction.

   A material which could be considered to be a potential explosive, is a chemical compound or a mixture of substances in a metastable state, which is capable of a

Tab. 1.4 Berthelot-Rot values for potentially explosive substances.

potentially explosive substance	$\rho_0/10^3$ kg m^{-3}	V_0/m^3 kg^{-1}	Q_v/kJ kg^{-1}	B_R/kJ m^{-3}
HMX	1.96	0.927	5253	18707
NG	1.60	0.782	6218	12448
TNT	1.65	0.975	3612	9588
gun powder	1.87	0.274	3040	2913
hydrazine	1.00	1.993	1785	3558
Oppauer salt	1.10	0.920	1072	1193

quick chemical reaction, without requiring additional reaction partners (e.g. atmospheric oxygen). In order to estimate how explosive a substance is, the Berthelot-Rot value B_R can be used (equation 1). Here ρ_0 (in kg m^{-3}) is the density of the potential explosive, V_0 (in m^3 kg^{-1}) is the volume of smoke and Q_v (in kJ kg^{-1}) is the heat of explosion.

$$B_R \left[\text{kJ m}^{-3} \right] = \rho_0^2 \, V_0 \, Q_v \tag{1}$$

Table 1.4 shows the Berthelot-Rot values for some well-known explosives. In general, compounds with a B_R value higher or equal to that of the "Oppauer salt" (55 % NH_4NO_3, 45 % $(NH_4)_2SO_4$) − the detonation of which in 1921 caused a massive and catastrophic explosion with over 1000 fatalities − are considered potentially explosive.

In contrast to the potentially explosive substances discussed above, explosion hazards are defined as follows. Hazardous explosive substances are compounds or mixtures of substances which give a positive result to at least one of the following tests:

− steel-sleeve test (Koenen test) with a nozzle plate with a 2 mm diameter hole
− impact sensitivity (using the BAM drop-hammer); more sensitive than 39 J,
− friction sensitivity; more sensitive than 353 N.

Energetic materials which contain the fuel as well as the oxidizer ignite on raising the temperature past the ignition temperature (due to the supply of external heat), forming a flame which generates heat as a result of the exothermic chemical reaction which is greater than the heat loss of the surroundings. In contrast to simple combustion, (e.g. a candle = fuel) which occurs without an increase in pressure and uses oxygen from the atmosphere, in a deflagration (oxidizer and fuel combined in the energetic material), pressure is formed (Fig. 1.20). The term **Deflagration** means that when using a mixture of fuel and oxidizer, a flame is propagated which is less than the speed of sound, but which still can be heard. The (linear) burn rate (r in m s^{-1}) is therefore the speed with which the flame (zone of reaction is on the surface) moves through the unreacted material. Since the temperature increases with increasing pressure (p), the burn rate is also pressure de-

pendent (equation 2). It is strongly influenced by the composition of the energetic material, as well as the confinement. In this context, β is a coefficient ($\beta = f(T)$) and a is the index of the burn rate which describes the pressure dependency. The index a is < 1 for energetic materials which deflagrate, and > 1 for detonating explosives.

$$r = \beta p^a \tag{2}$$

Under certain conditions (e.g. strong confinement), a deflagration can change to a **Detonation** (but not vice versa!). This occurs when the reaction front reaches the speed of sound in the material (typical values for the speed of sound in different materials are: air 340 m s^{-1}, water 1484 m s^{-1}, glass 5300 m s^{-1}, iron 5170 m s^{-1}) and then propagates supersonically from the reacted into the unreacted material. The transition from a deflagration to a detonation is known as a **Deflagration-to-Detonation Transition** (DDT). The term detonation is used to describe the propagation of a chemical reaction zone through an energetic material accompanied by the influence of a shock-wave at a speed faster than the speed of sound. The detonation zone moves through the explosive at the speed of detonation D, perpendicular to the reaction surface and with a constant velocity. All of the properties of the system are uniform within the detonation zone. When these chemical reactions occur with the release of heat at a constant pressure and temperature, the propagation of the shock-wave becomes a self-sustaining process. Chemical substances which are able to undergo a DDT, are described as explosives and the corresponding self-sustaining process is called a detonation (Figs. 1.20 and 1.21).

Under the influence of the dynamic properties of the shock-wave, a thin layer of still unreacted explosive from the original specific volume V_0 ($V_0 = 1/\rho_0$) along with the shock adiabat of the corresponding explosive (or Hugoniot adiabat) is compressed to volume V_1 (Fig. 1.22). The pressure increases from p_0 to p_1 as a consequence of the dynamic compression, which subsequently results in an increase of the temperature in the thin compressed layer of the explosive (Figs. 1.21 and 1.22), which causes initiation of the chemical reaction. At the end of the chemical
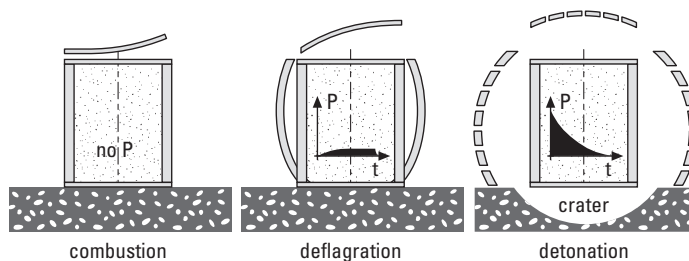
Fig. 1.20 Schematic representation of the pressure-over-time diagram of a combustion, a deflagration and a detonation.
(This diagram is reproduced with slight modification from the original of Prof. Dr. Manfred Held, who is herewith thanked for his permission to reproduce this.)
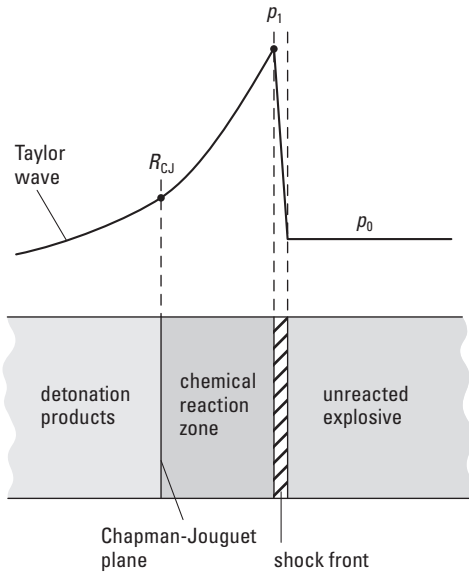
Fig. 1.21 Schematic representation of the detonation process and the structure of the detonation wave.
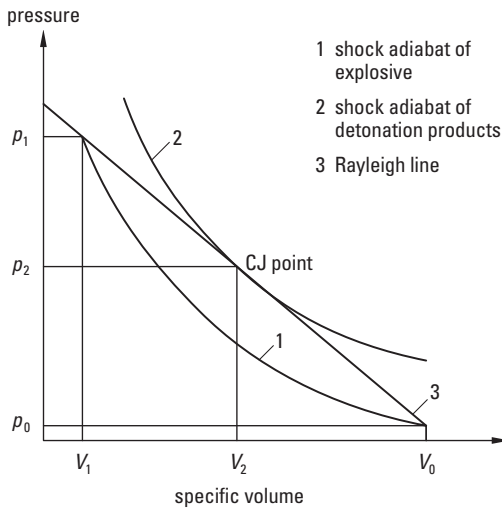
Fig. 1.22 Shock adiabat for an explosive and the detonation products (detonation in stationary state).

reaction, the specific volume and pressure have the values V_2 and p_2. At the end of the reaction zone the reaction products are in chemical equilibrium ($\Delta G = 0$) and the gaseous reaction products move at the local speed of sound, c. Mass, impulse and energy conservation apply. The requirement of a chemical equilibrium between

Tab. 1.5   Reaction types of an energetic material with $Q_{ex} = 1000$ kcal kg^{-1}.

reaction type	reaction speed/ m s^{-1}	mass flow/ m^3 s^{-1}	gaseous products/ m^3 s^{-1}	reaction time/ s m^{-3}
Combustion	$10^{-3}-10^{-2}$	$10^{-3}-10^{-2}$	$1-10$	10^2-10^3
Deflagration	10^2	10^2	10^5	10^{-2}
Detonation	10^4	10^4	10^7	10^{-4}

the reaction products is known as the Chapman-Jouguet condition. This state corresponds to the point of the detonation products on the shock adiabat (Fig. 1.22). At this point it is important to emphasize again, that in a deflagration the propagation of the reaction occurs as a result of thermal processes, whereas in the considerably faster detonation, a shock-wave mechanism is found.

Following the detonation model for the stationary state, the points (V_0, p_0), (V_1, p_1) and (V_2, p_2) lie on one line (Fig. 1.22), which is known as the **Rayleigh line**. The slope of the Rayleigh line is determined by the detonation velocity of the explosive. In accordance with Chapman and Jouguet's theory, the Rayleigh line is tangent to the shock adiabat of the detonation products and at this point corresponds to the end of the chemical reaction (V_2, p_2). This point is therefore also known as the **Chapman-Jouguet Point** (C-J point). At the C-J point an equilibrium is reached and the speed of the reaction products corresponds to that of the detonation velocity D. Now the gaseous products can expand and a dilution or Taylor wave occurs (Fig. 1.21). Concrete values for typical speeds of reactions and mass flow rates for combustion, deflagration and detonation are summarized in Table 1.5.

1.4 Combustion, Deflagration, Detonation – A Short Introduction

Fire, combustion, deflagration, and detonation are all terms used to describe exothermic oxidation reactions. They are distinguishable from each other by their reaction velocities.

1.4.1 Fire and Combustion

Generally speaking, combustion is a heat-releasing chemical oxidation reaction, which is often accompanied by the occurrence of a flame. Flame temperatures differ widely from approx. 2000 K for an open flame to approx. 3000 K for the flame of an acetylene cutting torch. Remarkably, the heats of combustion of explosives is generally lower than those of common fuels (pine wood with 12.9 % water: 4.422 kcal/g, acetylene: 11.923 kcal/g, dynamite 75 %: 1.290 kcal/g.

Fire is a simple example of a combustion reaction, despite it being less predictable and slower than pure combustion reactions. There are four factors which decide

how big a fire can get: fuel, oxygen, heat, and uninhibited chemical chain reactions. If one of these factors is restricted or even absent, the fire will become extinct. For example, lean fuel-air mixtures cannot be ignited because the ratio of fuel is too low and rich mixtures lack the sufficient oxygen ratio to be ignitable. Water as a fire extinguisher has a cooling effect and it therefore stops burning through heat restriction and heat transfer. During burning, a reducing agent (fuel, e.g. gasoline) reacts with oxygen. When heating an ignitable liquid, prior to reaching the actual boiling point of the liquid, a considerable amount of fumes can be observed on the surface of the liquid. As these gases mix with air, ignitable mixtures can develop. The temperature at which an ignitable fume layer is found directly on the liquid's surface is called the flash point of the substance. Liquids at temperatures exceeding the flash point are easily set on fire by a flame or spark. The flash point is usually found at temperatures lower than the boiling point. As the boiling liquid is heated further, the temperature of the heated fume-air mixture may become high enough to evoke a spontaneous oxidation. At this temperature, the fume-air mix will ignite itself spontaneously. The corresponding temperature is called the autoignition temperature (usually above 300 °C, for some compounds, e.g. diethyl ether, significantly lower). A comparable effect can be observed when water is added to overheated oil. As the oil is spilled in form of a finely dispersed cloud, an oil-air mixture is obtained at a temperature enabling rapid oxidation. The resulting hot oil cloud will ignite spontaneously. Thus when heating an ignitable liquid, the temperatures first reach the flash point, then the boiling point, and finally the autoignition point. In order to burn, liquid fuels must be evaporated to maximize contact with oxygen (air) and solid fuels must be sublimed first (e.g. camphor) or pyrolyzed into ignitable gases or fumes.

After a sufficient heat source starts the fire, it propagates through the fuel by heat carrying the uninhibited chemical chain reaction. Heat is transferred by convection, conduction and radiation. Convection is based on the lower densities of heated gases resulting in a gas flow. This is the base for the so-called Zone Model to predict heat flow and fire growth in rooms and spaces. In the Zone Model (e.g. CFAST program; Fire Growth and Smoke Transport Modeling with CFAST (version 6.1.1), National Institute of Standards and Technology (NIST), http://cfast.nist.gov), a room is divided into a cold gas layer (zone) at the floor and a hot zone at the ceiling. Heat transfer by conductivity is understood either as thin, when heat transfer within the object is faster than the rate at which the surface of the object is changed by heat transfer, or as thick, when there is a temperature gradient within the object and the unexposed surface has no significant influence on the heat transfer into the exposed surface. In thin materials (e.g. sheet metal), the temperature can be described by the one-dimensional heat transfer equation:

$$(\delta \rho C_{\mathrm{p}}) \frac{\partial T}{\partial x} = \dot{q}''_{\mathrm{rad}} + \dot{q}''_{\mathrm{con}} - \dot{q}''_{\mathrm{e}}$$

with the heat transfer rates $\dot{q}''_i$ (i = rad for radiation, con for convection and e for background loss) and the measurable material thickness δ, density ρ and heat capacity C_p. For thick materials, heat transfer within the material can be described one-dimensionally by

$$\rho C_p \frac{\partial T}{\partial t} = k \frac{\partial^2 T}{\partial x^2}$$

with the thermal conductivity k of the material. Heat transfer by radiation can be described by the model of black body radiation and Boltzmann's equation for the thermal energy emission of an ideal radiator

$$E_b = \sigma T^4$$

with the Boltzmann constant of σ. Unfortunately, in reality, most burning objects do not behave like ideal black body radiators and do not completely absorb thermal energy.

When a fire is started in the open the burning is fuel-limited. Since oxygen is abundant in the air, the rate at which fuel is supplied to the fire limits its growth. Even for fires in confined areas (rooms), the early stage of fire is fuel limited. The heat release of a fire is dependent on time. In the early stage of burning, the heat release will grow with the square of time until reaching a steady state. When the fire is extinguished, e.g. when all fuel or oxygen available is consumed, the heat release will decrease to zero. The heat release of a fire can be estimated from the height of its flames. In confined spaces, the initial stage of fuel limited burn will grow into a fully developed fire, wherein all burnable fuels in the room are burning. The fully developed fire will terminally be oxygen-limited as the amount of oxygen available to the chemical chain reactions will constrain the fire. The transition to a fuel-rich oxygen-limited fire will be indicated by a flashover, the transition to uniform burning of all burnable substances in the room, preceded by rollover, flaming-out and off-gassing. In the final oxygen-limited stage, more and more under-oxidized combustion products like CO, HCN and other potentially hazardous compounds are detected in the combustion product mixture.

Combustion reactions are excessively used in propellant systems. The impulse of the gaseous combustion products is used to propel a payload. For obvious technical reasons, the burning temperature of a rocket engine is of interest. The adiabatic flame temperature of combustion (T_{ad}) is the temperature at which reactants and products do not differ in enthalpy. The enthalpies of the components of the system have to be calculated from their standard enthalpy by adding of the enthalpy caused by heating to T_{ad}. This is where the specific heat capacity C_v comes into play. Unfortunately, the component ratios of the system are functions of the temperature, necessitating the use of iterative calculations of T_{ad}.

1.4.2 Deflagration and Detonation

Combustion reactions can be self-accelerating. The acceleration of chemical reactions is achieved by two routes: large increases in active particles and branching of exothermic chain reactions. Active particles, like radicals, are formed by the dissociation of molecules, a process expected to increasingly take place at elevated temperatures. The more active particles are generated, the more collisions between active particles can be observed which causes an accerleration of the overall reaction rate. Branching of chain reactions may occur whenever a single reaction produces more active particles than there were previously in this reaction. However, active particles are continuously de-activated by inevitable collisions. Chain branching then is in concurrence with chain termination. If the rate of chain branching is greater than the rate of chain termination, the reaction will be accelerated and explosion conditions can be obtained. If the energy release of the reaction exceeds the thermal heat loss, thermal explosion can be achieved. Since the loss of active particles does not require activation energy, the temperature's influence on the rate of chain branching is much bigger than it would be on chain termination. Taking the rates of active center creation, chain branching and chain termination into account, the critical temperature, below which explosion is impossible, is to be found.

When starting the reaction, there is an induction period, in which active particles are built up in the system. After the induction time, the number of active particles continues to rise without limit. From this time on, deflagration is observed which may develop into detonation.

Deflagration is the exothermic chemical reaction proceeding at subsonic speed, a detonation proceeds in a supersonic detonation wave. While deflagration can be initiated by mild energy release, e.g. a spark, detonation is triggered by localized explosions caused by the impact of a shock wave. Rapid release of a large amount of energy is typically needed to initiate detonations. However, there often is a transition from deflagration to detonation (a transition from detonation to deflagration is not apparent). This deflagration-to-detonation transition (DDT) is relevant because of its destructive potential. Experimental observations indicate that DDT rarely takes place in unconfined propagating flames. The presence of walls or other spatial confinements of the propagating flame greatly enhance the probability of DDT. In an unconfined burning, the pressure of the gaseous reaction products, which might form small shock waves, are able to expand freely without pressurizing the unburned composition. As the burning system becomes more and more confined, e.g. in a tube, the shock waves caused by the expansion of product gases can reflect from the walls, then form turbulences and fold to convulsions. These reflections, turbulences and convulsions may increase the flame velocity. The flame, which is thus accelerated by itself, can act with the flow of the product gases as piston in the refined system generating pressure and shock waves in the unreacted material. This may again contribute to an even faster and exponential self-

acceleration of the flame until a miniature explosion prompts the onset of detonation. The shock wave must be strong enough to raise the temperature in the system up to roughly 1500 K in order to initiate the reaction. For Chapman-Jouguet type detonations, Mach numbers of $\sim 6/7$ are found for the leading shock wave; DDT takes place when the velocity of the reaction wave approaches the local speed of sound. Experimentally, a tulip shaped or spiked flame front appears shortly before the transition to detonation is achieved. As soon as the DDT has taken place, the reaction proceeds through the unreacted material in a self-sustained detonation.

2 Classification of Energetic Materials

Energetic materials which derive their energy from a chemical reaction (in contrast to a nuclear reaction) can be classified according to their use as shown in Figure 2.1.
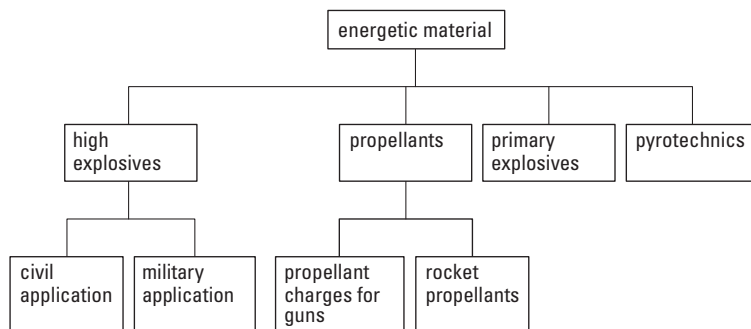
```
                          energetic material
        ┌────────────────────┬──────────┬──────────────┐
   high explosives       propellants   primary      pyrotechnics
                                        explosives
   ┌──────┴──────┐       ┌──────┴──────┐
 civil        military  propellant    rocket
 application  application charges for  propellants
                        guns
```

**Fig. 2.1** Classification of energetic materials.

2.1 Primary Explosives

Primary explosives are substances which unlike secondary explosives show a very rapid transition from combustion (or deflagration) to detonation and are considerably more sensitive towards heat, impact or friction than secondary explosives. Primary explosives generate either a large amount of heat or a shockwave which makes the transfer of the detonation to a less sensitive secondary explosive possible. They are therefore used as initiators for secondary booster charges (e.g. in detonators), main charges or propellants. Although primary explosives (e.g. $Pb(N_3)_2$) are considerably more sensitive than secondary explosives (e.g. RDX), their detonation velocities, detonation pressures and heat of explosions are as a rule, generally lower than those of secondary explosives (Tab. 2.1).

Typical primary explosives are lead azide and lead styphnate (see Fig. 1.17). The latter one is less powerful than LA but easier to initiate. Tetrazene (Fig. 2.2) is often added to the latter in order to enhance the response (sensitizer). (*N.B.* mercury fulminate used to be used as a sensitizer). Tetrazene is an effective primer which decomposes without leaving any residue behind. It has been introduced as an additive to erosion-free primers based on lead trinitroresorcinate. Unfortunately, tetrazene is hydrolytically not entirely stable and in long term studies decomposes at temperatures above 90 °C. Diazodinitrophenol (Fig. 2.2) is also a primary explo-

Tab. 2.1   Typical sensitivity and performance data of primary and secondary explosives.

|	typical primary explosives	$Pb(N_3)_2$	typical secondary explosives	RDX
sensitivity data				
impact sensitivity / J	≤ 4	2.5−4	≥ 4	7.4
friction sensitivity / N	≤ 10	< 1	≥ 50	120
ESD / J	0.002−0.020	0.005	≥ 0.1	0.2
performance data				
detonation velocity / m s^{-1}	3500−5500	4600−5100	6500−9000	8750
detonation pressure / kbar		343	210− 390	347
heat of explosion / kJ kg^{-1}	1000−2000	1639	5000−6000	5277 (H_2O(g))
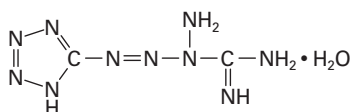
tetrazene
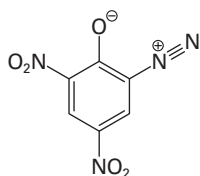
DDNP

Fig. 2.2   Molecular structure of tetrazene and diazodinitrophenol (DDNP).

sive and is primarily used in the USA. However, the compound quickly darkens in sunlight. SAcN (silver acetylide nitrate, $Ag_2C_2 \cdot 6\,AgNO_3$), mainly in combination with PETN, has also shown to be useful for the use in detonators [9].

HNS is a temperature stable secondary explosive, which is particularly useful for blasting in very hot oil deposits, because it is stable to approx. 320 °C. Problems in this area however relate to the initiator, since HNS is relatively difficult to initiate. The most useful initiator is cadmium azide, $Cd(N_3)_2$, ($T_{dec.}$ ca. 295 °C). However, since cadmium is toxic, alternatives are currently being sought after. The two most promising compounds to date to replace $Cd(N_3)_2$ are silver nitriminotetrazolate ($T_{dec.}$ = 366 °C) and di(silveraminotetrazole) perchlorate ($T_{dec.}$ = 319 °C) (Fig. 2.3) [10].
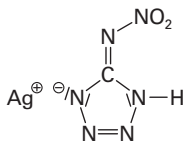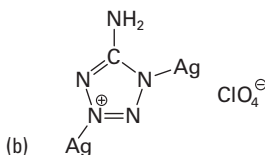
(a)   (b)

Fig. 2.3   Structures of silver nitraminotetrazolate and disilver(aminotetrazole) perchlorate.
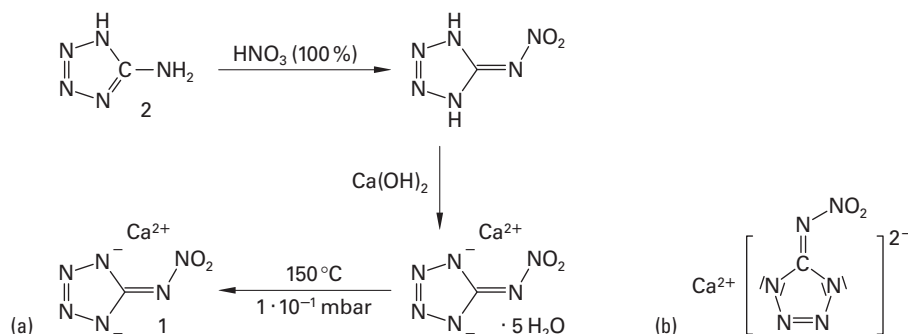
Fig. 2.4 Synthesis (a) and structure (b) of calcium (nitriminotetrazolate).

Calcium (nitriminotetrazolate) has shown huge potential due to its large thermal stability (T_{dec} = 360 °C) and relatively low sensitivity (impact sensitivity: 50 J, friction sensitivity 112 N, ESD = 0.15 J), but at the same time good initiation behavior with commercial pyroelectric initiators (Fig. 2.4). The corresponding cadmium salt is also a good primary explosive.

While the environmental impact of cadmium azide in deep oil deposits is relatively low, the long-term use of $Pb(N_3)_2$ and lead styphnate in military training grounds has resulted in considerable lead contamination (see Ch. 1.2.3, see Fig. 1.17). "On demand lead azide" (ODLA) is available from the reaction of lead acetate and sodium azide. The recently introduced iron and copper complexes of the type $[Cat]_2 [M^{II}(NT)_4(H_2O)_2]$ ($[Cat]^+$ = NH_4^+, Na^+; M = Fe, Cu; NT = 5-nitrotetrazolate) as "green" primary explosives [3] are relatively easily obtained and show similar initiator properties as those of lead azide (Tab. 2.2).

Tab. 2.2 Properties of lead azide (LA) and lead styphnate (LS) in comparison to new "green" primary explosives.

primary explosive	T_{dec} / °C	impact sensitivity / J	ESD / J	density / g cm^{-3}	detonation velocity / m s^{-1}
NH$_4$FeNT	255	3	> 0.36	2.2	7700
NaFeNT	250	3	> 0.36	2.2	not determined
NH$_4$CuNT	265	3	> 0.36	2.0	7400
NaCuNT	259	3	> 0.36	2.1	not determined
LA	315	2.4	0.005	4.8	5500
LS	282	3.4	0.0002	3.0	5200

2.2 High (Secondary) Explosives

Secondary explosives (also known as "high explosives" = HEs) unlike primary explosives can not be initiated simply through heat or shock. In order to initiate

primary explosives have to be used, whereby the shockwave of the primary explosive initiates the secondary. However, the performance of the secondary explosive is usually higher than that of the primary (see Tab. 2.1). Typical currently used secondary explosives are TNT, RDX, HMX, NQ and TATB (see also Tab. 1.2) and, for civil applications, HNS and NG e.g. in the form of dynamite for commercial use.

The current trends in the research of secondary explosives can be arranged into three branches (Fig. 2.5):

− Higher performance,
− Lower sensitivity (insensitive munition, IM),
− Lower toxicity of the explosives, their biological degradation products and the detonation products.

A higher performance for secondary explosives is of fundamental importance and always desired. The main performance criteria are:

1. heat of explosion Q (in kJ kg^{-1}),
2. detonation velocity D (m s^{-1}),
3. detonation pressure P (in kbar),

and less importantly,

4. explosion temperature T (K) and
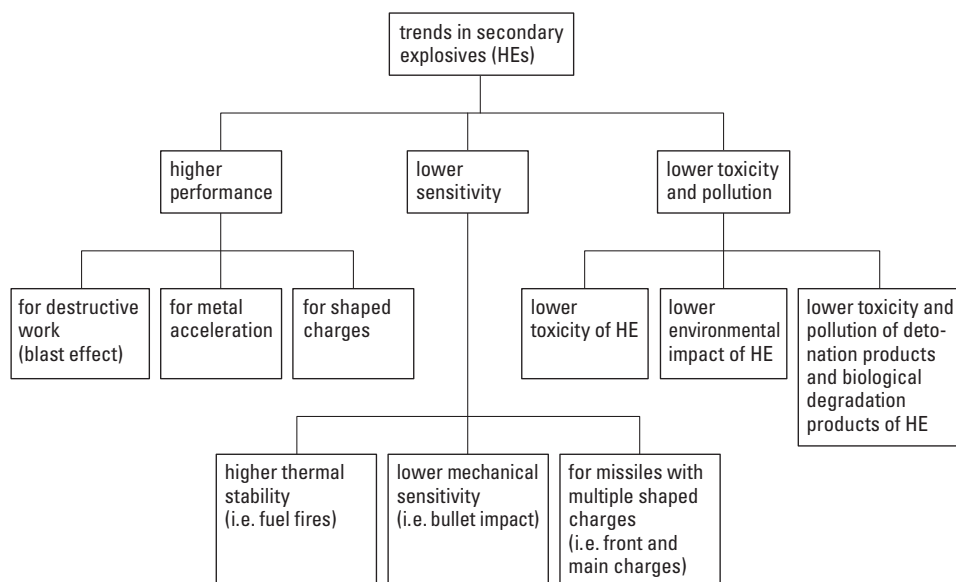5. volume of gas released V per kg explosive (in l kg^{-1}).

Fig. 2.5 Trends for new secondary explosives.

Depending on the location of the mission, one parameter can be more important than the other. For example, the performance (or brisance) of an explosive can not be described by one parameter alone. The term **brisance** describes the destructive fragmentation effect of a charge on its immediate vicinity. The higher the charge density (corresponding to the energy per volume) and the detonation velocity (corresponding to the reaction rate), the more brisant the explosive is. Furthermore, the detonation velocity as well as the detonation pressure increase with increasing density. According to Kast, the brisance value (B) is defined as the product of the loading density (ρ), the specific energy (F for "force of an explosive") and the detonation velocity D:

$$\text{Brisance: } B = \rho \times F \times D$$

The specific energy ("force") of an explosive (F) on the other hand can be calculated according to the general equation of state for gases:

$$\text{Specific energy: } F = p_e V = n\,R\,T$$

Here p_e is the maximum pressure through the explosion (not to be confused with the much higher values for the detonation pressure $p_{C\text{-}J}$ at the C-J point), V is the volume of detonation gases (in $l\,kg^{-1}$ or $m^3\,kg^{-1}$), n is the number of moles of gas formed by the explosion per kilogram of explosive, R is the gas constant and T is the temperature of the explosion. The specific energy also has the units $J\,kg^{-1}$. Consequently, the brisance can be given using the units $kg\,s^{-3}$.

Generally, the specific energy of secondary explosives is higher than that for propellant charges. This is due to the fact that in propellant charges the temperature of combustion is kept as low as possible in order to protect the barrel by preventing the formation of iron carbide (from the CO in the combustion). For shaped charges a high brisance and therefore a high specific energy and also high loading densities are particularly important. For typical general purpose bombs, a maximum heat of explosion (Q) and gaseous products (V) should be achieved.

As we have already seen above (see Fig. 1.20), the pressure vs. time diagram shows that the explosion pressure (not to be confused with the by magnitudes higher detonation pressure $p_{C\text{-}J}$) generated on detonation increases instantly and decreases exponentially with time. Figure 2.6 shows the typical time dependence of a blast wave. When the detonation occurs at time $t = 0$, the shock front reaches the "observer" i.e. the object, which is exposed to the shock front at time t_a. Afterwards, the pressure falls exponentially and for a certain period of time it falls beneath the pressure of its surroundings (atmospheric pressure).

As we can see in Figure 2.7, after a detonation, the shock wave naturally requires a certain amount of time t ($t_1 < t_2 < t_3 < t_4$), to reach a certain point. However, the maximum pressure p of the shockwave also decreases as the distance from the center of the detonation increases.
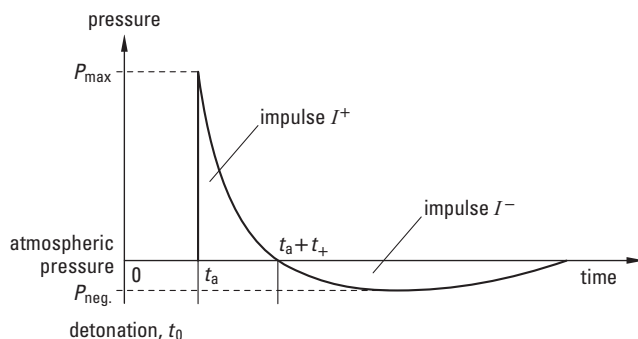
Fig. 2.6 Typical time dependent progression of a shock wave in the vicinity of a detonation. (This diagram is reproduced with slight modification from the original of Prof. Dr. Manfred Held, who is herewith thanked for his permission to reproduce this.)

Fig. 2.7 Pressure-distance-dependence of a progressing shock wave at different points in time t ($t_1 < t_2 < t_3 < t_4$) after a detonation.
(This diagram is reproduced with slight modification from the original of Prof. Dr. Manfred Held, who is herewith thanked for his permission to reproduce this.)
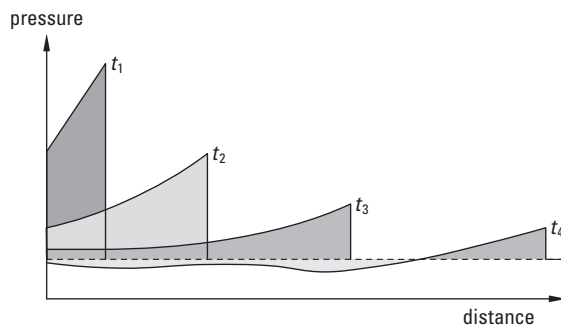
Generally, it can be said that the damaging effect of a shockwave produced by a detonation is proportional to its impulse (impulse = mass × velocity of the gaseous explosion products) and its maximum pressure, with the impulse being the most influential factor at smaller distances and the pressure being most important at larger distances. As a "rule of thumb", the distance D, which offers a chance of survival, is proportional to the cube route of the mass w of an explosive, while for typical secondary explosives at larger distances, the proportionality constant is approximately 2:

$$D = c\, w^{0.33} \approx 2\, w^{\,0.33}$$

It is important to note, that this approximation is only based on the pressure. The impulse of the shockwave and the fragment impact (e.g. from confined charges or fume-cupboard shields in lab) are *not* taken into consideration.
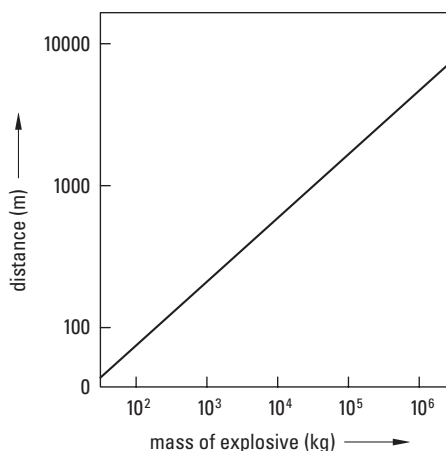
Fig. 2.8 "Safe" distance for occupied buildings from the detonation of a secondary explosive.

In order to work safely with highly energetic materials in the chemical laboratory the following rules must be obeyed:

− amounts used are to be kept as small as possible,
− the distance from the experiment is to be kept as large as possible (filled vessels are not to be transported by hand, but with well fitted tongs or clamps instead),
− mechanical manipulators are to be used when possible, particularly for larger quantities,
− vessels are never to be enclosed by hand (confinement),
− protective clothing (gloves, leather or Kevlar vest, ear protectors, face shield, anti-electrostatic shoes) is to be worn at all times.

Figure 2.8 shows a correlation between the mass of the secondary explosive used and the "safe" distance for occupied buildings. Of course this is only a very rough guide and it is dependent on the building and the nature of the explosive used.

In addition to formulations of secondary explosives (see Tab. 1.2), metallized mixtures are sometimes used as well. Metals such as beryllium, magnesium or aluminum which are air resistant, but at the same time easily oxidized in very exothermic reactions are suitable. In practice, aluminum is used almost exclusively. Since most formulations possess a negative oxygen balance, the aluminum does not contribute to raising the heat of detonation in atmospheric explosions a lot, but it combusts afterwards (post-detonation combustion, often a large fireball) using the surrounding air which increases the visibility (psychological effect) considerably. This is different for underwater explosions, e.g. torpedoes (see Tab. 1.2, TORPEX), because here the aluminum obtains the oxygen from the (liquid) water, which contains oxygen in a high density. Metallized formulations are also suitable for special missions (e.g. caves, tunnels e.g. in GWT), since in enclosed spaces the oxygen in the air needed to breathe for survival vanishes (see Ch. 13).
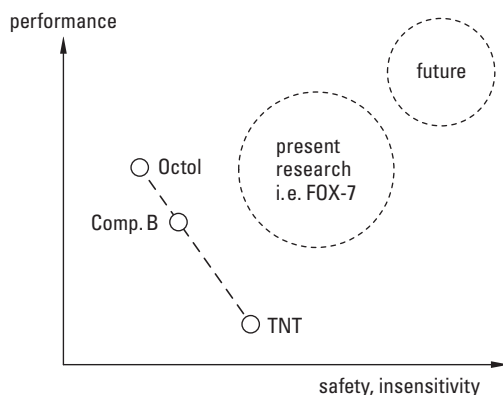
Fig. 2.9 Safety (insensitivity) and performance.

In attempts to strive for better performance, safety aspects (lower sensitivities) can not be ignored. For example, by using the formulations Composition B and octol (see Tab. 1.2) instead of TNT, the performance can be increased significantly (Fig. 2.1). However, the sensitivity increases as well which causes safety to decrease accordingly. The goal of current research is to develop considerably less sensitive secondary explosives, which offer maximum performance and a high safety standard (Fig. 2.9).

Particularly important in the area of explosives for torpedoes, missiles, war heads and bombs, which are transported by planes or submarine is, that if a fuel fire should occur, the charge is not thermally initiated. Insensitive, but high performing explosives also play a large role for shaped charges with several charges (front- and main charges) e.g. for operations against tanks, which are protected by Explosive Reactive Armour (ERA). Last but not least, insensitive also means that no accident can occur as a result of friendly fire or through enemy attack.

There still is a need for intensive research (Fig. 2.1) in the area of the latter aspect of new secondary explosives (and not only for those!) in terms of low toxicity and environmental impact. Conventional energetic materials (TNT, RDX), which are currently used by NATO armies for training purposes on their training grounds, have an extremely negative ecological impact, if they end up unwanted and uncontrolled in the environment as unexploded munition (UXOs = unexploded ordnance), or through low-order as well as high-order detonations. This necessitates expensive and very time-consuming remediation and detoxification operations. The development of alternative energetic materials, which are environmentally compatible, but still fulfil the performance and insensitivity requirements of the NATO armies (see above), i.e. safe handling, is an important step in the direction of developing ecologically compatible, non-toxic and sustainable highly energetic materials. For example, RDX is toxic when ingested or inhaled in large quantities, causing seizures, nausea and vomiting. For example, the EPA (Environmental Protection

Tab. 2.3 Ecological and toxicological problem areas of highly energetic materials.

class of energetic material	example	problem		possible solution
		environment	human	
primary explosive	$Pb(N_3)_2$	Pb contamination of training grounds	heavy metal toxicity of Pb	Pb-free primary explosives, e.g. Fe
secondary explosive	RDX	RDX and degradation products are toxic for plants, microorganisms and microbes (earthworms)	kidney toxin	new high-N, high-O compounds
	TNT	TNT and degradation products are ecologically toxic		new melt-castable high explosives, e.g. IMX-101: DNAN = dinitroanisole (binder) + NTO (filler)
	Comp.-B	contains RDX and TNT		IMX-104: DNAN (binder) + NTO and RDX (filler)
pyrotechnics	Ba (green)	heavy metal	heavy metal[a]	insoluble Ba compounds; Ba-free colorants, e.g. Cu
	ClO_4^- as Chlorine source		decrease of thyroxin synthesis due to inhibition of iodine storage[b]	
pyrotechnics	Pb resorcynate burn rate catalyst in min smoke missiles	heavy metal	heavy metal	Cu, Bi based burn rate modifiers; reactive metal nanopowders as burn rate catalysts/modifiers
solid rocket propellant	AP	HCl in atmosphere, ozone layer	decrease of thyroxin synthesis due to inhibition of iodine storage	$CaSi_2$ additives as HCl scrubbers; new HEDOs, e.g. ADN
monopropellant	N_2H_4		carcinogenic	new propellants, e.g. DMAZ
bipropellant	MMH		carcinogenic	new bipropellants, e.g. DMAZ
	HNO_3	NO_x	toxic	e.g. 100 % H_2O_2

[a] causes hypertension, muscular weakness, cardiotoxic effects, gastrointestinal effects
[b] EPA has recommended a max. level of 24.5 ppb ClO_4^- in drinking water.

Agency) has suggested a limit of $2 \, \mu g \, l^{-1}$ for RDX in drinking water. However, this value is marginally overstepped in some areas in the vicinity of troop training grounds. Limits for RDX have also been determined for the workplace by NIOSH (National Institute for Occupational Safety and Health). These are in general $3 \, \mu g \, m^{-3}$ air and $1.5 \, \mu g \, m^{-3}$ air for a 40 hour working week.

Table 2.3 shows a summary of examples of some ecological and toxicologic problem areas of highly energetic materials.

Particularly in the USA, but also in Germany, great efforts are being made by different institutions to reduce the environmental impact caused by the use of highly energetic materials. Leaders in this area are SERDP (Strategic Environmental Research and Development Program: http://www.serdp.org/) as well as ESTCP (Environmental Security Technology Certification Program: http://www.estcp.org/).

2.3 Propellant Charges

The oldest known propellant charge is blackpowder (or gunpowder) which is a mixture of 75% KNO_3, 10% sulfur and 15% charcoal dust. It is an easy to ignite powder with a burn rate of $600-800 \, m \, s^{-1}$, which is still used today as a charge in military and civil *pyrotechnic* munitions. NC powder was discovered in 1846 by Schönbein and burns almost without any residue. Its burn rates at atmospheric pressure is $0.06-0.1 \, m \, s^{-1}$, which is considerably slower than blackpowder, as long as no pressure is applied to the propellant charge on burning. In addition to the linear burn rate r (in $m \, s^{-1}$), the mass-weighted burning rate m (in $g \, s^{-1}$) is of interest as well (A: surface, in m^2; ρ: density, in $g \, m^{-3}$):

$$M = r \, A \, \rho$$

Single-base nitrocellulose powder is the oldest of all types of NC powders and is often referred to as "smokeless" powder. It is prepared by reacting cellulose with nitric acid.

Depending on the acid concentration used, NC is formed with different degrees of nitration (e.g. $11.5-14.0\%$). In addition to the nitrocellulose based, double- and triple-base propellants contain further substances such as nitroglycerine and nitro-guanidine.

While single-base propellant charges (NC) are used in weapons from pistols to artillery weapons, the higher performance double-base propellant charges (NC + NG) are used predominantly in pistols and mortars. The disadvantage of the double-base powder is the strong erosion of the gun barrel (see below), resulting from the significantly higher combustion temperatures as well as the appearance of a muzzle flash because of the explosion of some of the combustion gases upon contact with air. To prevent erosion and the muzzle flash, a triple-base powder (NC + NG + NQ) with an NQ content of up to 50% is used, particularly in large

Tab. 2.4   Parameters for single, double and triple-base propellant charges.

propellant charge	ρ/g cm^{-3}	Ω/%	T_c/K	I_{sp}/s	N$_2$/CO
NC[a]	1.66	-30.2	2750	232	0.3
NC[a]/NG (50:50)	1.63	-13.3	3308	249	0.7
NC[a]/NG/NQ (25:25:50)	1.70	-22.0	2683	236	1.4
Hy-At/ADN (50:50)	1.68	-24.7	2653	254	6.3

[a] NC-13.3 (N content 13.3%)

calibre tank and NAVY weapons. However, the performance of triple-base powders is lower than that of double-base powders (Tab. 2.4). In a triple-base powder, particularly in large tank and NAVY cannons, NQ is replaced by RDX in order to increase the performance. However, the barrels suffer increased erosion problems again due to the significantly higher combustion temperatures.

The velocity v of a projectile on ejection from the gun barrel can roughly be estimated using the following equation:

$$v = \left(\frac{2\,m\,Q\eta}{M} \right)^{0.5}$$

$$Q = \Delta U_f^\circ (\text{prop. charge}) - \Delta U_f^\circ (\text{combustion products})$$

Where m is the mass of the propellant charge (in g), M is the mass of the projectile (in g), Q is the heat of combustion (in J g^{-1}) and η is a constant, which is specific for the system. Here, the energy released in Q is once again of crucial importance.

The erosion problems in guns are generally caused by the formation of iron carbide (Fe from the gun barrel, C from CO) at high temperatures. Modern research on propellant charges is therefore focused on the development of powders which burn at lowest possible temperatures, but show good performance (see Ch. 4.2.3). Moreover, the N$_2$/CO ratio, which lies at approximately 0.5 for conventional propellant charges, should be increased as much as possible. The formation of N$_2$ instead of CO should also strongly reduce the amount of erosion, since iron nitride has a higher melting point than iron carbide (Fe$_3$C) and furthermore, it forms a solid protective layer on the inside of the gun barrel. New studies have shown that the introduction of propellant charges which are based on nitrogen-rich compounds such as e.g. triaminoguanidinium azotetrazolate (TAGzT) result in a considerably better N$_2$/CO ratio and the life-span of high calibre NAVY cannons can be increased by up-to a factor of 4 [11]. The synthesis of azotetrazolate salts (e.g. Na$_2$ZT) occurs in a facile route from aminotetrazole by oxidation using KMnO$_4$ in alkaline conditions (NaOH). *Note:* the reduction of Na$_2$ZT in acidic conditions (HOAc) using Mg forms the neutral compound bistetrazolylhydrazine (BTH).
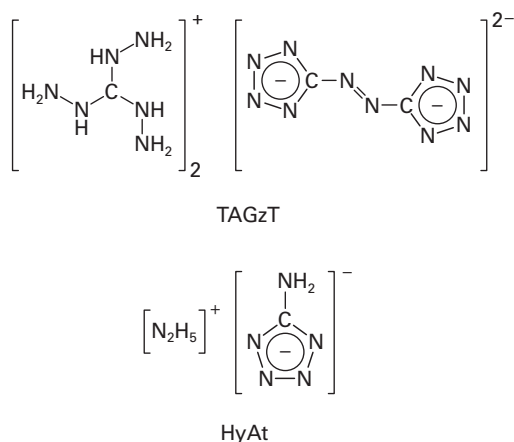
Fig. 2.10 Molecular structures of triaminoguanidinium azotetrazolate (TAGzT) and hydrazinium 5-aminotetrazolate (HyAt).

Also hydrazinium 5-aminotetrazolate (HyAt) appears to show good potential in this context (Tab. 2.4) [12] (Fig. 2.10).

For propellant charges the insensitivity is also playing an increasingly important role. Since approximately 1970 propellant charges have been developed and used under the title **LOVA** (low-vulnerability ammunition). Under bullet impact, shaped charge impact or fire they respond with fire in the worst case scenario, but not in deflagration and definitely not in detonation. As energetic fillers mainly RDX or HMX were used. As energetic binders, energy and gas generating polymers such as e.g. GAP (see Fig. 1.4) are particularly suitable. Such composite propellant charges are considerably less sensitive than powders based on NC.

2.4 Rocket Propellants

Rocket propellants are similar to the propellant charge powders discussed above, because they combust in a controlled manner and do not detonate. However, propellant charge powders burn considerably quicker than rocket propellants, which results in a significantly higher pressure for gun propellants in comparison with rocket propellants. Typical pressures in the combustion chambers of rockets are 70 bar, which can be compared with up to 4000 bar for large artillery and NAVY cannons.

As is the case for propellant charges, the specific impulse for rocket propellants is also one of the most important performance parameters.

The **specific impulse** (I_{sp}) is the change in the impulse (impulse = mass × velocity or force × time) per mass unit of the propellant. It is an important performance parameter of rocket motors and shows the effective velocity of the combustion

gases when leaving the nozzle, and is therefore a measure for the effectiveness of a propellant composition.

$$I_{sp} = \frac{\overline{F} \cdot t_b}{m} = \frac{1}{m} \cdot \int_0^{t_b} F(t) dt$$

The force F is the time dependent **thrust** $F(t)$, or the average thrust $\overline{F}$; t_b is the combustion time (in s) and m is the mass of propellant (in kg). Therefore the specific impulse has the units $N\ s\ kg^{-1}$ or $m\ s^{-1}$. Sometimes, predominantly in English speaking areas, the specific impulse is given based on the gravitation of the Earth g ($g = 9.81\ m\ s^{-2}$), which is on the mass of the propellant, and therefore has the unit seconds (s):

$$I_{sp}^* = \frac{I_{sp}}{g}$$

The specific impulse can be formulated exactly as follows:

$$I_{sp} = \sqrt{\frac{2\,\gamma\,R\,T_c}{(\gamma - 1)\,M}}$$

Whereby γ is the ratio of the specific heat capacities of the gas mixture, R is the gas constant, T_c is the temperature (K) in the combustion chamber and M is the average molecular weight (kg mol^{-1}) of the formed combustion gases:

$$\gamma = \frac{C_p}{C_V}$$

$$I_{sp}^* = \frac{1}{g} \sqrt{\frac{2\,\gamma\,R\,T_c}{(\gamma - 1)\,M}}$$

The average thrust of a rocket $\overline{F}$ can in accordance with the equation above be given simply as:

$$\overline{F} = I_{sp} \frac{\Delta m}{\Delta t}$$

Where I_{sp} is the specific impulse in (m s^{-1}), Δm is the mass of used propellant (in kg) and Δt is the duration of burning of the engine (in s). Therefore, the thrust has the units kg m s^{-2} or N and corresponds to a force.

In the following discussion we want to predominantly use the English term I_{sp}^*, which is smaller than the I_{sp} by a factor of approximately 10 and has the units s. Typical values for the specific impulse of solid boosters are 250 s, whereas for

bipropellants they are found at approx. 450 s. For chemistry it is important that the specific impulse is proportional to the square root of the ratio of the combustion chamber's temperature T_c and the average molecular mass of the combustion product M:

$$I_{sp} \propto \sqrt{\frac{T_c}{M}}$$

It is important in the discussion of the specific impulse I_{sp}^* below, that as a rule of thumb an increase of the specific impulse by 20 s, causes the maximum possible carried payload (warheads, satellites) to be approximately doubled.

A more detailed description to derive the thrust or the specific impulse of a rocket is given below: In order to propel a rocket, a rocket engine ejects combustion gases with low molecular mass but high velocity z through the nozzle. The rocket has the mass M and initially moves with velocity u. If the rocket ejects combustion gases of the mass of Δm within the time Δt and with the velocity z, a decrease in mass $M - \Delta m$ and an increase in the velocity to $u + \Delta u$ results. Due to the conservation of the impulse, the following can be derived:

$$
\begin{aligned}
M u &= (M - \Delta m)(u + \Delta u) + \Delta m\, z \\
\cancel{M u} &= \cancel{M u} + M \Delta u - \Delta m u - \Delta m \Delta u + \Delta m\, z \\
M \Delta u &= \Delta m\, (\underbrace{u + \Delta u - z}_{v_e}) \\
M \frac{\Delta u}{\Delta t} &= \frac{\Delta m}{\Delta t}\, v_e \\
M \frac{du}{dt} &= \frac{dm}{dt}\, v_e
\end{aligned}
$$

Therefore $v_e = u + \Delta u - z$ and is the velocity of the ejected combustion gases relative to the rocket. Here the force $(dm/dt)\,v_e$ corresponds to the **thrust** $F_{impulse}$, which originates from the impulse of the system:

$$F_{impulse} = \frac{dm}{dt}\, v_e$$

However, this is only equal to the total thrust F of the system when the pressure p_e at the end of the nozzle is the same as the pressure of its surroundings p_a. In general a correction term is needed which is called the pressure term $F_{pressure}$.

Figure 2.11 schematically shows the pressure profile which is one factor that influences rocket performance. The length of the arrows shows the contribution of the pressure from inside and outside the walls. While the atmospheric pressure outside is constant, the inside pressure of the combustion chamber is at its largest

and decreases in the direction of the nozzle end. The pressure term is proportional to the diameter A_e:

$$F = F_{\text{impulse}} + F_{\text{pressure}} = \frac{\mathrm{d}m}{\mathrm{d}t}\,v_e + (p_e - p_a)\,A_e$$

If the pressure at the end of the nozzle is smaller than the pressure of the surroundings (which occurs in the case of a so-called overexpanding nozzle), the pressure term then has a negative value and reduces the total thrust. Therefore, a pressure p_e which is the same or higher (underexpanding nozzle) than the air pressure is desirable.
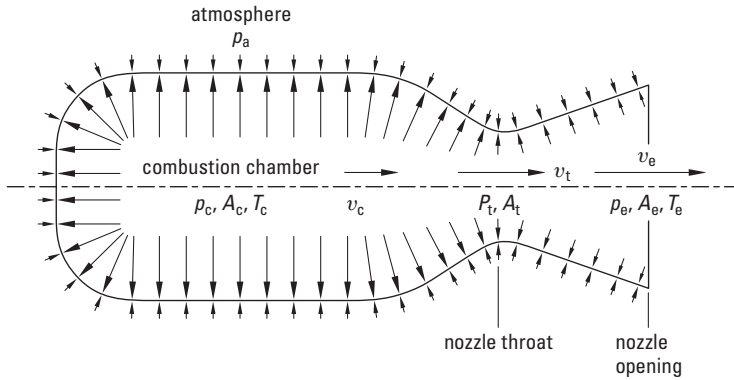
Fig. 2.11 Combustion chamber and nozzle.

Since the air pressure decreases with increasing flight altitude, at constant nozzle diameter, the total thrust increases with increasing flight altitude. This increase can correspond to approximately 10 to 30 % of the total thrust depending on the rocket. The maximum thrust is reached in vacuo. The so-called effective ejection velocity c_{eff} (of the combustion gases) is defined as the ratio between the thrust and the mass flux ($\mathrm{d}m/\mathrm{d}t$):

$$\frac{F}{\dfrac{\mathrm{d}m}{\mathrm{d}t}} = c_{\text{eff}} = v_e + \frac{(p_e - p_a)\,A_e}{\dfrac{\mathrm{d}m}{\mathrm{d}t}}$$

We can write:

$$F = \frac{\mathrm{d}m}{\mathrm{d}t}\,c_{\text{eff}}$$

The effective ejection velocity is an average. In reality the velocity distribution is not constant throughout the whole nozzle diameter. Assuming a constant ejection velocity allows a one-dimensional description of the problem.

The so-called total impulse I_t is the integral of the total thrust integrated over the total combustion time t:

$$I_t = \int_0^t F \, dt$$

The **specific impulse** is one of the most important values to characterize the performance of a rocket propulsion system. The higher this value is, the higher will the performance be. The specific impulse is defined as the total impulse per mass unit:

$$I_s^* = \frac{\int_0^t F \, dt}{g_0 \int_0^t \frac{dm}{dt} \, dt}$$

where $g_0 = 9.81$ m s^{-2} at sea level.

For constant thrust and mass flux, the equation above can be simplified to

$$I_{sp}^* = \frac{F}{\frac{dm}{dt} g_0}$$

Using the SI system, the specific impulse can be given in the units s^{-1}. However, the value g_0 is not always the same. Therefore, the specific impulse I_{sp} is often also given by the value

$$I_{sp} = \frac{F}{\frac{dm}{dt}}$$

This has the advantage that it is independent of the effect of gravity. It is given in the unit N s kg^{-1} or m s^{-1}. At sea level, both expressions are linked by a factor of approximately 10.

By inserting

$$F = \frac{dm}{dt} c_{eff}$$

in

$$I_{sp}^* = \frac{F}{\frac{dm}{dt} g_0}$$

the mass flux is shortened, and one obtains

$$I_{sp}^* = \frac{c_{eff}}{g_0}$$

The effective ejection velocity c_{eff} is different from the specific impulse I_{sp} only due to g_0 (see above).

The so-called **rocket equation** describes the fundamental equations of rocket propulsion. If we consider the simplest case, in which a monostage rocket accelerates in a gravity-free vacuum, i.e. a slow-down due to gravitation and friction is not taken into consideration. When the rocket has a velocity of zero at the start and ejects the propellant with a constant ejection velocity v_e, the velocity u of the rocket after time t corresponds to:

$$u(t) = v_e \ln\left(\frac{m(0)}{m(t)}\right)$$

Where $m(0)$ is the mass of the rocket at the start and $m(t)$ is the mass of the rocket at time t.

For rocket launches from earth, the formula must be changed to include the gravitation of Earth and corresponds to low altitudes with a constant earth gravitation g of 9.81 m s^{-2}:

$$u(t) = v_e \ln\left(\frac{m(0)}{m(t)}\right) - gt$$

Since g is dependent on the altitude, the following correction is needed:

$$u(t) = v_e \ln\left(\frac{m(0)}{m(t)}\right) - \int_0^t g(t')dt'$$

In addition to the gravitation of Earth a rocket launched from earth must also overcome the air resistance of the atmosphere, which means that the rocket equation for such cases is only an approximation. Planes, RAM and SCRAM jets which are propelled by jet engines, transport their fuel with them, but they also suck air in and use the oxygen from the air for the combustion of the fuel. They only carry the fuel but not the oxidizer with them. The rocket equation is not valid for such vehicles, which are referred to as air-breathing engines.

Generally, one can categorize rocket propellants into those for solid propellants and those for liquid propellants (Fig. 2.12). The **solid propellants** can be categorized further into double-base (homogeneous) and composite propellants (heterogeneous). The homogeneous propellants are generally based on NC, whereas the
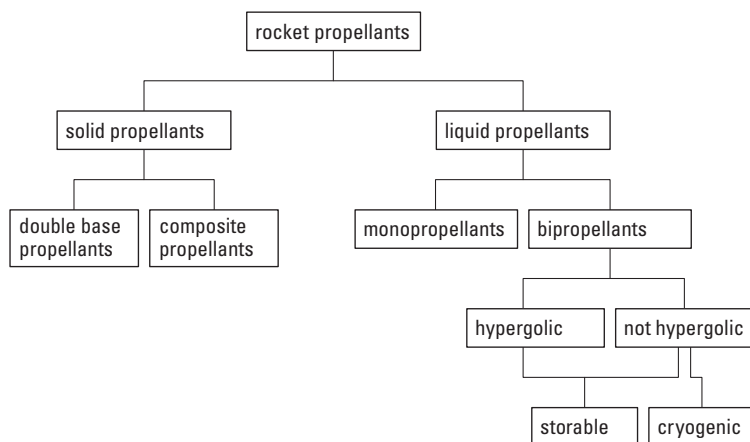
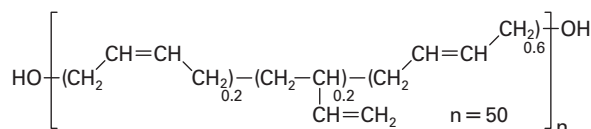**Fig. 2.12**   Classification of rocket propellants.

Fig. 2.13   Homopolymeric R45HT (hydroxyl terminated polybutadiene, HTPB).

heterogeneous propellants are generally based on AP. The double-base propellants are homogeneous NC/NG formulations. The composite propellants are mixtures of a crystalline oxidizer (e.g. ammonium perchlorate, AP) and a polymeric binder, which has been cured with isocyanate (e.g. hydroxy-terminated polybutadiene, HTPB/diisocyanate) and which contains the propellant (e.g. Al) (Fig. 2.13). The purpose of the polymer matrix (the binder) is to form a solid, elastic body of the propellant ingredients with sufficient mechanical properties. The binder is also used as a fuel because it contains mainly hydrogen and carbon. Two examples of double-base and composite propellants are given in Table 2.5.

Presently, research is on-going into trying to find alternatives to AP/Al (see also Ch. 1.2.4). The problems with the AP/Al mixtures which contain HTPB as a binder, are two-fold. On the one hand AP is toxic and should be substituted for this reason alone (see Ch. 1.2.4). On the other hand, such formulations are also problematic in slow cook-off tests (SCO test, see Ch. 6.2). It appears to be the case that here the AP slowly decomposes during the formation of acidic side-products. These acidic side-products then react with the HTPB binder, which can result in the formation of cracks und cavities in the composite, which consequently negatively affects the performance and sensitivity. Possible alternatives for AP are ADN, HNF and TAGNF. However, they cause other problems, such as, for example, the low thermal stability (ADN melts at 93 °C and already decomposes at 135 °C) and the binder compatibility is not always guaranteed either. Further research work is

Tab. 2.5 Solid propellants.

type	composition	I_{sp}^*/s	T_c/K
double-base	NC (12.6% N)[a] NG plasticizer other additives	200	2500
composite	AP Al HTPB additives	259	4273

[a] A typical double-base composition for minimum smoke missiles would be the M36 propellant with the following composition: NC (12.6% N) 49.0%, NG 40.6%, Di-n-propyl adipate 3.0%, 2-nitrodiphenylamine 2.0%, ballistic modifier (e.g. lead resorcinate) 5.3%, wax 0.1%.

absolutely necessary in order to find better oxidizers for solid propellants. In this context, the following requirements must be fulfilled:

1. density has to be as high as possible, if possible over 2 g cm^{-3},
2. oxygen balance has to be good, if possible better than that in AP,
3. melting point has to be above 150 °C,
4. vapor pressure has to be low,
5. decomposition temperature has to be above 200 °C,
6. synthesis has to be facile and economic,
7. compatible with binders (with HTPB),
8. sensitivity has to be as low as possible, definitely not more sensitive than PETN,
9. enthalpy of formation has to be as high as possible.

There are also advances in the area of propellants (Al). For example, attempts are being made to replace aluminum (which is normally used on the micro meter scale) with nano-Al. Thereby the combustion efficiency (quantitative combustion) would be increased, but the air (oxygen) sensitivity of the propellant would also increase significantly. ALEX is a nano material in the 20−60 nm region which is prepared by an electrical explosion (quick electrical resistance heating in vacuum or under an inert gas). The use of aluminiumhydrides, AlH_3, as replacements for pure Al are also being discussed currently, however these are even more sensitive to air (oxidation) when they are not stabilized through the use of wax.

Another possibility which is also currently being researched in order to increase performance is the replacement of the aluminum (Al) by aluminum hydride (AlH_3). Calculations have proven that the specific impulse (I_{sp}^*) can be increased by approximately 8% (or 20 s) by replacing Al by AlH_3. A further, however somewhat smaller improvement can theoretically be reached by substituting AP by ADN:

$$\begin{array}{llll} AP/Al & (0.70/0.30) & I_{sp}^* = 252 \text{ s} \\ AP/AlH_3 & (0.75/0.25) & I_{sp}^* = 272 \text{ s} \\ ADN/AlH_3 & (0.70/0.30) & I_{sp}^* = 287 \text{ s} \end{array}$$

Silanes, and in particular the higher silanes such as e.g. *cyclo*-pentasilane, Si_5H_{10}, have also been discussed recently as possible propellants. These could possibly be suitable for RAM and SCRAM jets, since in addition to forming SiO_2, they could burn using nitrogen from the air to form Si_3N_4 and thereby use not only the oxygen, but also the nitrogen from the air as oxidizers (air-breathing engines).

For **liquid rocket propellants**, there is a difference between mono and bipropellants. Monopropellants are endothermic liquids (e.g. hydrazine), which decompose exothermically − mainly catalytically (e.g. Shell-405; Ir/Al_2O_3) − in the absence of oxygen:

$$N_2H_4 \xrightarrow{\text{catalyst}} N_2 + 2\,H_2 \qquad \Delta H = -51 \text{ kJ mol}^{-1}$$
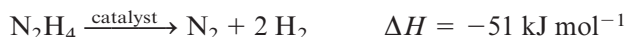
Monopropellants possess a relatively small energy content and a specific impulse and are therefore only used in small missiles and small satellites (for correcting orbits), where no large thrust is necessary. A summary of some monopropellants can be found in Table 2.6.

In a bipropellant system, the oxidizer and the fuel are transported in two tanks and are injected into the combustion chamber. The bipropellants can be separated into two different classes, either in cryogenic bipropellants, which can be handled only at very low temperatures and are therefore unsuitable for military applications (e.g. H_2/O_2) and storable bipropellants (e.g. monomethylhydrazine/HNO_3), or in accordance with their ignition behavior in hypergolic and non-hypergolic mixtures. **Hypergolic** describes rocket propellants whose components react spontaneously with one another (in less than 20 ms) when they are mixed or somehow contact each other. The components of hypergolic propellants are mostly oxidizers or reducing agents, which react immediately upon contact, and ignite partly explosively. Since the fuel reacts immediately by burning on contact with the oxidizer at the time of injection into the combustion chamber, it is not possible for too much fuel to accumulate in the combustion chamber prior to ignition which could lead to an explosion and damage of the rocket engine. A further important advantage is that the ignition definitely occurs, which is important for weapon systems such as intercontinental rockets, pulsed engines and upper stages of launch vehicles (re-ignition in space) for example. (*Note:* Hypergolic systems are also used in incendiary devices e.g. for mine clearance.) Hydrazine derivatives (hydrazine, MMH and UDMH) with HNO_3 or NTO (dinitrogen tetroxide) are practically the only hypergolic pro-

Tab. 2.6 Monopropellants.

monopropellant	formula	I_{sp}^*/s	T_c/K
hydrazine	$H_2N{-}NH_2$	186	1500
hydrogen peroxide	$HO{-}OH$	119	900
isopropylnitrate	$C_3H_7{-}O{-}NO_2$	157	1300
nitromethane	$CH_3{-}NO_2$	213	2400

Tab. 2.7 Bipropellants.

oxidizer	fuel	$T_c/°C$	T/K	I_{sp}^*/s
LOX	H_2	2740	3013	389
	H_2/Be (49:51)	2557	2831	459
	CH_4	3260	3533	310
	C_2H_6	3320	3593	307
	B_2H_6	3484	3762	342
	N_2H_4	3132	3405	312
F_2	H_2	3689	3962	412
	MMH	4074	4347	348
	N_2H_4	4461	4734	365
OF_2	H_2	3311	3584	410
FLOX (30/70)	H_2	2954	3227	395
N_2F_4	CH_4	3707	3978	319
	N_2H_4	4214	4487	335
ClF_5	MMH	3577	3850	302
	N_2H_4	3894	4167	313
ClF_3	MMH	3407	3680	285
	N_2H_4	3650	3923	294
N_2O_4, NTO	MMH	3122	3395	289
MON-25 (25% NO)	MMH	3153	3426	290
	N_2H_4	3023	3296	293
IRFNA (III-A)[a]	UDMH	2874	3147	272
IRFNA (IV HDA)[b]	MMH	2953	3226	280
	UDMH	2983	3256	277
H_2O_2	N_2H_4	2651	2924	287
	MMH	2718	2991	285

[a] IRFNA (III-A): 83.4% HNO_3, 14% NO_2, 2% H_2O, 0.6% HF
[b] IRFNA (IV HDA): 54.3% HNO_3, 44% NO_2, 1% H_2O, 0.7% HF

pellants used today. Table 2.7 shows a summary of different liquid bipropellant mixtures.

However, there are currently efforts to replace carcinogenic MMH and UDMH by toxicologically less damaging, but still hypergolic substances. One possible candidate is dimethylaminoethylazide (DMAZ) which has been produced by the company MACH I (PA):

DMAZ $>N-CH_2-CH_2-N_3$
Dimethylaminoethylazide
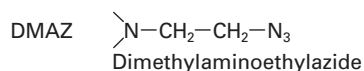
Out of the bipropellant mixtures shown in Table 2.7, only a few are used in practial applications. In particular, LOX/H_2 has proven useful in the cryogenic main engines of the civil Space Shuttle and Ariane V. The Aestus upper stage of the Ariane

V relies on using NTO/MMH. The engines of the Delta (RS-27) and Atlas rockets work with LOX/HC (HC = hydrocarbons). Russian rockets in particular often use UDMH, which is very similar to MMH. As storable oxidizers, practially only NTO or RFNA (red fuming nitric acid) are used. Despite the very good specific impulse of fluorine containing (F_2 or FLOX) oxidizers and beryllium containing propellants, they have not found application due to technical (handling and pumping of liquid fluorine) and ecological (toxicity of HF and Be compounds) grounds.

At this point, the more recent development of so-called **gel propellants** should be mentioned. We have seen above that for military missiles, hypergolicity is a desired property. On the other hand, transportation of IRFNA or NTO in combination with MMH or UDMH on a ship or submarine for example also carries high risks and danger if there is an accident with unwanted contact of the oxidizer with the fuel. Gel propellants try to combine the desired and positive properties of a liquid propellant (flow behavior, pulse-mode) with the reliability of a solid propellant. The term geled fuel is used to describe a fuel which has an additional gelling agent (approx. 5−6%) and an additive, so that it behaves like a semi-solid and only begins to liquefy under pressure. Inorganic (e.g. Aerosil 200, SiO_2 or aluminium octanoate) or organic substances (e.g. cellulose or thixatrol = modified castor oil derivative) are suitable gelling agents. The gel becomes semi-solid as a result of the presence of strong π-π- or van-der-Waals interactions and therefore it not only has a low vapor pressure but often also a higher density in comparison to pure fuel, which makes it very safe to handle. The gel only liquidizes under pressure while the viscosity decreases with increasing shear stress. There are certain problems still exist today in the production of oxidizer gels as a result of the high reactivity of WFNA, RFNA or NTO. Hypergolic alternatives to the stongly corrosive nitric acid derivaties are also sought after.

Hybrid rocket motors use propellants in two different states of matter, usually a solid fuel and a liquid or gaseous oxidizer. Like liquid rockets and unlike solid rockets a hybrid engine can be turned off easily but due to the fact that fuel and oxidizer (different states of matter) would not mix in the case of an accident, hybrid rockets fail more benignly than liquid or solid motors.

The specific impulse is generally higher than that for solid motors. A hybrid engine usually consists of a pressurized tank (oxidizer) and a combustion chamber containing the solid propellant (fuel). When thrust is desired, the liquid oxidizer flows into the combustion chamber where it is vaporized and then reacted with the solid fuel at chamber pressures of about 7−10 bar.

Commonly used fuels are polymers, e.g. HTPB or polyethylene which can be metallized (aluminized) in order to increase the specific impulse. Common oxidizers include gaseous or liquid oxygen or nitrous oxide.

Some of the disadvantages of the fuels presently used are a relatively low regression rate and a low combustion efficiency. Such problems could be overcome in the future by using cryogenic solid fuels like frozen pentane (@ 77 K). Such fuels would form a melt layer during the combustion process and have a higher regres-

sion rate. Alternatively, paraffin wax (not cryogenic) would also form a melt layer during combustion and could easily be aluminized. Such systems have specific impulses of up to 360 s.

The most commonly used oxidizers have the disadvantage of either being cryogenic (LOX) or toxic (N_2O_4). Newer oxidizer systems which are presently under investigation include refrigerated (approx. -40 to $-80\,°C$) mixtures of N_2O and O_2 ("Nytox", 80 % N_2O, 20 % O_2). The advantage of such a mixture would be a relatively high vapor pressure (compared to pure N_2O) and a high density due to the presence of O_2, but without being cryogenic. In combination with a metallized paraffin (wax) nytox as a fuel could help to overcome performance as well as toxicity issues.

Other developments go into the direction of adding up to approx. 10 % aluminum hydride (AlH_3) or $LiAlH_4$ to the HTPB fuel in order to increase the regression rate and deliver a specific impulse of up to 370 s.

2.4.1 Chemical Thermal Propulsion (CTP)

A further special area of propulsion systems is **Chemical Thermal Propulsion** (CTP). CTP is defined in contrast to STP (solar thermal propulsion) and NTP (nuclear thermal propulsion). In CTP, in a very exothermic chemical reaction in a closed system, heat but no pressure is generated since the products of the reaction are solid or liquid. The heat energy is then transferred to a liquid medium (the propellant) using a heat exchanger, which is responsible for the propulsion of for example, the torpedo. Suitable propellants are e.g. water (the torpedo can suck it in directly from its surroundsings) or H_2 or He, due to their very low molecular or atomic masses. The basic principles of CTP can also be used in special heat generators. A good example for a chemical reaction which is suitable for CTP is the reaction of (non-toxic) SF_6 (sulfur hexafluoride) with easily liquified lithium (m.p. $180\,°C$):

$$SF_6 + 8\,Li \rightarrow 6\,LiF + Li_2S \qquad \Delta H = -14727\,\text{kJ kg}^{-1}\ \text{(mixture)}$$

In comparison to this, the reaction of MMH with NTO generates only 6515 kJ per kilogramm of a stoichiometric mixture. Table 2.8 clearly shows the influence of the

Tab. 2.8 Specific impulse I_{sp}^* of the CTP reaction Li/SF_6 occurring at 10 bar and 2500 K, depending on the propellant used.

propellant	M (propellant)/ g mol^{-1}	I_{sp}^*/ s
H_2	2	900
He	4	500
H_2O	18	320
N_2	28	230

average molecular mass of the "combustion products" (in this case the propellants) on the specific impulse.

Further chemical reactions which are principally suitable for CTP are outlined in the following equations:

$$
\begin{array}{lll}
8\,Li + SF_6 & \rightarrow Li_2S + 6\,LiF & \Delta_r H = -3520\ \mathrm{kcal\ kg^{-1}} \\
4\,Li + OF_2 & \rightarrow Li_2O + 2\,LiF & -5415 \\
6\,Li + NF_3 & \rightarrow Li_3N + 3\,LiF & -3999 \\
8\,Li + SeF_6 & \rightarrow Li_2Se + 6\,LiF & -2974 \\
6\,Li + ClF_5 & \rightarrow LiCl + 5\,LiF & -4513 \\
6\,Li + BrF_5 & \rightarrow LiBr + 5\,LiF & -3212 \\
6\,Li + IF_5 & \rightarrow LiI + 5\,LiF & -2222 \\
4\,Li + ClF_3 & \rightarrow 3\,LiF + LiCl & -4160 \\
8\,Li + ClO_3F & \rightarrow 3\,Li_2O + LiCl + LiF & -4869
\end{array}
$$
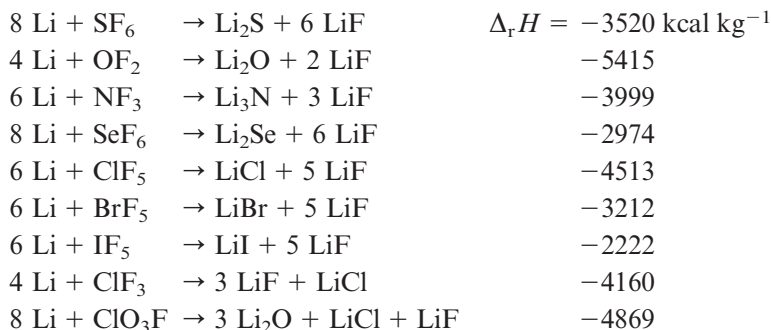
It is obvious that the Li/SF_6 system (although it is energetically lower than others) is preferred over other systems because it is easy to handle and has low health and environmental hazards in comparison to other mixtures involving different oxidizers.

2.5 Pyrotechnics

2.5.1 Detonators, Initiators, Delay Compositions and Heat-Generating Pyrotechnics

A pyrotechnic composition is a substance or mixture of substances designed to produce an effect by heat, light, sound, gas or smoke or a combination of these, as a result of non-detonative self-sustaining exothermic chemical reactions. Pyrotechnic substances do not rely on oxygen from external sources to sustain the reaction.

The term pyrotechnic is derived from ancient Greek and translates as 'the art of fire' or 'the art of handling fire'. Similarly, as with explosives or propellants, the effects of pyrotechnics are also based on strongly exothermic reactions, whereby explosives show the largest and propellants relatively speaking the lowest speeds of reaction. Pyrotechnics are located somewhere in between. In contrast to explosives which release large quantities of gas during a reaction, pyrotechnics form mainly solid as well as gaseous products. Generally every pyrotechnic consists of an oxidizer as well as a reducing agent. Moreover, depending on the intended use, they can also contain a binder, a propellant charge and a colorant as well as smoke and noise generating additives. In contrast to explosives, which often contain the oxidizer and reducing moieties combined in one molecule (e.g. TNT, RDX), traditionally pyrotechnics are mixtures of different substances. Many pyrotechnic reac-

Tab. 2.9   Applications of pyrotechnics.

pyrotechnic	area of application	example
heat generating pyrotechnics	first fires, primers	
	pyrotechnic mixtures in detonators (blasting caps, detonators or primers)	see Fig. 2.14
	electric "matches" in initiators ("first fires")	Ox: KNO_3, BaO_2 Fuel: Mg, Ti, Si see Fig. 2.14
	incendiary devices	
	percussion primers	$KClO_3$ + TNT + PbO_2, Sb_2S_3
	delay compositions (bombs, projectiles, grenades)	gassy: blackpowder gasless: metal oxide and −chromate + metal powder
	matches	head: Sb_2S_3 or S_8 + $KClO_3$ striking surface: P_{red} + glass
smoke-generating pyrotechnics	smoke munition	
light-generating pyrotechnics	signal flares	
	decoy munition (IR region) fireworks	MTV
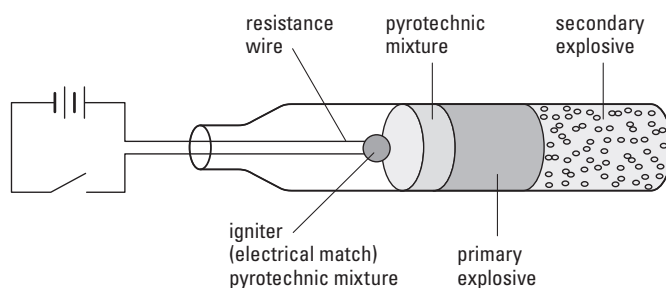
Fig. 2.14   Schematic representation of a detonator with an electric initiator.

tions are therefore solid state reactions, which result in a well-defined particle-size and highest possible homogeny. The energy released in a pyrotechnic reaction usually results in a flame and some smoke, light and also gas formation. Pyrotechnics have many applications, some of which are summarized in Table 2.9.

Pyrotechnic mixtures which are used for ignition in blasting caps or detonators or which are used as first fires in propellant charges, are very easy to initiate. Here the initiator generates a flame if it is hit with a metal (percussion primer) or if it is initiated electrically using resistance heating (bridge wire). The first fire then initiates the propellant charge (percussion primer) or the first fire of an electrical match initiates a pyrotechnic mixture in a detonator, which then initiates a primary

explosive which subsequently initiates a secondary explosive in the detonator. The shockwave of that detonator then initiates the main charge (not a component of the detonator). Figure 2.14 schematically shows the construction of a detonator which is initiated using an electrical match (initiator). For safety reasons, the initiator is introduced into the detonator only shortly before use. Typical examples for primary explosives used in detonators are lead azide and lead styphnate, and PETN for secondary explosives.

SINOXID (= without rust) is the trademark used for the traditional primer compositions of the company Dynamit Nobel. In contrast to the mixture of mercury fulminate and potassium chlorate which was used previously, SINOXID is made-up of lead styphnate (Fig. 1.17), tetrazene (Fig. 2.2), barium nitrate, lead dioxide, antimony sulfide and calcium silicide. SINOXID compositions feature very good chemical stability and storage life, they are abrasion-, erosion- and corrosion-free and ignite propellants with precision. **SINTOX-** (non-toxic) is a recently developed primer composition of Dynamit Nobel. It was developed specifically for ambient air in indoor firing ranges, which should not to be polluted with combustion products containing lead, antimony or barium. SINTOX consist essentially of diazodinitrophenol (or strontium diazodinitroresorcinate) and tetrazene as initial explosives and zinc peroxide as the oxidizer.

In fireworks, blackpowder is still used as the first fire.

Delay compositions are divided into two types: gasless (e.g. metal oxides or metal chromates with an elemental fuel) and gassy (e.g. blackpowder). Gasless delays are used in conditions of confinement (e.g. bombs, grenades, projectiles) or at high altitudes, where it is important that there are no variations of normal, ambient pressure. The desired burn rate (mm ms^{-1} to mm s^{-1}) is dependent on the purpose of use. Delay compositions with high burning rates for example are used in projectiles and bombs which should explode on impact, whereas those with low burning rates are primarily used in ground chemical munitions such as smoke pots, smoke grenades and tear pots. The following mixtures are examples of gasless delay compositions:
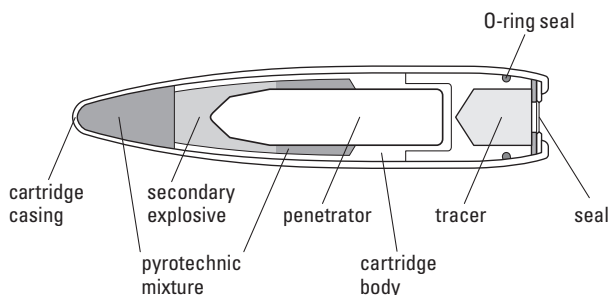
Fig. 2.15 Schematic representation of the construction of a 12.7 mm multipurpose projectile.

1 safety pin
2 striker
3 safety lever
4 fragmentation body
5 explosive filler / payload
6 primer
7 igniter
8 delay composition
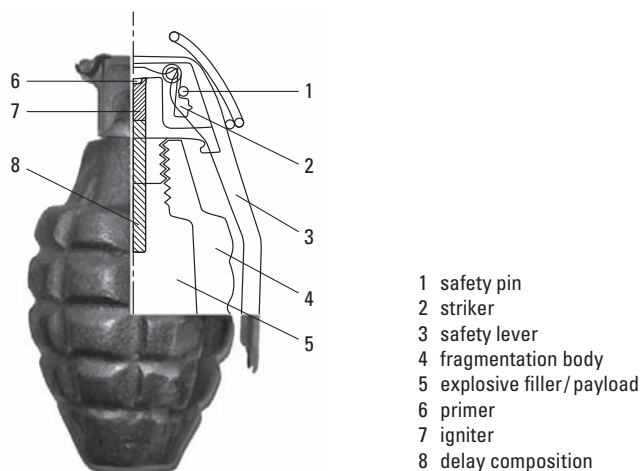
Fig. 2.16 Schematic representation of the construction of a hand grenade with a pyrotechnical delay device.

1. Fuel: B, Si   oxidizer: $K_2Cr_2O_7$,
2. Fuel: W   oxidizer: $BaCrO_4$, $KClO_4$,
3. Fuel: Mn   oxidizer: $PbCrO_4$, $BaCrO_4$,
4. Fuel: Cr   oxidizer: $BaCrO_4$, $KClO_4$.

A typical delay composition would be: $BaCrO_4$ (56 %), W (32 %), $KClO_4$ (11 %), VAAR ($\sim$ 1 %).

Figure 2.15 shows a schematic representation of the construction of a 12.7 mm multipurpose projectile with a pyrotechnic mixture (incendiary) and secondary explosive. Figure 2.16 schematically shows the construction of a hand grenade with a pyrotechnic delay composition. Bombs such as, for example, the MK 80 series, where approx. 45 % of the total mass is the explosive, usually contain pyrotechnic ("nose" or "tail") fuses.

2.5.2 Light-Generating Pyrotechnics

Pyrotechnic formulations which emit electromagnetic radiation in the visible region are used as parachutes or hand-held signal flares for large-area illumination or to mark specific positions (targets, landing areas for planes or paratroopers etc.). [13−16] For example, red is often used by aircraft personnel, to indicate their position in the event of an emergency landing or accident. Green and yellow are used by ground troops to mark their positions and white ($Mg + Ba(NO_3)_2 + KNO_3$; Al, Ti and Zr are also used as fuels for producing white lights) allows large-area illumination at night. The intensity and wavelength (color of the emitted light) depend on the components in the burning pyrotechnic mixture. Pyrotechnics which

Tab. 2.10 Spectra of the most important atoms and molecules for pyrotechnics.

element	emitter	wavelength / nm	color
Lithium	atomic Li	670.8	red
		460	blue
		413	violet
		497	blue/green
		427	violet
Sodium	atomic Na	589.0, 589.6	yellow
Copper	CuCl	420−460	blue/violet
		510−550	green
Strontium	SrCl	661.4, 662.0, 674.5, 675.6	red
	SrCl	623.9, 636.2, 648.5	orange
	SrCl	393.7, 396.1, 400.9	violet
	SrOH	605.0, 646.0	orange
		659.0, 667.5, 682.0	red
	atomic Sr	460.7	blue
Barium	BaCl	507, 513.8, 516.2, 524.1, 532.1,	green
		649	red
	BaOH	487,	blue/green
		512	geen
	BaO	604, 610, 617, 622, 629	orange
	atomic Ba	553.5,	green
		660	red

Tab. 2.11 Composition of selected illuminants in the visible region (%).

ingredient	Red Navy	Red Highway	Green Navy	Yellow Navy	White Navy
Mg	24.4		21.0	30.3	30
$KClO_4$	20.5	6.0	32.5	21.0	
$Sr(NO_3)_2$	34.7	74.0			varied
$Ba(NO_3)_2$			22.5	20.0	53
PVC	11.4		12.0		
$Na_2(COO)_2$				19.8	
Cu powder			7.0		
Bitumen	9.0			3.9	
Binder (VAAR)		10.0	5.0	5.0	5
S_8		10.0			

burn at approximately 2200 °C, usually contain perchlorates as the oxidizer as well as organic propellants (e.g. nitrocellulose). In order to increase the flame temperature to 2500−3000 °C, metal powders such as magnesium are added. The emission of specific spectral colors occurs as a result of the addition of other metals and other metal salts. Sodium is therefore used for yellow, strontium for red and barium is usually used for green. The main emitters of the corresponding spectral
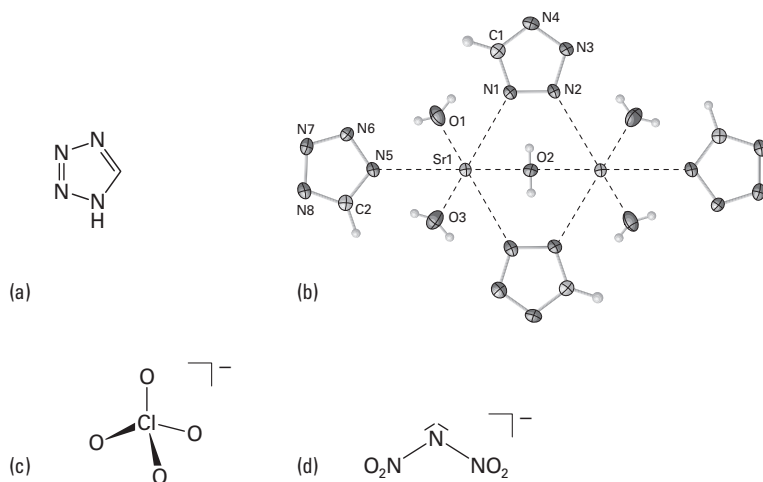
Fig. 2.17 Molecular structure of 1-H-tetrazole (a), the strontium compound as colorant in the environmentally friendly red pyrotechnic mixture (b), the perchlorate anion (c) and the dinitramide anion (d).

bands are atomic Na for yellow, $Sr^{(I)}OH$ and $Sr^{(I)}Cl$ for red as well as $Ba^{(I)}Cl$ and $Ba^{(I)}OH$ for green (Tab. 2.10). BaO is also a strong emitter in Barium illuminants (Tab. 2.10). The hydrogen necessary for the formation of the monohydroxides SrOH and BaOH comes from the decomposition products of the binder or the PVC (Tab. 2.10), the Cl atoms come from the perchlorate oxidizing agent but also from the PVC. Table 2.11 shows the composition of some important illuminants in the visible range.

However, from the ecological and toxicological point of view the relative high perchlorate content of all of the illuminating compositions (Tab. 2.11) as well as the use of the heavy metal barium in green illuminants is problematic; during the production and burning of the light-generating compositions, toxic perchlorate and soluble barium salts can get into ground water. The ClO_4^- anion is a possible teratogen and has shown negative effects on the thyroid function. The up-take of iodine into the thyroid is suppressed by chronic perchlorate up-take which in consequence causes thyroid subfunction. Moreover, the binders and other ingredients (PVC, Bitumen, sulfur) often result in burning with strong smoke. Current research is therefore concerned with the development of:

− Perchlorate-free red and green colored illuminants,
− Barium in the form of sparingly soluble Ba salts (not soluble $Ba(NO_3)_2$),
− Barium (heavy metal) free green illuminants,
− weakly / smoke-free red, green and yellow illuminants.

Many of the newly developed pyrotechnics are based on metal complexes with very nitrogen-rich ligands, mainly tetrazole derivatives (Fig. 2.17). Unlike conventional

energetic substances they do not derive their energy not through the oxidation of a carbon back-bone but through their high (positive) heat of formation. These compounds are suited for application as propellants, reducing agents or colorants − preferably with less toxic metal salts such as Cu^{II} instead of Ba^{II}.

Since environmentally compatible pyrotechnics should not contain perchlorates or heavy metals in the first instance, new red and green formulations are being developed which contain Cu instead of Ba and which contain other oxidizers (e.g. nitrate or dinitramide, Fig. 2.17) instead of perchlorates. The high nitrogen content also guarantees a significant reduction of the smoke and particulate matter released and consequently results in a considerably higher color brilliance.

Furthermore, high-N red and green formulations show an increase in burn time, an increase in luminous intensity and an increase in spectral purity. Two examples of new red and green formulations developed by ARDEC/LMU are:

red:	$Sr(NO_3)_2$	39%
	Mg	29%
	PVC	15%
	high-N Sr-tetrazolate salt	10%
	binder	7%

green:	$Ba(NO_3)_2$	46%
	Mg	22%
	PVC	15%
	high-N Ba-tetrazolate salt	10%
	binder	7%

In the above mentioned red and green formulations it is possible to replace the high-N metal tetrazolate salt with more metal nitrate and free aminotetrazole. This causes longer burn times but lower intensities.

The strontium formulation shows a reasonably high red color purity as can be seen from the chromaticity diagram in Fig. 2.19a. The color purity (p_e) of a visible flare with the chromaticity (x, y) is its difference from the illuminant's white point relative to the furthest point on the chromaticity diagram with the same hue (dominant wavelength for monochromatic sources): where (x_n, y_n) is the chromaticity of the white point and (x_I, y_I) is the point on the perimeter whose line segment to the white point contains the chromaticity of the stimulus.

$$p_e = \sqrt{\frac{(x - x_n)^2 + (y - y_n)^2}{(x_I - x_n)^2 + (y_I - y_n)^2}}$$

The color purity is the relative distance from the white point. Contours of constant purity can be found by shrinking the spectral locus about the white point. The points along the line segment have the same hue, with p_e increasing from 0 to 1
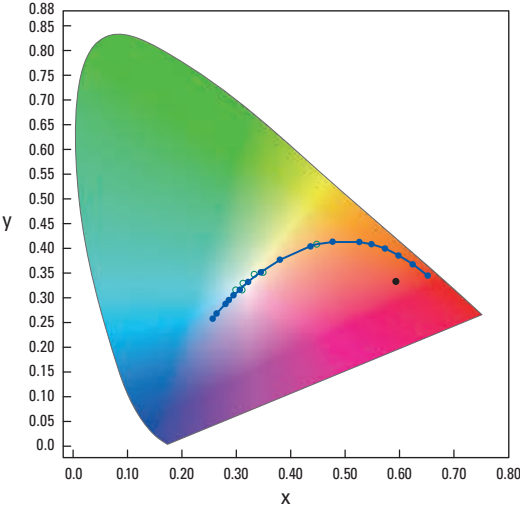
Fig. 2.19a Chromaticity diagram for the high-N strontium-based flare.

between the white point and position on the spectral locus (position of the color on the horseshoe shape in the diagram) or (as at the saturated end of the line shown in the diagram) position on the line of purples.

A breakthrough discovery was reported by Sabatini (ARDEC) in the area of green illuminants. Formulations without any heavy metal can be based on boron carbide (B_4C, fuel) with a suitable oxidizer (e.g. KNO_3). Table 2.12 shows the effect of boron carbide (B_4C) in pyrotechnic compositions. It can be seen that flares with 100% boron carbide as fuel show longer burn times and higher luminous intensity than the control barium nitrate based flare (M125 A1) while the spectral (color) purity is slightly lower.

Tab. 2.12 Effect of boron carbide in pyrotechnics.

fuel (B : B_4C) in formulation[a]	burn time [s]	luminous intensity [cd]	dominant wave-length [nm]	spectral purity [%]
control[b]	8.15	1357	562	61
100 : 0	2.29	1707	559	55
50 : 50	5.89	2545	563	54
40 : 60	6.45	2169	563	54
30 : 70	8.67	1914	562	53
20 : 80	8.10	1819	563	53
10 : 90	8.92	1458	562	52
0 : 100	9.69	1403	563	52

[a] Formulation: KNO_3 83%, fuel 10%, epoxy binder 7%.
[b] $Ba(NO_3)_2$ 46%, Mg 33%, PVC 16%, Laminac 4116/Lupersol binder 5%.
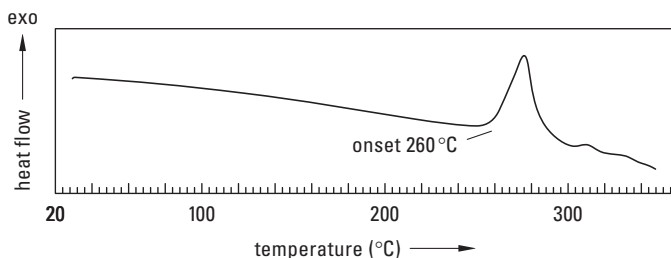
Fig. 2.18   DSC thermogram of the new environmentally friendly red mixture.

"Sustain the Mission – Secure the Future"

Fig. 2.19   Triple bottom line plus.

Extremely important for the safe handling of such pyrotechnic mixtures are, in addition to the chemical stability (compatability with the binder and other additional compounds) particular the thermal stability and the lowest possible impact, friction and electrostatic sensitivities. Figure 2.18 shows an example of a DSC thermogramm (Differential Scanning Calorimetry), which shows that the new environmentally friendly red mixture (colorant components from Figure 2.17) is thermally stable up to approx. 260 °C. But the sensitivity of the mixture towards electrostatic discharge (ESD) was lowered to 1 J (cf. typical values for the human body are within the range 0.005−0.02 J).

The protection of the environment through the use of sustainable technologies is one of the biggest and most important tasks of our time. Within the concept "triple bottom line plus" (mission, environment, community + economy) (Fig. 2.19), the U.S. Army in co-operation with leading scientists world-wide, is trying to implement the sustainability of their operations and missions. A good example of this is the research into new, less environmentally hazardous pyrotechnics, which contribute to a successful operation as a result of their properties, but don't damage the environment due to their "green" characteristics. Furthermore, they are of general economic interest (new innovative technology, reduce the cost of purifying ground water) and of particular interest for local communities (reduced exposure to particulate matter, heavy metals and perchlorate in the vicinity of troop training camps).

2.5.3 Decoy Flares

The terms decoy flare or countermeasure munition are used to denote a system, which imitates the IR signal of a plane and therefore ground-air, water-air or air-air rockets, so-called heat-seeking missiles, get lured away from their targets. One of the first and best-known IR seekers − "Sidewinder" − was developed in China Lake (Fig. 2.20).

The Sidewinder has a high explosive warhead and an IR-based heat-seeking guidance system. Its other components are an optical target detector, the fins and the rocket engine. The guidance-system directs the missile straight into the hot engine of the enemy's plane (or whatever the missile considers this to be). An infrared unit costs less than any other guidance-system. After it has been launched, the missile does not need anymore support from the launching platform and steers itself towards the target.

In order to be protected against such heat-seeking guided missiles, pyrotechnic decoy flares, which are based on blackbody radiation (or better greybody radiation), have been and are still being developed since the late 1950's. The specific radiant emittance of a radiating body (W in W cm^{-2}μm^{-1}) can be described using Planck's rule:

$$W\lambda = \frac{2\pi h c^2}{\lambda^5} \frac{1}{e^{hc/\lambda kT} - 1}$$
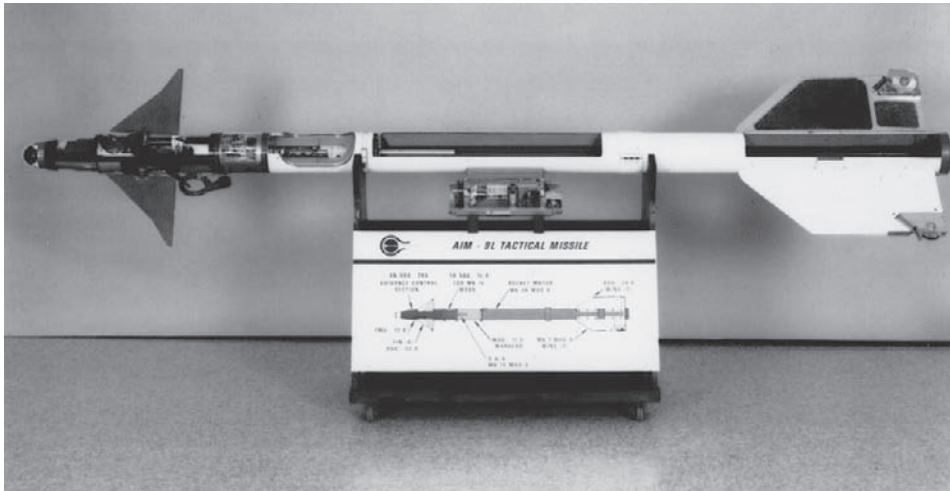
Fig. 2.20 The AIM-9 Sidewinder (AIM = Aerial Intercept Missile) is a heat-seeking guided missile for short-distance combat, which can be carried in most western fighter planes. In its 50 year history, more planes have been shot down using the Sidewinder than with any other device.

where λ (in µm) is the wavelength, h is Planck's constant ($6.626\ 10^{-34}$ W s^2), T is the absolute temperature of the radiator (in K), c is the speed of light ($2.998\ 10^{10}$ cm s^{-1}) and k is the Boltzmann constant ($1.38\ 10^{-23}$ W s K^{-1}).

In accordance with the rule of Wien, the maximum wavelength of the blackbody radiation λ_{max} (µm) shifts towards shorter wavelengths (higher energy) with increasing temperature:

$$\lambda_{max} = 2897.756\ \mu m\ K\ T^{-1}$$

Since in reality there is no actual blackbody radiator (for which the Planck law applies, W), but a more realistic so-called greybody radiator (W′), the value ε has been defined as the quotient W′/W, where ε can be given values between 0 and 1 (1 = genuine blackbody). For example, soot ($\varepsilon > 0.95$) behaves almost like a blackbody radiator, whereas MgO behaves more like a greybody radiator.

Heat-seeking missiles mainly work with photo-conductive IR detectors in the so-called α band (PbS, 2−3 µm) or in the β band (PbSe, 3−5 µm). While the hot tail pipes of a plane turbine typically emit a greybody radiation with λ_{max} between 2 and 2.5 µm, this is superimposed by the selective radiation of the hot exhaust gases (CO_2, CO, H_2O) in the region of $\lambda_{max} = 3-5$ µm. Figure 2.21 shows the typical IR signiature of a plane in the α and β bands. In order to imitate this signiature, initially Al/WO_3 thermites in graphite-balls were used (diameter 10 cm, thickness 2 mm), since graphite in the region < 2.8 µm emits a very good blackbody radiation with $\varepsilon = 0.95$. Nowadays, most of the pyrotechnic mixtures used are mixtures of Mg and perfluorinated polymers (Mg/Teflon/Viton, MTV), since the carbon soot ($\varepsilon \approx 0.85$) which is produced at very high temperatures (approx. 2200 K) is a good IR emitter. The schematic construction of a IR decoy flare is shown in Figure 2.22. The main reaction between Mg and Teflon can be formulated as follows, where m ≥ 2:

$$m\ Mg + -(C_2F_4)- \rightarrow 2\ MgF_2(l) + m\text{-}2\ Mg(g) + 2\ C + h\nu$$
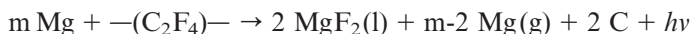
The highly exothermic reaction for the formation of MgF_2 heats up the carbon soot formed to approx. 2200 K, which then emits the IR radiation. Moreover, in Mg rich formulations (m ≥ 2), the evaporating Mg is oxidized in the gas phase (3100 K). In addition, the carbon which is formed from the reductive elimination of fluorine from Teflon can be oxidized further to CO or CO_2 by atmospheric oxygen:

$$m\ Mg + -(C_2F_4)- + O_2 \rightarrow 2\ MgF_2(l) + m\text{-}2\ MgO(s) + 2\ CO_2 + h\nu$$
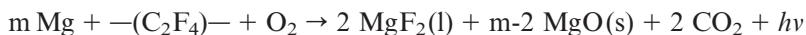
Therefore, during the radiation of a MTV decoy flare, the greybody radiation of the carbon soot (intensive) is superimposed with the less intensive selective radiation of the CO or CO_2, respectively. In addition to the typical wavelength depend-
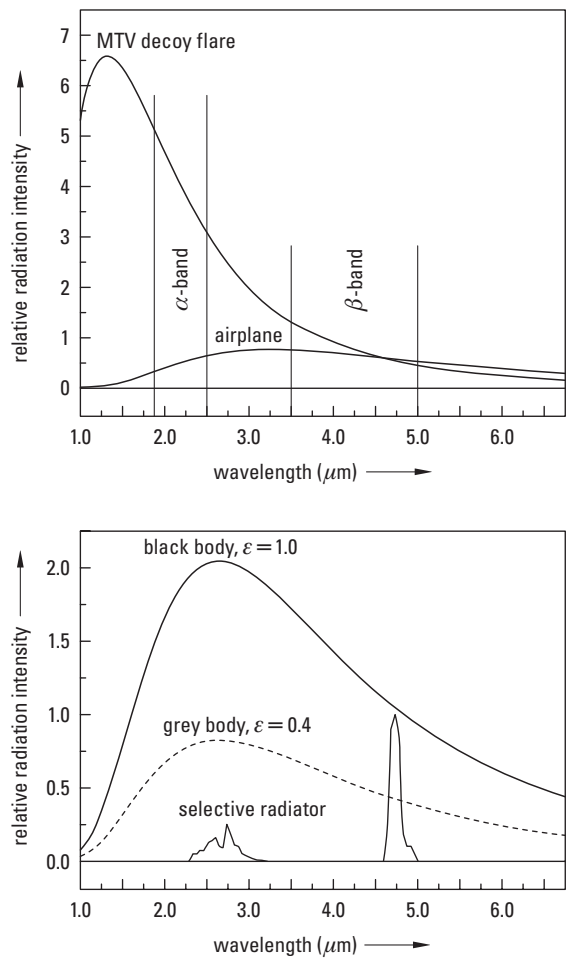
Fig. 2.21 Comparison of the relative radiation intensity of a plane and a MTV decoy flare.
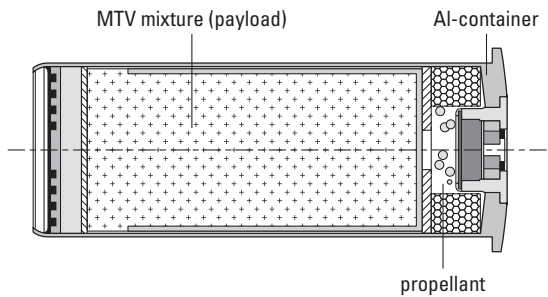
Fig. 2.22 Schematic construction of an IR decoy flare.

ent intensity of the radiation of a plane, Figure 2.21 also shows that of a MTV decoy flare.

Typical pyrotechnic compositions for the generation of blackbody radiation contain magnesium as the fuel and a fluorine-containing oxidizer such as e.g. polytetrafluorethylene, PTFE, $(C_2F_4)_n$. During the reaction, (1) large quantities of carbon form (which is a strong emitter in the IR region) and become thermally excited to radiation as a result of the heat of reaction. Decoy compositions are always rich in magnesium ($50-70$ weight-% Mg) and use the oxygen in the air as a complimentary oxidizer (2). This will now be described in greater detail by using a MTV countermeasure as an example, consisting of 63 weight-% Mg and 37 weight-% PTFE:

$$2.592 \text{ Mg(s)} + 0.3699 \text{ } (C_2F_4)_n \rightarrow 0.7398 \text{ MgF}_2\text{(s)} + 1.8522 \text{ Mg(s)}$$
$$+ 0.7398 \text{ C(gr)} + 532 \text{ kJ} \qquad (1)$$

$$1.8522 \text{ Mg(s)} + 0.7398 \text{ C(gr)} + \text{xs. O}_2 \rightarrow 1.8522 \text{ MgO(s)} + 0.7398 \text{ CO}_2$$
$$+ 1403 \text{ kJ} \qquad (2)$$
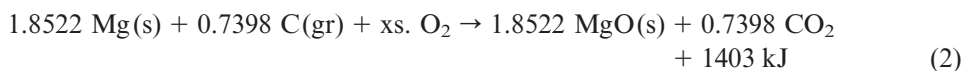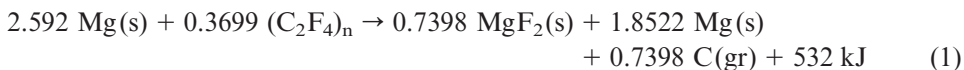
The primary reaction (1) contributes only about a third of the total heat of the reaction. Despite this, the primary reaction significantly influences the mass flow and the radiation characteristics. Therefore, it is sensible to increase the exothermicity of the primary reaction, in order to reach the highest possible spectral efficiency, E, $[J \text{ g}^{-1}\text{sr}^{-1}]$. For this reason, it has been suggested to use oxidizers which would result in a higher primary enthalpies of reaction than PTFE. Suitable substances with a higher molar enthalpy of reaction with magnesium than PTFE are graphite fluoride, $(CF_x)_n$, perfluorinated carbocyclene $(CF)_n$ or difluoroamine substituted compounds $\{C(NF_2)\}_n$.

The flame of a MTV composition consists of an inner zone of higher emission intensity, which contains a high concentration of carbon particles, which are formed through a primary reaction (1) (Fig. 2.22a). The primary reaction zone is surrounded by a second layer of lower emission intensity in which the oxidation of the magnesium and the carbon with oxygen from the air occurs (eq. 2). This intermediate zone is finally surrounded by an outer zone in which the cooling of the reaction products CO_2 and MgO occurs through radiation transfer and conduction of heat to the surrounding atmosphere. The high combustion temperature of the second layer heats up the inner zone even further and thereby influences the radiation characteristics considerably. Furthermore, the emission is also affected by the spatial expansion of the inner zone as well as the concentration of the carbon particles in it. Often, the concentration of the carbon particles in the inner zone is so high, that they cannot emit directly to the surroundings and therefore do not contribute to the radiation intensity. By dilution of the inner zone using an optically transparent gas such as e.g. nitrogen, the inner zone can be expanded and the concentration can also be reduced, so that a larger proportion of carbon par-

1 primary reaction zone
2 reaction zone of Mg and C with O_2 from air
3 outer dilution zone
4 MTV block
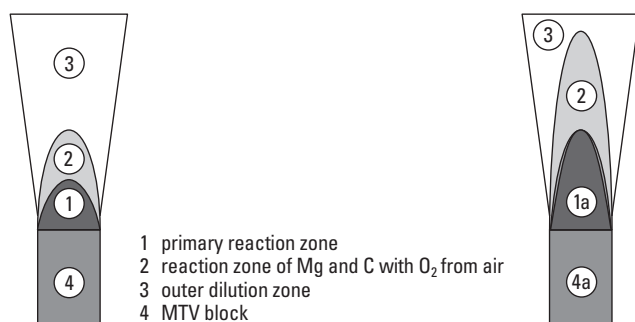
Fig. 2.22a Typical reaction zones of a conventional decoy flare (left) and a high-nitrogen flare based on perfluoroalkylated tetrazoles (right).

ticles can emit to the surroundings. Therefore, a radiation optimized decoy composition should deliver a sufficiently high proportion of nitrogen during combustion (Fig. 2.22a).

Recently it has been discovered that mixtures of magnesium and perfluoralkylated tetrazolates show a higher radiation intensity than compositions which are currently state-of-the-art and based on magnesium and e.g. PTFE, although the molar enthalpies of reaction for the reactions analogous to equation (1) are lower than e.g. MTV.

It is obvious that the intensity of the radiant intensity of MTV flares increases with the mass flow (kg s^{-1}, larger flares) and the burning rate. Current research is amongst other problems concerned with finding additives (e.g. 10% Zr powder), which raise the burning rate by a factor of up to 1.5. The largest influence on the burning rate r is the pressure p (see Ch. 1.3), while the coefficient β describes the influence of the temperature ($\beta = f(T)$) on the linear burning rate and the index a, the pressure dependence:

$$r = \beta p^a$$

To increase the temperature of reaction, components which have less negative heats of formation than PTFE can be used as well. Therefore, in some mixtures graphite fluoride or polycarbonmonofluoride (PMF) are used instead of PTFE. This achieves higher combustion enthalpies. Furthermore, PMF shows higher thermal stability than PTFE resulting in a better (longer) storability. A typical PMF mixture has the following approximate composition:

− $55-65\%$ Mg   (fuel),
− $30-40\%$ PMF (oxidizer),
− 5% Viton (binder).

As a result of the pressure dependence, the linear burn rate also decreases considerably with increasing altitude (Fig. 2.23).
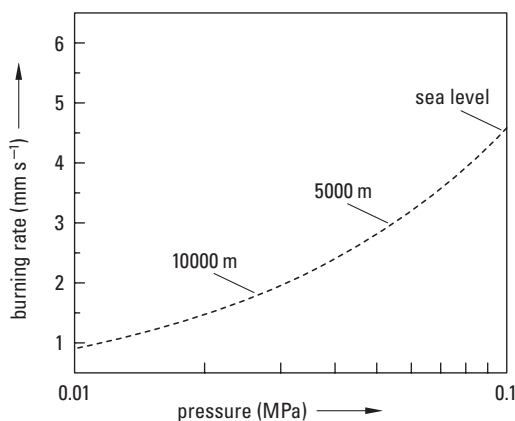
Fig. 2.23 Pressure dependence of the linear burning rate of a MTV mixture (50% Mg, 45% PTFE, 5% Viton).
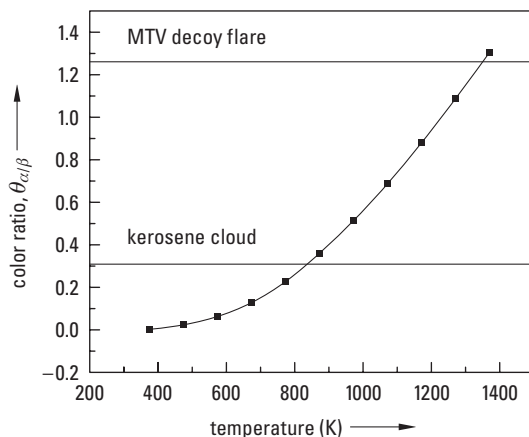
Fig. 2.24 Color ratio $\Theta_{\alpha/\beta}$ for a blackbody as a function of the temperature.

The biggest problem and therefore also the biggest challenge for research is however, the intensity ratio Θ of the relative intensities in the α (I_α) and β bands (I_β). Whereas the values for this relationship lie approximately between $1.3-1.4$ for MTV mixtures $\Theta(\text{MTV}) = (I_\alpha)/(I_\beta)$, planes show $\Theta(\text{plane}) = (I_\alpha)/(I_\beta)$ values of between approx. 0.5 to 0.8 (see Fig. 2.24). This means that modern heat-seeking guided missiles can differentiate between a real target (plane) and a MTV decoy flare. New decoy flares which show a strong emission (in β band) as a result of CO_2 or HBO_2 could solve this problem. One possibility would be to add organic substances (organic fuels) or boron compounds (formation of HBO_2) as well as additional oxidizers (AP) to the decoy flare compositions, but this often results in

a too low intensity of the radiation, which is problematic. This is a current area of research and cannot be answered conclusively at this time.

Figure 2.21 (see above) displays the relative radiant intensity for classical MTV flares and a target signature. It can be seen that the radiant intensity distribution is totally different for MTV compared to the actual target signature. While MTV yields ratios $\Theta_{a/\beta} = 1.33$, true targets exhibit ratios between $0.5 < \Theta_{a/\beta} < 0.8$ depending on the type of engine. Figure 2.24 shows the intensity ratio for both a and β bands as a function of the temperature. It is obvious that only a body with a temperature of less than 900 K will provide a color ratio $\Theta_{a/\beta}$ smaller than 0.8. The lower graph of Fig. 2.21 shows the total flame temperature of a plane taking into account the large amount of selective CO_2 radiation. In practice, this could mean the use of relatively cool continuous radiators, such as e.g. pyrophoric metal foils, or even the combustion of hydrocarbons to CO_2 and H_2O.

2.5.4 Smoke Munitions

Smoke-generating munition is used predominantly as obscurants for self-protection (camouflage in visible and IR regions), in smoke signals and for blinding of the enemy (Fig. 2.25). An obscurant smoke is an aerosol cloud brought into the line of sight between an observer and a target (Fig. 2.26). When considering an obscurant aerosol one has to distinguish between hygroscopic (P_4O_{10}) and non-
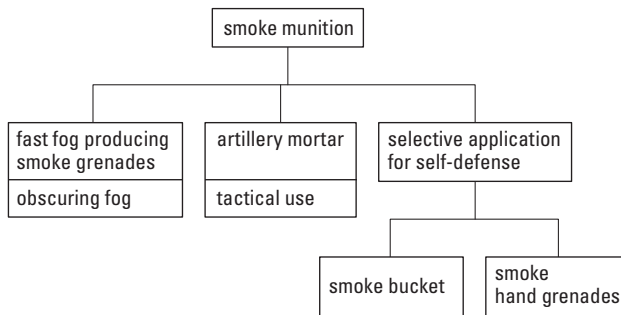
Fig. 2.25 Use of smoke munition.
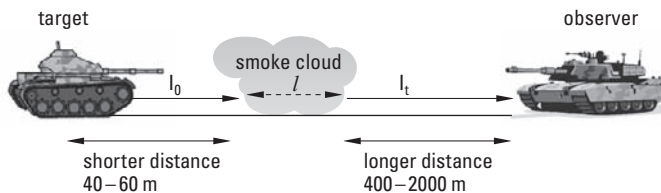
Fig. 2.26 Typical obscurant scenario (I_0 = intensity of the incoming light; I_t = intensity of the transmitted light; l = length of the fog cloud).
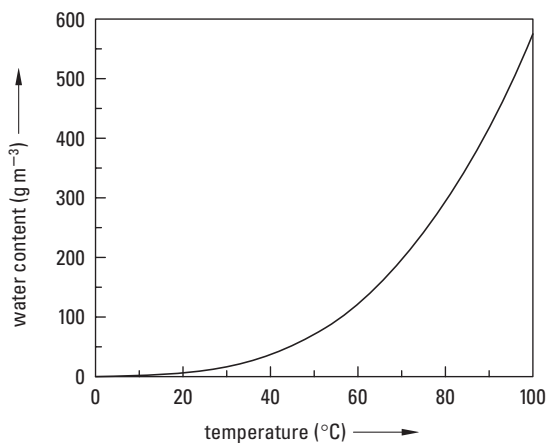
Fig. 2.27   Maximum water content of the atmosphere as a function of temperature.

hygroscopic aerosols. Almost all aerosols which are currently used are based on red phosphorus and are therefore hygroscopic, meaning that their effectiveness is also dependent on the relative humidity (Fig. 2.27).

In order to increase the combustion efficiency and the burning rate, formulations containing sodium nitrate or potassium nitrate, an organic binder as well as an aerosol agent (NH_4Cl) are used in addition to red phosphorus. Typical, simple smoke generating compositions, which are based on red phosphorus and contain approx. $10-75\%$ P are:

Composition 1	red phosphorus	smoke generator	10%
	KNO_3	oxidizer	30%
	NH_4Cl	aerosol additive	60%
Composition 2	red phosphorus	smoke generator	50%
	$CaSO_4$	oxidizer	37%
	boron	fuel & burn rate modifier	19%
	Viton	binder	3%
Composition 3	red phosphorus	smoke generator	75%
	CuO	oxidizer	10%
	Mg	fuel & burn rate modifier	11%
	various binders	binder	4%

Increasingly, a shielding in the mid and far IR region in addition to the simple obscurent effects in the visible region is desirable, since detection by the enemy is possible using electro-optical heat sensors. Although smoke generating formulations which are based on red phosphorus provide excellent shielding in the visible ($0.36-0.76\,\mu m$) and near IR regions ($0.76-1.3\,\mu m$), they screen only moderately in the mid and far IR regions; they are almost exclusively used for this region

because of their unsurpassed properties (aerosol formation, visible region, low tox-icity etc.). Therefore, the only way to guarantee a good shielding in the mid and far IR region as well is by achieving higher mass flow rates (per time) of red phosphorus. This can be achieved using, amongst others, the following strategies:

1. higher density of the formulations by pressing → better thermal conductivity
2. higher combustion pressure (see also Ch. 1.3.)
3. higher thermal conductivity of composite materials (metallic fuels or carbon fibers)
4. more strongly exothermic chemical reactions → higher temperatures
5. larger surface areas (no spherical particles which have a low surface to volume ratio)
6. better ignition process (detonative ignition)

Particularly interesting is aspect (4) which is concerned with more strongly exother-mic reactions. This makes the presence of an energetic additive necessary. Suitable additives are, for example:

a) Metals / Metal nitrates
b) Metals / fluorocarbons (see also Ch. 2.5.3)
c) Metals / Oxides
d) Other homogeneous highly energetic materials.

Examples of such "advanced" smoke-generating compositions are the following two formulations:

Composition 4	Mg	7−12%
	red phosphorus	65−70%
	PTFE	17%
	polychloroprene binder	6%

Composition 5	Mg	12%
	red phosphorus	66%
	KNO$_3$	16%
	polyvinylalcohol (PVA)	6%

One fundamental problem with formulations containing red phosphorus and mag-nesium, in particular in formulations which contain a substoichiometric quantity of oxidizer is that a thermodynamically favorable side-reaction between the phos-phorus and the magnesium can occur:

$$2\,P + 3\,Mg \rightarrow Mg_3P_2$$

The magnesium phosphide that is subsequently formed can react with atmospheric moisture to form phosphine, PH_3 which is toxic:

$$Mg_3P_2 + 6\,H_2O \rightarrow 3\,Mg(OH)_2 + 2\,PH_3$$
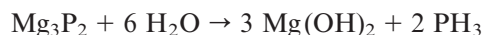
Tab. 2.13   Typical values using a 155 mm artillery smoke grenade.

	visible region (0.4−0.7 µm)	mid IR region (3−5 µm)	far IR region (8−14 µm)
duration of smoke	260 s	180 s	180 s
effective length	400 m	180 m	180 m
effective height	12−16 m	8−12 m	8−12 m
effective depth	ca. 40 m	ca. 40 m	ca. 40 m

This unwanted reaction can also occur very slowly if smoke munition is stored for several years. This can result in a considerable contamination of the munition depot (mainly bunkers or tunnel-shaped caves) with gaseous PH_3. For this reason, in modern formulations Mg is often replaced by Ti or Zr. These metals could in principal also form the corresponding metal phosphides, however, these metal phosphides do not react with water under normal conditions to form PH_3. Moreover, boron and/or silicon additives increase the shielding in the mid and far IR regions as a result of the formation of B_2O_3 (4−5 µm) or SiO_2 emmtters (9−10 µm). A typical Mg free smoke formulation, which also shields good in the mid and far IR regions is:

Composition 6	red phosphorus	smoke generator	58.5%
	KNO_3	oxidizer	21.1%
	Zr	energetic fuel	4.7%
	Si	energetic fuel	4.7%
	B	energetic fuel	4.7%
	chloroprene	binder	6.3%.

The size of the smoke cloud and its duration are of course strongly dependent on the amounts of smoke munition used (small hand grenades or 18 kg floating smoke pot) as well as the weather. While no good fog is formed (see Fig. 2.27) in extremely dry conditions, the duration of the cloud is significantly shorter in strong winds than in windfree conditions. Typical values e.g. for a 155 mm artillary smoke greande are summarized in Table 2.13.

Previously, ZnO / Al / hexachlorethane (HC) mixtures were used both as smoke- and fog-generating munitions as well. In those mixtures, the intermediate $ZnCl_2$ (and C, graphite) is formed, which then quickly hydrolyses forming HCl and ZnO. Such nonhygroscopic formulations are only used in handheld flares where the formation of acidic products (H_3PO_4) can't be tolerated. However, some of the side-products of the reactions have been found to be toxicologically and ecologically critical (e.g. hexachlorbenzol, hexachlorbutadiene, chlorinated dibenzofurane, dibenzodioxine), therefore research is underway to find suitable replacements for HC. Other munitions, which have to the knowledge of the author of this book, never been fielded by NATO countries contain TiO_2/Al/HC and also Ti/ZnO/HC.

$$C_2Cl_6 + 2\,Al \quad \rightarrow 2\,C + 2\,AlCl_3$$

$$2\,AlCl_3 + 3\,ZnO \rightarrow Al_2O_3 + 3\,ZnCl_2$$

$$3\,ZnCl_2 + 3\,H_2O \rightarrow 3\,ZnO + 6\,HCl$$
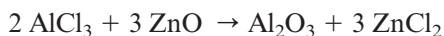
In addition to phosphorus-based obscurant smokes for self-protection there are also colored smoke compositions for signaling purposes, often in a military context. It can be produced by smoke grenades, or by various other pyrotechnical devices.

Smokes, in general, are cooler burning pyrotechnic mixtures. The reason is twofold. 1) A cooler burning smoke will rise gradually from the ground when deployed, which will serve as an effective screening/obscuration tool for military personnel. A smoke mixture which is too hot in temperature will result in a smoke rising too rapidly. When this happens, the screening/obscuration purposes of the smoke is lost. 2) A smoke which reaches high temperatures will result in combustion of the smoke dye (*i.e.* oxidation to carbon monoxide and carbon dioxide). Smoke dyes are added into smoke formulations for sublimation purposes. Not only does the sublimation event keep smokes cool (*i.e.* sublimation is an endothermic process), but it is the sublimation of the smoke dye which gives the smoke its distinct color (*i.e.* blue, red, yellow, green, black, etc.).

As has been commonly taught in smokes for years, the temperatures at which oxidizers and fuels melt is largely responsible for the temperature which a smoke will ultimately reach. Potassium chlorate has been identified as the "only oxidizer" to be used in smoke mixes because it has an exothermic decomposition, thus contributing energy to the pyrotechnic system, but also has a relatively low melting point. Scientists at ARDEC are currently looking at ways to replace potassium chlorate oxidizer in smoke mixes with other oxidizing agents. The EPA is looking at potassium chlorate now, and now environmentalists are questioning whether potassium chlorate is also bad like potassium perchlorate. Another problem with potassium chlorate is its sensitivity. Potassium chlorate used to be used in many of the early fireworks, but it was replaced by potassium perchlorate because potassium perchlorate was found to be inherently safer to work with.

As pointed out above, $KClO_3$ is much less stable than perchlorate and therefore more hazardous (especially mixtures with sulfur and phosphorus). On the other hand, it shows high burning rates and easy ignition. $KClO_3$ is slightly more hygroscopic than potassium nitrate and produces smoke of KCl. Furthermore, it can act as a chlorine donor.

The mixture used for producing colored smoke is usually a cooler-burning formula based on potassium chlorate oxidizer, $KClO_3$ (ca. 35 %) sugar as a fuel (ca. 20 %), and one or more dyes, with about 40−50 % content of the dye. About 2 % sodium bicarbonate may be added as a coolant, to lower the burning temperature. Its coolant properties arise because 2 moles of sodium bicarbonate will endothermically decompose into one mole each of sodium bicarbonate, carbon dioxide

and water. In addition to reducing flame temperatures of smokes, coolants are also used to reduce the sensitivity of smoke mixes, given the large amount of potassium chlorate used in these mixes. The presence of the coolants minimizes undesired acid formation and helps to prolong storage of the smoke mixes.

Typical colorants for smokes are:

Red: Disperse Red 9 (1-methylamino anthraquinone, a)
Orange: Sudan I, 1-phenylazonaphth-2-ol (b)
Yellow: Vat Yellow 4 (c) together with Benzanthrone (BZA)
Violet: Disperse Red 9 (a) with 1,4-Diamino-2,3-dihydroanthraquinone
         (1,4-Diaminoanthracene-9,10-dione)
Green: Vat Yellow 4 (c) together with with benzanthrone and Solvent Green 3
Black: naphthalene and anthracene
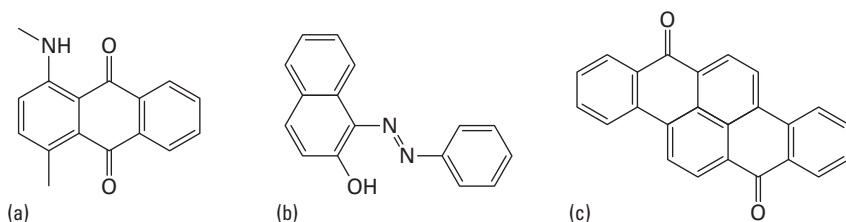
Fig. 2.28   Ingredients for colored smoke.

It should also be noted that white smokes are also of interest as well. There as several ways to produce a white smoke. In the old days, sublimation of sulfur did the trick (again, a low melting fuel), but the formation of sulfur dioxide always was seen as a problem. The hexachloroethane (HC) smokes was around for years (see above), which consisted of hexachloroethane, zinc oxide and aluminum. The trick in using the HC smoke was that it led to the formation of the Lewis acids zinc chloride and aluminum trichloride, and these smokes readily reacted with moisture in the air to produce aluminum hydroxide, zinc hydroxide, and most importantly from a smoke perspective, large amounts of hydrochloric acid. It was the hot HCl droplets that formed which produced a thick smoke upon cooling and pulling additional moisture from the air. Metal and metal oxide particles also contributed to the smoke production due to these finer particle scattering over a rather wide area. However, HC is now deemed toxic, and in fact, HC smokes are no longer being produced by the military in the USA. The military has been complaining about the lack of an HC replacement. Right now, the candidate to replace it is the terephthalic acid (TA) smoke mix. But this mix is not as good as HC in terms of efficiency (40−50 % of the mix is simply residue). It takes 2−3 TA grenades to equal the obscuration power of one HC grenade, and the TA smoke does not burn nearly as long. The smoke is less efficient for the TA smoke because instead of pulling moisture from the air and producing smoke with acid droplets, one is relying on sublimation and condensation of TA to produce the smoke. TA

does not pull moisture from the air, which hampers its ability as a smoke obscuration agent. Nonetheless, efforts are underway at ARDEC to find a quality replacement for the HC smoke mix. Another method of producing white smoke would be the volatilization of oil, but this has not been proven to work to any appreciable extent, even after much research.

It should also be mentioned that stearic acid or graphite is some times added in small amounts as an additive to smoke compositions. These materials serve as a lubricant, which really helps reduce sensitivities (especially to friction and impact) of smoke mixes. As for pyrotechnic binders in smokes, vinyl alcohol acetate resin (VAAR) has been used in the past. The most commonly used binder system now in smokes is polyvinyl alcohol (PVA), and it is applied wet.

2.5.5 Near-Infrared (NIR) Compositions

Since the mid-20th century, electro-optical systems such as night vision goggles and near infrared vision devices have become available. In general, these systems enable vision at night and make use of either non-visible photons and/or intensify the scarcely visible ones. The NIR range is considered to be between 700 nm and 2000 nm. However, for detection purposes, the range between 700−1000 nm is used extensively by several common detector materials in the UV, VIS and NIR range. For clandestine signalling and illuminating purposes in this range (700−1000 nm) pyrotechnic compositions based on either potassium (K) and/or cesium (Cs) compounds that are based on the intense emission lines of K and Cs in the infrared, are used. These flare compositions contain silicon as a high-energy non-luminous fuel, which is known to burn in the condensed phase. A typical composition is: KNO_3 70 %, hexamine 16 %, Si 10 %, binder 4 %. Furthermore, these compositions contain nitrogen-rich compounds like e.g. hexamine or azodicarbonamide as blowing agents to peel off the condensed reaction products. While hexamine is certainly a historically used fuel in pyrotechnic IR applications, especially given its relatively low light output due to its high-nitrogen content, one of the drawbacks of hexamine (at least in the USA), is a) the cost of the material is rising and b) hexamine is getting harder and harder to obtain. In this context, lactose monohydrate has potential to serve as a hexamine replacement. This would solve the supply issue and reduce cost if it can be used in IR applications, as lactose monohydrate is very cheap, and is a fraction of the cost of hexamine. It has a higher heat of combustion than hexamine, but still gives off a substantial amount of gas (i. e. lots of CO_2 and some CO). While materials with higher heats of combustion are likely to increase visible light output, this can be minimized or eliminated altogether by adjusting oxidizer/fuel ratios in the formulations. Presently research is focussing on compounds with an even higher nitrogen content such as potassium or cesium azotetrazolate or potassium or cesium bis(tetrazolyl)amine. Typical oxidizers are the peroxides or barium, strontium and zinc and stannic oxide. Besides NIR tracers, NIR illuminants comprise parachute signal flares as well as illuminating
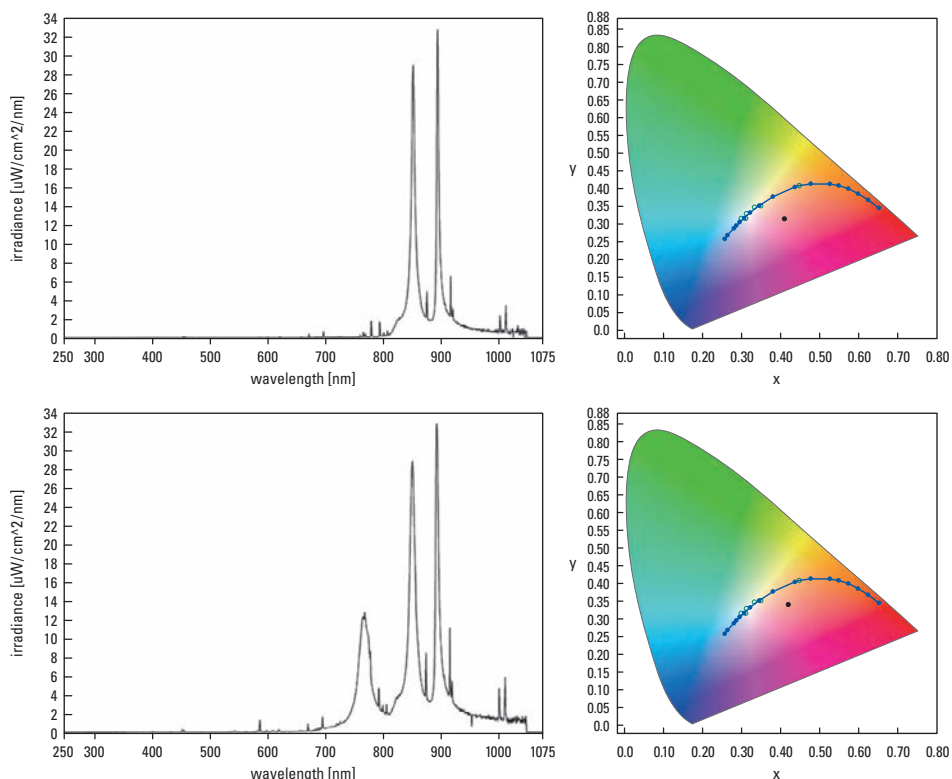
Fig. 2.29 NIR flare emission spectra (left) and chromaticity diagrams (right) for $CsNO_3$ based flares (top) and $KNO_3/CsNO_3$ based formulations (bottom).

rounds for mortars. For clandestine aerial reconnaissance, NIR illumination rockets can be used.

From Fig. 2.29 (top) it is clear that NIR flares based on pure cesium formulations ($CsNO_3$) are superior emitters in the NIR region, whereas cesium/potassium based formulations ($CsNO_3/KNO_3$) (Fig. 2.29 bottom) show a NIR color impurity with tailing into the visible red region.

The radiant intensity (I) is a measure of radiometric power per unit solid angle Ω ($\Omega = A/r^2$), expressed in watts per steradian (W sr^{-1}). The value of the solid angle Ω is numerically equal to the size of that area divided by the square of the radius of the sphere. For hand-held NIR flares one wants a reasonable burn time (ca. 45 s), a high concealment index X which is defined as the ratio of the radiant intensity in the near IR region (I_{NIR}, 700–1000 nm) over the radiant intensity in the visible region (I_{VIS}, 400–700 nm) and high radiant intensities in the NIR regions I_1(600–900 nm) and I_2(695–1050):

$X = I_{NIR}/I_{VIS} > 25$; $I_1 > 25$ W sr^{-1}; $I_2 > 30$ W sr^{-1}; luminous intensity (visible) < 350 cd.

3 Detonation, Detonation Velocity and Detonation Pressure

In Chapter 1.3 we defined a detonation as the propagation of a chemical reaction through an energetic material under the influence of a shock-wave at speeds faster than the speed of sound in the material. The velocity at which the energetic material decomposes is therefore only dependent on the velocity of the shock-wave. It is not determined by a heat-transfer process as it is the case for deflagration or combustion.

A detonation can result from either a continuously accelerating combustion (DDT, Deflagration-to-Detonation Transition) or from a shock (use of a primary explosive in a detonator to initiate a secondary explosive).

In the first case, we can assume that the linear burning rate increases proportionally to the pressure on the surface of the explosive:

$$r = \beta p^\alpha$$

Where β is the temperature dependent coefficient ($\beta = \mathrm{f}(T)$) and α is the index of the burning rate, which describes the pressure dependence. For deflagrations $\alpha < 1$, however, this value increases to $\alpha > 1$ for detonations. The DDT transition can occur when an explosive is ignited in a confined tube, where the gases formed cannot fully escape. This results in a sharp increase of the pressure and reaction velocity. Therefore, in a detonating explosive, the reaction velocity can increase above the speed of sound, turning the deflagration into a detonation.

In the second case we assume that an explosive is subjected to a shock-wave. This method is used in detonators (see Ch. 2.5.1); the shock-wave of a detonating primary explosive initiates a secondary explosive. This shock-wave compresses the secondary explosive enough to cause the temperature to increase to higher than the decomposition temperature through adiabatic heating and the explosive material that is directly behind the shock-wave front reacts. During this reaction the shock-wave accelerates as a result of the strongly exothermic reaction of the secondary explosive. As a result of the influence of the shock-wave, the density of the explosive shortly before the reaction zone increases to $1.3-1.5$ times the maximum density in the crystal (TMD), while in the thin (up to ca. 0.2 mm) chemical reaction zone directly behind the shockwave front, temperatures of up to and over 3000 K and at its end pressures of over 330 kbar can result. If the propagation of the shock-wave through the explosive occurs at speeds faster than the speed of sound, the process is described as a detonation. The shock-wave moves through the explosive under constant acceleration until it reaches a stationary state. The **stationary**
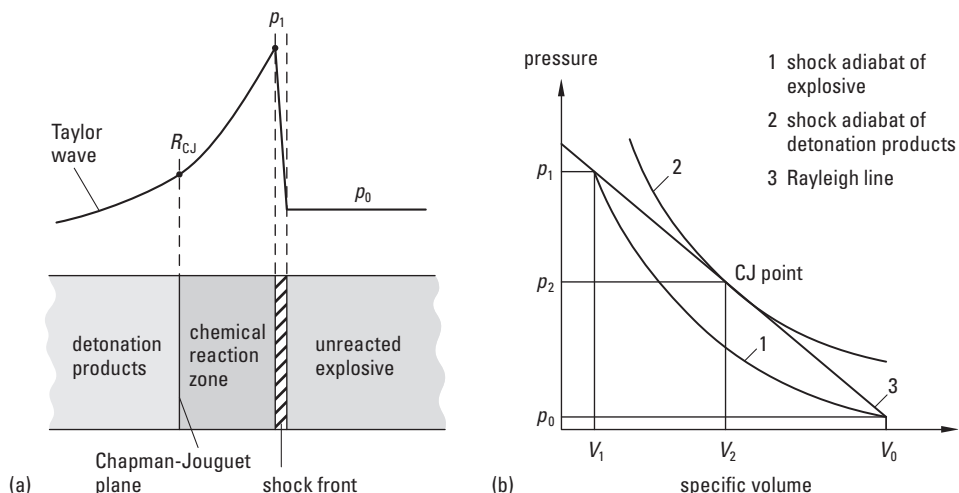
Fig. 3.1 Schematic representation of the detonation process and the shock-wave structure (a) as well as the shock adiabat for an explosive and the detonation products (detonation in a stationary state) (b).

state is reached, when the **free energy released** through this exothermic chemical reaction **is the same** as the **energy which is released to the surroundings as heat + the energy which is necessary to compress and move the crystal**. This means that when these chemical reactions occur with the release of heat at constant pressure and temperature, the propagation of the shock-wave will become a self-sustaining process.

Under the influence of the dynamic behavior of the shock-wave, a thin layer of still unreacted explosive gets compressed alongside the schock adiabat of the corresponding explosive (or Hugoniot adiabat) from the original specific volume V_0 ($V_0 = 1/\rho_0$) to volume V_1 (Fig. 3.1). As a consequence of the dynamic compression, the pressure increases from p_0 to p_1, which in turn causes an increase in the temperature in the thin compressed layer of the explosive (Fig. 3.1), which causes an initiation of the chemical reaction results. At the end of the chemical reaction, the specific volume and pressure have the values V_2 and p_2. This state corresponds to the point of the detonation product on the shock adiabat (Fig. 3.1). At this point it is important to emphasize again that in a deflagration, the propagation of the reaction occurs through thermal processes, while for the considerably quicker occurring detonation a shockwave mechanism occurs.

The desirable situation for the occurrence and linear propagation of a detonation for homogeneous explosives exists in confined tubes or cylindrical shaped explosives, in which the system should not fall below the critical diameter (characteristic for every individual explosive) as it otherwise causes the wave front to be disturbed ("loss" of energy to outside) and therefore the detonation velocity will be reduced.
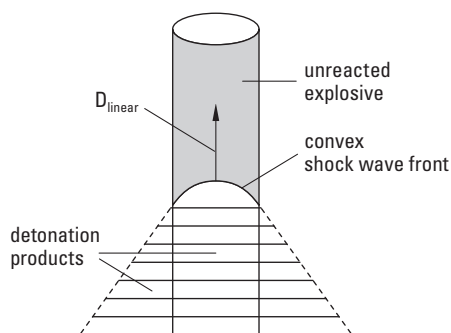
Fig. 3.2 Schematic propagation of a shock wave in a cylindrical shaped explosive.

While for many secondary explosives one inch is a "good" tube diameter, for primary explosives often considerably smaller diameters of 5 mm are sufficient. Figure 3.2 schematically shows the propagation of a shockwave in a cylindrical shaped explosive. Since the wave front is convex and not level, the linear detonation velocity is highest in the centre of the cylindrical explosive and decreases towards the surface. For large diameters this effect plays a negligible role, but for very small diameters the surface effects can become dominant, which causes the wave front to be unstable. This so-called critical diameter must be taken into account for measurements of the detonation velocity, so that one stays above the critical diameter.

   As previously stated, this discussion is valid for homogeneous explosives, such as the ones used in the military, since their reactions are predominantly intramolecular. Such explosives are often referred to as "ideal" explosives, in particular when they can be described using the steady state model of Chapman and Jouguet. In heterogeneous explosives (non-ideal), which are currently used in civil applications, intermolecular (diffusion controlled) mechanisms are predominant for the air bubbles, cavities or cracks (etc.). As a general rule detonation velocities increase proportional to the diameter.

   In accordance with the detonation model for the stationary state, the points (V_0, p_0), (V_1, p_1) and (V_2, p_2) lie on one line (Fig. 1.22) which is called the **Rayleigh line**. The gradient of the Rayleigh line is determined by the detonation velocity of the explosive. In agreement with the postulate of Chapman and Jouguet, this Rayleigh line is also a tangent to the shock adiabat of the detonation products at exactly the point which corresponds to the end of the chemical reaction (V_2, p_2). This point is therefore also referred to as the **Chapman-Jouguet Point** (C-J point).

   Generally, for homogeneous explosives, the **detonation velocity** increases proportional to the density of the energetic formulation. This means that reaching the maximum loading density is essential in order to obtain good performance. Different technical processes can be used in order to achieve the highest possible density including pressing, melt casting or extruding processes. For pure sub-

stances, the limiting, theoretical maximum density (TMD) is that of the single crystal (obtained from X-ray data at room temperature).

Kamlet and Jacobs suggested an empirical relationship between the detonation velocity and the **detonation pressure**. In this, the detonation velocity D is linear and the detonation pressure $p_{C\text{-}J}$ to the power of two dependent on the loading density ρ_0 (in g cm^{-3}) [17 − 19]:

$$p_{C\text{-}J}[\text{kbar}] = K\,\rho_0^2\,\Phi$$

$$D[\text{mm}\,\mu s^{-1}] = A\,\Phi^{0.5}(1 + B\,\rho_0)$$

The constants K, A and B are defined as follows:

$$K = 15.88$$
$$A = 1.01$$
$$B = 1.30$$

The value Φ is therefore

$$\Phi = N(M)^{0.5}(Q)^{0.5},$$

where N is the number of moles of gas released per gram of explosive, M is the mass of gas in gram per mole of gas and Q is the heat of explosion in cal per gram.

Table 3.1 shows how the detonation velocity and the detonation pressure are dependent on the density for selected explosives.

Tab. 3.1 Loading density dependency of the detonation velocity D and the detonation pressure $p_{C\text{-}J}$ (experimental data) [20].

explosive	density, $\rho/\text{g cm}^{-3}$	detonation velocity, $D/\text{m s}^{-1}$	detonation pressure, $p_{C\text{-}J}/\text{kbar}$
TNT	1.64	6950	210
	1.53	6810	171
	1.00	5000	67
RDX	1.80	8750	347
	1.66	8240	293
	1.20	6770	152
	1.00	6100	107
PETN	1.76	8270	315
	1.60	7750	266
	1.50	7480	240
	1.26	6590	160

4 Thermodynamics

4.1 Theoretical Basis

As we have already discussed above, the main performance criteria for secondary explosives are:

1. heat of explosion Q (in kJ kg^{-1}),
2. detonation velocity D (m s^{-1}),
3. detonation pressure p (in kbar),

and, slightly less importantly,

4. explosion temperature T (K) and
5. volume of gas released V per kg explosive (in l kg^{-1}).

To calculate the detonation velocity and the detonation pressure we require (see Ch. 3) thermodynamic values such as e.g. the heat of detonation, from which the detonation temperature can be obtained.

   Before we are concerned with detailed thermodynamic calculations, it is important not to forget that for the good design of a secondary explosive, a balanced oxygen content (**oxygen balance Ω)** is desirable. Generally, oxygen balance describes the relative amount of oxygen excess or defect (with negative sign "$-$"), to achieve a balanced ratio between the oxidizer and the combustable components (fuel). A mixture of substances with a balanced oxygen balance ($\Omega = 0$) can be converted into fully oxidized products by heating them in a closed container, without any added external oxygen and without any excess oxidizer or fuel. In accordance with this definition, a CHNO-containing explosive is completely converted to CO_2, H_2O and N_2. For a compound with the general formula $C_aH_bN_cO_d$, the oxygen balance Ω (in %) is defined as follows:

$$\Omega = \Omega_{CO_2} = \frac{\left[d - (2a) - \left(\dfrac{b}{2}\right)\right] \times 1600}{M} \; ; \qquad \Omega_{CO} = \frac{\left[d - a - \left(\dfrac{b}{2}\right)\right] \times 1600}{M}$$

while M is the molecular mass of the explosive. For example, TNT has a molecular mass of M (TNT) = 227 g mol^{-1} and a composition with the formula $C_7H_5N_3O_6$. Therefore the oxygen balance for TNT is Ω (TNT) = -74%:

$$C_7H_5N_3O_6 \rightarrow 7\ CO_2 + 2.5\ H_2O + 1.5\ N_2 - 10.5\ O$$
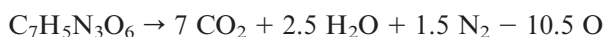
Tab. 4.1   Oxygen balances of some secondary explosives.

secondary explosive	formula	oxygen balance, $\Omega_{CO_2}/\%$
Ammonium nitrate, AN	NH_4NO_3	+20.0
Nitroglycerine, NG	$C_3H_5N_3O_9$	+ 3.5
Nitropenta, PETN	$C_5H_8N_4O_{12}$	−10.1
RDX	$C_3H_6N_6O_6$	−21.6
HMX	$C_4H_8N_8O_8$	−21.6
Nitroguanidine, NQ	$CH_4N_4O_2$	−30.7
Picric acid, PA	$C_6H_3N_3O_7$	−45.4
Hexanitrostilbene, HNS	$C_{14}H_6N_6O_{12}$	−67.6
Trinitrotoluene, TNT	$C_7H_5N_3O_6$	−74.0
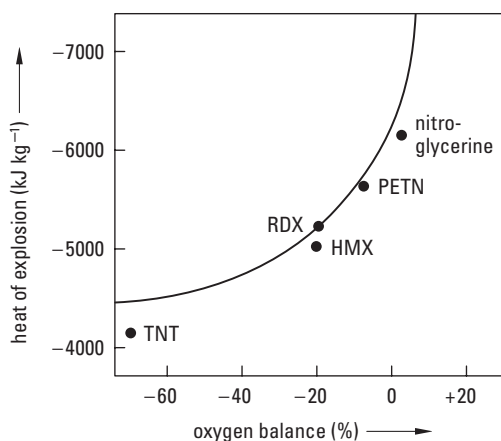
Fig. 4.1   Influence of the oxygen balance Ω on the heat of explosion Q.

Table 4.1 shows a summary of the oxygen balances of important secondary explosives.

Figure 4.1 shows the influence of the oxygen balance on conventional CHNO-explosives. Usually (this is the case for very nitrogen-rich compounds as well) a good oxygen balance results in a greater (more negative) heat of explosion and therefore leads to a better performance of the explosive.

The oxygen balance of an explosive alone does not help, when the thermodynamics of the reaction are to be estimated. In this case, it is (particularly for compounds with too-low oxygen balances) necessary to estimate how much of the oxygen gets converted into CO, CO_2 and H_2O. Additionally, since all explosions occur at high temperatures (approx. 3000 K), even with oxygen balances of $\Omega = 0$, not only CO_2 but also CO will form as stated in the Boudouard equilibrium. An approximate, but very simple scheme for the estimation of the detonation products is given by the so-called modified **Springall-Roberts rules**. These are given below and must be applied in order from 1 to 6:

1. C atoms are converted into CO
2. if O atoms remain, they oxidize hydrogen to H_2O
3. if there are remaining O atoms, they oxidize the already formed CO to CO_2
4. all nitrogen is converted to N_2
5. one third of the CO formed is converted into C and CO_2
6. one sixth of the CO formed originally is converted into C and water.

As an example, in Table 4.2, the Springall-Roberts-Rules have been applied to work out the detonation products of TNT.

Tab. 4.2 Determination of the detonation products of TNT ($C_7H_5N_3O_6$) according to the Springall-Roberts-Rules.

C atoms are converted into CO	$6\,C \rightarrow 6\,CO$
if O atoms remain, they oxidize hydrogen to H_2O	all oxygen is already used-up
if there are remaining O atoms, they oxidize the already formed CO to CO_2	all oxygen is already used-up
all nitrogen is converted to N_2	$3\,N \rightarrow 1.5\,N_2$
one third of the CO formed is converted into C and CO_2	$2\,CO \rightarrow C + CO_2$
one sixth of the CO formed originally is converted into C and water	$CO + H_2 \rightarrow C + H_2O$
total reaction	$C_7H_5N_3O_6 \rightarrow 3\,CO + CO_2 + 3\,C + 1.5\,H_2 + H_2O + 1.5\,N_2$

Therefore, the enthalpy of explosion (ΔH_{ex}) for TNT corresponds to the reaction enthalpy for the following reaction:

$$C_7H_5N_3O_6(s) \rightarrow 3\,CO(g) + CO_2(g) + 3\,C(s) + 1.5\,H_2(s) + H_2O(g) + 1.5\,N_2(g)$$
$$\Delta H_{ex}(TNT)$$
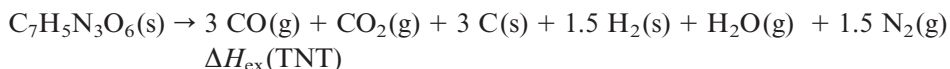
In contrast, the **enthalpy of combustion** for TNT (ΔH_{comb}) corresponds to the change in enthalpy for the following reaction and is more negative (more exothermic) than the explosion:

$$C_7H_5N_3O_6(s) + 5.25\,O_2(g) \rightarrow 7\,CO_2(g) + 2.5\,H_2O(g) + 1.5\,N_2(g)$$
$$\Delta H_{comb}(TNT)$$

For the definition of the enthalpy of combustion (ΔH_{comb}), it is important to check if there are values are given for $H_2O(g)$ or $H_2O(l)$.

Since the exact standard enthalpies of formation for all possible detonation products are known (see e.g. http://webbook.nist.gov/chemistry/), the enthalpy of detonation can easily be calculated, as long as only the enthalpy of combustion is exactly known from the experimental data, which unfortunately is not always the case.

According to the first fundamental law of thermodynamics, energy is conserved in any process involving a thermodynamic system and its surroundings. It is convenient to focus on changes in the assumed internal energy (U) and to regard them as due to a combination of heat (Q) added to the system and work done by the system (W). Taking ΔU as an incremental change in internal energy, we can write:

$$\Delta U = W + Q$$

Since work, W is defined as:

$$W = - \int_{V_1}^{V_2} p \, dV = -p \, \Delta V$$

for $V = $ const. $\Delta U = Q_v$
and for $p = $ const. $\Delta U = Q_p - p \, \Delta V$

For propellant charges, which burn in a gun barrel with constant pressure and for secondary explosives, a good approximation is $V = $ const. (isochoric) and therefore $\Delta U = Q_v$, while for rocket fuels (free expansion of the gases in the atmosphere) $p = $ const. and therefore $\Delta U = Q_p - p \, \Delta V$ is a good approximation.

Since the equation of state H (enthalpy) is defined as $H = U + pV$, the following generalization can be made:

$$\Delta H = \Delta U + p \, \Delta V + V \, \Delta p$$

Therefore, for $p = $ const.: $\Delta H = Q_p$.

This means that we can generalize as follows:

$$Q_v = \Sigma \Delta_f U^\circ_{(\text{detonation products})} - \Sigma \Delta_f U^\circ_{f(\text{explosive})}$$

and

$$Q_p = \Sigma \Delta_f H^\circ_{(\text{detonation products})} - \Sigma \Delta_f H^\circ_{f(\text{explosive})}$$

The molar energies of formation U and enthalpies H for a given explosive with the composition $C_a H_b N_c O_d$ can be connected as follows:

$$H = U + \Delta n \, R \, T$$

here, n is the chance of moles of the *gaseous* substances and R is the general gas constant. If we consider the hypothetical "equation of formation (from the elements)" for TNT for example, the change of moles is negative and Δn corresponds to -7:

$$7 \, C(s) + 2.5 \, H_2(g) + 1.5 \, N_2(g) + 3 \, O_2(g) \rightarrow C_7 H_5 N_3 O_6(s)$$
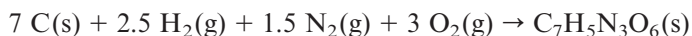
In practice, in a good approximation H and U can often be taken to be equal.

The liberated volume of detonation gases (V_0, usually back-calculated for standard conditions of 273 K and 1 bar) is also an important parameter when assessing the performance of an explosive. V_0 can easily be calculated using the reaction equation derived from the Springall-Roberts rules and applying the ideal gas law and it is usually given in $l \, kg^{-1}$.

Table 4.3 shows a summary of typical values for the volumes of gas released during an explosion (under STP).

Tab. 4.3 Calculated volumes of gas released in an explosion (under STP).

explosive	$V_0 / l \, kg^{-1}$
NG	740
PETN	780
RDX	908
HMX	908
NQ	1077
PA	831
HNS	747
TNT	740

The **Explosive Power** has been defined as the product of the volume of gas released V_0 (STP) and the heat of explosion Q. Traditionally Q is given in $kJ \, kg^{-1}$, and V_0 in $l \, kg^{-1}$ (Tab. 4.3). The value of the explosive power is usually compared with the explosive power of a standard explosive (picric acid) resulting in power indices, as shown below (Tab. 4.4).

$$\text{Explosive power} = Q(kJ \, kg^{-1}) \times V_0(l \, kg^{-1}) \times 10^{-4} \, (kg^2 \, kJ^{-1} \, l^{-1})$$

$$\text{Power index} \quad = \frac{Q \times V_0}{Q_{PA} \times V_{PA}} \times 100$$

Tab. 4.4 Explosive power and power index.

explosive	$-Q/kJ \, kg^{-1}$	$V_0/l \, kg^{-1}$	explosive power	power index
$Pb(N_3)_2$	1610	218	35	13
NG	6195	740	458	170
PETN	5794	780	452	167
RDX	5036	908	457	169
HMX	5010	908	455	169
NQ	2471	1077	266	99
PA	**3249**	**831**	**270**	**100**
HNS	3942	747	294	109
TNT	4247	740	314	116

The detonation or explosion temperature T_{ex} is the theoretical temperature of the detonation products, assuming that the explosion occurs in a confined and

undestroyable adiabatic environment (adiabatic conditions). The detonation temperature can be calculated with the assumption that the heat content of the detonation products must be the same as the calculated heat of detonation (Q). We can assume, that the detonation products of the initial temperature T_i (normally 298 K) will be brought up to a temperature of T_{ex} due to the heat of detonation, i. e. T_{ex} is dependent on Q. The connection between Q and T is given in the following equation, whereby C_V is the molar heat capacity of the detonation products:

$$Q = \Sigma \int_{T_i}^{T_{ex}} C_V \, dT \quad \text{with:} \quad C_V = \left(\frac{\partial Q}{\partial T}\right)_V = \left(\frac{\partial U}{\partial T}\right)_V$$

$$\text{and} \quad C_P = \left(\frac{\partial Q}{\partial T}\right)_P = \left(\frac{\partial H}{\partial T}\right)_P.$$

Therefore, the detonation temperature T_{ex} can be estimated as follows:

$$T_{ex} = \frac{Q}{\Sigma C_V} + T_i$$

If a value which is slightly too low and a value which is slightly too high are used for the detonation temperature and the value for Q is calculated using the values given in Table 4.5, the "correct" detonation temperature T_{ex} can be estimated iteratively.

Tab. 4.5 Average heat capacities C_V (in J K^{-1} mol^{-1}).

T_{ex}/K	CO_2	CO	H_2O	H_2	N_2
2000	45.371	25.037	34.459	22.782	24.698
2100	45.744	25.204	34.945	22.966	24.866
2200	46.087	25.359	35.413	23.146	25.025
2300	46.409	25.506	35.865	23.322	25.175
2400	46.710	25.640	36.292	23.493	25.317
2500	46.991	25.769	36.706	23.665	25.451
2600	47.258	25.895	37.104	23.832	25.581
2700	47.509	26.012	37.485	23.995	25.703
2800	47.744	26.121	37.849	24.154	25.820
2900	47.965	26.221	38.200	24.309	25.928
3000	48.175	26.317	38.535	24.260	26.029
3100	48.375	26.409	38.861	24.606	26.129
3200	48.568	26.502	39.171	24.748	26.225
3300	48.748	26.589	39.472	24.886	26.317
3400	48.924	26.669	39.761	25.025	26.401
3500	49.091	26.744	40.037	25.158	26.481
3600	49.250	26.819	40.305	25.248	26.560
3700	49.401	26.891	40.560	25.405	26.635
3800	49.546	26.962	40.974	25.527	26.707
3900	49.690	27.029	41.045	25.644	26.778
4000	49.823	27.091	41.271	25.757	26.845
4500	50.430	27.372	42.300	26.296	27.154
5000	50.949	27.623	43.137	26.769	27.397

4.2 Computational Methods

4.2.1 Thermodynamics

The thermodynamic data as well as the detonation parameters can nowadays be very reliably obtained by using quantum-mechanical computer calculations. On the one hand it is important to check experimental results, and on the other hand − and even more importantly − it is important to predict the properties of potential new energetic materials without any prior experimental parameters, for example during the planning of synthetic work. Moreover, such computational methods are ideal for the estimation of the detonation parameters of newly synthesized compounds, which have not been obtained in the $50-100$ g quantities which are necessary for the experimental determination of such detonation parameters (e.g. detonation velocity).

In order to be able to calculate the detonation parameters of a particular neutral or ionic compound, it is advisable to calculate the enthalpy (H) and free energy (G) quantum chemically with very exact methods (e.g. G2MP2, G3 or CBS-4M). To achieve this, the Gaussian (G03W or G09W) programme is suitable. In the following section, we will concentrate on the CBS-4M method developed by Petersson and co-workers. In the CBS method, (complete basis set) the asymptotic convergence behavior of natural orbitals is used, in order to extrapolate the energy limit for an infinitely large basis set. The CBS method begins with a HF/$3-21$G(d) calculation in order to optimize the structure and for the calculations of the zero-point energy. Then, using a larger basis set, the so-called base-energy is calculated. A MP2/$6-31+$G calculation with a CBS extrapolation gives the perturbation-theory corrected energy, which takes the electron correlation into account. A MP4(SDQ)/$6-31+$(d,p) calculation is used, to estimate the correlation contributions of a higher order. The most widely used CBS-4M version today is a re-parametrization of the original CBS-4 version, which contains additional empirical correction terms (M stands for "minimal population localization" here).

The enthalpies of the gaseous species M can now be calculated using the method of the atomisization energies [21−23]:

$$\Delta_f H^\circ(g,m) = H^\circ_{\text{(molecule)}} - \Sigma H^\circ_{\text{(atoms)}} + \Sigma \Delta_f H^\circ_{\text{(atoms)}}$$

Two examples should be considered for further discussion: the covalent nitroglycerine (NG) and the ionic ammonium dinitramide (ADN). The calculated enthalpies (H) and free energies (G) for NG, the ions NH_4^+ and $N(NO_2)_2^-$ as well as the relevant atoms H, C, N and O using the CBS-4M method, are summarized in Table 4.6.

Tab. 4.6   CBS-4M values for NG, the ions NH_4^+ and $N(NO_2)_2^-$ and the relevant atoms H, C, N and O.

	$-H^{298}$ / a. u.	$-G^{298}$ / a. u.
NG,	957.089607	957.149231
NH_4^+	56.796608	56.817694
$N(NO_2)_2^-$	464.499549	464.536783
H	0.500991	0.514005
C	37.786156	37.803062
N	54.522462	54.539858
O	74.991202	75.008515

Therefore in Table 4.6 we already have the $H^\circ_{(molecules)}$ and $H^\circ_{(atom)}$ values (given in a. u. = atomic units; 1 a. u. = 1 H = 627.089 kcal mol^{-1}). The values for $\Delta_f H^\circ_{(atoms)}$ are easily obtained from the literature and are summarized in Table 4.7.

Tab. 4.7   Literature values for $\Delta_f H^\circ_{(atoms)}$ (in kcal mol^{-1})

	Ref. [21]	NIST [24]
H	52.6	52.1
C	170.2	171.3
N	113.5	113.0
O	60.0	59.6

According to the equation given above, we can now easily calculate the standard enthalpies of formation $\Delta_f H^\circ(g)$ for the gas phase species NG, NH_4^+ and $N(NO_2)_2^-$ (Tab. 4.8).

Tab. 4.8   Calculated standard enthalpies of formation $\Delta_f H^\circ(g)$ for the gas-phase.

gas-phase species	formula	$\Delta_f H^\circ(g)$ / kcal mol^{-1}	$\Delta_f H^\circ(g)$ / kJ mol^{-1}
NG	$C_3H_5N_3O_9$	$-$ 67.2	-281.1
ammonium ion	NH_4^+	$+151.9$	$+635.5$
dinitramide ion	$N(NO_2)_2^-$	$-$ 29.6	-123.8

In order to be able to convert the standard enthalpies of formation $\Delta_f H^\circ(g)$ for the gas-phase into values for the condensed phase, for covalent molecules (NG) we additionally require the enthalpy of sublimation $\Delta H_{sub.}$ (for solids) or the enthalpy of vaporization $\Delta H_{vap.}$ (for liquids). Both values can be estimated using the Trouton's rule, in which T_m is the melting point of the solid and T_b is the boiling point of the liquid [25]:

$$\Delta H_{sub.} \text{ [J mol}^{-1}] = 188\, T_m \text{[K]}$$
$$\Delta H_{vap.} \text{ [J mol}^{-1}] = 90\, T_b \text{[K]}$$

NG is a liquid and its extrapolated boiling point is 302 °C (= 575 K). Therefore, the enthalpy of vaporization is calculated to be $\Delta H_{vap.}(NG) = 51.8$ kJ mol^{-1} (12.3 kcal mol^{-1}).

In the case of ionic solids of the type AB, AB$_2$ or A$_2$B, the lattice energy (ΔU_L) and lattice enthalpy (ΔH_L) can be calculated by using the Jenkin's method proposed [26−29]. Only the molecular volumes of the ions are required. These can be most easily obtained from single crystal X-ray diffraction data:

$$\Delta U_L = |z_+||z_-|\, v \left[\frac{a}{\sqrt[3]{V_M}} + \beta \right]$$

Here $|z_+|$ and $|z_-|$ are the dimensionless charges of the cations and anions and v is the number of ions per 'molecule' (2 for ADN, 3 for Ba (DN)$_2$). V_M is the volume in nm^3 of a formula unit (e.g. $V_M(ADN) = V_M(NH_4^+) + V_M(DN^-)$; $V_M(Ba(DN)_2) = V_M(Ba^{2+}) + 2\,V_M(DN^-)$). The constants a and β are dependent on the composition of the salt, and are summarized in Table 4.9.

Tab. 4.9 The values for the constants a and β for calculating the lattice energy by using the Jenkin's method.

salt type	a / kJ mol^{-1}	β / kJ mol^{-1}
AB	117.3	51.9
AB$_2$	133.5	60.9
A$_2$B	165.3	−29.8

The lattice energy ΔU_L can easily be converted into the corresponding lattice enthalpy ΔH_L:

$$\Delta H_L(A_pB_q) = \Delta U_L + \left[p \left(\frac{n_A}{2} - 2 \right) + q \left(\frac{n_B}{2} - 2 \right) \right] R\,T$$

n_A, n_B: = 3 for monoatomic ions
5 for linear, polyatomic ions
6 for non-linear, polyatomic ions.

From X-ray diffraction data it is known that the molecular volume of ADN 110 Å^3 is 0.110 nm^3 [30]. If this value was not known, it could have been calculated using the literature values for the volumes of $V_M(NH_4^+) = 0.021$ nm^3 and $V_M(DN^-) = 0.089$ nm^3 as being $V_M(ADN) = 0.110$ nm^3. Therefore, the following values for ADN can be written:

$\Delta U_L(ADN) = 593.4$ kJ mol^{-1}
$\Delta H_L(ADN) = 598.4$ kJ mol^{-1}

Since the enthalpy of vapourization for NG and the lattice enthalpy for ADN are known, the gas-phase enthalpy values can easily be converted into the standard enthalpies of formation for the condensed phase:

$$\Delta_f H°(\text{NG}) \quad = -332.9 \text{ kJ mol}^{-1} = -80 \text{ kcal mol}^{-1}$$
$$\Delta_f H°(\text{ADN, s}) \quad = \quad -86.7 \text{ kJ mol}^{-1} = -21 \text{ kcal mol}^{-1}.$$

A comparison with experimental values from literature shows that the calculation outlined here gives a good result, without having to rely on experimental data (with the exception of the density and the molecular volume):

$$\Delta_f H°(\text{NG}) \quad = -88 \text{ kcal mol}^{-1}$$
$$\Delta_f H°(\text{ADN}) \quad = -36 \text{ kcal mol}^{-1}$$

As we have already shown in Chapter 1.4, the molar energies of formation U and enthalpy H for a given explosive with the composition $C_a H_b N_c O_d$ are related as follows:

$$H = U + \Delta n\, R\, T$$

Here n is the change in the number of moles of gaseous substances and R is the ideal gas constant. Therefore, for NG ($\Delta n = -8.5$) and ADN ($\Delta n = -6$) the following values can be written:

$$\Delta_f U°(\text{NG}) \quad = -311.8 \text{ kJ mol}^{-1} = -1373.0 \text{ kJ kg}^{-1}$$
$$\Delta_f U°(\text{ADN}) = \quad -71.8 \text{ kJ mol}^{-1} = \quad -579.0 \text{ kJ kg}^{-1}$$

4.2.2 Detonation Parameters

There now are various different codes available for computing detonation parameters (e.g. TIGER, CHEETAH, EXPLO5 etc.). In this discussion, we will concentrate on the application of one such code, namely the program EXPLO5. This program is based on the chemical equilibrium, a steady-state model of detonation. It uses the Becker-Kistiakowsky-Wilson's equation of state (BKW EOS) for gaseous detonation products and Cowan-Fickett's equation of state for solid carbon [31−34]. The calculation of the equilibrium composition of the detonation products is done by applying the modified White, Johnson and Dantzig's free energy minimization technique. The program is designed to enable the calculation of detonation parameters at the C-J point (see Ch. 3).

The ideal gas law of the form

$$pV = n\, R\, T$$

with the ideal gas constant R enables us to calculate an ideal gas the pressure p for a certain temperature T and also the volume V for a known molar amount n.

To calculate the detonation pressure, this equation is however not good enough, because there are strong deviations from the ideal gas behavior. The Becker-Kistiakowsky-Wilson equation of state (BKW-EOS)

$$\frac{pV}{RT} = 1 + x\,e^{\beta x} \qquad x = \frac{k}{VT^{\alpha}}$$

which contains the covolume constant k takes into account the residual volume of the molecules of the gaseous components. The α and β parameters are obtained by comparisons with the experimental data (fitted empirically). For extremely low temperatures, however, the pressure becomes infinitely large. Cowan and Fickett developed the Becker-Kistiakowsky-Wilson equation of state to:

$$\frac{pV}{RT} = 1 + x\,e^{\beta x} \qquad x = \frac{\kappa\,\Sigma X_i\,k_i}{V(T + \theta)^{\alpha}}$$

whereby also $(\delta p / \delta T)_V$ remains positive. The covolume constant is replaced by the weighted sum of the products of the mole fractions X_i and the geometric covolumes k_i of the gaseous components i. The Becker-Kistiakowsky-Wilson-Neumann parameters α, β, κ and θ were obtained empirically by adapting the computational results to the experimental data.

However, this equation can not be used for solids. For such cases Cowan and Fickett suggest an equation of the following form with the factors $p_1(V)$, $a(V)$ and $b(V)$ as polynomial functions of the compression of the material η relative to the crystal density of the solid in the standard state, which is known as the Cowan-Fickett equation of state for solids:

$$p = p_1(V) + a(V)T + b(V)T^2$$

$$\eta = \frac{V^{\circ}(T^{\circ})}{V} = \frac{\rho}{\rho^{\circ}}$$

The $p(V)$ diagram shows the shock adiabat of the explosive, which is also called the Hugoniot curve or Hugoniot adiabat (see Fig. 1.22). The shock adiabat can be calculated for both the non-reacted explosive as well as for the reaction products (see Fig. 1.22). The C-J point, which represents the point where the C-J conditions are fulfilled, is therefore the point where the shock adiabat of the reaction products touches the Raleigh line (tangent), which is described by the following equation:

$$p - p_0 = \rho_0^2\,U^2(V_0 - V)$$

Here, ρ_0 is the material density of the unreacted explosive, u is the impact velocity and V and V_0 are the specific volumes. The Raleigh line is a straight line with the slope D^2/V^2 connecting (V_0, p_0), (V_1, p_1) and (V_2, p_2) in the $p(V)$ diagram.

At the point where the Raleigh line touches the schock adiabate of the reaction products the slope of both functions is the same, and the following relationship, where U is the velocity of the products, is valid:

$$\frac{\partial p}{\partial V} = \frac{D^2}{V^2} = \frac{U^2}{V^2}$$

Under the assumption of a steady-state model of detonation, the EXPLO5 program allows the calculation of the detonation parameters and also the chemical composition of the system at the C-J point. For the calculations, the BKW equation of state is applied for gases, where X_i is the mole fraction of the i-th gaseous component and k_i is the molar covolume of the i-th gaseous detonation products:

$$\frac{pV}{RT} = 1 + x\,e^{\beta x} \qquad x = \frac{\kappa\,\Sigma\,X_i\,k_i}{V(T+\theta)^\alpha}$$

$\alpha = 0.5, \quad \beta = 0.176, \quad \kappa = 14.71, \quad \theta = 6620$ (EXPLO5 V5.03)

$\alpha = 0.5, \quad \beta = 0.096, \quad \kappa = 17.56, \quad \theta = 4950$ (EXPLO5 V5.04)

For solid carbon, the Cowan-Fickett equation of state is applied in the following form, with the presumption that carbon is present in the graphite modification:

$$p = p_1(V) + a(V)T' + b(V)T'^2$$

where:

$T' \quad = T/11605.6$ K,
$p_1(V) = -2.467 + 6.769\,\eta - 6.956\,\eta^2 + 3.040\,\eta^3 - 0.3869\,\eta^4,$
$a(V) \quad = -0.2267 + 0.2712\,\eta,$
$b(V) \quad = 0.08316 - 0.07804\,\eta^{-1} + 0.03068\,\eta^{-2},$

compression of the material η: $\quad \eta = \dfrac{V^\circ(T^\circ)}{V} = \dfrac{\rho}{\rho^\circ}.$

The minimization of the free energy in accordance with White-Johnson-Dantzig allows the determination of the composition of the detonation products in equilibrium state. The thermodynamic parameters (enthalpy, entropy, free enthalpy, free energy) of the detonation products can be calculated using functions based on the enthalpy $H_T^\circ - H_0^\circ$. The coefficients $c_0, \ldots c_4$ can be found in literature [*J. Chem. Phys* **1958**, *28*, 751−755; *Prop., Expl. Pyrotech.* **1985**, *10*, 47−52]:

$$(H_T^\circ - H_0^\circ) = c_0 + c_1 T + c_2 T^2 + c_3 T^3 + c_4 T^4.$$

The EXPLO5 program calculates the parameters of state of the products along the shock adiabat, starting from a density of a given explosive (ρ_0) and then increasing it in an arbitrary chosen step up to the density of about $1.5 \cdot \rho_0$. Then, it determines the C-J point as a point on the shock adiabat at which the detonation velocity has a minimum value (this minimum, D_{min}, is determined by the minimum of the first derivative of the Hugoniot adiabat, see Fig. 4.2). Once the C-J point is determined the detonation parameters can be calculated applying the well-known relationships between them.

The hydrodynamic detonation theory allows to correlate the detonation parameters on the basis of the laws of mass, impulse and energy conservation and to calculate them independently of p and V:

$$\frac{D}{V_0} = \frac{D - U}{V}$$

$$\frac{D^2}{V_0} + p_0 = \frac{(D - U)^2}{V} + p$$

$$U_0 + D^2 + p_0 V_0 = U + 1/2 \, (D - U)^2 + pV$$

From this, for the detonation velocity and the velocity of the shock front the following equations can be written:

$$D = V_0 \sqrt{\frac{p - p_0}{V_0 - V}}$$

$$U = (V_0 - V) \sqrt{\frac{p - p_0}{V_0 - V}}$$
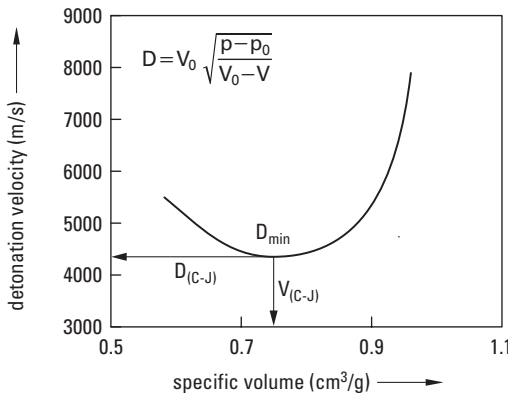
Fig. 4.2 Change of detonation velocity with specific volume of detonation products.

Tab. 4.10   Calculated and experimentally determined detonation parameters.

explosive	density	method	$D/\mathrm{m\,s^{-1}}$	$p_{\text{C-J}}/\mathrm{kbar}$	T_{ex}/K	$Q_{\text{C-J}}/\mathrm{kJ\,kg^{-1}}$
NG	1.60	experimental	7700	253	4260	
		EXPLO5	7819	242	4727	−6229
TNT	1.64	experimental	6950	210		
		EXPLO5	7150	202	3744	−5087
RDX	1.80	experimental	8750	347		
		EXPLO5	8920	345	4354	6033
HNS	1.65	experimental	7030	215		
		EXPLO5	7230	212	4079	−5239
PETN	1.76	experimental	8270	315		
		EXPLO5	8660	311	4349	5889

The detonation parameters for NG, TNT and RDX calculated using the EXPLO5-program are summarized in Table 4.10, as well as the experimental data for comparison.

4.2.3 Combustion Parameters

Using the calculated thermodynamic data outlined in 4.2.1, not only the detonation parameters (4.2.2) but also the most important performance parameters for rocket propellants can be calculated. For this there are various programs which are available as well, from which we are going to refer back to and concentrate again on the EXPLO5 code.

The combustion of an energetic material is an irreversible process in which mainly gaseous and to a lesser extent solid combustion products are formed. One can differentiate between two borderline cases of combustion:

1. isobaric
2. isochoric

In an **isobaric combustion**, the combustion occurs without any loss of heat to the surroundings (adiabatic) and at a constant pressure (isobar), while the combustion products are found in a chemical equilibrium (e.g. rocket propellants).

In an **isochoric combustion** it is also assumed that the combustion occurs without any loss of heat to the surroundings (adiabatic) but at a constant volume (isochoric) and the combustion products are found in chemical equilibrium (e.g. gun propellants).

For **rocket propellants**, as we have already seen in Chapter 4.1, the assumption of free expansion of the gases in the atmosphere or in space, $p = $ const. (and thereby $\Delta U = Q_{\text{p}} - p\Delta V$) is a good approximation and therefore the process is
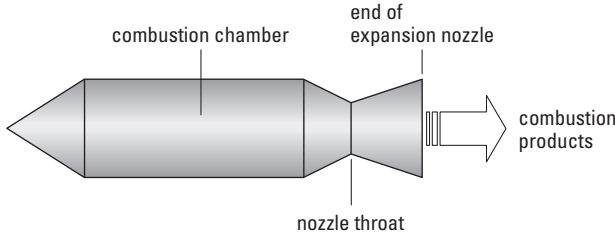
Fig. 4.3 Schematic representation of a rocket combustion chamber with expansion nozzle.

best described as **isobaric**. For the theoretical calculation of the performance of rocket propellants, the following assumptions are made:

1. the pressure in the combustion chamber and at the nozzle throat is constant,
2. energy and momentum conservation equations are applicable,
3. the velocity of the products of combustion in the combustion chamber is equal to zero,
4. there is no temperature and velocity lag between condensed and gaseous species,
5. the expansion in the nozzle (nozzle, Fig. 4.3) occurs isentropically (a change of state is isentropic, when the entropy S remains constant, i.e. S = const. or $\mathrm{d}S = 0$).

The important performance parameters for the performance of a rocket propellant are the thrust F and the specific impulse I_{sp}^{*}.

As we have already seen above (Ch. 2.4), the average thrust and the specific impulse I_{sp} are related to each other as follows ($I_{sp}^{*} = I_{sp}/g$):

$$\overline{F} = I_{sp}\,\frac{\Delta m}{\Delta t}$$

For the thrust we can finally write:

$$F = \frac{\mathrm{d}m}{\mathrm{d}t}\,v_{e} + (p_{e} - p_{a})A_{e}$$

Here, v_{e} is the velocity of the combustion gases at the end of the expansion nozzle (see Fig. 2.20), p_{e} and p_{a} are the pressure at the end of the expansion nozzle and atmospheric pressure respectively and A_{e} is the cross section at the end of the expansion nozzle.

Therefore, we can write the following for the specific impulse:

$$I_{sp} = \frac{F}{\dfrac{\mathrm{d}m}{\mathrm{d}t}} = v_{e} + \frac{(p_{e} - p_{a})A_{e}}{\dfrac{\mathrm{d}m}{\mathrm{d}t}}$$

Using the EXPLO5 programme, we can calculate the following performance parameters (amongst others) for rocket propellants under isobaric conditions for different pressures in the combustion chamber:

- isobaric heat of combustion Q_p (kJ kg^{-1})
- isobaric combustion temperature T_c (K)
- composition of the products of combustion
- temperature and pressure at the nozzle throat
- flow velocity at the nozzle throat
- temperature at the end of the expansion nozzle ($p_e = 1$ bar)
- specific impulse

For isochoric combustion processes, the following parameters (amongst others) can be calculated:

- isochoric heat of combustion Q_v (kJ kg^{-1})
- total pressure in closed systems (bar)
- composition of the combustion products
- specific energy: $F = n\,R\,T_c$ (J kg^{-1}),
  T_c = isochoric combustion temperature.

Currently, a new propellant is being researched. This propellant is hydrazinium aminotetrazolate (**2**), which is obtained in a facile route from hydrazine and aminotetrazole (**1**) (Fig. 4.4) [35a].
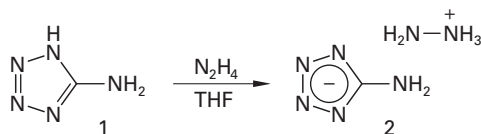
Fig. 4.4 Synthesis of hydrazinium aminotetrazolate (**2**, Hy-At).

The programme EXPLO5 was used to calculate the rocket propellant parameters for this compound in combination with ADN as the oxidizer while presuming a combustion chamber pressure of 45 bar (Tab. 4.11)

We can see that the specific impulse of a 70:30 mixture of Hy-At is approximately 5 s higher than that of a stoichiometric mixture of AP and Al. Therefore, the new fuel Hy-At in combination with the environmentally friendly ADN (in contrast to AP) could potentially be of interest.

For **gun propellants** we can assume isochoric combustion with the specific energy f_E or force or impetus ($f_E = n\,R\,T$), the combustion temperature T_c (K), the co-volume b_E (cm^3 g^{-1}) and the pressure p (bar; 3000–4000 bar) being the most important parameters. Moreover, a large N_2/CO ratio is desirable in order to avoid erosion problems. The loading densities are by far not as important as for high explosives. Comparing M1 and EX-99 with the newly developed high-nitrogen propellant (HNP) which is based triaminoguanidinium azotetrazolate (TAGzT)

Tab. 4.11 Calculated combustion parameters for hydrazinium aminotetrazolate- Hy-At /
ADN formulations with p = 45 bar.

oxidizer ADN[a]	fuel Hy-At	ρ / g cm^{-3}	Ω / %	T_c / K	I_{sp} / s
10	90	1.573	−65.0	1863	227
20	80	1.599	−55.0	1922	229
30	70	1.625	−44.9	2110	236
40	60	1.651	−34.8	2377	246
50	50	1.678	−24.7	2653	254
60	40	1.704	−14.6	2916	260
70	30	1.730	− 4.5	3091	261
80	20	1.756	+ 5.6	2954	250
90	10	1.782	+15.7	2570	229
AP[b]	Al[c]				
70	30	2.178	−2.9	4273	255

[a] ADN, ammonium dinitramide; [b] ammonium perchlorate, [c] aluminum.

and with NICO (based on TAG$_2$BT) (Tab. 4.11a), very similar performance values
for M1, HNP, NICO, but a greatly reduced errosion coefficient (N$_2$/CO) can be
found (Tab. 4.11b, Fig. 4.4a). It is also worth mentioning that the HNP and NICO
are similar in their performance to NILE (Navy Insensitive Low Erosion Propel-
lant: 40 % RDX, 32 % GUDN, 7 % acetyl triethyl citrate, 14 % cellulose acetate
butyrate, 5 % hydroxyl propylcellulose, 2 % plasticizer).

The most common equation of state for interior ballistics is that of Nobel-Abel:

$$p\,(v - b_E) = n\,R\,T$$

(with: b_E = co-volume, n = mol number, R = gas constant).

The co-volume is a parameter which takes the physical size of the molecules and
any intermolecular forces created by their procimity to one another into account.
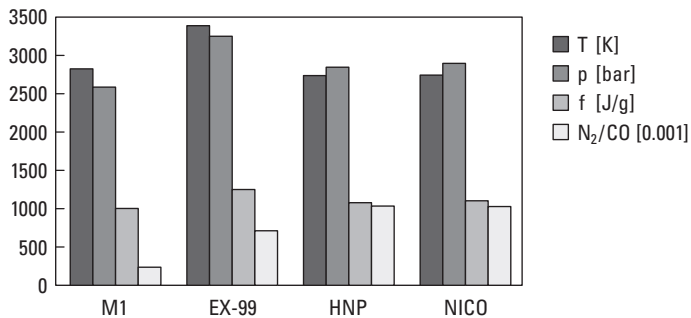
Fig. 4.4a Calculated performance of various gun propellants (HNP = High-N-2, NICO =
TAG$_2$-BT-High-N-2).

Tab. 4.11a Propellant charge compositions.

propellant charge formulation	ingredient	amount/% (weight)
M1	NC (13.25)	86
	2,4-DNT	10
	dibutyl phthalate (DBP)	3
	diphenyl amine (DPA)	1
EX-99	RDX	76
	cellulose acetate	12
	BDNPA/F[a]	8
	NC (13.25)	4
High-N-1	RDX	56
	TAGzT	20
	cellulose acetate	12
	BDNPA/F[a]	8
	NC (13.25)	4
High-N-2 (HNP)	RDX	40
	TAGzT	20
	FOX-12/GUDN	16
	cellulose acetate	12
	BDNPA/F[a]	8
	NC (13.25)	4
TAG_2-BT-High-N-2 (NICO)	RDX	40
	TAG_2-BT[b]	20
	FOX-12/GUDN	16
	cellulose acetate	12
	BDNPA/F[a]	8
	NC (13.25)	4

[a] Bis(dinitropropyl)acetal (BDNPA) : Bis(dinitropropyl)formal (BDNPF) = 50 : 50
[b] TAG_2-BT = $(CN_6H_9)_2$-5,5′-Bistetrazolate

Tab. 4.11b Calculated performance of various gun propellants[a].

	T_c/K	$p_{max.}$/bar	f_E/kJ g^{-1}	b_E/cm^3 g^{-1}	N_2/CO (w/w)
M1	2834	2591	1.005	1.125	0.23
EX-99	3406	3249	1.257	1.129	0.71
High-N-1	2922	3042	1.161	1.185	0.95
High-N-2 (HNP)	2735	2848	1.088	1.181	1.05
TAG_2-BT-High-N-2 (NICO)	2756	2896	1.105	1.185	1.03

[a] loading density = 0.2 g cm^{-3}; virial equations of state (real gas)

If experimental test results (manometric pressure bomb) for the maximum pressure using different loading densities are available, the force f_E and the co-volumes b_E can be calculated as follows:

$$f_E = \frac{p_2}{d_2} \times \frac{p_1}{d_1} \times \frac{d_2 - d_1}{p_2 - p_1}$$

$$b_E = \frac{\dfrac{p_2}{d_2} - \dfrac{p_1}{d_1}}{p_2 \; p_1}$$

where:

f_E force,
b_E co-volume,
p_1 maximum pressure at the lower density d_1,
p_2 maximum pressure at the higher density d_2,
d_1 lower loading density,
d_2 higher loading density.

Assuming that the powder combustion occurs at a temperature equal to the explosion temperature T_{ex} and under consideration of the fact, that after combustion, the specific volume V and the charge density (d) are equal, the following equation applies:

$$\frac{p_{max}}{d} = b_E \; p_{max} + f_E$$

The EXPLO5 code can also be used for the calculation of the thermodynamic properties of propellant gases and shows an error of usually less than 5% (loading densities ca. 0.2 g cm^{-3}) when the maximum pressure, the specific energy and the co-volume are considered.

4.2.4 Example: Theoretical Evaluation of New Solid Rocket Propellants

Solid propellants of essentially all solid rocket boosters are based on a mixture of aluminum (Al, fuel) and ammonium perchlorate (AP, oxidizer).

Ammonium perchlorate (AP) has applications in munitions, primarily as an oxidizer for solid rocket and missile propellants. It is also used as an air-bag inflator in the automotive industry, in fireworks, and is a contaminant in agricultural fertilizers. Because of these uses and ammonium perchlorate's high solubility, chemical stability, and persistence, it has become distributed widely in surface and ground water systems. There is little information about the effects of perchlorate in these systems or on the aquatic life that inhabits them. However, it is known that perchlorate is an endocrine disrupting chemical that interferes with normal thyroid function and that thyroid dysfunction impacts both growth and development in vertebrates. Because perchlorate competes for iodine binding sites in the thyroid, the addition of iodine to culture water has been examined in order to determine if
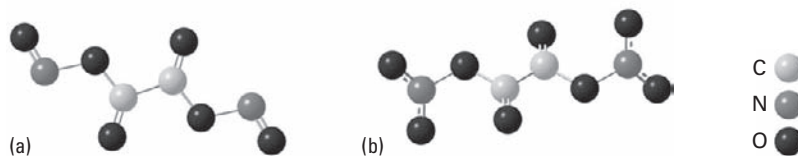
Fig. 4.5 Optimized molecular structures of $(ON)O_2C-CO_2(NO)$ (a) and $(O_2N)O_2C-CO_2(NO_2)$ (b).

Tab. 4.12 Solid state energies of formation ($\Delta_f U°$).

	$\Delta_f H°(s)/\text{kcal mol}^{-1}$	Δn	$\Delta_f U°(s)/\text{kcal mol}^{-1}$	$M/\text{g mol}^{-1}$	$\Delta_f U°(s)/\text{kJ kg}^{-1}$
$[NO_2]_2[O_2C-CO_2]$	$-\ 86.6$	-5	$-\ 83.6$	180.0	-1943.2
$[NO]_2[O_2C-CO_2]$	-107.0	-4	-104.6	148.0	-2957.1
$O_2N-O_2C-CO_2-NO_2$	-113.5	-5	-110.5	180.0	-2568.5
$ON-O_2C-CO_2-NO$	$-\ 96.5$	-4	$-\ 94.1$	148.0	-2660.2

perchlorate effects can be mitigated. Finally, perchlorate is known to affect normal pigmentation of amphibian embryos. In the US alone the cost for remediation is estimated to be several billion dollars, money that is deeply needed in other defense areas.

In the course of the emerging global interest in high-energetic, dense materials (HEDM) the LMU group is currently developing new energetic materials, which preferably have a positive oxygen balance value (see Ch. 4.1) [35b].

The objectives of the ongoing work is to explore the chemical synthesis of possible replacements for AP as an oxidizer in tactical missile rocket motors. The synthesis, sensitivities, thermal stability, binder compatibility and decomposition pathways of these new high-oxygen materials are currently being researched. In the following example, we theoretically want to evaluate, the suitability of nitrosyl (NO^+) and nitronium (NO_2^+) oxalate as a potential ingredient for solid rocket propellants.

The molecular structures of neutral $(ON)O_2C-CO_2(NO)$ and $(O_2N)O_2C-CO_2(NO_2)$ were fully optimized without symmetry constraints in both cases to C_i symmetry (Fig. 4.5).

Table 4.12 presents the calculated energies of formation for the solid neutral species and salts based on the CBS-4M method (see Ch. 4.2.1.). Furthermore we see from table 4.12 that for the nitronium ($[NO_2]^+$) species the covalently bound form is favored over the ionic salt by 26.9 kcal mol^{-1} while for the nitrosonium species ($[NO]^+$) the salt is favored over the covalent isomer by 10.5 kcal mol^{-1}. This change from the preferred covalent form of $-NO_2$ compound (actually a nitrato ester) to the ionic nitronium salt can be attributed almost exclusively to the

increased lattice enthalpy of the (smaller!) NO^+ species ($\Delta H_L(NO^+ - NO_2^+$ salt) = 31.4 kcal mol^{-1}) (*N.B.* The difference in the ionization potentials of NO (215 kcal mol^{-1}) and NO_2 (221 kcal mol^{-1}) is only marginal).

For a solid rocket propellant free expansion of the combustion products into space (or atmosphere) with p = const. can be assumed and therefore the below equation is a good approximation, i.e. the combustion process as isobaric can be considered:

$$\Delta U = Q_p - p\,\Delta V$$

In this study we assume firing the rocket motor against an ambient atmosphere (p = 1 bar) as it is commonly the case for tactical missiles.

The following combustion calculations were carried out under isobaric conditions, based on the assumption that the combustion of fuel proceeds without any heat loss to the surroundings (i.e. adiabatically) and that the state of chemical equilibrium establishes in the combustion products. The calculation of the theoretical rocket performances was based on the following assumptions:

1. the pressure in the combustion chamber and the chamber cross-section area are constant
2. the energy and momentum conservation equations are applicable
3. the velocity of the combustion products at the combustion chamber is equal to zero
4. there is no temperature and velocity lag between condensed and gaseous species
5. the expansion in the nozzle is isentropic (*N.B.* In thermodynamics, an isentropic process or isoentropic process is one during which the entropy of the system remains constant.)

The theoretical characteristics of the rocket motor propellant may be derived from the analysis of the expansion of the combustion products through the nozzle. The first step in the calculation of the theoretical rocket performance is to calculate the parameters in the combustion chamber, and the next step is to calculate the expansion through the nozzle (see Fig. 4.3). The expansion through the nozzle is assumed to be isentropic ($\Delta S = 0$). The EXPLO5 and ICT program code provide the following options:

− *frozen* flow (composition of combustion products remains unchanged, frozen, during the expansion through the nozzle, i.e. equal to composition in the combustion chamber),
− *equilibrium* flow (composition of combustion products at any station in the nozzle is defined by chemical equilibrium).

The frozen performance is based on the assumption that the composition of combustion products remains constant ("frozen"), while equilibrium performance is

Tab. 4.13 Combustion properties (solid rocket motor) of Al formulations with essentially zero oxygen balance (frozen expansion).

	$O_2N\!-\!O_2C\!-\!CO_2\!-\!NO_2$: Al $= 0.70 : 0.30$	$[NO]_2[O_2C\!-\!CO_2]$: Al $= 80 : 20$	AP : Al $= 0.70 : 0.30$
condition	isobaric	isobaric	isobaric
p / bar	70	70	70
ρ / g cm^{-3}	1.93	1.82	2.18
Ω / %	-2.0	-0.6	-2.8
Q_p / kJ kg^{-1}	-6473	-5347	-6787
$T_{comb.}$ / K	4642	4039	4290
I_{sp}^* / s	223	220	243

based on the assumption of instantaneous chemical equilibrium during the expansion in the nozzle.

The specific impulse I_{sp} is the change of the impulse (impulse = mass $\times$ velocity, or force $\times$ time) per propellant mass unit. The specific impulse is an important parameter for the characterization of rocket propellants and can be interpreted as the effective exhaust velocity of the combustion gases when exiting the expansion nozzle:

$$I_{sp} = \frac{\overline{F} \times t_b}{m} = \frac{1}{m} \int_0^{t_b} F(t)\, dt$$

The force F is the time-dependent thrust, $F(t)$, or the average thrust, $\overline{F}$, t_b is the burning time of the motor and m the mass of the propellant. Therefore, the unit of the specific impulse I_{sp} is N s kg^{-1} or m s^{-1}.

It is conventional to divide the specific impulse I_{sp} by g_0 (standard gravity, $g_0 = 9.81$ m s^{-2}) so that the resulting specific impulse I_{sp}^* has the unit s (seconds):

$$I_{sp}^* = \frac{I_{sp}}{g_0}$$

The specific impulse I_{sp}^* can also be defined according to the following equation with $\gamma = C_p / C_\upsilon$.

$$I_{sp}^* = \frac{1}{g} \sqrt{\frac{2\,\gamma\,R\,T_C}{(\gamma - 1)\,M}} \qquad\qquad \gamma = \frac{C_p}{C_\upsilon}$$

Table 4.13 summarizes the calculated propulsion parameters for aluminized formulations in which the Al content has been varied in order to achieve an oxygen balance that is close to zero (with respect to CO_2, see eq. 2). Table 4.13 contains the corresponding values for a AP/Al formulation for comparison as well. Finally, Table 4.14

Tab. 4.14 Specific impulses (solid rocket motor) of Al formulations calculated using different codes (EXPLO5 and ICT).

	$O_2N{-}O_2C{-}CO_2{-}NO_2 : Al$ $= 0.70 : 0.30$		$[NO]_2[O_2C{-}CO_2] : Al$ $= 80 : 20$		$AP : Al$ $= 0.70 : 0.30$	
formulation	**I**		**II**		**III**	
	EXPLO5	ICT	EXPLO5	ICT	EXPLO5	ICT
condition	isobaric		isobaric		isobaric	
p / bar	70		70		70	
ρ / g cm^{-3}	1.82		1.74		2.13	
Ω / %	-1.8		-0.5		-2.85	
I_{sp}^* / s						
frozen	223	206	220	215	243	229
equilibrium	226	245	225	230	247	257
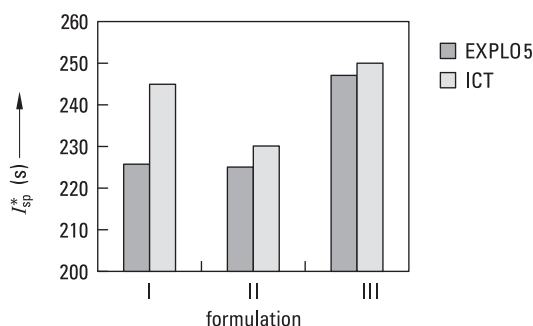
Fig. 4.6 Graphical representation of the calculated equilibrium specific impulses for the optimized formulations **I**: covalent $O_2N{-}O_2C{-}CO_2{-}NO_2$ / Al, **II**: ionic $[NO]_2[O_2C{-}CO_2]$ / Al and **III**: AP / Al (see Tab. 4.14).

shows the calculated specific impulses for equilibrium expansion for the three optimized formulations (covalent $O_2N{-}O_2C{-}CO_2{-}NO_2$ /Al, ionic $[NO]_2[O_2C{-}CO_2]$/ Al and AP /Al). The results of Table 4.14 are graphically summarized in Figure 4.6.

From Table 4.13 and Figure 4.6 we can conclude that generally the agreement between the EXPLO5 and ICT calculated equilibrium specific impulses is reasonably good with the ICT code always predicting a slightly better performance. It is further apparent that the formulation with covalent $O_2N{-}O_2C{-}CO_2{-}NO_2$ and Al results in better performance than the formulation using ionic $[NO]_2[O_2C{-}CO_2]$ and Al. The specific impulse of the chlorine and perchlorate-free formulation with covalent $O_2N{-}O_2C{-}CO_2{-}NO_2$ and Al (**I**) is just slightly lower than that of the AP/Al (**III**) formulation. Therefore it can be concluded that bis(nitronium) oxalate (or oxalic acid dinitrato ester), $O_2N{-}O_2C{-}CO_2{-}NO_2$, may be a promising new perchlorate-free and environmentally benign oxidizer for formulations to be used in solid rocket motors.
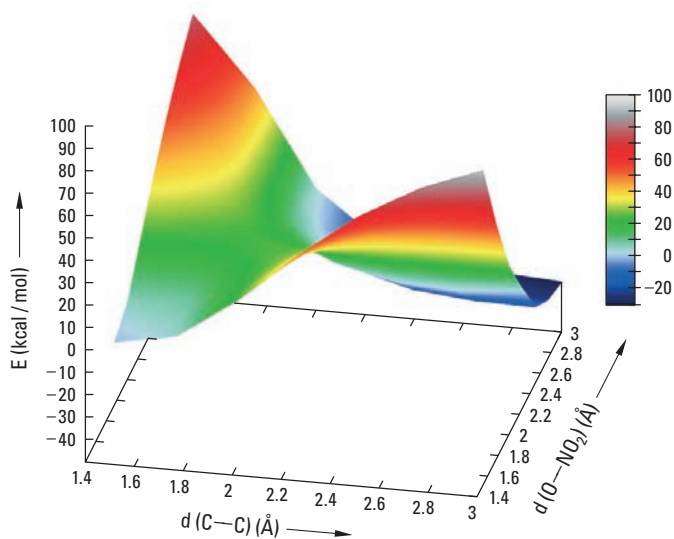
Fig. 4.7 Potential energy hypersurface for the simultaneous dissociation of O_2N—O_2C—CO_2—NO_2 into CO_2 and NO_2 at B3LYP/6−31G* level of theory.

The above discussion clearly revealed that the covalently bound oxalic acid dinitrate ester is the most promising candidate as a high oxidizer and potential replacement for AP in this series. In order to evaluate its thermodynamic and kinetic stability we calculated the decomposition into CO_2 and NO_2. The reaction enthalpy of $\Delta H = -56.5$ kcal mol^{-1} clearly indicates that oxalic acid dinitrate ester is (as expected) thermodynamically unstable with respect to its decomposition into CO_2 and NO_2.

$$O_2N\text{—}O_2C\text{—}CO_2\text{—}NO_2 \text{ (s)} \xrightarrow[\Delta H = -56.5 \text{ kcal mol}^{-1}]{} 2\ CO_2 \text{ (g)} + 2\ NO_2 \text{ (g)}$$
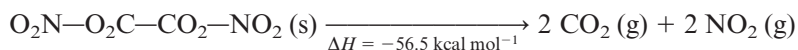
In order to evaluate the kinetic stability of covalently bound O_2N—O_2C—CO_2—NO_2 it was decided to compute a two dimensional potential energy hypersurface (Fig. 4.7) at B3LYP/6−31G* level of theory. As one can see, the simultaneous dissociation of O_2N—O_2C—CO_2—NO_2 into CO_2 and NO_2 has a relatively high activation barrier (Fig. 4.7). The transition state (Fig. 4.8) was located 37.1 kcal mol^{-1} (CBS-4M) above the dinitrate ester. It is interesting that in agreement with Hammond's postulates the transition state lies more towards the higher-energy starting material.

The electrostatic potential (ESP) of covalent O_2N—O_2C—CO_2—NO_2 was computed at the optimized structure at the B3LYP/6−31G(d) level of theory. Figure 4.9 shows the electrostatic potential for the 0.001 electron/bohr^3 isosurface of electron density evaluated at the B3LYP level of theory. The colors range from
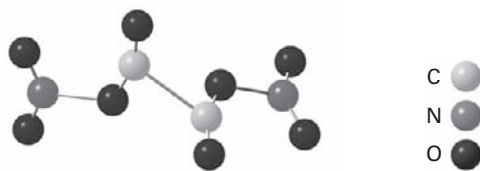
Fig. 4.8 Transition state structure for the simultaneous dissociation of $O_2N-O_2C-CO_2-NO_2$ into CO_2 and NO_2 at CBS-4M level of theory (NIMAG = 1, $v_1 = -817\ \text{cm}^{-1}$, $d(C-C) = 2.33\ \text{Å}$, $d(O-NO_2) = 1.91\ \text{Å}$).

−0.06 to +0.06 hartrees with green denoting extremely electron-deficient regions ($V(r) > 0.06$ hartree) and red denoting electron-rich regions ($V(r) < -0.06$ hartrees). It has recently been proven by Politzer, Murray et al. and extensively used by Rice et al. (see Ch. 8) [39−44] that the patterns of the computed electrostatic potential on the surface of molecules can generally be related to the sensitivity of the bulk material. The electrostatic potential at any point r is given by the following equation in which Z_A is the charge on nucleus A, located at R_A.

$$V(r) = \sum \frac{Z_A}{|R_A - r|} - \int \frac{\rho(r')}{|r' - r|}\, dr'$$

Politzer et al. were able to show that impact sensitivity can be expressed as a function of the extend of this anomalous reversal of the strengths of the positive and negative surface potentials. In most nitro ($-NO_2$) and nitrato ($-O-NO_2$) systems the regions of positive potential are stronger than the negative, contrary to the usual situation. This atypical imbalance between stronger positive regions and weaker negative regions can be related to the impact sensitivities. The calculated electrostatic potential of $O_2N-O_2C-CO_2-NO_2$ (Fig. 4.9) shows strong positive regions over the nitro ($-NO_2$) groups with the positive areas extending into the $O-NO_2$ region (oxygen$-NO_2$ bond). Furthermore, there is also a strong positive region over the relatively weak C$-$C bond. This is in good accord with the labile $O-NO_2$ and C$-$C bonds and also accounts for the easy bond cleavage. In comparison, free oxalic acid (Fig. 4.9) does not show any positive regions over the bonds in the molecule.

From this computational study the following conclusions can be drawn:

1. Covalently bound and ionic nitronium and nitrosonium oxalate were researched with respect to their potential use as energetic materials or oxidizers for solid rocket motors. None of these compounds can be expected to be a good high explosive. However, the covalent molecule oxalic acid dinitrate ester, $O_2N-O_2C-CO_2-NO_2$, was identified to be a potentially interesting oxidizer.
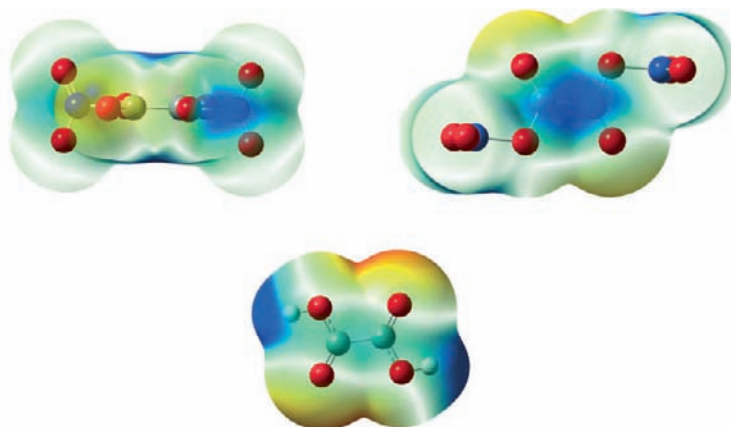
Fig. 4.9 Electrostatic potential of $O_2N-O_2C-CO_2-NO_2$ and oxalic acid (B3LYP/6$-$31G(d), 0.001 e bohr^{-3} isosurface, energy values -0.06 H to $+0.06$ H); color coding: red (very negative), orange (negative), yellow (slightly negative), green (neutral), turquoise (slightly positive), light blue (positive), dark blue (very positive).

2. The computed specific impulse of a $O_2N-O_2C-CO_2-NO_2$/Al formulation (80 : 20) is comparable to that of a conventional AP/Al (70 : 30) formulation, however, it is free of toxic perchlorate or any halogen.
3. Oxalic acid dinitrate ester, $O_2N-O_2C-CO_2-NO_2$ is metastable with respect to decomposition into CO_2 and NO_2. The reaction barrier (transition state) for the monomolecular dissociation was calculated to be 37 kcal mol^{-1} at CBS-4M level of theory.
4. The computed electrostatic potential of $O_2N-O_2C-CO_2-NO_2$ shows strong positive areas at the 0.001 s bohr^{-3} isosurface over the $O-NO_2$ and $C-C$ bonds indicating the relative weakness of the particular bonds.

The results obtained in this study should encourage synthetic work in order to prepare oxalic acid dinitrate ester, $O_2N-O_2C-CO_2-NO_2$ on a laboratory scale and to experimentally evaluate its properties, first and foremost its thermal stability.

4.2.5 Example: EXPLO5 Calculation of the Gun Propellant Properties of Single, Double and Triple Base Propellants

In order to elucidate the different properties of single, double and triple base gun propellants and to compare these values with the ones obtained for a new high-nitrogen propellant (e.g. NILE, see above), we calculated the relevant combustion parameters using the EXPLO5 code under the assumption of isochoric combustion. The results are summarized in Table 4.15.

Tab. 4.15 Computed (EXPLO5) gun propellant parameters for a single, double and triple base propellant in comparison with a new high-nitrogen formulation (isochoric conditions).

propellant	$\rho\,/$ g cm^{-3}	loading density / g cm^{-3}	$f_E\,/$ kJ g^{-1}	$b_E\,/$ cm^3 g^{-1}	$T_{comb.}\,/$ K	$p_{max}\,/$ bar	$N_2\,/$ CO
NC (12.5)	1.66	0.2	1.05	1.08	3119	2674	0.26
NC : NG (50 : 50)	1.63	0.2	1.21	1.02	3987	3035	0.59
NC : NG : NQ (25 : 25 : 50)	1.70	0.2	1.13	1.06	3256	2875	1.25
TAGzT : NC (85 : 15)	1.63	0.2	1.09	1.22	2525	2875	6.07

The general trend in terms of performance can clearly be seen in the calculated results shown in Table 4.15. While a double-base propellant performs much better than a single-base formulation (much higher force and pressure), the combustion temperature is also considerably higher (over 360 K) which causes increasing erosion problems. The triple-base propellant on the other hand shows performance in between the single- and double-base propellant while having a combustion temperature only slightly higher (137 K) than that of the single base propellant.

The experimental formulation of a new high-nitrogen propellant with 85 % TAGzT (triaminoguanidinium azotetrazolate) and 15 % NC has the lowest combustion temperature of all shown formulations (nearly 600 K below $T_{comb.}$ of the single-base propellant). Furthermore, the performance of the new high-nitrogen formulation can be expected to be similar (e.g. same maximum pressure as a triple-base propellant) to a triple-base propellant. Equally important, the $N_2\,/$ CO ratio of a triple-base propellant increases from 1.25 to 6.07. This, together with the significantly reduced combustion temperature should help to drastically reduce erosion problems. Initial field studies using TAGzT based propellants for large caliber (105 Howitzer) guns have indicated that the life-time of a gun barrel could possibly be increased by a factor of up to 4. This would justify the (still) higher cost for high-nitrogen formulations because of the increased life-time and therefore drastically reduced cost of the gun system.

5 Initiation

An explosive can be initiated using different stimuli (e.g. heat or shock) and can then either ignite, deflagrate and turn into a detonation, or directly detonate, if it is initiated using a strong shock (Fig. 5.1). The ignition occurs at an ignition temperature which is characteristic for individual substances, if the linear loss of heat of the surroundings is smaller than the heat generated through the exothermic reaction.
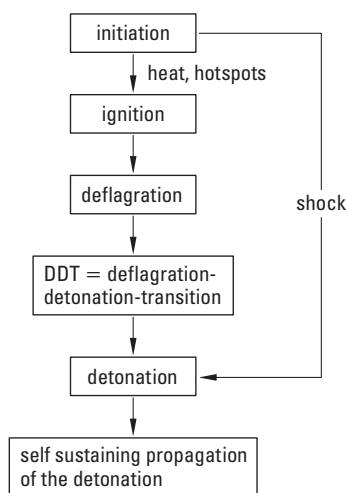
Fig. 5.1 Transition from initiation to detonation.

Generally, it can be said that the **initiation** of explosives is mostly a **thermal process**. However, the ignition (initiation) of an explosive can also occur by impact linking-via the low frequency vibrational modes (doorway modes) between 200 and 600 cm^{-1}. In cases where the initiation occurs through a shock-wave, we also observe strong warming-up through adiabatic compression. If mechanical (impact, friction) or electrostatic (ESD) mechanisms are the cause, it can be assumed, that the mechanical or electric energy is also first converted into heat. This occurs, for example, during the formation of so-called **hotspots**. Here, there are small gas bubbles $(0.1-10 \text{ μm})$, which are then strongly heated (up to $900\,°C$) as well through adiabatic compression and therefore initiate the explosive. These can either be gas bubbles in liquids or in solids. The larger the difference in pressure between the original pressure (p_1) and the final pressure on compression p_2, the higher the jump in temperature:

$$T_2 = T_1 \left(\frac{p_2}{p_1} \right)^{\frac{\gamma-1}{\gamma}}$$

Another type of possible hotspots are small, very hard crystals or crystal needles. Prior to breaking the crystal, energy must be applied either through friction or through pressure, in order to bring charges of the same sign closer together. This energy is released again on breaking of the crystals and can result in the formation of a hotspot. However, not every hotspot results in an ignition and finally in detonation. When e.g. the energy is released to the surroundings without resulting in an initiation. Generally it can be said, that the temperature in a hotspot must be at least 430 °C, in order to be sufficient enough to cause the initiation of a secondary explosive. Consequently, explosives with melting points below 430 °C can not be initiated by hotspots. On the other hand, liquids (e.g. NG) can be initiated through hotspots (gas bubbles of dissolved gases) as well through adiabatic compression. On average hotspots exist only for $10^{-3}-10^{-5}$ s.

When crystals rub together, hotspots can form only through **friction**, as a result of the friction heat and the (in comparison to metals) low heat conductivity.

Usually it is assumed, that on **impact** most primary explosives are initiated by hotspots from inter-crystalline friction. For secondary explosives, as a general rule, initiation by impact results in the formation of hotspots, which originate (adiabatic compression) from gas bubbles between the crystals. Such hotspots only exist for approximately 10^{-6} s.

The thermal energy of hot spots must be efficiently transferred to appropriate molecular vibrational modes, a process called "up-pumping", if bond-breaking and subsequent exothermic decomposition and detonation are to be achieved. The term "trigger linkage" has been applied to the key bond or bonds that are initially ruptured. Any dissipation of hot spot energy, for instance by diffusion, will lessen the likelihood of these processes. Thus Kamlet suggested that free rotation around the trigger linkage (e.g. $C-NO_2$, $N-NO_2$, $O-NO_2$ can have a desensitizing effect, since it uses energy that could otherwise go into bond-breaking vibrational modes. Furthermore, Kamlet recognized the significance of decomposition steps that follow the initial bond rupture, for example the autocatalysis (by NO_2 radicals) for the decomposition of nitramines.

The fact that solids composed of very small particles are less sensitive can now be explained on the grounds that these will have smaller hot spots and thus require higher temperatures for ignition.

It should also be noted that initiation of detonation can occur even in a homogeneous (defect-free) solid (which doesn't really exist). This can occur, for example, if there is efficient anharmonic coupling to channel energy from lattice into the critical molecular vibrations.

Finally, let us consider the situation in TATB which is well known for its remarkable insensitivity. An outstanding feature of TATB is the strong and extensive hy-

drogen bonding, both inter- and intramolecular, between the NO_2 and NH_2 groups. This would be anticipated from its molecular structure, and has been confirmed by X-ray diffraction. The intermolecular H-bonding gives rise, in the solid, to a two-dimensional network, to which is attributed the relatively high thermal conductivity of TATB. In terms of the hot spot concept, this is a desensitizing factor, since it results is a more rapid dissipation of their energy through thermal diffusion. This is also a reason why TATB requires a high ignition temperature. On the other hand, the strong intermolecular H-bonding should increase the NO_2 rotational barrier, an expectation for which DFT calculations provide support. By Kamlet's reasoning (see above), this should have a sensitizing effect, since it diminishes the loss of energy through rotation and makes more of it available for the key NO_2 vibrational modes. It is believed that $C\text{-}NO_2$ homolysis is the first or one of the first steps in TATB initiation.

6 Experimental Characterization of Explosives

6.1 Sensitivities

As we have seen in the previous chapter, energetic materials are often initiated using thermal processes. However, the explosion stimuli could also come from mechanical or electrostatic sources. Therefore, it is important to know the exact sensitivities for explosive compounds. The important values that have to be determined are:

1. the impact sensitivity
2. the friction sensitivity
3. the electrostatic sensitivity (ESD) and
4. the thermal sensitivity

Testing the response of solid, liquid or pasty substances to impact, friction and thermal stimuli is required in various standards such as EEC, Official Journal of the European Communities as well as UN Recommendations on the Transport of Dangerous Goods, 13.4.2 Test 3(a)(ii) BAM drop hammer.

The **impact sensitivity** of solid, liquid or gelatinized explosives is determined by using the drophammer method. The drophammer essentially consists of a cast steel block with a cast base, a round anvil, a column fixed at the steel block, hardened, smoothed guide bars and the drop weight with retaining and releasing device. The heavy iron block is essential in order to adsorb the shock waves caused by the falling weight. Both guide bars are attached to the column with three brackets. An adjustable metre rule allows an exact measurement of the drop height.

In this test the sample (approx. 40 mg) to be investigated is placed in the plunger assembly, consisting of two steel rollers, a hollow steel collar and a centering ring for fixation (Fig. 6.1). The assembly is placed onto a small anvil. The impact energy (energy = work $\times$ distance = mass $\times$ acceleration $\times$ distance) can be varied by changing the drop-height (approx. $0.1-1$ m) and the mass (approx. $0.1-10$ kg). The minimum impact energy is determined by looking at which one had at least one out of five samples explode. It is important that while determining the impact sensitivity of crystals the size of the crystals must be given; smaller crystals are generally less impact sensitive than larger crystals of the same substance.

In order to determine the **friction sensitivity** according to the BAM regulations, the sample is placed onto a rough porcelain plate ($25 \times 25 \times 5$ mm). This plate is
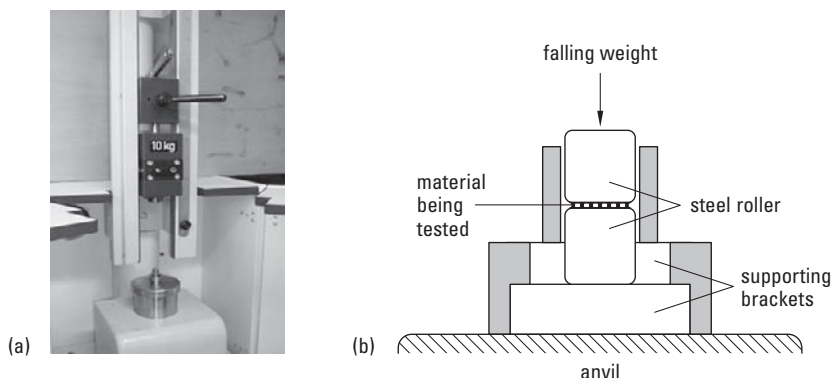
Fig. 6.1 Drophammer in accordance with the BAM (a) and detailed sketch of the drop-hammer test with the two steel rollers, a hollow steel collar and a centring ring for fixation (b).
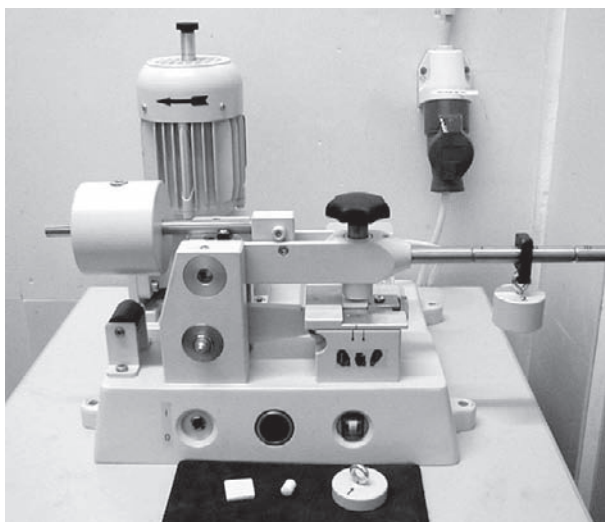
Fig. 6.2 Friction tester according to BAM regulations.

clamped onto the moving platform of the friction apparatus (Fig. 6.2). The friction force between the moving porcelain plate and a static porcelain peg (10×15 mm) (curvature radius 10 mm) causing sample initiation is determined. A set of 13 weights supplied with the instrument allow to achieve friction forces in the range of $0.5-360$ N (*N.B.* The force applied (at end points of the lever) is proportional to the ratio of the length of the lever arm measured between the fulcrum and application point of the force applied at each end of the lever. This test method is applicable both for sensitive primary explosives and less sensitive high explosives. The porcelain plate moves back and forth under the porcelain peg. The minimum

Fig. 6.3 Electrostatic test equipment.

force of friction is determined. During this process at least one sample out of six ignites, turns black, makes a cracking sound or explodes. As discussed above for the impact sensitivity, before determining the friction sensitivity, the sample should be sieved in order to perform the test on a sample with a uniform and defined crystal size.

Electrostatic discharge is one of the most frequent and the least characterized cause of accidental explosions of energetic materials. It is therefore imperative in R&D, manufacture, processing, loading or demilitarization to have reliable data on electrostatic spark sensitivities of energetic materials. The **electrostatic sensitivity** (electrostatic discharge sensitivity, ESD) is determined by using an ESD test apparatus. Different spark energies (usually between 0.001 and 20 J (Fig. 6.3) can be applied, by using variable capacitive resistances C (in Farad, F) and loading voltages V (in Volt, V):

$$E = \frac{1}{2} C U^2$$

This is a particularly important test for the safe handling of explosives since the human body can be electrically charged (depending on the type of clothing worn and humidity etc.) which on discharge can cause spark formation. Typical values for the human body are:

$$C = 0.0001 - 0.0004 \; \mu F$$
$$U = 10000 \; V$$
$$E = 0.005 - 0.02 \; J.$$
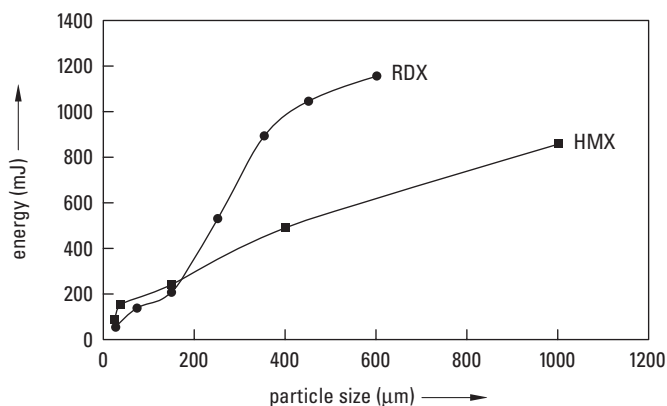
Fig. 6.4 Dependence of the ESD sensitivity on the particle size for hexogen (RDX) and octogen (HMX).

Tab. 6.1 Values for the impact, friction and electrostatic sensitivities of some primary and secondary explosives.

explosive	impact sensitivity / J	friction sensitivity / N	ESD sensitivity / J
primary explosive			
$Pb(N_3)_2$	2.5−4	0.1−1	0.005
secondary explosive			
TNT	15	> 353	0.46 − 0.57
RDX	7.5	120	0.15 − 0.20
β-HMX	7.4	120	0.21 − 0.23
PETN	3	60	0.19
NQ	> 49	> 353	0.60
TATB	50	> 353	2.5 − 4.24

As is shown in Figure 6.4, the ESD values are greatly influenced by the particle size; in these tests the sample must be carefully sieved prior to measuring. The finer the powder of a particular sample is, the higher the ESD sensitivity values are. Usually, compounds with ESD < 0.1 J are classified as sensitive, those with ESD > 0.1 J as insensitive.

Table 6.1 shows a summary of typical values for the impact, friction and electrostatic sensitivities of some primary and secondary explosives.

In accordance with the UN guidelines for the transport of dangerous/hazardous goods, the substances in Table 6.2 have been classified based on their impact and friction sensitivities.

For the thorough classification of a substance (which is necessary for safe handling), the **thermal stability** must also be determined. The first indication of the thermal stability of energetic compounds or formulations can be obtained from DSC data (see Fig. 2.19, Ch. 2.5.2). The so-called steel-sleeve test (or Koenen test)

Tab. 6.2 UN classification for the transport of dangerous goods.

	impact sensitivity / J	friction sensitivity / N
insensitive	> 40	> 360
less sensitive	35−40	ca. 360
sensitive	4−35	80−360
very sensitive	< 4	10− 80
extremely sensitive		< 10
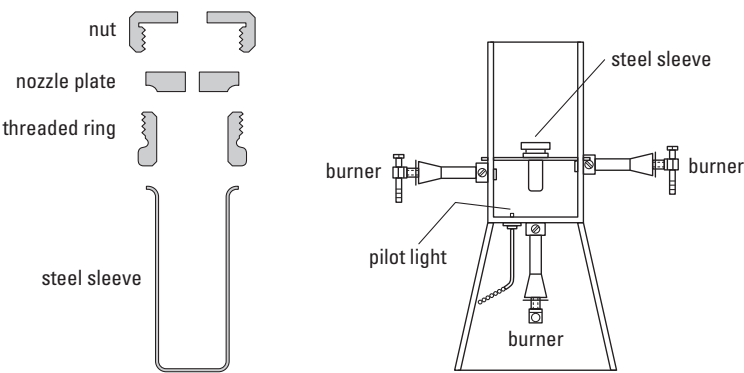
Fig. 6.5 Schematic construction of a steel sleeve test.
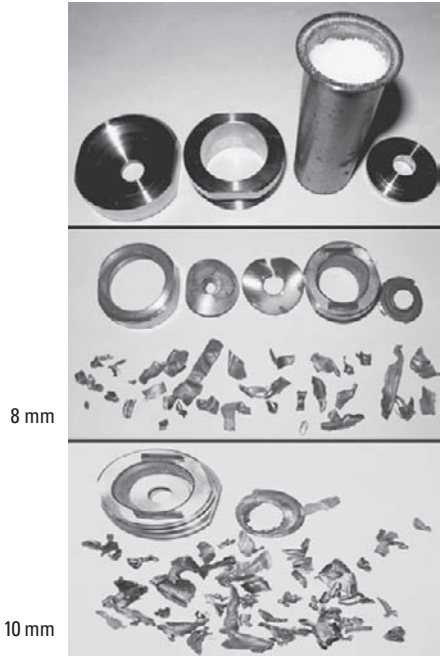
Fig. 6.6 Results of steel sleeve tests for a new explosive with 8 and 10 mm holes in the nozzle plate.

Tab. 6.3 UN hazard classification.

UN classification	hazard potential
1.1	mass detonation with possible formation of fragments
1.2 (18)	no mass detonation, whereby most fragments land within the stated distance (in m)
1.2 (12)	
1.2 (08)	
1.2 (04)	
1.3	mass fire
1.4	moderate fire

is used particularly for assessing the transport safety. In this test, the substance is filled into a steel sleeve (internal diameter: 24 mm, length: 75 mm, wall thickness: 0.5 mm, $V = 25$ mL) up to a height of 15 mm beneath the top edge and then the sleeve is closed with a nozzle plate. Nozzle plates are available with an orifice of $1.0-20$ mm. The steel sleeve is attached to the nozzle plate with a two-part threaded socket. It is then heated simultaneously by four burners. By varying the orifice diameters, the critical diameter can be determined. It is the diameter at which the pressure increase on burning and the subsequent explosion destroys the sleeve into at least four small splinters. Figure 6.5 schematically shows, the construction of a steel sleeve test and Figure 6.6 shows the results of some tests.

According to UN guidelines, all energetic materials can be divided into four main categories based on their potential danger/hazard. These UN classifications are summarized in Table 6.3.

6.2 Long-Term Stabilities

Simple **DSC measurements** (Differential Scanning Calorimetry) are an ideal method to quickly investigate the thermal stability of a substance while only using very small quantities of substance, which is particularly important when dealing with dangerous samples. During the DSC measurements, heating rates of $5\,°C$ min^{-1} are commonly used to give an initial indication of the thermal stability and decomposition temperature (see Ch. 2.5.2). However, it is necessary to research the long-term stability by using additional measurements. In this context, the so-called isotherm safety calorimeter can be used for example. They can investigate the thermal stability of a substance at a certain temperature (e.g. $30\,°C$ below the decomposition temperature) for 48 hours or longer. In isoperibolic long-term evaluations (approximately isothermal; heat exchange), the stability of substances or mixtures of substances in a sample cell (RADEX cell) can be investigated, with or without an additional pressure sensor.
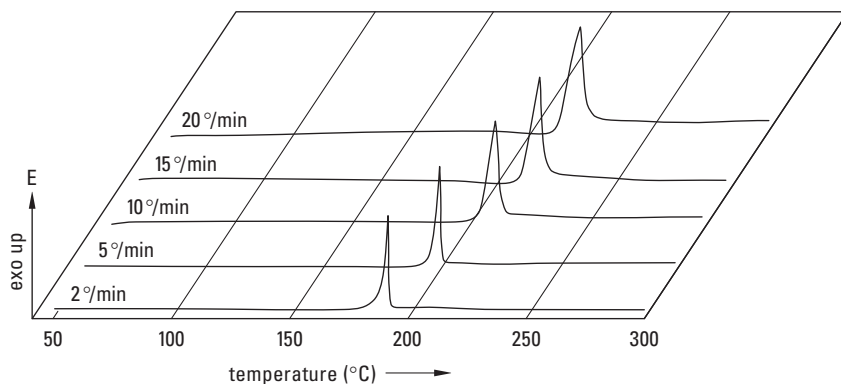
Fig. 6.7 DSC plot for ammonium 1-methyl-5-nitriminotetrazolate using different heat rates (up = exo).
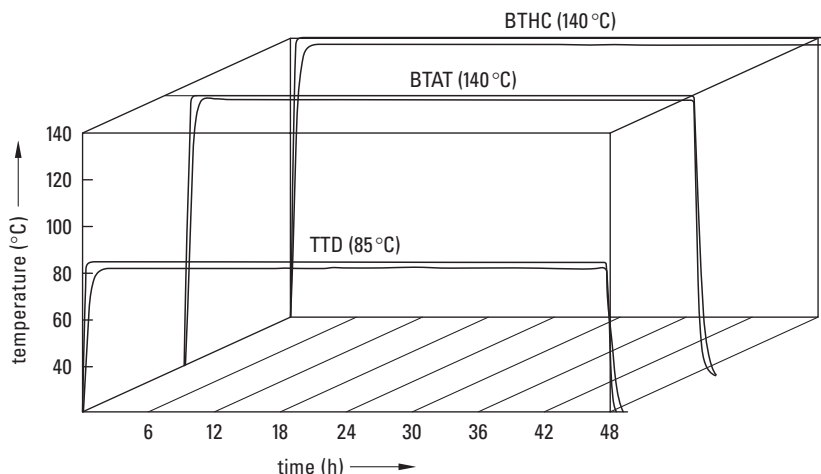
Fig. 6.8 Isothermal long-term measurement (48 h) for TTD, BTAT and BTHC without decomposition.

Figure 6.7 shows an example of DSC plots of a highly energetic material (ammonium 1-methyl-5-nitriminotetrazolate) using different heat rates, while Figure 6.8 shows the long-term stability of various other compounds in a **FlexyTSC** safety calorimeter.

For the unambiguous determination of the thermal stability of a substance or mixture of substances, it is generally necessary to determine the heat flow rate P (in $\mu W\ g^{-1}$). The substance can be considered to be thermally stable at a certain temperature, if the heat flow corresponds to a value not higher than $300\ \mu W\ g^{-1}$ over a time period of 7 days. Figure 6.9 shows an example of such an investigation for diaminotetrazolium nitrate (HDAT nitrate, Fig. 6.10) at a temperature of $89\ °C$. Here it can be observed that the substance is thermally stable at this temperature.
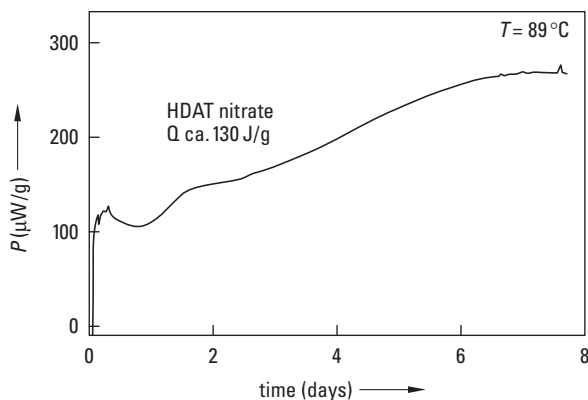
Fig. 6.9   Heat flow for HDAT nitrate at 89 °C.
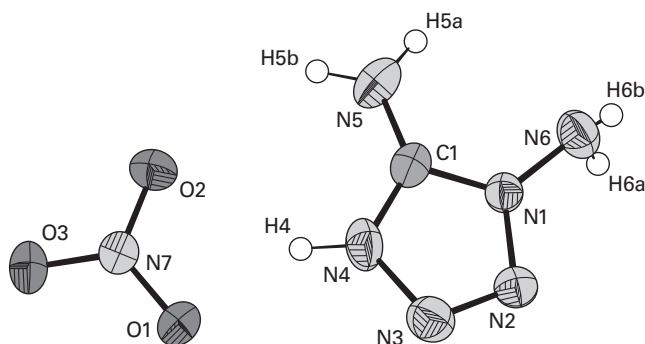
Fig. 6.10   Molecular structure of HDAT nitrate.

The so-called **Kneisl-Test** is a simple method which can be used for the estimation of the long-term thermal stability, particularly for primary explosives. A defined quantity (e.g. 100 mg) of the substance under investigation is air sealed in a glass ampoule. This ampoule is then placed in an oven for 100 h at the temperature for which thermal stability should be determined. The ampoule is then opened, the remaining mass of substance weighed and any gaseous decomposed products which may have been formed are analyzed (IR, MS, GC-MS). In order to "pass" the test, the mass lost due to decomposition should not exceed 2 % of the original sample mass.

6.3 Insensitive Munitions

The term insensitive munition (IM) is used to describe munition which is particularly safe to handle and which is difficult to initiate accidentally, but at the same

Tab. 6.4 Categories for insensitive munition.

	German	English
NR	Keine Reaktion	No reaction
V	Abbrand	Burning
IV	Deflagration	Deflagration
III	Explosion	Explosion
II	Teilweise Detonation	Partial detonation
I	Vollständige Detonation	Detonation

Tab. 6.5 IM tests.

scenario	IM test	test procedure	allowed response for IM (see Tab. 6.4)
small arms attacks	BI	attack (bullet impact) with three 12.7 mm bullets with 850 m s^{-1}	V − burning
fragmenting munitions attacks	FI	attack with five 16−250 g-fragments with 2530 m s^{-1}	V − burning
magazine, store, plane, ship or truck in fuel fire	FCO	fast cook-off-test, simulation of a fuel fire (s. Fig. 6.11)	V − burning
fire in adjacent magazine, store or vehicle	SCO	slow cook-off-test (SCO) with a heat rate of 3.3 °C/h	V − burning
shaped charge weapon attack	SCI	impact of a shaped charge between 50 und 62 mm	III − no detonation
detonation in magazine, plane, truck etc.	SR	reaction to detonation of a neighboring charge (sympathetic reaction)	III − no detonation
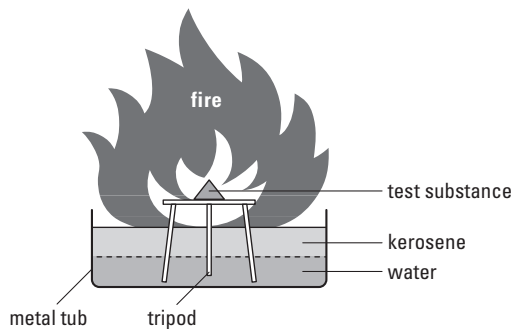
Fig. 6.11 Simple construction of an FCO test (fast cook-off test).

time has the power and reliability to fulfil the requirements necessary to complete the mission. The insensitivity of munition can be tested and classified into six categories (Tab. 6.4).

Six tests are performed on each substance in order to classify them into one of these categories. The results of these tests can range from "no reaction" to "complete detonation". Those tests are briefly summarized in Table 6.5.

Since this area is so important, NATO has founded a Munitions Safety Information Analysis Center (MSIAC).

6.4 Gap Test

In the so-called gap test the sensitivity towards shockwaves is determined [36]. The apparatus for the gap test (Fig. 6.12) is used to measure the ability of a material to propagate a detonation by subjecting it to a detonating booster charge under confinement in a polycarbonate tube. The gap test enables the determination of the minimum shock wave pressure that can cause complete detonation of the tested explosive. The explosive under investigation is subjected to the action of the shock wave of a known pressure. Such a wave is generated by a booster and a shock wave pressure attenuator. Whether or not the shock wave causes the complete detonation of the explosive can be concluded on the basis of the mechanical effects produced after the detonation of the explosive: hole cutting in a steel plate, dent depth in a witness steel block or compression of a copper cylinder. In this test, the gap medium (usually water) stops flying particles and direct heat transmission, serving as a heat filter. Consequently, the shock wave is the only energy transmitted to the explosive. If other factors are constant, the possibility of the transmission
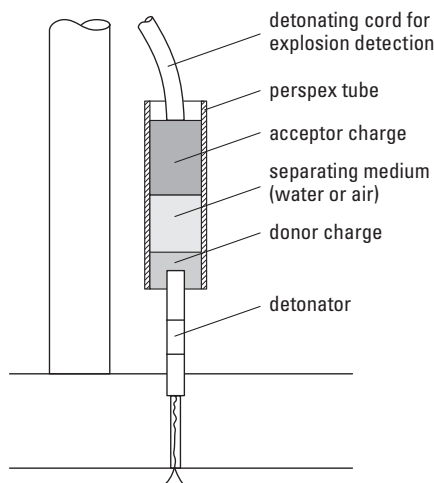
Fig. 6.12   Schematic set-up of a gap test.

of the detonation is determined mostly by both the sensitivity of the acceptor charge and by the initiating strength of the donor charge. The gap test method is based on the determination of the distance between the donor and the acceptor charge of given masses at which transmission or failure of detonation occurs.

Figure 6.12 schematically shows the set-up of the gap test. Typical values for the donor charge are 10 g RDX (with 0.6 g PETN detonator). The medium is water (or alternatively air), the confinement is a Plexiglass tube of approx. 20 mm diameter. With such an experimental set-up, values for the initiation limits are approx. 25−27 mm for PA and 21−23 mm for Tetryl. In contrast, the value for TNT (less impact sensitive) is only 7−8 mm. The extremely insensitive compound FOX-12 only shows a response at 2 mm under similar conditions.

6.5 Classification

If new energetic materials are synthesized in a research laboratory and are sent to other institutes for further analysis, various stability tests have to be carried out, so that the materials can initially be classified (IHC, **interim hazard classification**) as being at least hazard class "1.1 D" (see Ch. 6.1). The requirements to "pass" the

Tab. 6.6 Required UN tests 3a−3d to obtain an IHC (interim hazard classification).

UN test	test	conditions	+
UN 3a	impact sensitivity	5 tests; positive, if 50 % of the tests give positive results	≤ 3.5 J
UN 3b	friction sensitivity	5 tests; positive, if one out of five test is positive	≤ 184 N, visible sparks, visible flames, explosion heard, clear crackling noise
UN 3c	thermal stability	75 °C, 48 h	visible examination: − color change, − explosion, − ignition (burning) weight loss (except adsorbed moisture) RADEX: self-heating max. 3 °C (RADEX, see Ch. 6.2)
UN 3d	small-scale-burning test (see Fig. 6.13)	sawdust soaked in kerosene, not confined	explosion or detonation
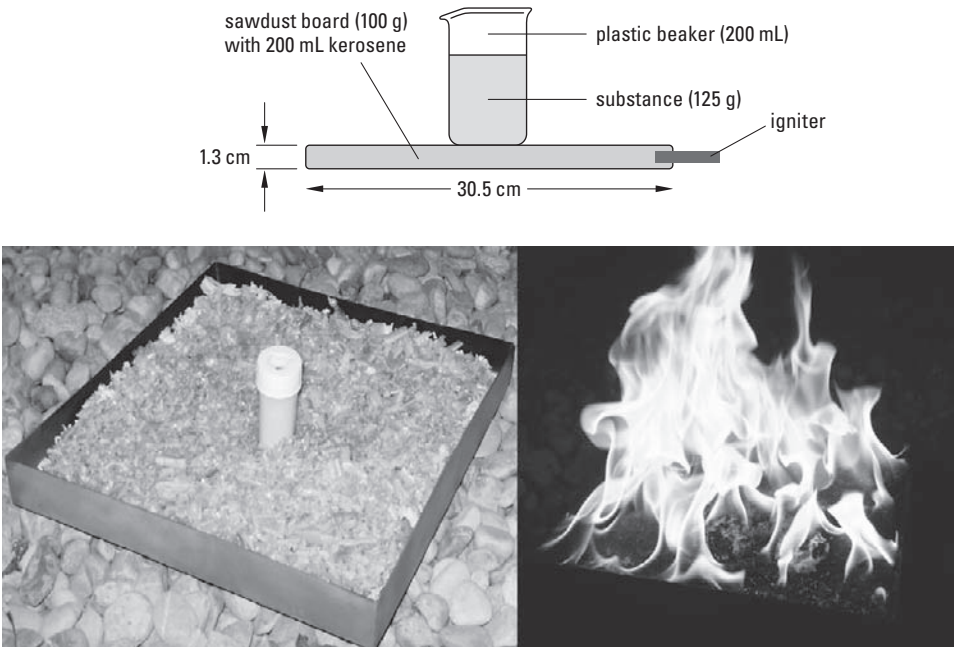
Fig. 6.13   Experimental set-up for a small-scale-burning test (UN 3d).

Tab. 6.7   UN tests 4a and 4b(ii) to establish an IHC (interim hazard classification).

UN test	test	conditions	+
UN 4a	thermal stability of packed and unpacked energetic materials	75 °C, 48 h	visible examination: − color change, − explosion, − ignition (burning) weight loss (excluding adsorbed moisture) RADEX: Self-heating max. 3 °C (RADEX, see Ch. 6.2)
UN 4b(ii)	free fall from 12 m height	12 m free fall (see Fig. 6.14)	fire, explosion or detonation (damage of the packaging does not count as a "fail")
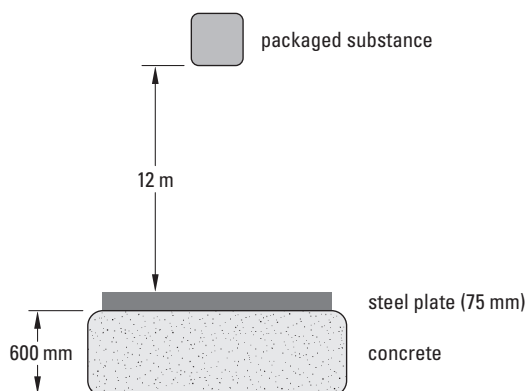
Fig. 6.14 Set-up for the free fall test (UN 4b(ii)).

necessary tests (UN 3a−UN 3d) are summarized in Table 6.6. A positive test results (+) means that the substance did *not* pass the test.

If a sample does not pass test 3c, but is shown to be thermally stable using a DSC, test 4a must additionally be performed. If the substance is thermally unstable, it can not be transported. In the case of a sample not passing tests 3a, 3b or 3c, test 4b(ii) must be performed (Tab. 6.7). A preliminary transportation certificate can then only be issued if the sample passes tests 3a−3d or 4a and 4b(ii).

7 Special Aspects of Explosives

7.1 Shaped Charges

A **shaped charge** is an explosive charge which is shaped to focus the effect of the explosive's energy [37]. In contrast to an explosion of a solid cylindrical explosive charge which creates a relatively wide but only moderately deep crater (Fig. 7.1), a shaped charge consisting of a solid cylinder of explosive (with rotational symmetry) with a conical hollow in one end and a central detonator causes a much deeper though narrower crater (Fig. 7.1). A shaped charge with a metal-lined conical cavity (e.g. Cu or W liner) creates an even deeper and narrower crater (Fig. 7.1). The extremely high pressure generated by the detonation of the explosive drives the liner contained within the hollow cavity inward whereby it collapses upon its central axis. The resulting collision forms and projects a high-velocity jet of metal forward along the axis (see Fig. 7.2). Most of the jet material originates from the innermost layer of the liner and remains below the melting point solid in the jet. A typical modern lined shaped charge can penetrate armor steel to a depth of seven or more times the diameter of the charge's cone.

Ideally, the liner consists of a malleable metal of high density. For this reason copper is most commonly used. Tungsten and tantalum are also in use because of their extremely high densities, while depleted uranium, though in use for kinetic energy munition (see below) has not found widespread application as liner material for shaped charges. The pyrophoric effects of tantalum (and DU) further enhance the damage caused by the lined shaped charge after penetrating the armor steel.
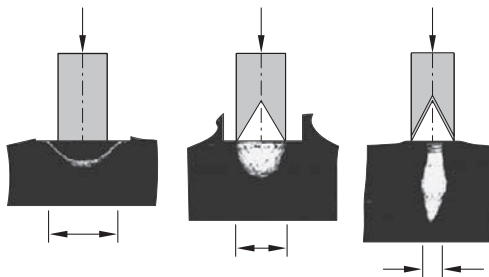
Fig. 7.1 Conventional cylindrical explosive charge, shaped charge, shaped charge with metal liner.
(This diagram is reproduced with slight modification from the original of Prof. Dr. Manfred Held, who is herewith thanked for his permission to reproduce this.)
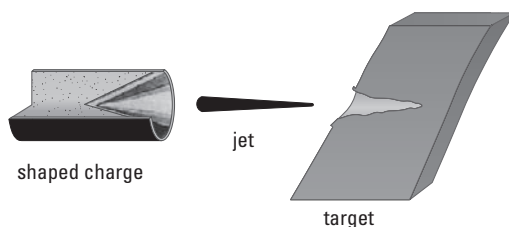
Fig. 7.2 Jet formation from a metal-lined shaped charge.
(This diagram is reproduced with slight modification from the original of Prof. Dr. Manfred Held, who is herewith thanked for his permission to reproduce this.)

The velocity of the jet depends on the brisance of the high explosive used and the internal apex angle of the metal liner. The smaller the angle is, the higher is the velocity of the jet. But very small angles can result in jet bifurcation or even failure of the jet to form at all. For this reason a "good" compromise needs to be found (usually $40-90°$). In any case, most of the jet formed moves at hypersonic speed with its tip reaching speeds of up to $7-12 \text{ km s}^{-1}$, the tail at a lower velocity of $1-3 \text{ km s}^{-1}$ and the slug at still lower velocity ($< 1 \text{ km s}^{-1}$). The high velocity of the jet combined with the high density of the material of the metal liner gives the jet a very high kinetic energy. When the jet hits the target, a very high pressure is formed as a result. A typical jet velocity of 10 km s^{-1} results in a pressure of about 200 GPa. The penetration process therefore generates enormous pressures, and therefore it may be considered to be hydrodynamic (Fig. 7.3). At such a pressure the jet and armor may be treated like an incompressible fluid (if their material strengths are ignored) in order to get a good approximation so that the jet penetrates the target (armor steel plate) according to the laws of hydrodynamics like a liquid (Fig. 7.3). The general penetration behavior of a projectile as a function of its velocity is shown in Table 7.1.

Since the jet needs some time and space to fully form, most shaped charges have a long ballistic cap to guarantee the correct standoff distance. When the ballistic

Tab. 7.1 Penetration behavior of a projectile as a function of its velocity.

velocity of projectile (km s^{-1})	effect	launch method
< 50	elastic, plastic	mechanical, air rifle
50– 500	plastic	mechanical, air rifle
500– 1 000	plastic or hydrodynamic, target material appears to be very viscos	powder gun
3 000–12 000	hydrodynamic, target material appears to be liquid	explosive acceleration
> 12 000	explosive, evaporation of the colliding solids	explosive acceleration
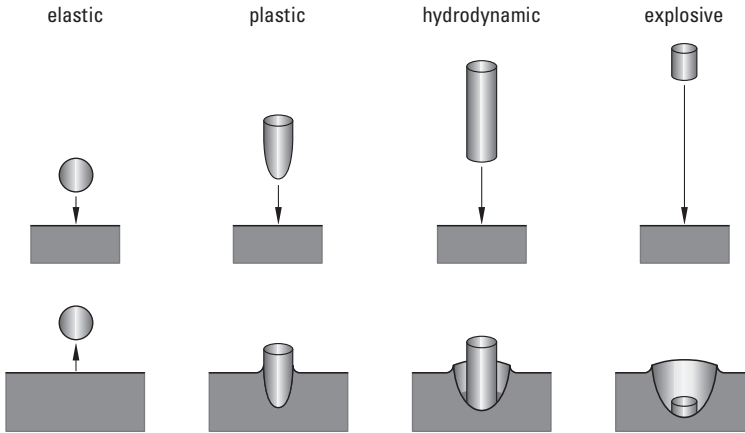
Fig. 7.3 Penetration behavior: elastic, plastic, hydrodynamic, explosive.
(This diagram is reproduced with slight modification from the original of Prof. Dr. Manfred Held, who is herewith thanked for his permission to reproduce this.)
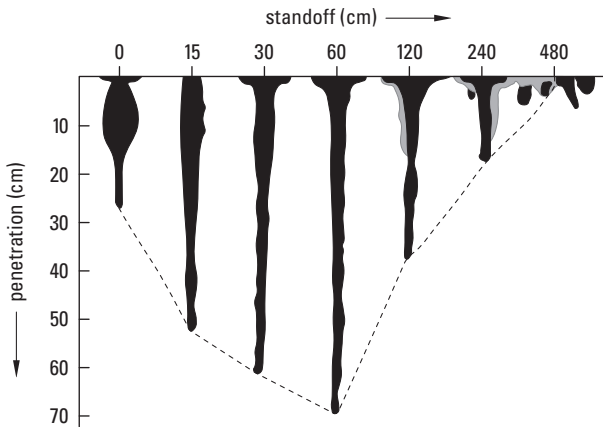
Fig. 7.4 Influence of the standoff distance on the penetration depth of a typical shaped charge with metal liner (diameter: 10 cm, length: 18 cm).
(This diagram is reproduced with slight modification from the original of Prof. Dr. Manfred Held, who is herewith thanked for his permission to reproduce this.)

cap hits the target the main charge gets detonated while still being at sufficient (for the jet formation) distance from the target surface. If, however, the standoff distance is too large, the jet stretches (due to different tip and tail velocities) and eventually breaks up into particles which dramatically lowers the penetration depth. Figure 7.4 shows the influence of the standoff distance on the penetration depth for a typical metal-lined shaped charge (diameter: 10 cm, length: 18 cm).
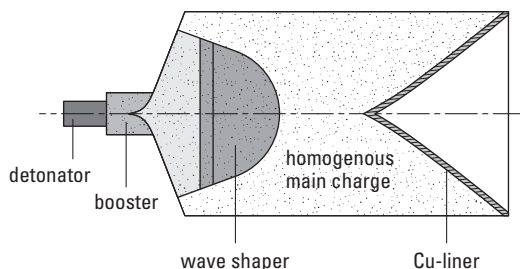
Fig. 7.5 Schematic design of a shaped charge with metal liner and wave shaper.
(This diagram is reproduced with slight modification from the original of Prof. Dr. Manfred
Held, who is herewith thanked for his permission to reproduce this.)
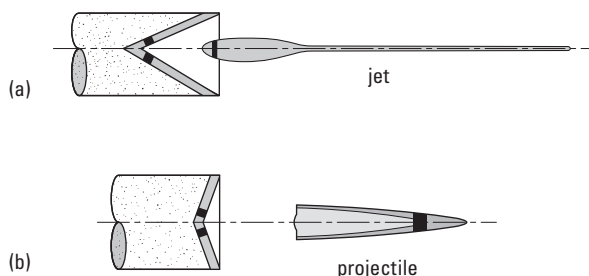
Fig. 7.6 Comparison between a shaped charge (a) and an explosively formed projectile (b).
(This diagram is reproduced with slight modification from the original of Prof. Dr. Manfred
Held, who is herewith thanked for his permission to reproduce this.)

Because of the extremely high jet velocity the (low) speed with which the shaped
charge travels towards its target is relatively unimportant. For this reason, relatively
slow and repercussion-free projectiles are often used to carry the shaped charge.
The advantage of such systems is that they do not require a big and heavy launch
platform which makes the entire system more mobile. Shaped charges are fre-
quently used as warheads in anti-tank missiles and also as gun-fired projectiles,
rifle grenades, mines, bomblets, torpedos and as various types of air-, land- or sea-
launched guided missiles. Figure 7.5 shows the schematic design of a shaped charge
with a metal liner.

Wide angle cones and other liner shapes such as plates or dishes with apex angles
greater than 100° do not jet, but instead give an **explosively formed projectile or
explosively formed penetrator (EFP)** (Fig. 7.6). The projectile forms through dy-
namic plastic flow and has a velocity of $1-3$ kms^{-1}. Target penetration is much
smaller than that of a jet, but the hole diameter is larger with more armour back-
spall.

An EFP uses the action of the explosive's detonation wave (and to a lesser extent
the propulsive effect of its detonation products) to project and deform a plate or
dish of ductile metal (such as copper or tantalum) into a compact, high-velocity
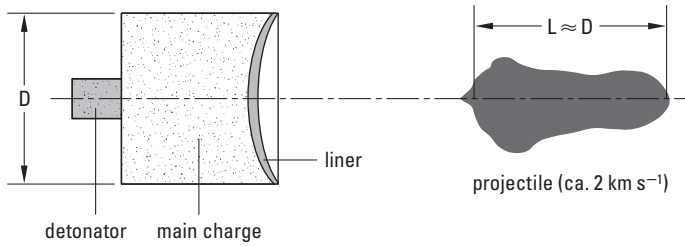
Fig. 7.7 Schematic design of a charge to generate an explosively formed projectile (EFP). (This diagram is reproduced with slight modification from the original of Prof. Dr. Manfred Held, who is herewith thanked for his permission to reproduce this.)
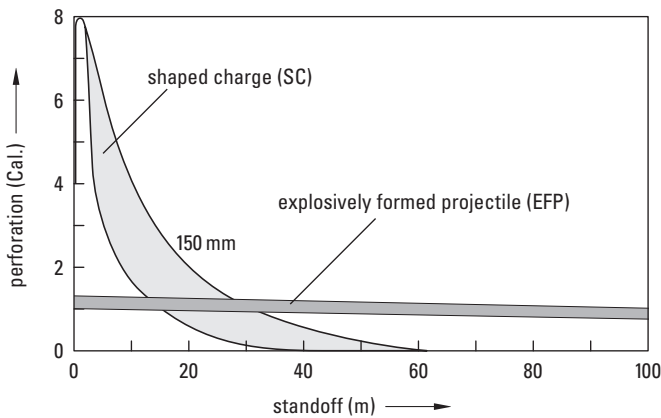
Fig. 7.8 Influence of the standoff distance on the perforation depth for shaped charges (SC) and explosively formed projectiles (EFP).
(This diagram is reproduced with slight modification from the original of Prof. Dr. Manfred Held, who is herewith thanked for his permission to reproduce this.)

projectile, commonly called the slug (Fig. 7.7). This slug (one projectile with homogeneous velocity) is projected towards the target at about two kilometers per second. The main advantage of the EFP over a conventional shaped charge is its effectiveness at very large standoff distances, which is equal to hundreds of times the charge's diameter (perhaps a hundred meters for a practical device) (Fig. 7.8).

A **fragmenting warhead** is a special type of shaped charge or device that explosively forms projectiles. In such a device many EFPs of the shape of cones or cups are combined into one multi-projectile warhead (Fig. 7.9). Such devices which send out the projectiles in a cylindrical geometry are particularly suitable for targets in the air.

A further strategy to penetrate or perforate a target is the use of so-called **kinetic energy (KE) munition**. In this context the term "kinetic energy" indicates that the

cones   cups   fragmentation charge
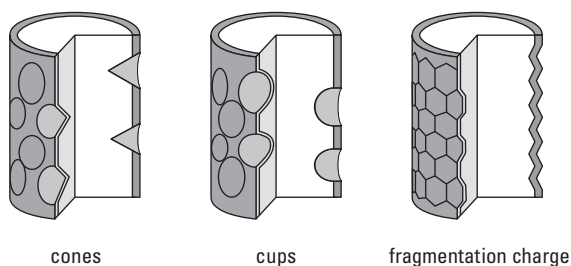
Fig. 7.9 Schematic presentation of a multi-projectile warhead.
(This diagram is reproduced with slight modification from the original of Prof. Dr. Manfred Held, who is herewith thanked for his permission to reproduce this.)

destructive energy of the munition originates from its high kinetic energy ($T = \dfrac{1}{2} mv^2$). For this reason, a high mass (m) and a high velocity (v) of the penetrator are desirable. The Bernoulli equation shows the relationship between the penetration depth (P) and the length of the penetrator (L) with the densities of the penetrator (ρ_P) and the target (ρ_T):

$$P \sim L \sqrt{\frac{\rho_P}{\rho_T}}$$

The constant η depends on the velocity of the penetrator (v_P). For a typical penetrator velocity of 1600 m s^{-1} the constant η is about 0.66:

$$P = \eta L \sqrt{\frac{\rho_P}{\rho_T}} = 0.66 \times L \sqrt{\frac{\rho_P}{\rho_T}} \qquad (\text{for } v_P = 1600 \text{ m s}^{-1}).$$

Since the density of the target material is usually 7.85 g cm^{-3} (armor grade steel) one can only influence the penetration depth by the velocity, density and length of the penetrator. Table 7.2 summarizes the penetration depths depending on the penetrator material used (penetrator density). It is apparent why from a strategical point of view penetrators made of highly dense (and pyrophoric) depleted uranium are very suitable.

Tab. 7.2 Penetration depth as a function of the penetrator material used (density) for a typical penetrator of 80 cm lengthwith a velocity of 1600 m s^{-1}.

penetrator material	penetrator density / g cm^{-3}	Penetration depth / cm
armor steel	7.85	53
tungsten	19.3	83
depleted uranium (DU)	19.0	82
tantalum	16.7	77
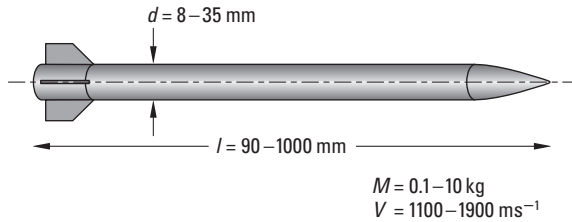
Fig. 7.10 Typical kinetic energy munition (KE) which is stabilized by tail fins. (This diagram is reproduced with slight modification from the original of Prof. Dr. Manfred Held, who is herewith thanked for his permission to reproduce this.)

It should also be noted that increasing the length of the penetrator is not always easy because long penetrators need to be stabilized by tail fins to avoid spinning and to guarantee a hitting angle of exactly 0° (Fig. 7.10). (*N.B.* The NATO hitting angle is defined as the angle between the penetrator's trajectory and a line perpendicular to the target surface. This means that with a NATO angle of 0° the penetrator hits the target directly perpendicular to the target surface, as desired.)

While a relatively small shaped charge (see above) travels with relatively low velocity and therefore requires only a small launch platform, kinetic energy munitions (KE) usually need large and therefore less mobile cannons to achieve the high velocities required. This makes shaped charges particularly useful for launching from highly mobile platforms such as helicopters. But the lower velocity of a shaped charge device compared to kinetic energy munition makes the shaped charge device more vulnerable during the duration of its flight.

7.2 Detonation Velocities

In the discussion of shaped charges (see above) it was shown that the brisance (see Ch. 2.2) of the main charge used is of utmost importance. The brisance value (B) is defined as the product of the loading density (ρ), the specific energy (F for "force of an explosive") and the detonation velocity D:

$$\text{brisance: } B = \rho F D$$

The specific energy ("force") of an explosive (F) on the other hand can be calculated according to the general equation of state for gases:

$$\text{specific energy: } F = p_e V = n R T$$

Therefore, we can conclude that for shaped charges the loading density of the high explosive and its detonation velocity (or to be more precise the Gurney velocity, see Ch. 7.3) are relevant performance parameters.
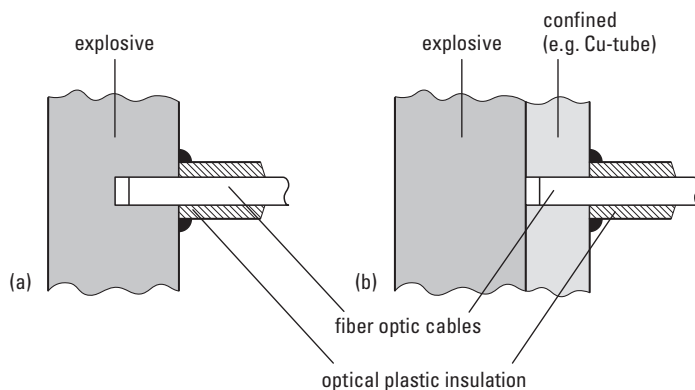
Fig. 7.11 Position of an optical fiber in case of an unconfined (a) and a confined (b) explosive charge.

In Chapter 4.2.2 we already discussed methods for the theoretical calculation of the detonation velocity and detonation pressure. In this chapter we now want to focus on the experimental determination of the detonation velocity. Bearing in mind that detonation velocities of known high explosives may reach up to 10,000 m s^{-1}, the experimental determination of the detonation velocity is not easily achieved. There are several methods which are suitable to measure the detonation velocity [38]. Most of these methods are based on the fact that the detonation process is accompanied by the emission of light (autoluminous process). Depending on the measuring equipment selected, the methods for the detonation velocity determination can be divided into,

1. optical methods, which are based on the use of different types of high-speed cameras (distance-time curves) and
2. electrical methods, which are based on the use of different types of velocity probes combined with an electronic counter or an oscilloscope.

In recent years, the fiberoptic technique has widely been used for the determination of the detonation velocity. Optical fibers are capable of detecting and transmitting a light signal accompanying the detonation wave front. This light signal may be recorded by optical methods (using a high-speed streak camera), or it may be transformed into an electric signal (by a fast photodiode) which is then recorded by a suitable ultrafast signal recording technique (fast-storage oscilloscope or multi-channel analyzer). The optical fibers also serve as a convenient means of transporting the signal from the experimental assembly in the firing area to the recording shed. The length of the optical fiber may exceed 20 m. Usually highly flexible optical fibers with a relatively low attenuation factor, 1 mm core diameter and 2.2 mm outside diameter of the black plastic jacket may be used. If the explosive charge is unconfined, the optical fibers are placed directly into the explosive
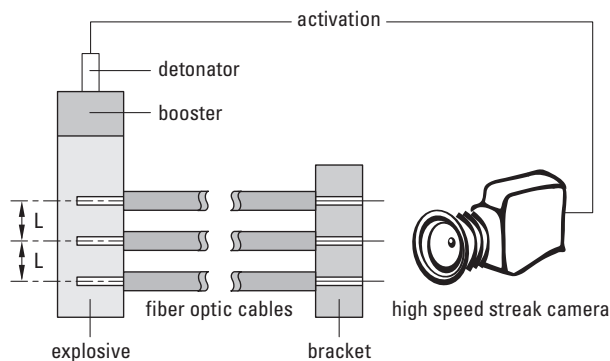
Fig. 7.12 Schematic representation of the determination of the detonation velocity using the optical fiber/streak camera technique.
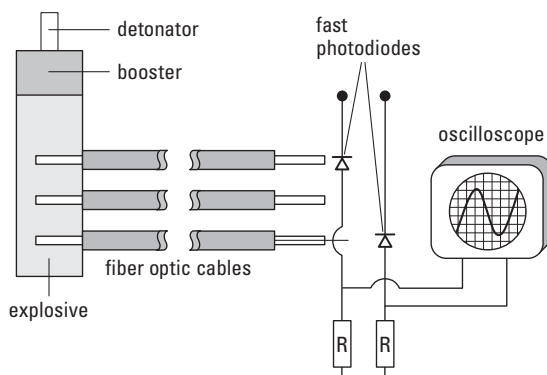
Fig. 7.13 Schematic representation of the test arrangement for the determination of the detonation velocity using the optical fiber/fast photodiode/oscilloscope technique.

charge to a depth of 2/3 of the charge diameter. If the explosive charge is confined, the fiber is placed through a hole in the wall of the metal or plastic confinement right to the inner surface of the tube (Fig. 7.12).

Figures 7.12 and 7.13 show the experimental set-up for using a high-speed streak camera or a fast photodiode/oscilloscope for the determination of the detonation velocity.

As discussed above, a convenient way of measuring the detonation velocity is to convert the light signal using a fast photodiode that has a rising time of about 10 ns into an electric signal that may be recorded by either a fast oscilloscope (Fig. 7.13) or a multi-channel analyzer (Fig. 7.14)

For the experimental measurement of the detonation velocity in a chemical laboratory (indoors), it is advisable to carry out the detonation experiment in a so-called detonation chamber (Fig. 7.15). Usually, the explosive is filled (pressed or melt-cast) into a plastic or metal tube (sealed on one end) which is wider than the

Fig. 7.14   Recording the detonation velocity (VOD, velocity of detonation) using a multi-channel analyzer.
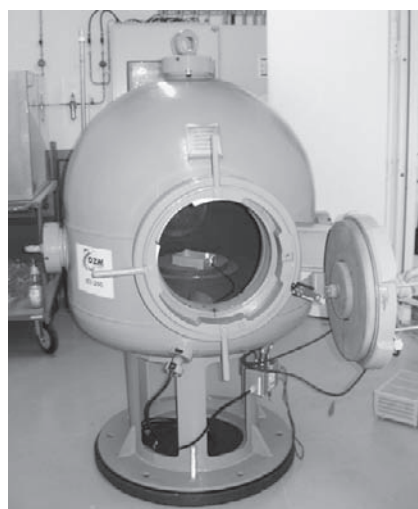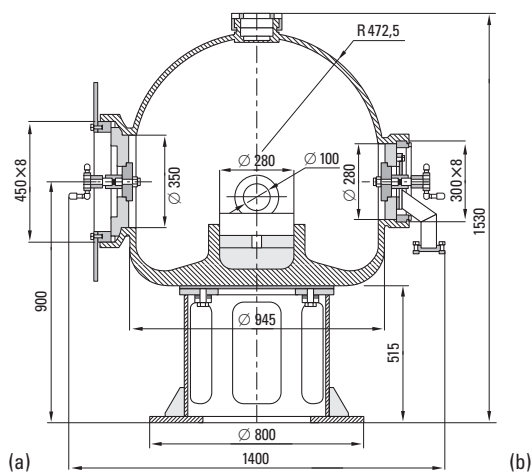
Fig. 7.15   Schematic representation (right) and photo of a KV-250 detonation chamber (up to 250 g TNT or equivalent).
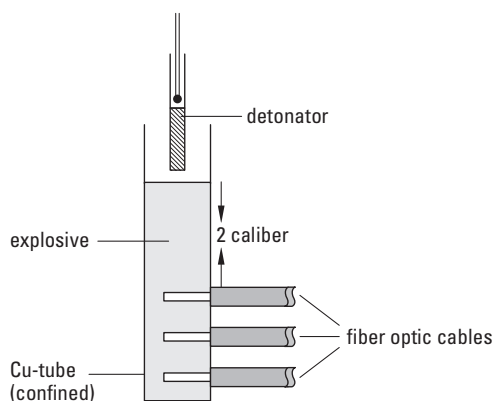
Fig. 7.16 Schematic set-up of a test for the determination of the detonation velocity using the optical fiber method.
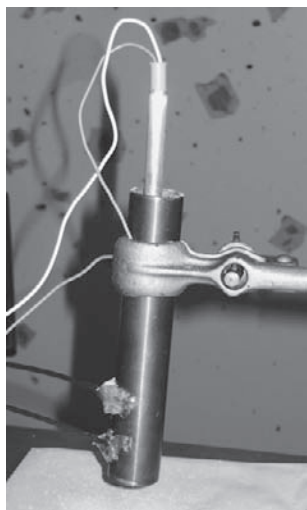
Fig. 7.17 Typical set-up for a simple determination of the detonation velocity using the optical fiber method.

critical diameter. This tube contains at least two, but preferably more (for mean value calculation) holes for the optical fibers a distance of approx. 1 in. An experimental set-up for measuring the detonation velocity using the optical fiber method is shown in Figures 7.16 and 7.17. For the measurement it is important to address the following:

1. The density of the explosive under investigation in the tube has to be constant and known exactly.
2. The diameter of the confinement tube has to be above the critical diameter (see Ch. 3, Fig. 3.2). While for many secondary explosives 1 inch is a "good" dia-

meter to start with, for primary explosives usually much smaller diameters (ca. 5 mm) are sufficient. In any case measurements with different tube diameters are recommended in order to ensure convergence of the detonation velocity on increasing tube diameter (to make sure to be above the critical diameter)

3. The closest optical fiber should not be closer to the detonator than one, preferably two calibers, to ensure that the detonation wave can stabilize and that it originates exclusively from the explosive under investigation (and not from the detonating device).

Table 7.3 and Figure 7.18 show the dependency of the calculated (EXPLO5, see Ch. 4.2.2) and experimentally measured (optical fiber method, multi channel analyzer) detonation velocities of a new high explosive (NG-A) on the loading density. The good agreement between the calculated and measured detonation velocity values reflects the quality of the measurement (time accuracy: $\pm$ 0.1 µs, accuracy of the measured detonation velocity $\pm$ 0.2 %, highest measurable velocity 10,000 m s^{-1}) and gives credence to the theoretically calculated parameters.

Tab. 7.3   Measured and calculated detonation velocities of NG-A as a function of the loading density.

loading density / g cm^{-3}	D / m s^{-1} (measured)	D / m s^{-1} (calculated)
0.61	4181	4812
1.00	6250	6257
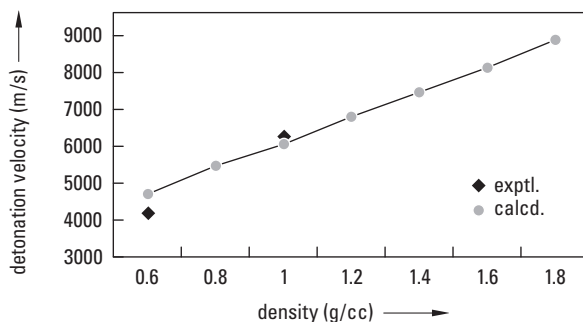
Fig. 7.18   Measured (exptl.) and calculated (calcd.) detonation velocity (det. vel.) of NG-A as a function of the loading density (density).

7.3 Gurney Model

As was already discussed in Chapter 7.1 (shaped charges), it is not only the detonation velocity, but also the so-called Gurney velocity, that determines how quickly metal fragments are ejected from an explosive charge with a specific shape (bombs,
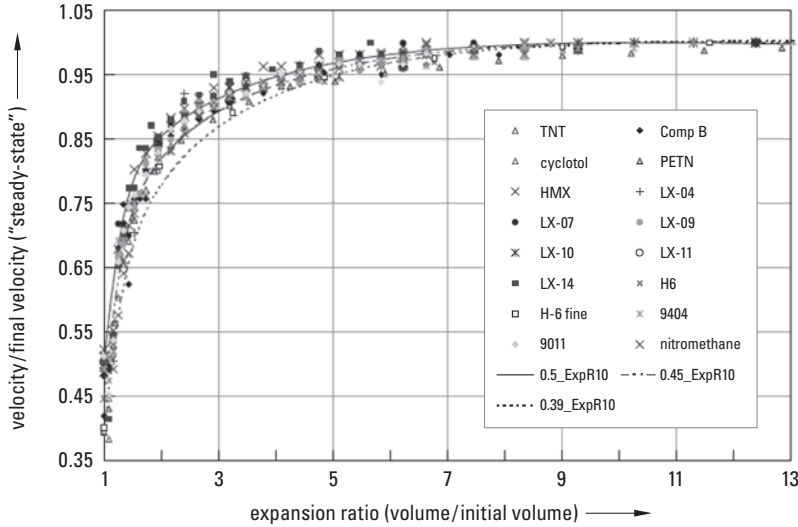
Fig. 7.19 Dependence of the normalized fragment velocity of 16 explosives (Cu cylinder) on the expansion volume. Steady-state at velocity/final Velocity = 1.

grenades). This question was researched by Ronald W. Gurney in 1943. Gurney suggested that there is a simple dependence releating to the mass of the metal confinement (M) and the explosive (C) on the fragment velocity (V). The simple Gurney model developed in Aberdeen (MD) assumes the following:

- The energy released on detonation is essentially completely changed into the kinetic energy of the detonation gases *and* kinetic energy of the metal fragments.
- The energy used for the deformation or fragmentation of the material used for confinement can essentially be ignored.
- During detonation, the explosive is spontaneously ($\Delta t = 0$) transformed into homogeneous and chemically completely changed, gaseous products under high pressure.
- The gaseous detonation products expand with uniform density and a linear velocity gradient.
- The chemical detonation energy of the explosive is changed into kinetic energy, until the fragments have a steady-state velocity (Fig. 7.19), from which the Gurney velocity can be calculated.

The fragment velocity is largely dependent on the shape of the charge. For cylindrical charges (which are a good approximation for most bomb and missile (rocket) warheads) (Fig. 7.20):

$$\frac{V}{\sqrt{2E}} = \left(\frac{M}{C} + \frac{1}{2}\right)^{-0.5}$$
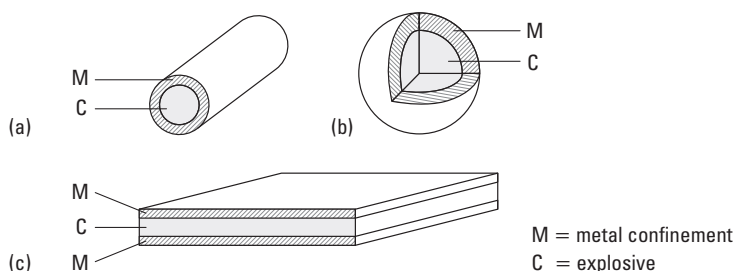
Fig. 7.20 Construction of a cylindrical (a), a spherical (b) and a sandwich configuration (c).

The constant $\sqrt{2E}$ is the so-called Gurney velocity (in km s^{-1}), which is dependent on the nature of the explosive.

Spherical charges (Fig. 7.20) which have initiating charges in the centre and are used as an approximation for grenades (and many cluster bombs), have a similar relationship:

$$\frac{V}{\sqrt{2E}} = \left(2\,\frac{M}{C} + \frac{3}{5}\right)^{-0.5}$$

Charges in the shape of a symmetrical sandwich (Fig. 7.20) (e.g. reactive armor) obey the following relationship:

$$\frac{V}{\sqrt{2E}} = \left(2\,\frac{M}{C} + \frac{1}{3}\right)^{-0.5}$$

The Gurney velocity $\sqrt{2E}$ is decisive for the performance of the explosive used. As we already saw in Ch. 3, Kamlet and Jacobs introduced the Φ parameter which relates the detonation velocity and the detonation pressure for $C_aH_bN_cO_d$ explosives with the heat of detonation Q (in cal g^{-1}), where M is the molecular weights of the gaseous detonation products (in g mol^{-1}) and N is the number of moles of gaseous detonation products per gram of explosive (for charge densities of $\rho > 1$ g cm^{-3}):

$$\Phi = N\sqrt{MQ}$$

To approximate the Gurney velocity, Hardesty, Kamlet et al. have suggested the following relationship:

$$\sqrt{2E} = 0.6 + 0.54\sqrt{1.44\,\Phi\,\rho}$$

Tab. 7.4 Dependence of the Gurney velocity $\sqrt{2E}$ on the detonation velocity ($D = V_0 D$)

explosive	charge density ρ/g cm^{-3}	D/km s^{-1}	$\sqrt{2E}$/km s^{-1}
Composition A-3[a]	1.59	8.14	2.64
Composition B[b]	1.71	7.89	2.56
HMX	1.835	8.83	2.87
octol (75/25)[c]	1.81	8.48	2.75
PETN	1.76	8.26	2.68
RDX	1.77	8.70	2.82
tetryl	1.62	7.57	2.46
TNT	1.63	6.86	2.23
tritonal[d]	1.72	6.70	2.18

[a] 88% RDX, 12% binder and plasticizer
[b] 60% RDX, 39% TNT, 1% binder
[c] 75% HMX, 25% RDX
[d] 80% TNT, 20% Al

therefore

$$\sqrt{2E} = 0.877 \, \Phi^{0.5} \, \rho^{0.4}$$

It was only in 2002 that A. Koch et al. could show that the Gurney velocity $\sqrt{2E}$ and the detonation velocity (D = VoD) of an explosive can roughly be described using the following simple relationship:

$$\sqrt{2E} = \frac{3\sqrt{3}}{16} D \approx \frac{D}{3.08}.$$

Therefore, there is a simple approximation for the Gurney velocity $\sqrt{2E}$ for either a pure explosive or for an explosive formulation, when the charge density ρ and detonation velocity are known (Tab. 7.4).

A very simple approach to approximate the Gurney velocity for $C_a H_b N_c O_d$ explosives (density ρ, in g cm^{-3}) was introduced in 2008 and is based on the following equation:

$$\sqrt{2E} \, [\text{km s}^{-1}] = 0.404 + 1.020 \, \rho - 0.021 \, c + 0.184 \, (b/d) + 0.303 \, (d/a)$$

Some results are summarized in Table 7.5. However, this method fails for explosives which do not contain hydrogen atoms and is also only recommended for preliminary categorization.

Of course, the Gurney velocity can also be determined experimentally by using the measured fragment velocity V. It can be concluded that the relationship discussed above provides a good approximation, but that the Gurney velocity is also dependent on other factors including, for example, the material of the confinement used (in particular its density). This can be seen in Table 7.6.

Tab. 7.5 Gurney velocity $\sqrt{2E}$ obtained according to method A: $\sqrt{2E} = D/3.08$ (see Tab. 1.1) and Method B: $\sqrt{2E} = 0.404 + 1.020\,\rho - 0.021\,c + 0.184\,(b/d) + 0.303\,(d/a)$.

explosive	charge density $\rho/\text{g cm}^{-3}$	$D/\text{km s}^{-1}$	$\sqrt{2E}/\text{km s}^{-1}$ method A	$\sqrt{2E}/\text{km s}^{-1}$ method B
HMX	1.835	8.83	2.87	2.90
PETN	1.76	8.26	2.68	2.97
RDX	1.77	8.70	2.82	2.87
tetryl	1.62	7.57	2.46	2.41
TNT	1.63	6.86	2.23	2.42

Tab. 7.6 Dependence of the experimentally determined Gurney velocities $\sqrt{2E}$ on the cylinder material used.

explosive	$\sqrt{2E}$ (steel)$/\text{m s}^{-1}$	$\sqrt{2E}$ (copper)$/\text{m s}^{-1}$
Composition A-3	2416	2630
Composition B	2320	2790
octol (75/25)	2310	2700
TNT	2040	2370
tetryl	2209	2500
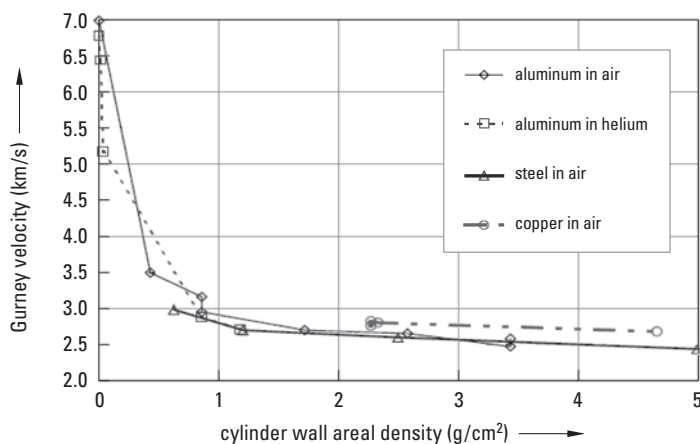
Fig. 7.21 Dependence of the Gurney velocity $\sqrt{2E}$ on the surface density (in g cm^{-2}) of the cylinder walls for Composition B ($\rho = 1.71\,\text{g cm}^{-3}$).

Figure 7.21 also shows that the Gurney velocity for a specific explosive, with a particular charge density, is only constant when the surface density (in g cm^{-3}) of the cylinder walls is above a critical value of approx. $1\,\text{g cm}^{-2}$.

The most recent work, which has mainly been reported by Joe Backofen, shows that the Gurney velocity is not only dependent on the explosive, the mass of the

confinement, and the shape of the charge, but that it is also dependent on the properties of the material (see Table 1.2 and Fig. 7.20). Subsequently he proposed a two-step model to describe this: a brisant shock-dominated first step, followed by a gas-dynamic second (propulsion) step.

7.3.1 Example: Calculation of the Gurney Velocity for a General Purpose Bomb

The MK80 GBP series is the abbreviation for a series of flying bombs whose effect is based on pressure and splitter effect. All variations of this series show an optimized aerodynamic shape so that they can be used in quick-flying fighter planes. The MK80 series consists of bombs which are predominantly composed of the explosive payload (TNT, Composition B, tritonal ……), one or more fuses (nose and tail) and the tail unit with stabilizing fins or breaking facility. Typically, the mass of the explosive corresponds to approximately half of the total mass.

The MK84 (Fig. 7.22) is the largest bomb in the MK80 series. With a length of 3.8 m and a diameter of 46 cm they can be considered for the calculation of the Gurney velocity as being cylindrical. The total mass of the MK84 is 907 kg and the mass of the HE is approximately 430 kg.

Fig. 7.22   MK84 general purpose bomb.

Assuming that the payload of 430 kg of HE is only made up of Tritonal (80% TNT, 20% Al), the detonation velocity can be calculated to be $D = 6.70$ km s^{-1}, based on a density of $\rho = 1.72$ g cm^{-3}. Following the relationship discussed above:

$$\sqrt{2E} = \frac{3\sqrt{3}}{16} D \approx \frac{D}{3.08}$$

The Gurney velocity can be calculated to be

$$\sqrt{2E} = 2.175 \text{ km s}^{-1}.$$

Therefore, if it is assumed to be a cylindrical charge, the fragment velocity can be approximated as follows:

$$\frac{V}{\sqrt{2E}} = \left(\frac{M}{C} + \frac{1}{2}\right)^{-0.5}$$

and

$$V = \sqrt{2E}\left(\frac{M}{C} + \frac{1}{2}\right)^{-0.5}$$

$$V = 2.175 \text{ km s}^{-1}\left(\frac{477 \text{ kg}}{430 \text{ kg}} + \frac{1}{2}\right)^{-0.5} = 3.5 \text{ km s}^{-1}.$$

8 Correlation between the Electrostatic Potential and the Impact Sensitivity

8.1 Electrostatic Potentials

In Chapters 4.2.2 and 4.2.3 we have seen that it is often possible to predict performance parameters using quantum mechanics without requiring experimental data. There are also huge efforts being made towards being able to theoretically predict, not only the performance but also the sensitivity parameters (if possible using quantum mechanical ab initio or DFT calculations), and particularly to allow a prediction of the sensitivity of new molecules which have not been synthesized previously. This would mean that the preparation of sensitive molecules which would have little chance of ever being used as energetic materials could be avoided. In addition, such sensitivity predictions would help to increase safety and also improve financial issues related to for synthetic projects so that they could be used more effectively for more specific targets. In comparison to computer calculations, the synthetic work in chemical laboratories requires a lot more effort and is much more time consuming and therefore considerably more expensive. As discussed previously in Chapter 6.1, the impact sensitivity is one of the most important parameters for the estimation of the sensitivity of highly energetic compounds. At this point it is worthwhile to repeat that although the drop-hammer method for the determination of the impact sensitivity uses a mechanical method, the initiation most likely also occurs as a result of hotspots. Thus it occurs thermally. It is thanks to the work of Peter Politzer, Jane Murray and Betsy Rice [39−44] in particular, that it was realized that for covalently bonded molecules, the electrostatic potential (ESP) of an isolated molecule can be correlated with the (bulk) material properties of the compound in the condensed phase.

The electrostatic potential $V(r)$ for a particular molecular hypersurface (normally 0.001 electron bohr^{-3} surface) is defined as follows:

$$V(r) = \sum_i \frac{Z_i}{|R_i - r|} - \int \frac{\rho(r')}{|r' - r|} \, dr'$$

Here Z_i and R_i are the charge and coordinates (position) of atom i and $\rho(r)$ is the electron density. The electrostatic potential can be obtained either from X-ray diffraction investigations, but more commonly it is obtained using quantum chemical calculations. Regions in which the ESP is positive are electron deficient and
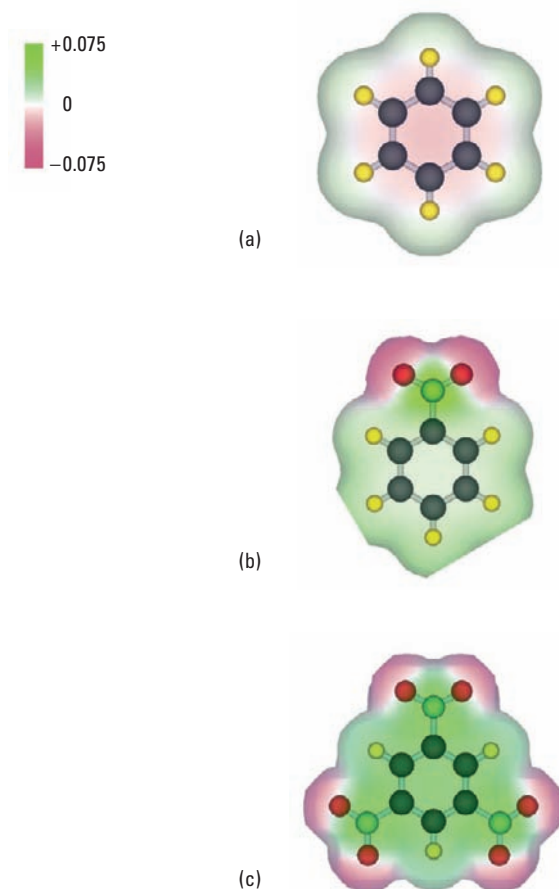
Fig. 8.1 Electrostatic potential for benzene (a), nitrobenzene (b) and trinitrobenzene (c) on the 0.001 electron bohr^{-3} hypersurface with the color code from +0.075 a.u. (green) to −0.075 a.u. (red).

their electron density is low in this area. In contrast, regions which have negative potentials are electron rich and have a higher electron density. The relative magnitude and extension of positive and negative potentials on a given hypersurface of a molecule are of decisive importance for the impact sensitivity of the compound. In the following section, the 0.001 electron bohr^{-3} hypersurface will always be considered. For "typical", non-impact sensitive organic molecules, the areas of the negative potentials are smaller but significantly stronger than the positive ones. In contrast to this, in impact sensitive compounds the regions of positive potentials are still larger, but as strong as or stronger than the negative regions (Fig. 8.1). Politzer and Rice were able to show that the impact sensitivity can be described as a function of this anomalous behavior. Figure 8.1 shows the calculated electrostatic

Tab. 8.1 Conversion of $h_{50\%}$ values into the Si consistent impact sensitivity in J.

compound	$h_{50\%}/\text{cm}$	impact sensitivity / J
PETN	13	3
RDX	28	7
HMX	32	8
HNS	54	13
FOX-7	126	31
NTO	291	71

potentials of benzene, nitrobenzene (both insensitive) and trinitrobenzene (impact sensitive). It can also be said that the less evenly the electron density is distributed (without taking into account extreme values due to charges above atoms of the electron donating or electron withdrawing substituents) the more sensitive a compound will behave. Moreover, it could be determined that for aromatic compounds (see Fig. 8.1) the impact sensitive species show a stronger electron deficient region above the aromatic ring (more positive potential) in comparison with the less sensitive species. It appears to be the case that the more impact sensitive compounds are significantly more electron deficient in the centre of their structures (more positive potential) than their insensitive analogues. Above the $C-NO_2$ bond in the more impact sensitive trinitrobenzene there also is a region of positive potential.

In addition to the qualitative conclusions (see Fig. 8.1), attempts have also been made to be able to quantitatively predict the impact sensitivity, in particular for the important organo-nitro compounds. In this, the average electrostatic potential V_{Mid} (kcal mol^{-1}) at the "mid point" of the C—N bond, or the averaged potential V^*_{Mid} (kcal mol^{-1}) for all C—N bonds in the molecule, plays an important role:

$$V_{\text{Mid}} = \frac{Q_C}{0.5\,R} + \frac{Q_N}{0.5\,R}$$

$$V^*_{\text{Mid}} = \frac{1}{N} \sum_{i=1}^{N} \left(\frac{Q_C}{0.5\,R} + \frac{Q_N}{0.5\,R} \right)$$

For organo-nitro compounds, the following correlation between V^*_{Mid} and the (widely used in the USA) $h_{50\%}$ value has been proposed by Rice et al. [44]:

$$h_{50\%} = y_0 + a \exp. (-b\,V^*_{\text{Mid}}) + c\,V^*_{\text{Mid}}$$

The $h_{50\%}$ value is directly correlated to the impact sensitivity and corresponds to the drop-height in cm, for which 50 % of the samples explode in a drop hammer

test using a 2.5 kg mass (Tab. 8.1). In the equation above, y_0, a, b and c are constants with the following values:

$$
\begin{aligned}
a &= 18922.7503 \text{ cm,} \\
b &= 0.0879 \text{ kcal mol}^{-1}, \\
c &= -0.3675 \text{ cm kcal}^{-1} \text{ mol}^{-1}, \\
y_0 &= 63.6485 \text{ cm.}
\end{aligned}
$$

On this basis, it should also be possible for other classes of compounds to establish similar correlations, in order to predict the impact sensitivities at least semi-quantitatively.

8.2 Volume-Based Sensitivities

Politzer, Murray et al. have also researched the possibility of a link between the impact sensitivities of energetic compounds and the space available for their molecules in the crystal lattices [39f, g]. To measure this space, they used the equation

$$
\Delta V = V_{\text{eff.}} - V(0.002)
$$

where $V_{\text{eff.}}$ is the effective molecular volume obtained from the crystal density and $V(0.002)$ is that enclosed by the 0.002 a.u. contour of the molecule's gas phase density, determined computationally. When the experimental impact sensitivity (h_{50} values) was plotted against ΔV for a series of 20 compounds (Fig. 8.2, a), the nitramines (▲) formed a separate group showing little dependence on ΔV. Their
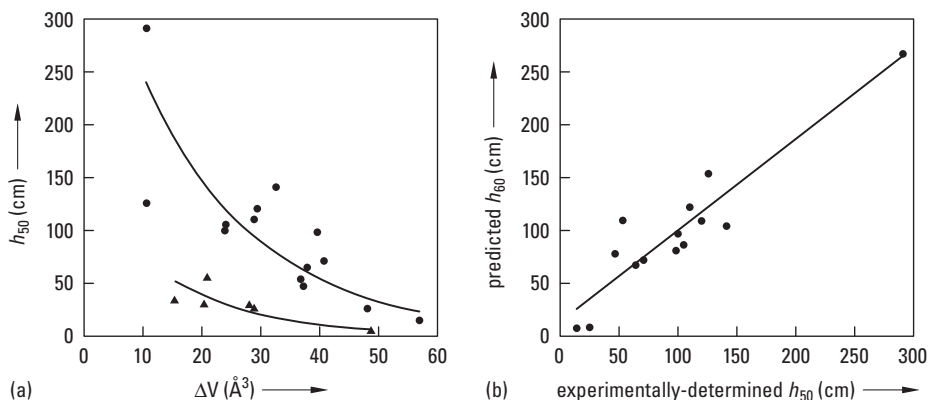
Fig. 8.2 Measured impact sensitivities (h_{50} values) plotted against computed ΔV for various energetic compounds (▲ = nitramines, ● = non-nitramine energetic compounds) (a). Comparison of impact sensitivities predicted on an electrostatically corrected volume-based model [39f,g] (b).

impact sensitivities correlate well with an anomalous imbalance in the electrostatic potentials on their molecular surfaces, which is characteristic of energetic compounds in general (see above, Ch. 8.1). The imbalance is symptomatic for the weakness of the N—NO$_2$ bonds, caused by depletion of electronic charge. Thus, for compounds (e.g. nitramines) in which trigger-linkage-rupture is a key step in detonation initiation, the surface potential imbalance can be symptomatic of sensitivity. The impact sensitivities of non-nitramines (Fig. 8.2, a), on the other hand, depend on ΔV a lot more, and can be quite effectively related to it if an electrostatically-based correction term is added (Fig. 8.2, b). Why might this be a factor? Perhaps the availability of more space enhances the molecule's ability to absorb and localize the external energy coming from the impact, for example either vibrationally or translationally.

The volume-based (ΔV) h_{50} values for the non-nitramine energetic compounds were predicted using the equation

$$h_{50} = a\,(\Delta V)^{\frac{1}{3}} + \beta v \sigma_{\text{tot}}^2 + \gamma$$

where a (-234.83), β (-3.197) and γ (962.0) are constants, $\sigma_{\text{tot}}^2 = \sigma_+^2 + \sigma_-^2$ (with σ_+^2, σ_-^2 and σ_{tot}^2 being the positive, negative and total variances of the electrostatic potential) and v being an electrostatic balance parameter defined as $v = (\sigma_+^2\,\sigma_-^2)\,/\,(\sigma_+^2\,+\sigma_-^2)^2$.

9 Design of Novel Energetic Materials

9.1 Classification

As we have already discussed above, secondary explosives (or high explosives) are homogeneous substances which can either be covalent or ionic. However, in both cases it is important that the oxidizer and fuel are combined within *one* molecule (i.e. in one covalent molecule or in one ionic formula unit). For example, this is the case for TNT, in which the three nitro groups correspond to the oxidizer, and the C—H backbone acts as the fuel. Such molecules belong to the "**oxidation of the carbon backbone**" group of substances (Tab. 9.1).

In the TNT molecule, all of the angles involving the C atoms are approximately 120° (C_6 ring) or 109° (CH_3 group) and they therefore correspond almost to the ideal angles for a sp^2 and sp^3 hybridized atom. If one now considers a strained ring or cage structure, for example in CL-20, the energy of the molecule is increased as a result of the ring or **cage strain**. Consequently, in the explosive decomposition forming CO, CO_2, H_2O and N_2, more energy is released than would be in an unstrained system (Tab. 9.1).

Principally, members of both of the above mentioned classes of compounds (oxidation of the molecule back-bone; ring and cage strain) can be exothermic or endothermic compounds. An example of the former is TNT with $\Delta_f H° = -295.5$ kJ kg^{-1}, while RDX shows a positive standard enthalpy of formation of $\Delta_f H° = +299.7$ kJ kg^{-1}.

A third class of highly energetic materials is always endothermic and is called **nitrogen-rich molecules** (Tab. 9.1). The reasons why nitrogen-rich molecules are par-

Tab. 9.1 Overview of different approaches for the design of highly energetic compounds.

type	example	comments	structure
oxidation of the C back-bone,	TNT, PETN, RDX	compound can be exothermic or endothermic, compounds can be covalent or ionic	Fig. 1.3
ring or cage strain	CL-20, ONC	most endothermic, most covalent	Fig. 1.6
nitrogen-rich molecules	TAGzT, Hy-At	always endothermic, compounds can be covalent or ionic	Fig. 2.2
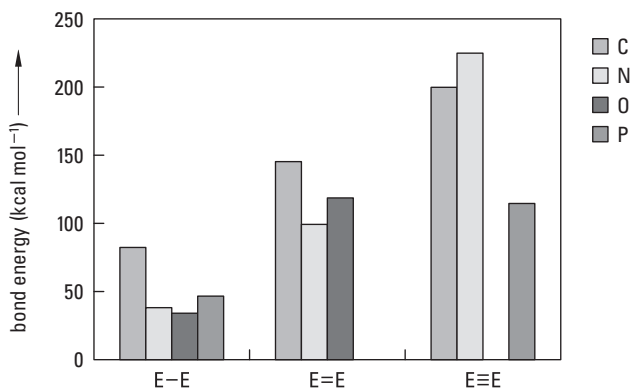
Fig. 9.1 Approximate bond energies for C—C, N—N, O—O and P—P single, double and triple bonds (in kcal mol^{-1}).
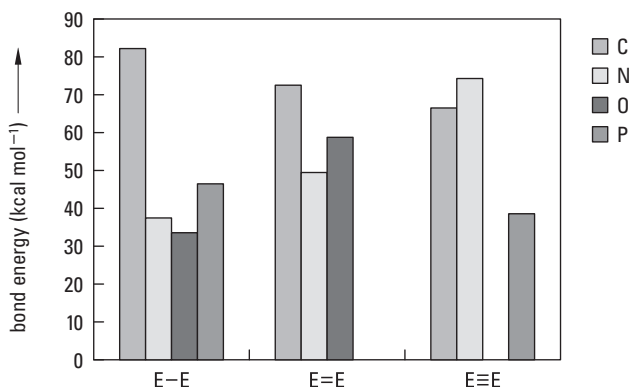
Fig. 9.2 Average element-element bond energies per 2-electron bond (in kcal mol^{-1}).

ticularly interesting as highly energetic compounds will be considered in more detail in the next section.

If we first consider the bond energies for typical C—C, N—N and O—O single, double and triple bonds, we can see that the bond strength increases from single to double to triple bonds (which is unsurprising) (Fig. 9.1).

However even more important is the question whether an element-element double bond is twice as strong as a single bond, and a whether a triple bond is three times as stable as a single bond. This means that we have to average the bond energy per 2-electron bond. This situation is illustrated in Figure 9.2.

Now we can see that the element nitrogen is unique as the bond energy per 2-electron bond increases from a single to a double to a triple bond. The surprising enormously high bond energy of the N≡N triple bond is responsible for the fact that all nitrogen-rich and polynitrogen compounds show a strongly exothermic decomposition when N_2 is formed. Furthermore, we can see that unlike nitrogen,

carbon prefers single bonds over double or triple bonds. This means that thermodynamically, acetylene H—C≡C—H trimerizes in an exothermic reaction forming benzene, while thermodynamically, N≡N would never oligomerize or polymerize to N_x (x = 4, 6, 8). The reason for the particular stability of the N≡N triple bond in comparison to carbon can be found in the small size of the N atoms (better overlapping) (covalent radii: N = 0.70 Å, C = 0.77 Å), and also as a result of the different hybridization of N in N_2 in comparison with C in HCCH, in which the N—N σ bond in N_2 has a considerably higher p-character than the C—C bond in acetylene does:

N≡N:	σ-LP(N)	64 % s	36 % p
	σ-(N—N)	34 % s	66 % p
H—C≡C—H	σ(C—C)	49 % s	51 % p
	σ(C—H)C	45 % s	55 % p
	H	100 % s	

The large jump in the average 2-electron bond energies between the double and the triple bonds is particularly valuable for nitrogen. This means that during the development of new energetic substances with a very high nitrogen content (N > 60 %) and a N—N bond order smaller than or equal to 2, large amounts of energy (for explosions or rocket propulsion) will be released on decomposition to molecular dinitrogen.

9.2 Polynitrogen Compounds

It would be particularly interesting to take polynitrogen compounds into consideration (100 % N). However, no other modification of nitrogen except N_2 is known which is metastable under normal conditions (1 atm, 298 K) in the condensed phase.

In recent years, however, the search for further energy-rich forms of nitrogen has intensified using both theoretical and experimental methods. Apart from their purely theoretical interest, the possible potential uses of metastable forms of N_x as highly energetic materials, which would only produce hot air (hot dinitrogen) on decomposition, has made N_x molecules particularly interesting. Generally, calculations show that the decomposition of highly energetic forms of poly-nitrogen to N_2 should release over 10 kJ/g energy. This energy release per gram of condensed material is much higher than that of any of the state-of-the-art propellants or explosives used today. Some of the forms of nitrogen we will consider in the following section have already been identified as being vibrationally stable, thermodynamically metastable N_x molecules. Particularly interesting in this context is the N_6 molecule, which has been most intensively investigated theoretically. The nitrogen
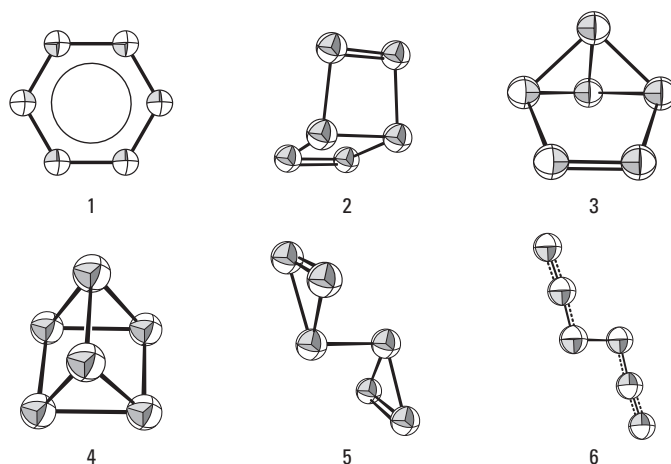
Fig. 9.3 Structures of six different N_6 isomers [45−46].

Tab. 9.2 Compilation of N_6 isomers and their isoelectronic organic CH analogues [45−46].

N_6 form (see Fig. 7.4)	point group	stability	rel. energy (in kJ mol^{-1})	CH analogue	point group
1	D_{6h}	unstable	899	Benzene	D_{6h}
2	C_{2v}	stable	1037	Dewar benzene	C_{2v}
3	C_{2v}	stable	890	Benzvalene	C_{2v}
4	D_{3h}	stable	1384	Prismane	D_{3h}
5a	C_{2h}	transition state	1020	Bicyclopropene	C_{2h}
5b	C_{2v}	transition state	1041	Bicyclopropene	C_{2v}
6a	C_1	transition state	769	−	−
6b	C_2	transition state	769	−	−
N_2	$D_{\infty h}$	stable	0	Acetylene	$D_{\infty h}$

triazide molecule $N(N_3)_3$, has also been investigated by using theoretical calculations and its synthesis has been attempted, but only the formation of five equivalents of N_2 and large quantities of energy were observed. The six most important possible structures of N_6 are summarized in Figure 9.3, while Table 9.2 shows a comparison of the N_6 molecules with some known, isoelectronic organic C—H compounds. For the different N_6 structures (**1−6**) five have (**1−5**) classic analogues in organic chemistry, however only the N_6 analogues **2, 3** and **4** represent stable minimum structures. The diazide structure **6** is the only isomer which doesn't have a classic analogue in organic chemistry and represents a transition state.

Since only isomers **2, 3** and **4** are stable minima, we will concentrate on them in the following discussion. Structure **3** contains an almost pre-formed N_2 unit (N1—N2) and in-depth studies show that this compound is therefore not kinetically stabilized enough for it to be of practical interest. The relative energies of **2** and **4**
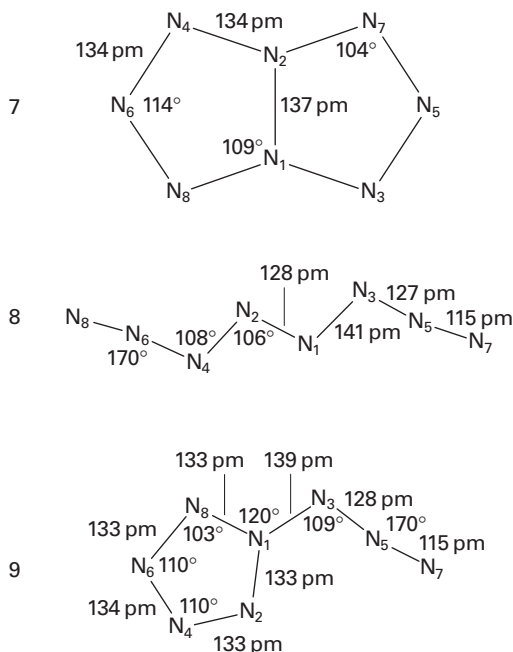
Fig. 9.4   Structures of three different N_8 isomers (**7−9**).

are 1037 and 1384 kJ mol^{-1} higher than that of N_2. These values correspond to specific energies of 14 and 19 kJ/g. These energies are noticeably high, considering that the high-performance explosives used today have typical values of 6 kJ/g.

Furthermore, both molecules **2** and **4**, have relatively high values for the lowest frequency normal vibration which is found at approximately 450 cm^{-1}. These values suggest, that the structures of these two isomers are relatively rigid and that the highly thermodynamically favorable decomposition reaction (see above) to N_2 should have a significant activation energy. Therefore, we can summarize that the N_6 analogues of Dewar benzene (**2**) and prismane (**4**) are the best candidates for N_6 for real high-energy materials. Structure **4** appears to be the most promising preparatively, since the unimolecular dissociation into three N_2 molecules is symmetry forbidden (4 + 4 + 4) and would possess considerable activation energy.

On the basis of quantum mechanical calculations, it has also recently been shown that azidopentazole (**9**, Fig. 9.4) is possibly the global minimum on the N_8 energy hypersurface. Azidopentazole has a significant energy barrier with respect to the ring closing reaction (**9 → 7**) and it can be expected that azidopentazole is also stable, also with respect to reverse cyclization. Therefore azidopentazole probably represents not only the global minimum on the N_8 energy hypersurface, but should also be a synthetically realistic target. But how could one attempt to synthesize azidopentazole? The most promising route is probably the reaction of phenylpentazole (prepared from the corresponding diazonium salt and the azide ion) with a

Tab. 9.3 Summary of N_8 isomers.

N_8 isomer	point group	stability	rel. energy (in kJ mol^{-1})
Pentalene bicycle (**7**)	D_{2h}	stable	245.1
N_8 chain (**8**)	C_s	stable	246.9
Azidopentazole (**9**)	C_s	stable	229.7
N_2	$D_{\infty h}$	stable	0.0

covalent azide compound. The structures and relative energies of the three most probable N_8 isomers are summarized in Figure 9.4 and Tab. 9.3.

$$C_6H_5{-}NH_2^+ \xrightarrow{\text{NaNO}_2,\ \text{HCl},\ 0\,°C} C_6H_5{-}N_2^+Cl^-$$

$$C_6H_5{-}N_2^+Cl^- + AgPF_6 \rightarrow C_6H_5{-}N_2^+PF_6^- + AgCl$$

$$C_6H_5{-}N_2^+PF_6^- + NaN_3 \rightarrow C_6H_5{-}N_5 + NaPF_6$$

$$C_6H_5{-}N_5 + R{-}N_3 \rightarrow N_5{-}N_3\ (\textbf{9}) + C_6H_5{-}R$$
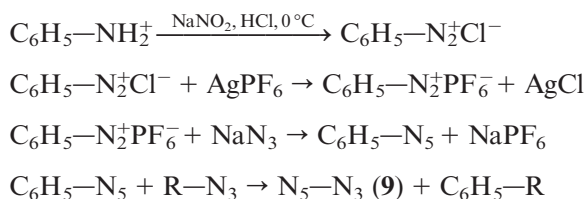
It is interesting to note at this point that polynitrogen compounds are not only of great interest as explosives, but also as rocket propellants. For example, a specific impulse of 408 s and a combustion chamber temperature of 7500 K have been predicted for N_4 (T_d) (and for N_8 an I_{sp} of 500 s). From experience, since an increase in the specific impulse of 20 s results in a doubling of the payload, this would be a massive improvement. Furthermore, since polynitrogen compounds exhibit smoke-free combustion, they are also of big interest for tactical rockets.

Although currently some very nitrogen-rich compounds are known, there is no all-nitrogen/polynitrogen compound in use or even under investigation. Nonetheless, the (calculated) advantages of this class of compounds is summarized again in the following:

- only gaseous reaction products (N_2)
- large positive standard enthalpies of formation ($\Delta_f H°$)
- large propulsive or explosive power
- very high specific impulse (200 % > value for hydrazine)
- very high (adiabatically calculated) reaction temperature (up to 7500 K)
- smoke-free combustion
- minimal signature of a rocket engine
- low erosion of gun barrels (no formation of iron carbide)

In recent years it has been possible to increase the static pressure during material synthesis and investigations by more than a factor of 50. This means that it is possible to access pressures which were previously unthinkable. This breakthrough was made possible by the huge advances in the diamond-cell technique. The pressure at the centre of the earth corresponds to a value of approximately 3 500 000 bar

$= 3\,500\,\text{kbar} = 3.5\,\text{Mbar}$. The highest pressure that has been reached using the diamond-cell is 5.5 Mbar. It has been assumed, that the highest possible pressure accessible using this technique should be approximately 7.5 Mbar. At this pressure, the metallization of diamond begins, which is linked to a large decrease in volume, so that as a result the diamonds crack. The change of the inner energy (U) of a substance is dependent on the variables temperature (T) and pressure (p):

$$\Delta U = T\Delta S - p\,\Delta V$$

Due to the temperature dependent term $T\Delta S$, the state (solid, liquid, gas) can be changed, e.g. by melting or evaporation. However, the pressure-dependent term $p\,\Delta V$ is more dominant, because the pressure can be increased to a much greater extent than the temperature. Table 9.4 summarizes the effects at static pressures of $5\,000$ bar, $50\,000$ bar or $500\,000$ bar, that can be achieved for a compound which shows a decrease in volume of $\Delta V = 20\,\text{cm}^3\,\text{mol}^{-1}$.

Tab. 9.4 Correlation of the applied pressure and material changes.

$p\,/\,\text{bar}$	$p\Delta V\,/\,\text{kcal mol}^{-1}$	effect
5 000	2	pressing the substance
50 000	20	deformation of bonds
500 000	200	formation of new bonds with new electronic states

The application of static pressures in the range of $5\,000$ to $50\,000$ bar has relatively speaking only the small effect of pressing the substance together and bending of the bonds. These effects can also be achieved by changing the temperature at ambient pressure. When the pressure reaches $500\,000$ bar, a completely new situation arises: old bonds can be broken, new bonds made and new electronic states occupied, which result in drastic changes to the physical properties of the substance.

As a highlight of such investigations, the results of the high-pressure research on nitrogen should be mentioned. As a result of the triple bond in the dinitrogen molecule, N_2, it is one of the most stable diatomic molecules. At low temperatures and pressures nitrogen can be condensed, but this solid still contains diatomic N_2 molecules and is an insulator with a large band gap.

In 1985 McMahan and LeSar predicted that the triple bond in molecular nitrogen should be breakable under very high pressures and a solid should be formed which consists of trivalent (i.e. three-coordinate) nitrogen atoms (pressure-coordination rule). Such structures already exist at normal pressures for the other group 15 elements phosphorus, arsenic, antimony and bismuth. The transformation pressure for nitrogen should lie in a range between 500 and 940 kbar. An estimation of the bond energies predicts $38\,\text{kcal mol}^{-1}$ for a single bond and $226\,\text{kcal mol}^{-1}$ for a triple bond. This predicts a difference of $188\,\text{kcal mol}^{-1}$, and corresponds to the value of $200\,\text{kcal mol}^{-1}$ (cf. Tab. 9.4).
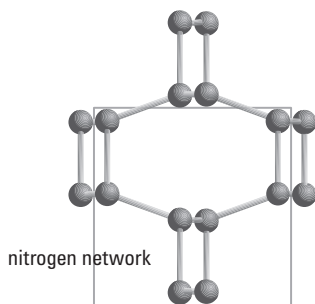
Fig. 9.5 Singly bonded polymeric nitrogen (cubic modification). (Reproduced with permission from Prof. Dr. J. Evers, http://www.cup.uni-muenchen.de/ac/evers/index.html)

The preparation of trivalent nitrogen was achieved in 2004 by Eremets et al. in a diamond cell at 1 150 000 bar and 2 000 K [47−49]. The crystallographic data for the trivalent nitrogen is: cubic, lattice parameter $a = 3.4542(9)$ Å. A three-dimensional structure which consisted of trivalent nitrogen atoms (Fig. 9.5) was found. The N—N bond length at 1.1 Mbar is 1.346 Å, and the NNN angle is 108.8°. The nitrogen atoms form screws of trivalent atoms which are connected to form a three-dimensional network.

Unfortunately, this cubic polynitrogen is not stable under normal conditions and already decomposes back to molecular dinitrogen at a pressure of approximately 42 GPa.

9.3 High-Nitrogen Compounds

One synthetic approach is to synthesize nitrogen-rich compounds (N > 60 %), which also contain oxidizing groups (e.g. nitro: —NO_2, nitrimino: =N—NO_2, Fig. 9.6), in order to achieve the best possible oxygen balance (Ω). This is important because in principal, it is always better to have the oxidizer and fuel combined in *one* molecule (in contrast to mixtures), because this generally results in superior detonation parameters such as a higher detonation velocity and detonation pressure. Of course, the new compounds synthesized also should not be worse in any of the positive properties RDX shows (e.g. thermal stability, low sensitivity etc.).
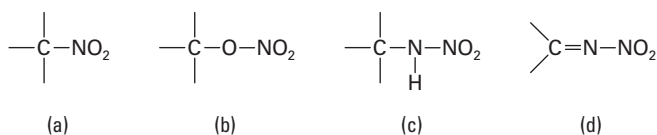
Fig. 9.6 Oxidizing groups which can facilitate a positive oxygen balance; Nitro (a), Nitrato (b), Nitramino (c), Nitrimino (d).

Tab. 9.5 Desired properties of new nitrogen-rich highly energetic compounds.

performance	detonation velocity	$D > 8500 \text{ m s}^{-1}$
	detonation pressure	$p > 340 \text{ kbar}$
	heat of explosion	$Q > 6000 \text{ kJ kg}^{-1}$
stability	thermal stability	$T_{\text{dec.}} \geq 180\,°C$
	impact sensitivity	$IS > 7 \text{ J}$
	friction sensitivity	$FS > 120 \text{ N}$
	electrostatic sensitivity	$ESD > 0.2 \text{ J}$
chemical properties	hydrolytically stable,	
	compatible with binder and plasticizer,	
	low water solubility[a] (or non-toxic),	
	smoke-free combustion,	
	long-term stable (> 15 years under normal conditions)	

[a] low octanol-water partition coefficient

Table 9.5 shows a summary of the desired properties for new, nitrogen-rich highly energetic compounds.

Of course, it is difficult to fulfill all these criteria, in particular as further practical aspects also have to be taken into account, including: simplest possible synthesis, a cheap and sustainable synthesis (no chlorinated solvents), as well as being able to automate the individual synthetic steps [50, 51]. So far it has been possible to identify two classes of compounds which show many of the properties mentioned above:

− tetrazole compounds [52, 53],
− trinitroethyl compounds [54].

9.3.1 Tetrazole and Dinitramide Chemistry

While triazole compounds are not often energetic enough and pentazole species are kinetically too labile, the tetrazole derivatives often combine the desired endothermicity with kinetic stability (Fig. 9.7). Aminotetrazole (AT) and diaminotetrazole (DAT) are good starting materials for the synthesis of new highly energetic, nitrogen-rich compounds. AT and DAT can be synthesized in accordance with the synthetic schemes outlined in Figure 9.8. For DAT, the synthesis starts from thiosemicarbazide (easily obtained from KSCN and hydrazine) in acidic medium.

Often, energetic compounds composed of salts show advantages over their covalent analogues; they show a lower vapor pressure for example, essentially eliminat-
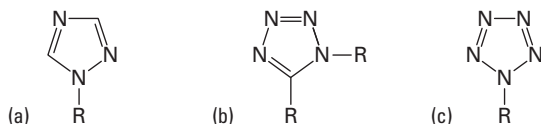
Fig. 9.7 The basic structures of 1,2,4-triazole (a), tetrazole (b) and pentazole compounds (c)
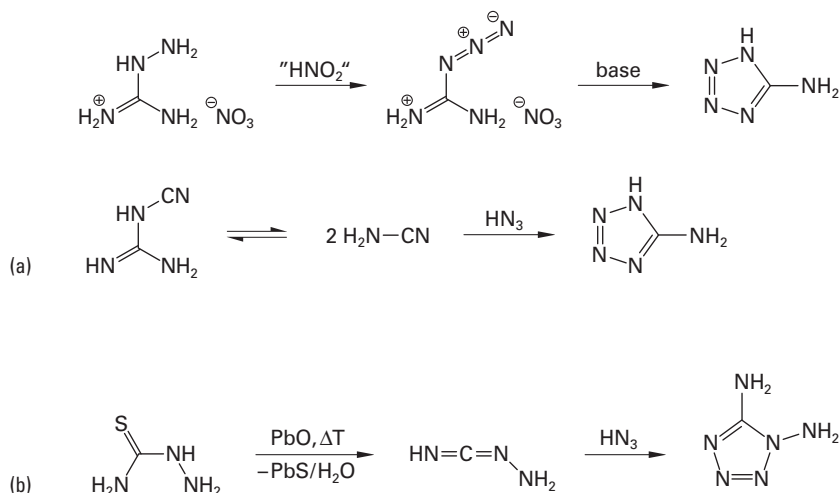
Fig. 9.8 Two synthetic routes for the synthesis of aminotetrazole (AT, a) and the synthetic route for diaminotetrazole (DAT, b).

ing the risk of inhalation of toxic compounds. Furthermore ionic compounds usually have higher densities, higher thermal stabilities and larger critical diameters (IM) [55]. On the other hand, salts are often water soluble and hygroscopic, which is negative. The solid state density (ρ) is a particularly important parameter since not only the detonation pressure (p) but also the detonation velocity (D) are directly dependent on the density, which we have already seen using the simple relationship of Kamlet and Jacobs which was discussed in Chapter 3 [10].

$$p_{\text{C-J}} \,[\text{kbar}] \quad = \text{K}\,\rho_0^2\,\Phi$$
$$D\,[\text{mm}\,\mu\text{s}^{-1}] = \text{A}\,\Phi^{0.5}(1 + \text{B}\,\rho_0)$$

The constants K, A and B are defined as follows:

$$\text{K} = 15.88$$
$$\text{A} = 1.01$$
$$\text{B} = 1.30$$

The parameter Φ is therefore

$$\Phi = N(M)^{0.5}(Q)^{0.5}$$

where

- N is the no. of moles of gas released per gram of explosive,
- M the mass of gas in gram per mole of gas and
- Q is the heat of explosion in cal per gram.
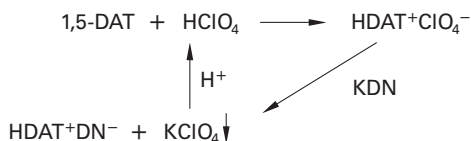
Fig. 9.9 Synthesis of diaminotetrazolium dinitramide (HDAT⁺DN⁻).
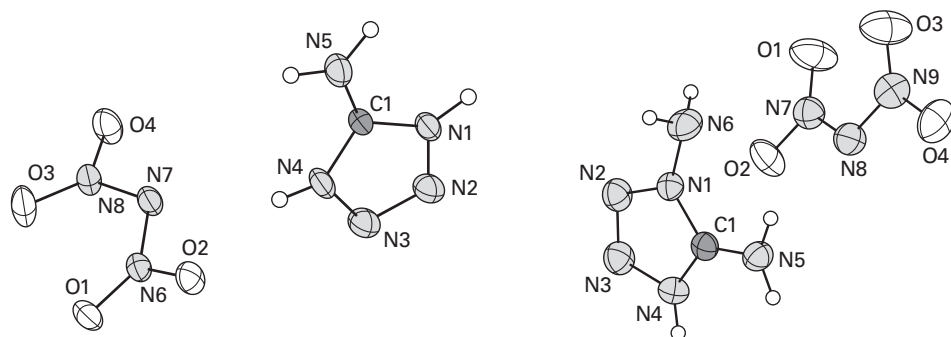
Fig. 9.10 Structures of aminotetrazolium dinitramide (HAT⁺DN⁻, left) and diaminotetra-zolium dinitramide (HDAT⁺DN⁻, right).
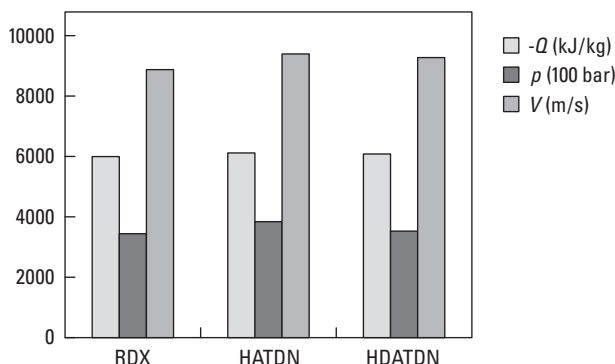
Fig. 9.11 Comparison of the performance data for aminotetrazolium dinitramide (HAT⁺DN⁻), diaminotetrazolium dinitramide (HDAT⁺DN⁻) and hexogen (RDX).

Aminotetrazole (AT) and diaminotetrazole (DAT) can easily be converted into the perchlorate salts, which can subsequently be converted into the highly energetic salts HAT⁺DN⁻ and HDAT⁺DN⁻ by reaction with potassium dinitramide (KDN). Figure 9.9 shows the synthesis of diaminotetrazolium dinitramide. The structures of both high-energy salts was determined using single crystal X-ray diffraction (Fig. 9.10).

The most important parameters for the characterization of the performance of secondary explosives for use in energetic formulations in war heads and general
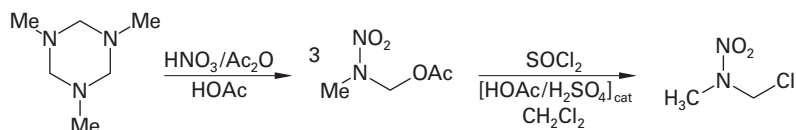
Fig. 9.12 Synthesis of 1-chloro-2-nitro-2-azapropane.
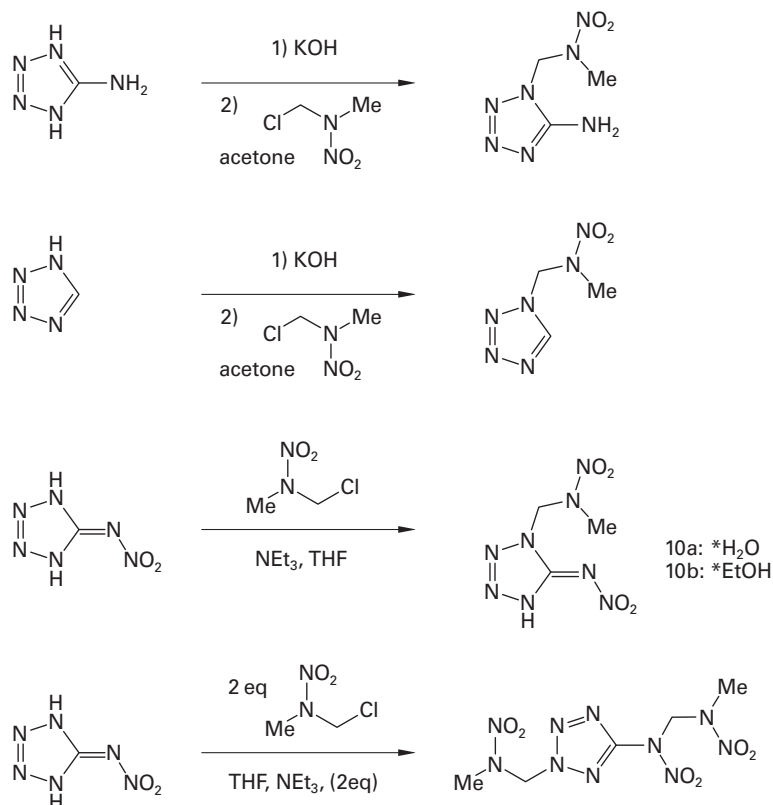
Fig. 9.13 Synthesis of tetarazole compounds with energetic side-chains.

purpose bombs (GPBs) are the heat of detonation (Q), the detonation pressure (p) and the detonation velocity (D). For comparison, Figure 9.11 shows a summary of the important values for aminotetrazolium dinitramide (HAT$^+$DN$^-$), diaminotetrazolium dinitramide (HDAT$^+$DN$^-$) and RDX.

Tetrazole compounds are also good starting materials for the synthesis of energetic materials with substituted side-chains attached to the tetrazole skeleton. For example, tetrazole can be alkylated by reaction with 1-chloro-2-nitro-2-azapropane and converted into various energetic compounds (Figs. 9.12 and 9.13).

Compound **8** for example is stable up to 184 °C (melting point of 150 °C), is not impact sensitive (IS > 100 J) and is only slightly friction (FS = 120 N) and electro-
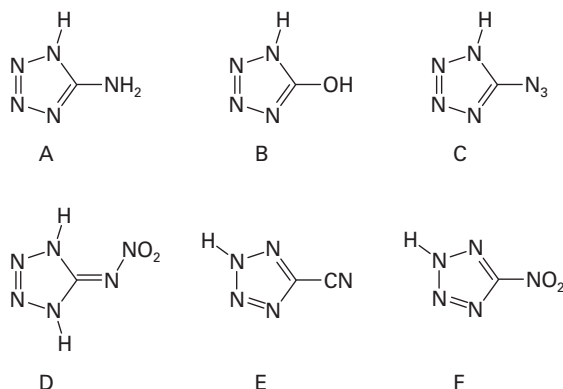
Fig. 9.14 Tetrazole derivatives with different substituents.

static sensitive (ESD = 0.22 J). The performance parameters such as the detonation velocity (8467 m s^{-1}), detonation pressure (273 kbar) and heat of explosion (5368 kJ kg^{-1}) are significantly higher than the values for TNT and only marginally lower than those of RDX.

Out of the different possible derivatives of tetrazoles, we have so far only discussed (**A**) and nitriminotetrazole (**D**) (Fig. 9.14) in more detail. Although the azide-substituted tetrazole compound of type **C** is very energetic, it is still not useful for practical application since it is extremely sensitive. Additionally of interest are the neutral and ionic nitrotetrazole derivates of type **F,** which are more stable (Fig. 9.14).

While free nitrotetrazole is extremely sensitive and only of limited thermal stability, the salts of nitrotetrazole are, at least thermally, often significantly more stable. The best synthetic route starts from 5-aminotetrazole via the corresponding copper salt (M = alkali metal):
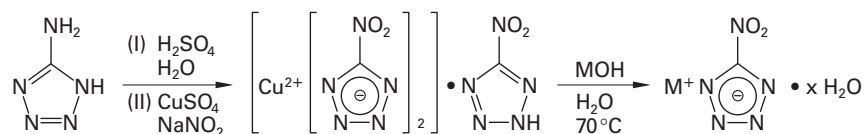
Although AgNT can be obtained from NaNT and AgNO$_3$, ammonium nitrotetrazolate is best prepared as the hemihydrate (Fig. 9.15) by the acidification of sodium nitrotetrazolate with sulfuric acid, followed by extraction and reaction with ammonia gas. This compound is particularly suited to the synthesis of further energetic nitrotetrazolate salts such as, for example the hydrazinium, guanidinium, aminoguanidinium, diamonoguanidinium and triaminoguanidinium salts (Fig. 9.15).

Even though they are mainly of academic interest, the nitrotetrazole compounds are very suitable species to study using ^{15}N NMR spectroscopy. Figure 9.16 shows
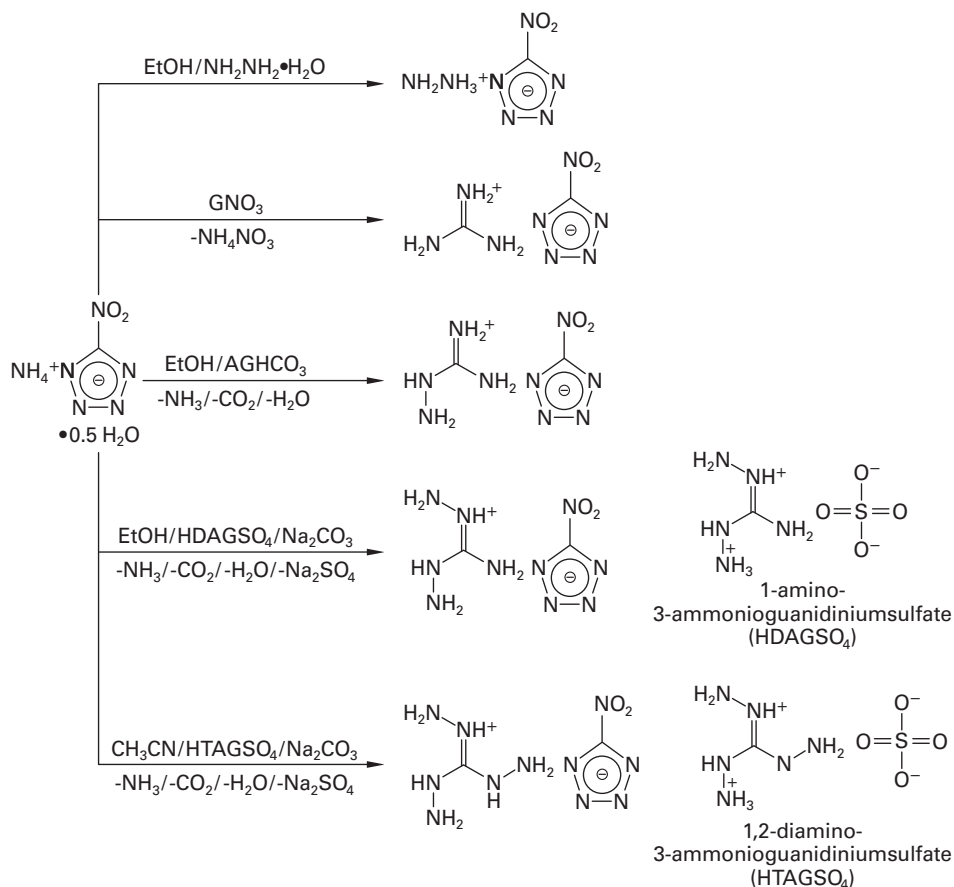
Fig. 9.15 Synthesis of various energetic nitrotetrazolate salts.

an example of very nicely resolved ^{15}N NMR spectra of free nitrotetrazole, as well as of both the methylated isomers.

A very interesting approach to the synthesis of new, ethyl-bridged, energetic tetrazole compounds, both neutral and ionic has been reported recently by Shreeve and co-workers [56a,b]. They react *in situ* generated cyanazide, N_3CN, with 1,2-diaminoethane to form the bridged tetrazole derivative **A** (Fig. 9.17), which can subsequently be converted with HNO_3 to the corresponding neutral nitrimino derivative **B**. Finally, using hydrazine, compound **B** can be converted to the energetic hydrazinium salt **C**, which is surprisingly thermally stable (m. p. = 223 °C).

Another very promising tetrazole compound, bistetrazolylamine (H_2BTA), can be obtained directly from sodium dicyanamide and sodium azide [56c]:

$$NaN(CN)_2 + 2\ NaN_3 \xrightarrow{\text{HCl}} H_2BTA \cdot H_2O \xrightarrow{-H_2O} H_2BTA$$
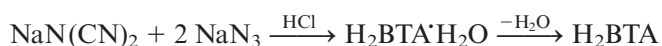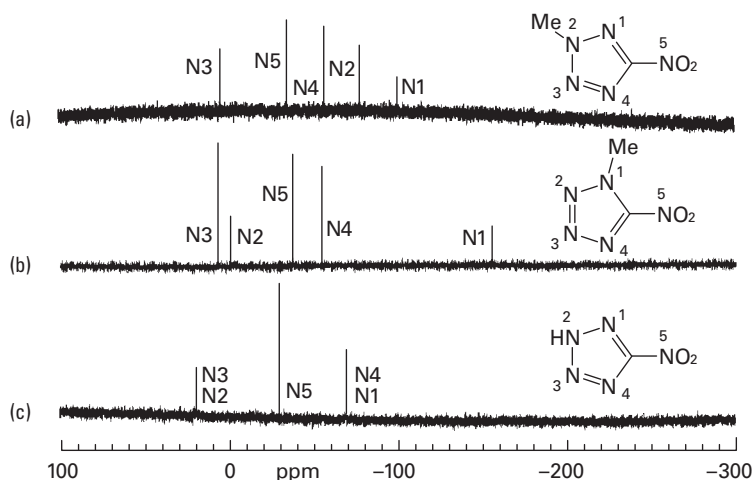
Fig. 9.16 ^{15}N NMR spectra of 2-methyl- (a), 1-methyl-nitrotetrazole (b) and nitrotetrazole (c).
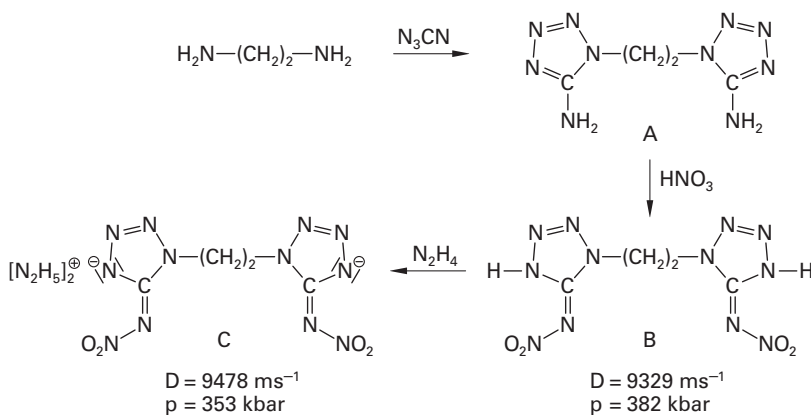
Fig. 9.17 Synthetic scheme for the preparation of briged nitriminotetrazole compounds.

The anhydrous compound has a density of 1.86 g cm^{-3}, good performance data ($V_0D = 9120$ m s^{-1}, $p_{C-J} = 343$ kbar) but a very low sensitivity (impact > 30 J, friction > 360 N). Energetic salts of the type [Cu(H$_2$BTA)$_2$][NO$_3$]$_2$ are also known.

A new synthetic approach for high-nitrogen compounds has recently been suggested by Charles H. Winter et al. which uses poly(pyrazolyl)borate complexes [56d]. Since a borate anion [BR]$_4^-$ carries only one negative charge but can include four heterocyclic ring systems R, theoretically, up to 8 N$_2$ molecules can get liberated if R is a tetrazole ring system, i. e. if we are talking about a tetrakis(tetrazolyl)borate anion.

9.3.2 Tetrazole, Tetrazine and Trinitroethyl Chemistry

Through the combination of very oxygen-rich trinitroethyl groups with the nitrogen-rich and endothermic tetrazole and tetrazine ring systems, the syntheses of three highly energetic trinitroethyl derivatives were achieved:

1. trinitroethyl-tetrazole-1,5-diamine (TTD),
2. bis(trinitroethyl)-tetrazole-1,5-diamine (BTTD),
3. bis(trinitroethyl)-1,2,4,5-tetrazine-3,6-diamine (BTAT).

The synthesis of these compounds is relatively facile using trinitroethanol and the corresponding amines, while for the synthesis of TTD diaminotetrazole, BTTD TTD and for BTAT, diamino-tetrazine was used (Fig. 9.18). At pH values above 6, trinitroethanol behaves as an acid, so that for the Mannich reaction shown in Figure 9.18, two different mechanisms can be discussed.
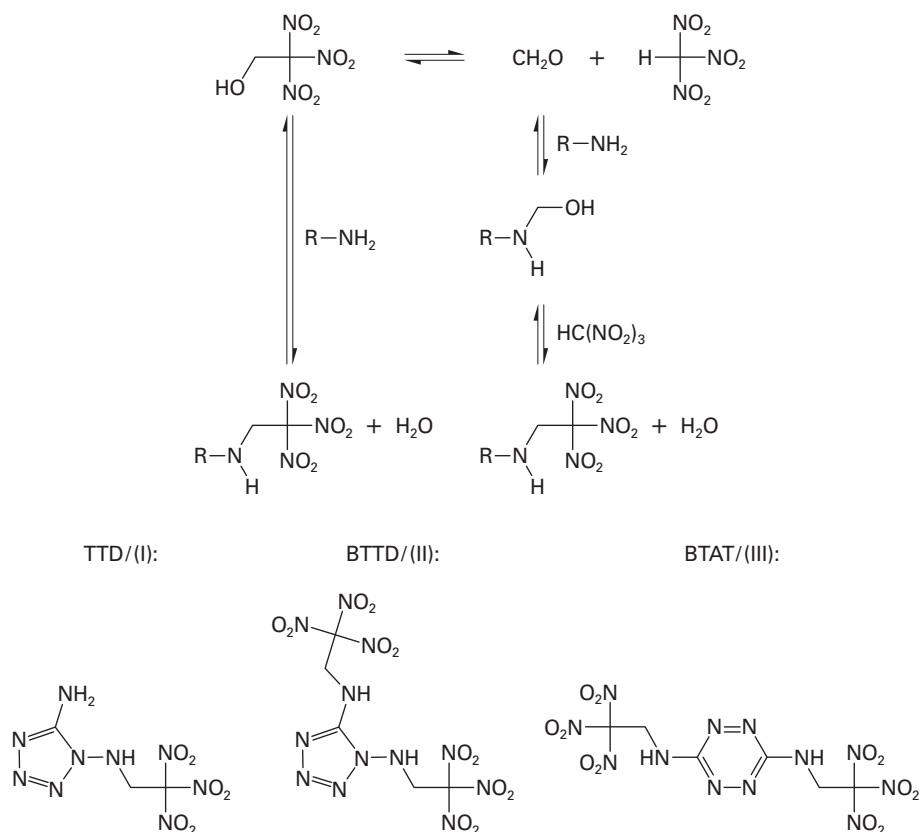
Fig. 9.18 Mannich reaction for the synthesis of trinitroethyl-tetrazole-1,5-diamine (TTD), bis(trinitroethyl)-tetrazole-1,5-diamine (BTTD) and bis(trinitroethyl)-1,2,4,5-tetrazine-3,6-diamine (BTAT).
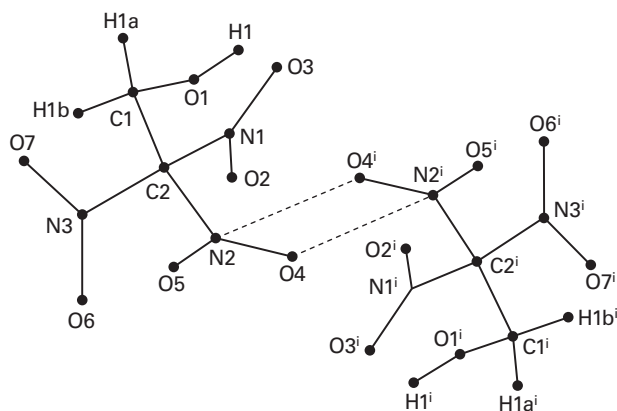
Fig. 9.19 Intermolecular dipolar nitro group interactions in trinitroethanol.

Tab. 9.6 Properties of TTD and BTAT in comparison with RDX.

	TTD	BTAT	RDX
formula	$C_3H_5N_9O_6$	$C_6H_6N_{12}O_{12}$	$C_3H_6N_6O_6$
$\Omega/\%$	−15.2	−10.9	−21.6
$\Delta_fH°(s)/kJ\,mol^{-1}$	+356	+336	+85
$\Delta_fU°(s)/kJ\,kg^{-1}$	1443	852	280
$T_{dec.}/°C$	126	184	202
$\rho/g\,cm^{-3}$	1.831	1.886	1.80
$D/m\,s^{-1}$	9194	9261	8894
$p_{C\text{-}J}/kbar$	370	389	338
T_{ex}/K	4650	4867	4290
$Q_{C\text{-}J}/kJ\,kg^{-1}$	6018	6135	5875
$V_0/l\,kg^{-1}$	788	743	797
impact sensitivity / J	30	7	7
friction sensitivity / N	40	160	120

An important characteristic of these compounds is that due to the dipolar nitro groups, the molecules form strong intra and intermolecular interactions including hydrogen bonds, which contribute not only to an increase in the thermal stability, but also to a higher density. This is particularly clear in trinitroethanol due to its intermolecular dipolar nitro group interactions (Fig. 9.19). The molecular structures of TTD, BTTD and BTAT which were obtained using single crystal X-ray diffraction are shown in Figures 9.20−9.22. The high densities, combined with the endothermic character of the tetrazole or tetrazine moieties and the good oxygen balance of the trinitroethyl group, all result in very good detonation parameters (Tab. 9.6).

As can be observed in Table 9.6, TTD and BTAT have good to very good performance parameters with acceptable sensitivities, however, since TTD decomposes
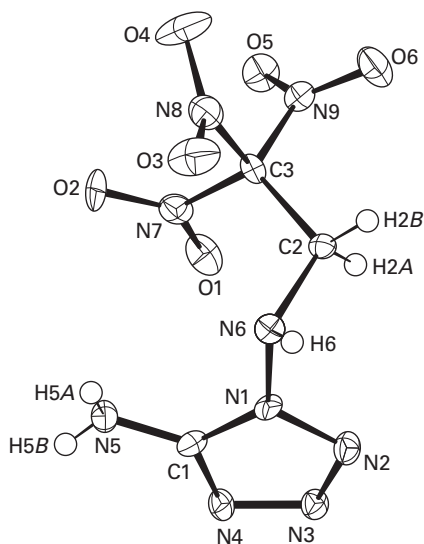
Fig. 9.20 Molecular structure of trinitroethyl-tetrazole-1,5-diamine (TTD) from single crystal X-ray diffraction data.
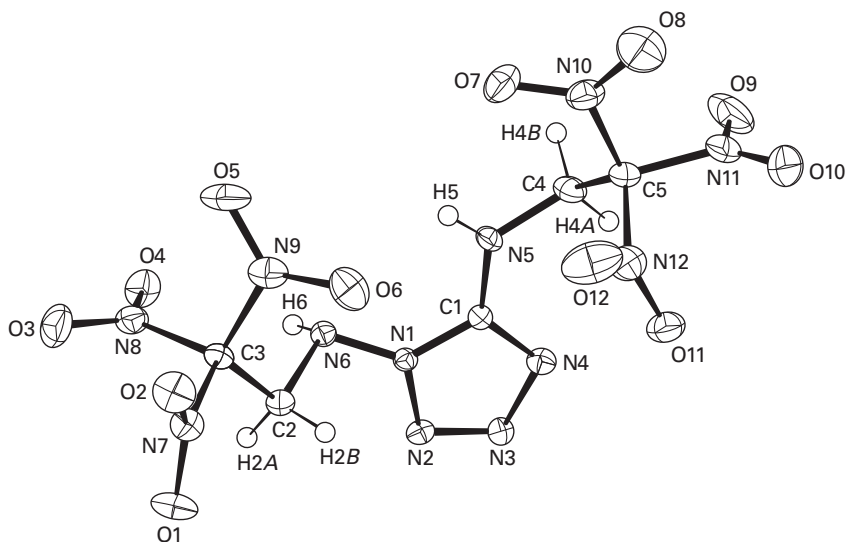
Fig. 9.21 Molecular structure of bis(trinitroethyl)-tetrazole-1,5-diamine (BTTD) from single crystal X-ray diffraction data.

at 126 °C, its thermal stability is too low. In contrast, BTAT is stable to 184 °C (DSC, 5 °C/min). A long-term study at 140 °C for 48 h also showed no decomposition of BTAT.
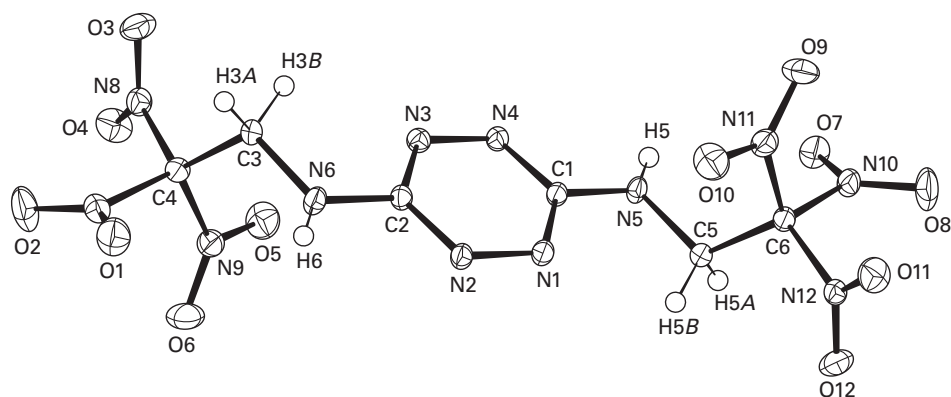
Fig. 9.22 Molecular structure of bis(trinitroethyl)-1,2,4,5-tetrazine-3,6-diamine (BTAT) from single crystal X-ray diffraction data.

$C_6H_6N_{12}O_{12}$, $T_{dec} > 180\,°C$, $\Sigma\,(O,N) > 82\,\%$, $D = 9261\ m\ s^{-1}$, $P_{CJ} = 389\ kbar$
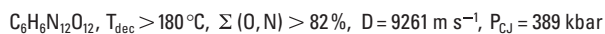
Fig. 9.23 Explosion of bis(trinitroethyl)-1,2,4,5-tetrazine-3,6-diamine (BTAT) in Koenen test.

At this point it should be pointed out, that BTAT has the same CHNO composition as CL-20, but it is significantly less sensitive than the energetic ε modification of CL-20. Figure 9.23 shows a photo of a steel-sleeve test (Koenen test) performed using BTAT with a critical diameter of 10 mm (see Ch. 6.1).

As we have already seen, trinitromethane and trinitroethanol are important starting materials in the synthetic chemistry of highly nitrated compounds. The precursor potassium trinitromethanide can be prepared best from tetranitromethane (TNM):
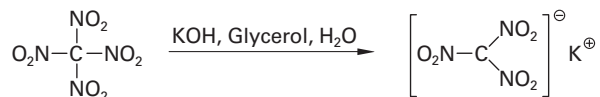
Free trinitromethane can be obtained by acidification with phosphoric acid:

$$K^+[C(NO_2)_3]^- \xrightarrow{H_3PO_4} H{-}C(NO_2)_3$$
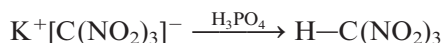
Tetranitromethane can itself be prepared in good yield by the nitration of acetic anhydride or isopropanol using conc. HNO_3. The synthesis requires very exact control of the reaction conditions and is not without danger.

$$4\,(CH_3CO)_2O + 4\,HNO_3 \rightarrow C(NO_2)_4 + 7\,CH_3COOH + CO_2$$

Finally, trinitroethanol (TNE) can be obtained by the condensation of trinitromethane with formaldehyde (paraformaldehyde) in acidic conditions:

$$H{-}C(NO_2)_3 + H_2CO \rightarrow HO{-}CH_2{-}C(NO_2)_3$$
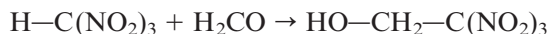
The corresponding chlorocarbonate can be obtained by the reaction of free TNE with phosgene, and is also an important building block in the chemistry of poly-nitro-compounds (Fig. 9.24).
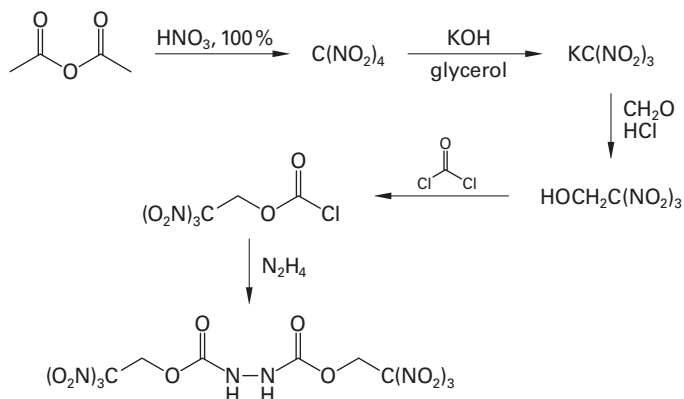
Fig. 9.24 Synthesis of trinitroethanol and trinitroethylchlorocarbonate.

A better method for obtaining the chlorocarbonate is by stirring a mixture of TNE, FeCl$_3$, CCl$_4$ and a few drops of water under reflux for an hour.

The synthesis of hydrazinium nitroformate (HNF) occurs best through the reaction of anhydrous hydrazine with trinitromethane (nitroform) in methanol or diethyl ether:

$$H\text{—}C(NO_2)_3 + N_2H_4 \rightarrow [N_2H_5]^+[C(NO_2)_3]^-$$
$$HNF$$
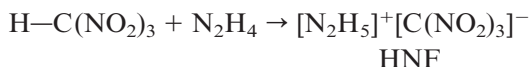
9.3.3 Ionic Liquids

The term ionic liquids refers to liquids that exclusively contain ions. They are liquid salts which do not need to be dissolved in a solvent such as water. As a rule, the term ionic liquids is used when the corresponding salts are liquid at temperatures lower than 100 °C. Examples of suitable cations are alkylated imidazolium, pyridinium, ammonium or phosphonium ions. The size and the symmetry of the participating ions prevents the formation of a strong crystal lattice, meaning that only small amounts of thermal energy are needed to overcome the lattice energy and break up the solid crystal structure.

Current research is focused on finding suitable nitrogen-rich anions, so that ionic liquids could also be used as fuels in bipropellants (see Ch. 2.2 and Ch. 2.4). In comparison with the currently used fuels such as MMH and UDMH, ionic liquids would possess a negligible low vapor pressure and therefore considerably reduce the inhalation toxicity. Initial investigations have shown that the dicyanamide anion, $[N(CN)_2]^-$, in combination with the 1-propargyl-3-methyl-imidazolium cation may be a suitable ionic liquid for rocket propulsion. However, using WFNA as the oxidizer, the ignition delay is 15 ms, comparative to 1 ms for the MMH / NTO system and 9 ms for MMH / WFNA [57].

Ionic liquids should also be very suitable for use as monopropellants, but the salts used must contain either the oxidizer and fuel combined, or salt mixtures which contain both oxidizing and reducing salts. Since these mixtures are homogeneous systems which contain both the oxidizer and fuel, they can be labeled as monopropellants, just as hydrazine is. Particularly interesting are salt mixtures which are less toxic and have a lower vapor pressure than hydrazine. Such mixtures are also known as "green propellants". Suitable anions are the nitrate or dinitramide ions [58]. A combination which has already been studied intensively as an oxidizer is the HAN, hydroxylammonium nitrate system. ADN, ammonium nitrate (AN) and hydrazinium nitrate (HN) have also been investigated. As fuels, hydroxylammonium azide (HAA), ammonium azide (AA) or hydrazinium azide (HA) may be appropriate. As a rule, these salt mixtures are not used as pure substances on safety grounds, but with 20 or 40 % water added; they then decom-

Tab. 9.7   Influence of the water content on the specific impulse (in s) of oxidizing and reducing salt mixtures.

oxidizer	fuel	I^*_{sp} (0% water)	I^*_{sp} (20% water)	I^*_{sp} (40% water)
HAN	HAA	372	356	319
HAN	AA	366	342	303
HAN	HA	378	355	317
ADN	HAA	376	352	317
ADN	AA	362	335	303
ADN	HA	373	347	314
AN	AA	349	324	281
AN	HAA	366	342	303
AN	HA	359	334	293
HN	AA	374	349	309
HN	HAA	401	354	316
HN	HA	379	354	314
	Hydrazine	224		

R^1, R^2 = Me, Et, $CH_2CH_2\text{-}N_3$, NH_2
R^3 = H, Me, NH_2, $CH_2\text{-}N_3$
X   = NO_3^-, $N(NO_2)_2^-$, ClO_4^-, N_3^-
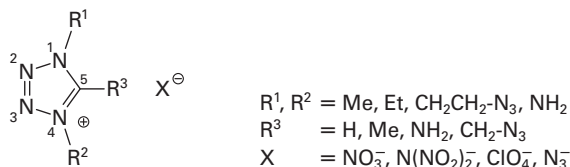
Fig. 9.25   1,4,5-Substituted tetrazolium cation with different energetic anions X.

pose catalytically in an exothermic reaction. Table 9.7 shows the dependence of the calculated specific impulses on the water content for such salt mixtures.

Quite recently several new energetic ionic liquids (EILs) have been synthesized either consisting of imidazole salts or 1,2,4-triazole salts but until now only few EILs from derivatives of tetrazole have been described in the literature. Tetrazoles are built of 5-membered heterocycles with four nitrogen atoms in the ring. The heats of formation ($\Delta_f H°$) get more and more positive with increasing number of nitrogen atoms (imidazole $\Delta_f H° = +58.5$ kJ mol^{-1}, 1,2,4-triazole $\Delta_f H° = +109.0$ kJ mol^{-1}, 1,2,3,4-tetrazole $\Delta_f H° = +237.2$ kJ mol^{-1}). Furthermore the use of tetrazoles is of great interest since the generation of molecular nitrogen as an end-product of propulsion is highly desirable. Also the formation of carbon residues can be minimized. Tetrazoles can be synthesized by many different synthetic routes, which are mostly low in price and also portable in larger scales.

In the future, 1,4,5-substituted tetrazolium salts with the general formula depicted in Fig. 9.25 should be synthesized and evaluated. Due to the introduction of hydrophobic side chains (except for NH_2) one would expect these compounds to have melting points below 100 °C.

It should be advantageous to introduce methyl-, ethyl-, ethylazide- and amino-groups, on the 1- and 4-position of the tetrazole ring system as well as hydrogen,

$X = NO_3^-$ (**1**), $N(NO_2)_2^-$ (**2**), ClO_4^- (**3**), N_3^- (**4**)
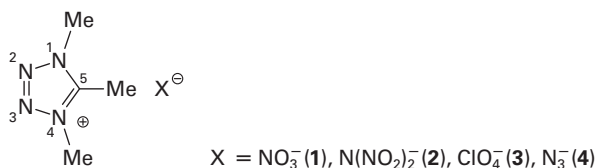
Fig. 9.26   Energetic Ionic Liquids based on the 1,4,5-trimethyltetrazolium ($TMTz^+$) cation.

Tab. 9.8   Calculated gas phase heats of formation of **1**–**4**.

	1	2	3	4
$\Delta H°f(g)$ / kcal mol^{-1}	128	173	136	248

methyl-, amino- and methylazido groups to the 5-position. Theoretical calculations have shown that these tetrazolium salts in combination with classic energetic and oxidizing anions like nitrate (NO_3^-), dinitramide ($N(NO_2)_2^-$), perchlorate (ClO_4^-) or azide (N_3^-) should have high heats of formation and, consequently, high specific impulses. For example, the 1,4,5-trimethyltetrazolium cation (Fig. 9.26), which is not able to form classical hydrogen bonds, has a calculated gas phase enthalpy of formation of 127.6 kcal mol^{-1}. In combination with the energetic anions X = nitrate, dinitramide, perchlorate, and azide (Fig. 9.25) four new EILs, with high heats of formation can be discussed. Table 9.8 summarize the calculated thermodynamic parameters.

A significant step to a lower-toxicity bipropulsion system would be the demonstration of hypergolicity (spontaneous ignition) between an ionic liquid, which is a paragon of low vapor toxicity, and a **safer oxidizer**. Apart from cryogens, hydrogen peroxide seems to be especially promising because of its high performance, less-toxic vapor and corrosivity, and its environmentally benign decomposition products, which make handling this oxidizer considerably less difficult than N_2O_4 or HNO_3. A high fuel performance can be fostered by light metals with large combustion energies and relatively light products. Elements with considerable performance advantages and nontoxic products are aluminum and boron. The need for light combustion products through the production of hydrogen gas and water vapor is fulfilled by a high hydrogen content. Aluminum and boron are well known for their ability to serve as hydrogen carriers in neutral and ionic molecules.

Quite recently, Schneider and other researchers from the Air Force Research Laboratory at Edwards AFB tested various ILs with 90 % and 98 % H_2O_2 [57b]. In view of the advantages of high hydrogen content, ILs containing $[Al(BH_4)_4]^-$ ions may be viewed as a densified form of hydrogen stabilized by metal atoms. In this recently published study, Schneider et al. investigated the new compounds trihexyltetradecylphosphonium tetrahydridoborate [THTDP][BH$_4$] (**1**) and [THTDP][Al(BH$_4)_4$] (**2**) (Fig. 9.27).
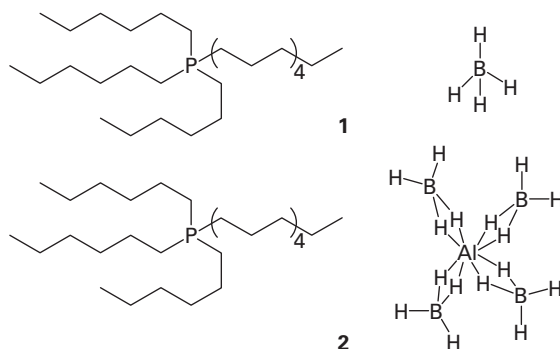
Fig. 9.27   Borohydride based ionic liquids [THTDP][BH$_4$] (**1**) and [THTDP][Al(BH$_4$)$_4$] (**2**).

Tab. 9.9a   Drop test results of **2** on four oxidizers.

	90% H$_2$O$_2$	98% H$_2$O$_2$	N$_2$O$_4$ (NTO)	WFNA[a]
reaction	ignition	ignition	ignition	explosion
ignition delay/ms	< 30	< 30	ignition in vapor phase before the liquids combined	–

[a] WFNA = white fuming nitric acid

Tab. 9.9b   Computed equilibrium I_{sp} values[a].

O/F (mass %)	NTO/MMH	N$_2$H$_4$/H$_2$O$_2$	(THTDP)[Al(BH$_4$)$_4$] (**2**)
50/50	287	292	218
60/40	311	**304**	226
70/30	**321**	303	257
80/20	286	269	291
85/15			**302**
90/10			286

[a] chamber pressure = 15 bar, expansion pressure = 0.05 bar

Compounds **1** and **2** were subjected to drop tests to determine their reactivity with common propulsion oxidizers, including 90% and 98% H$_2$O$_2$ (Table 9.9a). While **1** lights only 3 s after dropping onto H$_2$O$_2$, the ignition delay of **2** was quite short. The hypergolic dicyanamide ILs display changes in delay times (with white fuming nitric acid, WFNA) from 30 ms to 1000 ms upon reversal of the order of addition of oxidizer and fuel. In contrast, the ignition of **2** is equally fast regardless of the order of addition. These simple drop tests place only upper limits on the ignition delays because ignition may be initiated by hydrogen, which burns with an almost invisible flame. However, these tests do demonstrate that an IL with a

complex $[Al(BH_4)_4]^-$ anion is universally reactive with traditional rocket oxidizers including lower hazard H_2O_2. The computed specific impulses for various H_2O_2/**2** ratios in comparison with the systems $NTO(N_2O_4)$/MMH and N_2H_4/H_2O_2 are summarized in Tab. 9.9b. Furthermore, this new class of ILs holds the potential for enabling high-performing, noncryogenic, green bipropulsion for the first time.

9.4 Dinitroguanidine Derivatives

Exceeding the detonation performance of known explosives such as RDX (1,3,5-trinitro-1,3,5-hexahydrotriazine) is a long term research goal in the field of new energetic compounds. The development of strained cages like CL-20 (HNIW: 2,4,6,8,10,12-hexanitro-2,4,6,8,10,12-hexaazaiso-wurzitane) or ONC (octanitrocubane) has attracted lots of interest, however both materials have several drawbacks. The existence of polymorphs as well as a cost intensive preparation makes both compounds disputable for contemporary application. As an aside, highly nitrated compounds like HNB (hexanitrobenzene) show the most promising properties, but their chemical stability towards acids or bases is often not good enough. As the material density is the key for well performing high explosives, a different approach has been started with the concept of zwitterionic structures. A molecule capable of fulfilling these requirements is 1,2-dinitroguanidine (DNQ), which has been reported and well described in the literature previously. The crystallographic characterization of DNQ shows different nitro group surroundings, contrary to dissolved DNQ which shows rapid prototropic tautomerism. The presence of an acidic nitramine (pK_a = 1.11) in DNQ makes it possible to produce monoanionic dinitroguanidine salts. Nucleophilic substitution reactions involving the dinitroguanidine anion are reported in literature as well.

1,2-Dinitroguanidine (**1**) can easily be synthesized as reported by Astrat'yev. The synthetic route is shown in Figure 9.28. Since it is known that strong nucleophiles like hydrazine or ammonia can substitute nitramine groups at elevated temperatures, **ADNQ** (ammonium dinitroguanidine) was produced from a stoechiometric amount of ammonium carbonate to avoid the free base. 1,7-Diamino-1,7-dinitrimino-2,4,6-trinitro-2,4,6-triaza-heptane (**APX**) was also synthesized according to the method of Astrat'yev, starting from 1,3-bis(chloromethyl)nitramine (**2**) and potassium dinitroguanidine (**3**). The former compound is readily available from the nitrolysis of hexamine with subsequent chlorination.

Differential scanning calorimetry (DSC) measurements were used to determine the decomposition temperatures of APX and ADNQ, and indicate that decomposition of APX starts with an onset temperature of 174 °C. In contrast to this behavior the decomposition temperature of the ionic compound ADNQ is 197 °C. In addition, both compounds were tested according to the UN3c standard in a Systag, FlexyTSC Radex oven at 75 °C for 48 hours with the result, that no weight loss or decomposition products were detected.
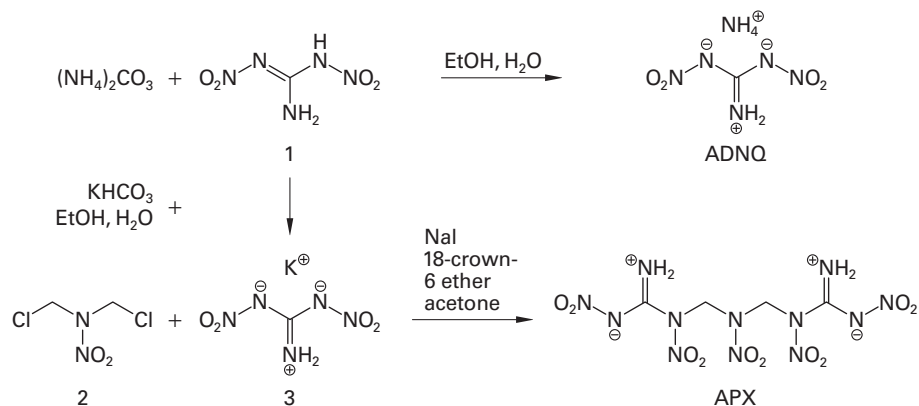
Fig. 9.28 Synthesis of ammonium dinitroguanidine (ADNQ) and 1,7-Diamino-1,7-dinitrimino-2,4,6-trinitro-2,4,6-triaza-heptane (APX).

The detonation parameters calculated with the EXPLO5 program using the experimentally determined densities (X-ray) as well as some sensitivity values are summarized in Table 9.8. Especially the detonation parameters of APX are particularly promising exceeding those of TNT and RDX and in part even those of HMX. The most important criteria of high explosives are the detonation velocity (D = APX: 9540, ADNQ: 9066, TNT: ~7178, RDX: 8906, HMX: 9324 m s^{-1}), the detonation pressure ($p_{\text{C-J}}$ = APX: 398, ADNQ: 327, TNT: 205, RDX: 346, HMX: 393 kbar) and the energy of explosion (Q_v = APX: −5943, ADNQ: −5193,TNT: 5112, RDX: −6043, HMX: −6049 kJ kg^{-1}) [59a].

The sensitivity and performance values (Tab. 9.10) revealed that ADNQ may be a high-performing but still relatively insensitive high explosive, while APX needs to be classified as a primary explosive due to its high impact sensitivity.

Tab. 9.10 Detonation parameters.

	APX	APX + 5% PVAA	ADNQ
ρ / g cm^{-3}	1.911	1.875	1.735
Ω / %	−8.33	−16.28	−9.63
Q_v / kJ kg^{-1}	−5935	−5878	−5193
T_{ex} / K	4489	4377	3828
$p_{\text{C-J}}$ / kbar	398	373	327
D / m s^{-1}	9540	8211	9066
V_0 / l kg^{-1}	816	784	934
IS / J	3	5	10
FS / N	80	160	252
ESD / J	0.1	−	0.4

9.5 Co-Crystallization

Until recently, co-crystallization methods have only been used in pharmaceuticals. However, the hope in the energetics area is that due to strong intermolecular interactions (π stacking, H-bonding) one could reduce the sensitivity of a particular good performer which is too sensitive (e.g. CL-20, APX etc.) when co-crystallized with another compound. Unfortunately, when a high explosive is co-crystallized with a non-energetic compound, the energetic component inevitably sees its explosive power diluted. Quite recently, Matzger et al. reported the first energetic-energetic co-crystal composed of CL-20 and TNT in a 1:1 molar ratio [59c]. The co-crystal CL-20˙TNT also exemplifies the capabilities of aliphatic, highly nitrated compounds to co-crystallize despite their lack of strong, predictable interactions. With no available π-π stacking, this co-crystal forms based on a series of CH hydrogen bonds between nitro group oxygens and aliphatic hydrogens as well as interactions between the electron-deficient ring of TNT and nitro groups of CL-20 (Fig. 9.29). The co-crystal CL-20˙TNT has a density of 1.91 g cm^{-3}, which is somewhat lower than those of CL-20 polymorphs (1.95−2.08 g cm^{-3}), but still substantially higher than that of TNT (1.70−1.71 g cm^{-3}). The impact sensitivity of CL-20˙TNT was measured using a drop test and determined to be approximately half as sensitive as CL-20. Therefore, incorporating insensitive TNT into a co-crystal with sensitive CL-20 greatly reduces its impact sensitivity, potentially improving the viability of CL-20 in explosive applications. This initial study holds promise that more energetic−energetic co-crystals may be discovered from among the nitro-rich, non-aromatic compounds that dominate the field.
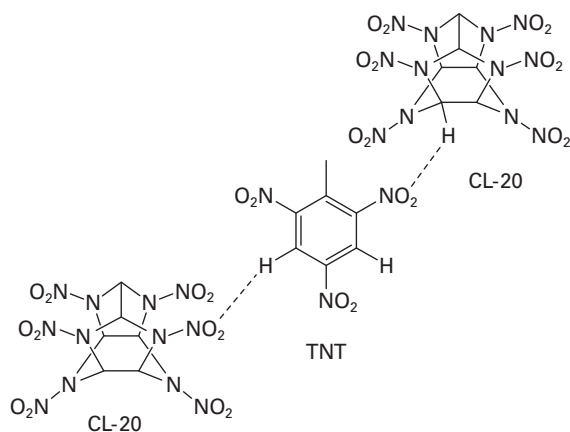
Fig. 9.29 Molecular assembly in the co-crystal CL-20˙TNT.

9.6 Future Energetics

Great strides have been made in increasing performance and decreasing sensitivity in energetic materials since the first commercialization of nitroglycerine (NG) in the form of dynamite in 1867 by Alfred Nobel. However, the DoD continues rely on traditional, half-century old energetics to meet their combat needs. New energetic materials must be developed to enable DoD to advance beyond traditional thought on energetic capabilities, to transition to the next stage in combat, and to maintain a lethality overmatch with all enemies.

Energetic materials are most commonly used in either high explosives or propellant formulations. Certain parameters are important in determining the effectiveness of new molecules in these formulations, including high densities (ρ), good oxygen balance (Ω) and high detonation/combustion temperatures and high specific impulses (I_{sp}) for rocket propellant formulations and lower combustion temperatures combined with a high force and pressure and a high N_2/CO ratio of the reaction gases for gun propellants.

Using the heat of explosion (Q), the detonation velocity (D) and the detonation pressure (P) as a measure for the performance of a high explosive, one can clearly see from Fig. 9.30 that since the time NG was taken into service the performance of chemical explosives has improved substantially.

In spite of the many years of research, there are limited possibilities to realize a substantial increase in performance from conventional C-H-N-O explosives. Recent advances in energetics energy output have come in improved processing or inclusion of energetic binders to increase overall formulation energy, but limited success has been realized in the development of novel energetics. One reason for this is that conventional nitramine and nitroaromatic explosives such as TNT, RDX, HMX and other similar molecules share the same three limitations (Table 9.11):

(i)   they are not nitrogen-rich ($N \leq 50\%$);
(ii) the oxygen-balance is not close to zero;
(iii) formulations (mixtures of various HEs) are required to achieve a good oxygen balance.
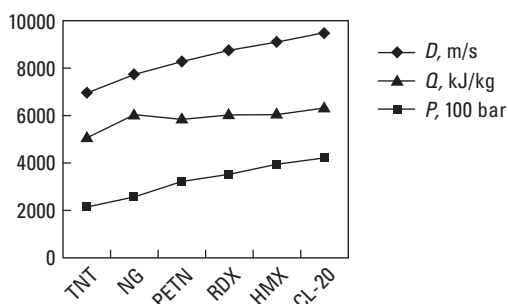
Fig. 9.30 Performance of chemical explosives.

Table 9.11 Nitrogen content (N) and oxygen balance (Ω) of conventional HEs.

	N / %	Ω / %
TNT	18.5	-73.9
PETN	17.7	-10.1
RDX, HMX	37.8	-21.6
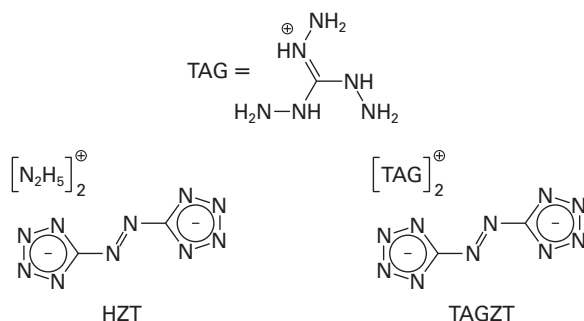
Fig. 9.31 Chemical Structure for HZT and TAGZT

Nitrogen rich molecules are desired as energetics because of the high energy content in N—N bonds. Oxygen balance is defined as the percentage of used oxygen that remains or is needed after an oxidation reaction and can therefore be positive or negative. Materials with an oxygen balance close to zero are typically, but not always, more effective energetics since all of the oxygen is used up in reaction. An oxygen balance can be modified through formulation additions to bring the overall formulation oxygen balance close to zero.

Researchers have already realized the energy content limit for CHNO based molecules. Research needs to expand beyond this way of thinking and increase efforts to explore different molecular structures and molecular make-up in order to realize the substantial increase in performance that will be required for future combat systems. Early research has shown that materials with a high nitrogen content offer many advantages to those with carbon backbones, including the potential for vastly increased energy content. Research into molecules with high nitrogen content ($> 50\%$) has shown potential for a substantial increase in available energy. The first generation of high-nitrogen compounds, such as hydrazinium azotetrazolate (HZT) and triamino-guanidinium azotetrazolate (TAGZT) (Fig. 9.31), did indeed meet the criteria for being nitrogen rich and proved to be very desirable ingredients in erosion-reduced gun propellants (see Fig. 4.4a), however, due to the unfavorable oxygen balance such compounds are not suitable as energetic fillers in high explosive compositions (Tab. 9.12).

The second generation of high-nitrogen compounds which have improved oxygen balances such as TKX-50 and ABTOX (Fig. 9.32), combines desirable high nitrogen content with a good oxygen balance (Tab. 9.12). These compounds are

Tab. 9.12 N content and Ω of high-N compounds.

		N / %	Ω / %
1st generation	HZT	85	-63
	TAGZT	82	-73
2nd generation	TKX-50	59	-27
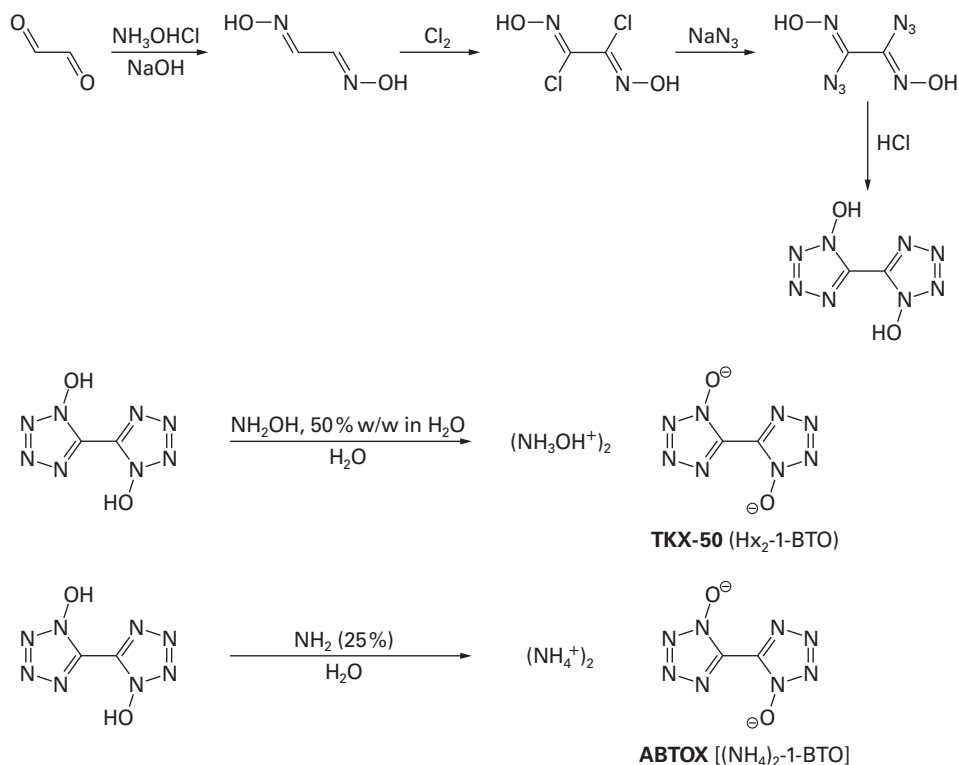
Fig. 9.32 Synthesis of 1-BTO from DAGL (top) and synthesis of TKX-50 and ABTOX (bottom)

therefore more suitable for use in high-explosive formulations. Moreover, materials with an oxygen balance close to zero are also suitable as powerful ingredients in solid rocket propellants. An increase of the I_{sp} of only 20 s would be expected to increase the payload or range by ca. 100 %. Related to this, Fig. 4.4a shows the computed performance parameters for conventional and high-N gun propellants.

The computed and predicted performance values not only exceed the first generation of high-nitrogen compounds (*e.g.* HZT) but, in case of TKX-50, also the performance values of RDX and HMX (Fig. 9.33).
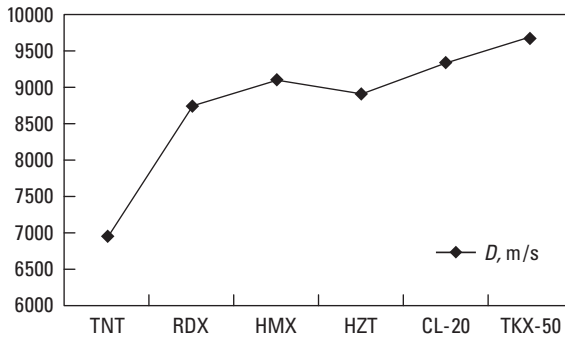
Fig. 9.33 Performance of conventional and high-nitrogen explosives (D = VoD)

Future research will lead to even more powerful, high-nitrogen high-oxygen explosives with enhanced and superior detonation parameters to fulfil the lethality requirements of all forces. New energetics will provide vastly increased energy content over RDX, up to several times the energetic performance. In addition, these materials will have a high energy density with a high activation energy.

With these capabilities, DoD will be able to develop new applications for energetic materials and vastly improve performance in current munitions. The increased performance of the next generation of energetics will enable DoD to meet the same strategic goals with fewer munitions and less energetic material. The increase in energy output can be harnessed in munitions that require a fraction the amount of energetics to deliver the same payload or thrust profile. This will allow engineers to put energetics in munitions that have never had them before.

10 Synthesis of Energetic Materials

10.1 Molecular Building Blocks

Most inorganic or organic energetic materials contain at least one of the building blocks shown in Table 10.1 and can therefore be classified by their functional groups.

Tab. 10.1   Molecular building blocks for energetic materials.

group	energetic substance	example
—O—O—	organic peroxo compounds	TATP
ClO_3^-	chlorate	$KClO_3$
ClO_4^-	perchlorate	AP
—NF_2	organic difluoramine derivatives	HNFX-1
—NO_2	organic nitro compounds	TNT
—O—NO_2	organic nitrato- or nitroesters	NG, PETN, NG-A
NO_3^-	nitrate	AN
—N=N—	organic or inorganic diazo compounds	TAGzT
—N_3	covalent azides	GAP
N_3^-	ionic azides	$[N_2H_5][N_3]$, hydrazinium azide
—NH—NO_2, —NR—NO_2	nitramino compounds	RDX, HMX
$N(NO_2)_2^-$	dinitramide	ADN
=N—NO_2	nitrimino compounds	nitriminotetrazole
—CNO	fulminates	$Hg(CNO)_2$, mercury fulminate
—C≡C—	acetylides	Ag_2C_2, silver acetylide

The molecular structures of nitriminotetrazole and tetrakis(difluoramino)octahydro-dinitro-diazocine (HNFX) have not been discussed so far and are shown in Figure 10.1.

It is interesting that nitriminotetrazole contains an oxidizing nitrimino group in addition to the endothermic ring, which helps to create a more positive oxygen balance ($\Omega = -12.3\%$). HNFX works similarly as it corresponds to a HMX molecule in which two of the nitramine groups are exchanged for $C(NF_2)_2$ groups. In this example, the two remaining nitramine groups and the introduced difluoroamine groups act as strong oxidizers.
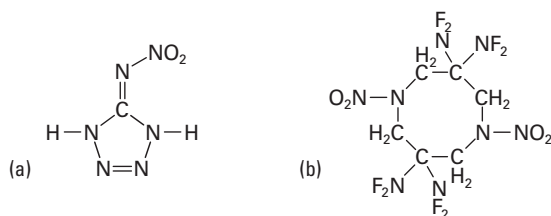
Fig. 10.1   Molecular structures of nitriminotetrazole (a) and tetrakis(difluoramino)octahydro-dinitro-diazocine (HNFX) (b).

10.2 Nitration Reactions

As we have seen in Table 1.2, practically all formulations used by the military contain TNT, as well as RDX and/or HMX. Additionally, PETN and nitroglycerine (in dynamite) play an important role. All these substances are obtained by nitration reactions. An overview of different types of nitration is given in Table 10.2.

Tab. 10.2   Possible nitration reactions.

reaction	C nitration	O nitration	N nitration
product	nitro compounds, $R-NO_2$	nitrate ester, $R-O-NO_2$	nitramine, $R-NH-NO_2$
examples	TNT, PA, tetryl, TATB, HNS	NC, NG, PETN, NG-A	RDX, HMX, NQ
nitrating agent	mixed acid: HNO_3/H_2SO_4	mixed acid: HNO_3/H_2SO_4	mixed acid: HNO_3/H_2SO_4, HNO_3 (100%)

The nitration of organic compounds still occurs almost exclusively using mixed acid or 65 % to 100 % HNO_3. Mixed acid is a mixture of concentrated nitric acid and concentrated sulfuric acid, which acts as a very strong nitrating agent due to the presence of the NO_2^+ ion.

$$HNO_3 + H_2SO_4 \rightarrow H_2ONO_2^+ + HSO_4^-$$

$$H_2ONO_2^+ + HSO_4^- + H_2SO_4 \rightarrow NO_2^+ + H_3O^+ + 2\,HSO_4^-$$
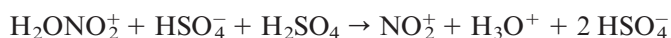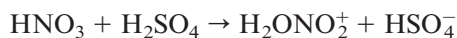
Aromatic hydrocarbons can be converted into nitro compounds via an electrophilic substitution using mixed acid. For example, trinitrotoluene is obtained by the direct nitration of toluene using mixed acid. Other good nitrating agents are $NO_2^+BF_4^-$ and $NO_2^+OSO_2CF_3^-$ (nitronium triflate) in CH_2Cl_2 with ultrasonic activation.

A good example of an N-nitration which can be undertaken using mixed acid or 100 % HNO_3, is the nitration of aminotetrazole to nitriminotetrazole (Fig. 10.2) [59b]:
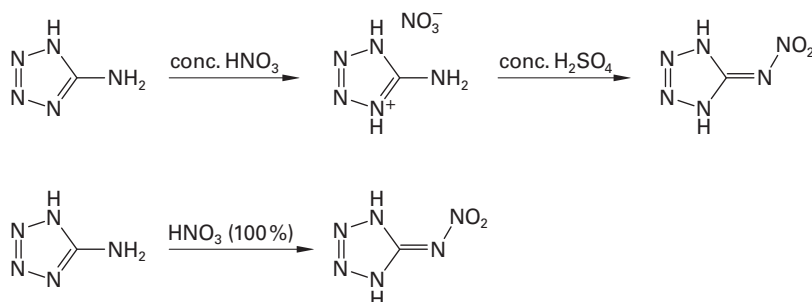
Fig. 10.2   Nitration of aminotetrazole to nitriminotetrazole.

Nitriminotetrazole can also be obtained in good yield by the diazotization of nitroaminoguanidine to nitroguanylazide and subsequent cyclization under alkaline conditions (Fig. 10.3).

nitroaminoguanidine   nitroguanylazide
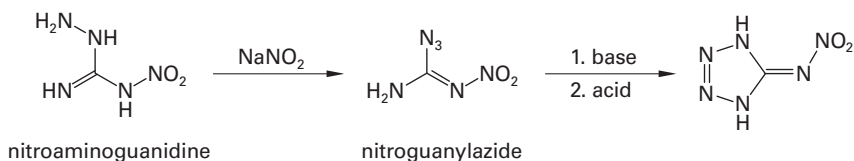
Fig. 10.3   Synthesis of nitriminotetrazole from nitroaminoguanidine.

A further example of a nitration using nitric acid is the preparation of RDX from hexamethylentetramine (HMTA) via triacetyltriazine (TART) in a two-step reaction (Fig. 10.4):

HMTA   TART   RDX
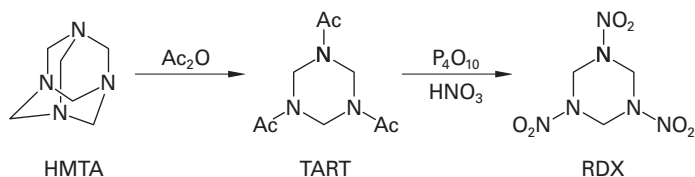
Fig. 10.4   Synthesis of hexogen (RDX) from hexamethylentetramine (HMTA) via triacetyltriazine (TART).

In modern synthetic chemistry N_2O_5 can also be used as a nitrating agent; it is advantageous because anhydrous conditions can be used and, if pure N_2O_5 is used, there are no acidic impurities present. If acidic impurities do not matter, a mixture of N_2O_5 and HNO_3 is also a good and strong nitrating agent.

Previously, technical N_2O_5 was mainly obtained by the dehydration of nitric acid at $-10\,°C$, as N_2O_5 is the anhydride of nitric acid. It is an easily sublimed solid (subl. $32\,°C$, 1 bar).

$$12\ HNO_3 + P_4O_{10} \xrightarrow{-10\,°C} 6\ N_2O_5 + 4\ H_3PO_4$$
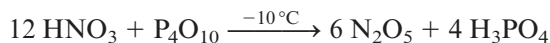
Since 1983, the technical synthesis usually used follows that developed by Lawrence Livermore National Laboratory, in which the electrolysis of nitric acid in the presence of N_2O_4 results in the formation of a approx. $15-20\,\%$ solution of N_2O_5 in anhydrous nitric acid.

$$2\ HNO_3 \xrightarrow{N_2O_4,\ 2e^-} N_2O_5 + H_2O$$
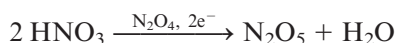
In the following, we want to look at a further way to produce pure and almost acid-free N_2O_5. This was developed into a semi-industrial process (pilot plant) as late as 1992 in the DRA Laboratories (Defence Research Agency). This method involves the gas-phase ozonization of N_2O_4 using an ozone-oxygen mixture with an approx. $5-10\,\%$ ozone content [60, 61].

$$N_2O_4 + O_3 \rightarrow N_2O_5 + O_2$$
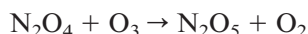
Solutions of pure N_2O_5 in chlorinated organic solvents (CH_2Cl_2, $CFCl_3$) are mild nitrating agents, which have recently found a wide range of applications (Tab. 10.3).

An example of a ring-opening nitration reaction is shown below.

$$\text{cyclo-}(CH_2)_nX \xrightarrow{N_2O_5,\ CH_2Cl_2,\ 0-10\,°C} O_2NO-(CH_2)_n-X-NO_2$$

$(n = 2\ \text{oder}\ 3;\ X = O\ \text{oder}\ NR\ (R = Alkyl))$
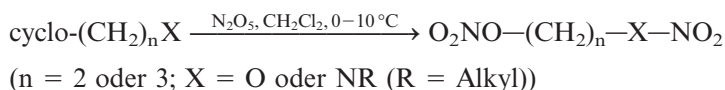
If the substituent on nitrogen is an H atom and not an alkyl group, the nitration occurs with preservation of the cyclic, four-membered ring structure.

$$\text{cyclo-}(CH_2)_3NH \xrightarrow{N_2O_5,\ CH_2Cl_2,\ 0-10\,°C} \text{cyclo-}(CH_2)_3N(NO_2)$$
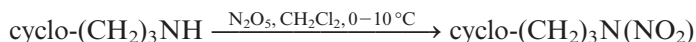
Tab. 10.3 Synthetic application of CH_2Cl_2 / N_2O_5 solutions.

reaction type	product
aromatic nitration	$C-NO_2$
nitrolysis	$N-NO_2$
ring opening reactions	$N-NO_2$ or $O-NO_2$
selective nitration	$O-NO_2$ (rarer $N-NO_2$)

In a similar synthetic route, the strong oxidizers TNAZ (trinitroazetidine) and CL-20 were prepared (Fig. 1.7).

ADN is a unique highly energetic material, because it does not contain carbon, chlorine or fluorine. ADN is an environmentally benign high energy inorganic oxidizer salt, first synthesized in 1971 at the Zelinsky Institute of Organic Chemistry in Moscow. It is claimed that ADN-based solid propellants are in operational use in Russian TOPOL intercontinental ballistic missiles and that ADN was previously produced in ton-scale quantities in the former USSR. ADN forms colorless crystals and is a very oxygen-rich nitrogen oxide, which possesses excellent properties for use as an explosive (in combination with strong reducing agents such as aluminum, aluminum hydride or organic compounds) or solid rocket propellant. Additionally, the absence of halogens makes ADN an environmentally friendly solid rocket propellant and makes RADAR detection of the rocket emission more difficult. ADN is currently being tested as one of the most promising replacements for ammonium perchlorate [62].

Ab initio calculations predict a structure with C_2 symmetry for the free dinitramide ion, $N(NO_2)_2^-$ (Fig. 10.5), while in solution and in the solid state the local symmetry is essentially C_1. This can be explained on the basis of weak cation-anion interactions or interactions with the solvent, since the dinitramide ion is very easy to deform because of the very small barrier to rotation of the NNO_2 moiety (< 13 kJ mol^{-1}) [63].
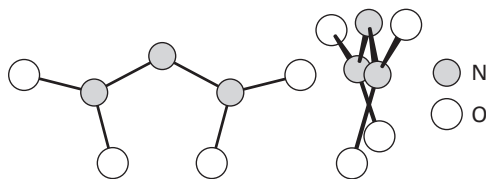
Fig. 10.5 Two different views of the dinitramide ion with C_2 symmetry.

Although ADN is already industrially prepared, the lab synthesis is not trivial and depends on the precise control of the reaction conditions. Normally, ADN is synthesized by the nitration of ammonia using N_2O_5 (prepared by the ozonization of NO_2) in a chlorinated solvent (Fig. 10.6):

synthesis of N_2O_5:
$$2\,NO_2 + O_3 \longrightarrow N_2O_5 + O_2$$

synthesis of ADN:
$$NH_3 + N_2O_5 \longrightarrow (O_2N)NH_2 + HNO_3$$
$$(O_2N)NH_2 + N_2O_5 \longrightarrow (O_2N)_2NH + HNO_3$$
$$(O_2N)_2NH + NH_3 \longrightarrow [NH_4^+][N(NO_2)_2]^-$$
$$2\,HNO_3 + 2\,NH_3 \longrightarrow 2\,[NH_4^+][NO_3]^-$$
$$\overline{4\,NH_3 + 2\,N_2O_5 \longrightarrow [NH_4^+][N(NO_2)_2]^- + 2\,[NH_4^+][NO_3]^-}$$
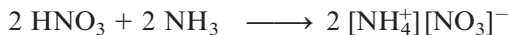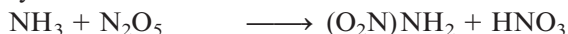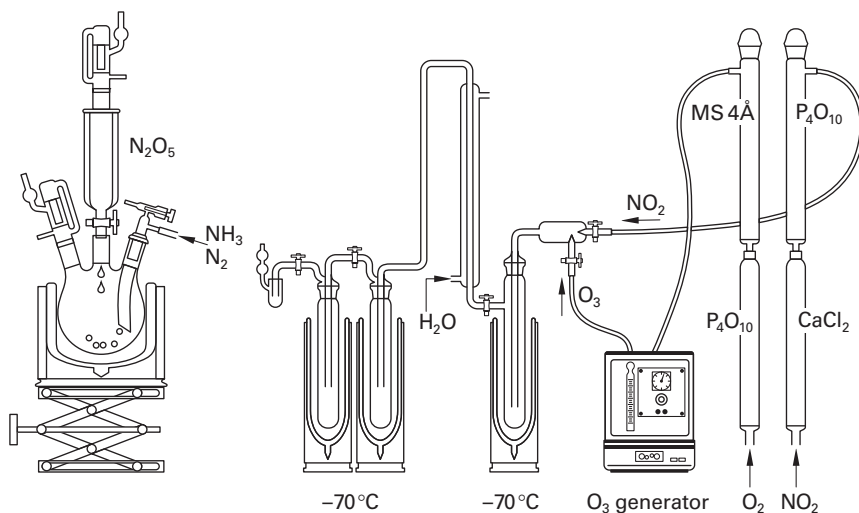
Fig. 10.6 Schematic diagram of the apparatus used for the small-scale lab-preparation of N_2O_5 (right) and ADN (left).

Note: Free dinitraminic acid is a very strong acid with a pK_A value of -5.6. It is unstable however and decomposes quickly to N_2O and HNO_3.

Industrially, ADN is commonly prepared by the nitration of urea. In the first stage, urea is converted into urea nitrate using dilute nitric acid, which is then dehydrated to form nitrourea by reaction with concentrated sulfuric acid. The 1,1-dinitrourea isomer can subsequently be obtained by nitrating nitrourea with a strong nitrating agent ($NO_2^+BF_4^-$, N_2O_5); the dinitrourea then reacts with gaseous ammonia to form ADN and urea:

$$H_2N-CO-NH_2 \xrightarrow{\text{dil. HNO}_3} [H_2N-CO-NH_3]^+[NO_3]^-$$
$$[H_2N-CO-NH_3]^+[NO_3]^- \xrightarrow{\text{konz. H}_2\text{SO}_4} H_2N-CO-NH(NO_2)$$
$$(O_2N)HN-CO-NH_2 \xrightarrow{\text{N}_2\text{O}_5} (O_2N)_2N-CO-NH_2$$
$$(O_2N)_2N-CO-NH_2 + 2\ NH_3 \longrightarrow [NH_4^+][N(NO_2)_2]^- + H_2N-CO-NH_2$$
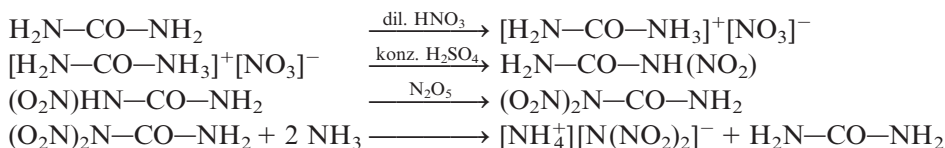
Using a new process, ADN can be prepared in a very environmentally friendly manner (without the use of chlorinated organic solvents) by the direct nitration of salts (potassium or ammonium) of sulfamic acid (amidosulfonic acid, H_2N-SO_3H) using mixed acid (HNO_3/H_2SO_4):

$$H_2N-SO_3^- \xrightarrow{\text{HNO}_3/\text{H}_2\text{SO}_4,\, T<-25\,°C} N(NO_2)_2^-$$
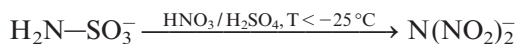
Sulfamic acid (amidosulfonic acid) itself can be obtained simply from urea and pyrosulfuric acid (disulfuric acid, $H_2S_2O_7$):

$$CO(NH_2)_2 + H_2S_2O_7 \rightarrow 2\ H_2N-SO_3H + CO_2$$
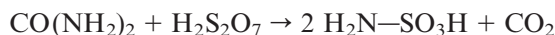
Conversion of ADN into different metal salts of ADN is facile by reaction with the corresponding metal hydroxide:

$$MOH + [NH_4][N(NO_2)_2] \rightarrow [M][N(NO_2)_2] + NH_3 + H_2O$$
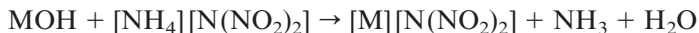
10.3 Processing

Most explosives which are used by the military are solids under normal conditions and are usually obtained as granules on a technical scale. These granules are then mixed with other explosives and energetic (e.g. binder, plastiziser) or non-energetic additives (anti-oxidants, wetters, wax) and made into their final form using one of the following technical processes:

1. melting, mostly under vacuum
2. pressing, often under vacuum
3. extruding at high pressures

Melting (melt-casting) is one of the oldest technical processes and is normally used for formulations which contain TNT as the melt-castable component and RDX or HMX as the energetic filler. This is essentially the reason why TNT is still often used today. TNT melts at approx. 80 °C and has a very high ignition temperature of 240 °C (Fig. 10.7). The melting and decomposition points of RDX and HMX lie close together, while other energetic compounds such as NQ or TATB decom-
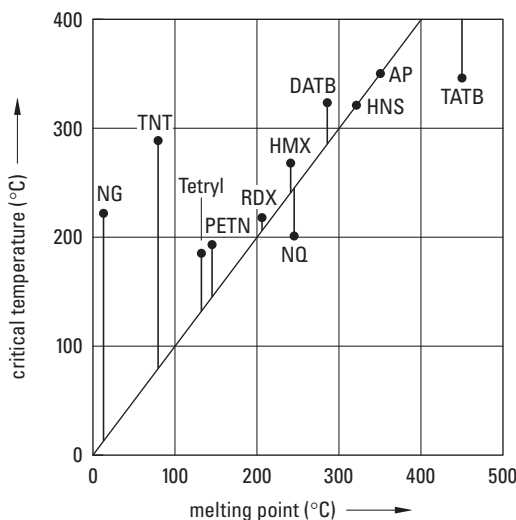
Fig. 10.7   Melting points and critical temperatures of some energetic materials. (This diagram is reproduced in slightly modified form from the original with permission from Prof. Dr. Manfred Held.)

pose at much lower temperatures than their estimated melting points (Fig. 10.7). The main disadvantage of the melt process is, that during cooling cracks can form in the explosive, which has a negative influence on its performance and sensitivity.

To overcome the shortcomings of melt-casting, liquid polymers (e.g. HTPB, GAP etc.) are used as binders while explosives such as RDX or HMX are used as fillers for PBXs. In this so-called **normal-casting** process, the explosive (RDX, HMX) is mixed with a binder (HTPB) which may be crosslinked with a diisocya-nate to provide a cured and dimensionally stable matrix. This process is often performed under vacuum, and filling can also be agitated by vibration in order to remove any gas bubbles trapped in the matrix. This type of casting is generally adopted for large caliber warheads.

A powder is generally used in **pressing**, which is mainly undertaken under vac-uum. The advantage in comparison with the melt process is the low temperature. However, this process is also more hazardous which is why it is always automated or remote controlled. The subsequent mechanical processing of the finished explo-sive block is also relatively dangerous and should always be carried out using remote-control.

Extruding is usually carried out using a screw-type extruding machine as it is known from the plastic industry. In this process, the explosive and polymer binder are pre-mixed and then mixed, compressed and extruded through a small hole under high pressure using the extruder. This process is particularly suitable for the preparation of polymer bound explosives (PBXs).

11 Safe Handling of Energetic Materials in the Laboratory

11.1 General

A chemical research laboratory is different from an industrial production facility for many reasons. First of all, only much smaller quantities of energetic materials are handled in a chemical research laboratory and secondly, during research, the properties of new, energetic materials are not known and therefore particular care must be taken. One of the most important safety rules can be worked out from the "rule of thumb", which relates the distance D (in m), which offers a chance of survival, to the mass w (in kg) of the explosive. For a typical secondary explosive at large distances, the proportionality constant is approximately 2:

$$D = c\,w^{0.33} \approx 2\,w^{0.33}$$

It is important to note that this approximation is based only on the pressure/impulse of the shock wave and does not take into account the fragment formation (e.g. from confined charges, fume-cupboard front shields in the laboratory, reaction vessel glass).

In order to work safely with highly energetic materials in the chemical laboratory, the following rules must be obeyed:

- use smallest possible quantities,
- keep maximum distance from the experiment (vessels containing compounds not to be transported by hand, but with well fitting tongs or clamp instead),
- mechanical manipulation is to be used if possible, particularly for larger amounts,
- vessels never to be encased by hand (confinement),
- protective clothing is to be used (gloves, leather or Kevlar vest, ear protectors, face shield).

Additionally, one must bear in mind that although primary explosives are much more dangerous to handle − based on the probability of unexpected initiation due to their higher sensitivity − secondary explosives exhibit a much higher performance and if initiated, result in much larger damage than a primary explosive.

With regards to research into new energetic materials, a rule of thumb is that all synthetic attempts should first of all be carried out in 250 mg quantities while various sensitivity data is obtained (impact, friction and electrostatic sensitivity,

thermal stability). Only when all of these values are known, can increasing the synthesis to 1 g be considered (only if the properties are suitable). Later, increasing it to 5 and perhaps eventually to 10 g quantities could be possible depending on the sensitivity data obtained. Further tests such as the long-term stability (DSC, long-term heat-flux measurements etc.) must then be carried out.

11.2 Protective Equipment

In addition to the clothing that every chemist should wear in the lab (lab coat, safety glasses, enclosed shoes, non-flammable clothing), one can be protected further during work with small quantities (see above) of explosives. Possibilities include:

− Suitable protective gloves (see below)
− Kevlar® wrist protectors
− Full-visor face shield with polycarbonate shield (to be worn over normal safety glasses)
− Ear protectors
− Shoes with conducting soles against electrostatics (it is important that the floor is also conducting and earthened, especially for handling primary explosives)
− Protective leather jacket (made from 2 mm thick leather) or Kevlar protective vest with groin protector.

Finally, only spatulas made out of conducting plastic instead of metal spatulas should be used. Furthermore, it is important to make sure that the lab equipment, and certainly the vessels for storing the energetic materials are also made out of conducting plastic and stored on a conducting surface.

Injuries to hands are one of the most common accidental injuries in a lab where energetic materials are handled. Safety gloves are available in different materials. In addition to the protective effect, the fine-feel also has to be taken into account. There are several opinions with respect to the most suitable protective gloves. Some
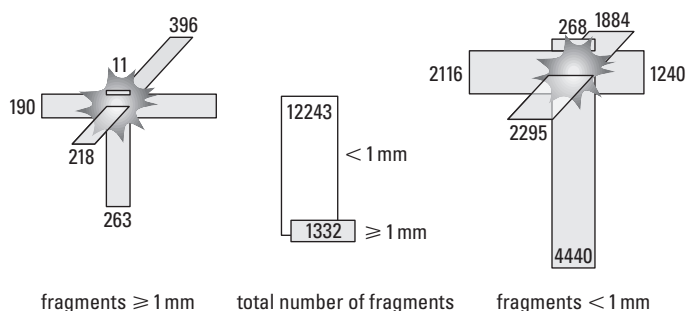
Fig. 11.1 Size and fragment distribution after an explosion with a quantity of 1 g $Pb(N_3)_2$ in a 10-ml glass vessel.
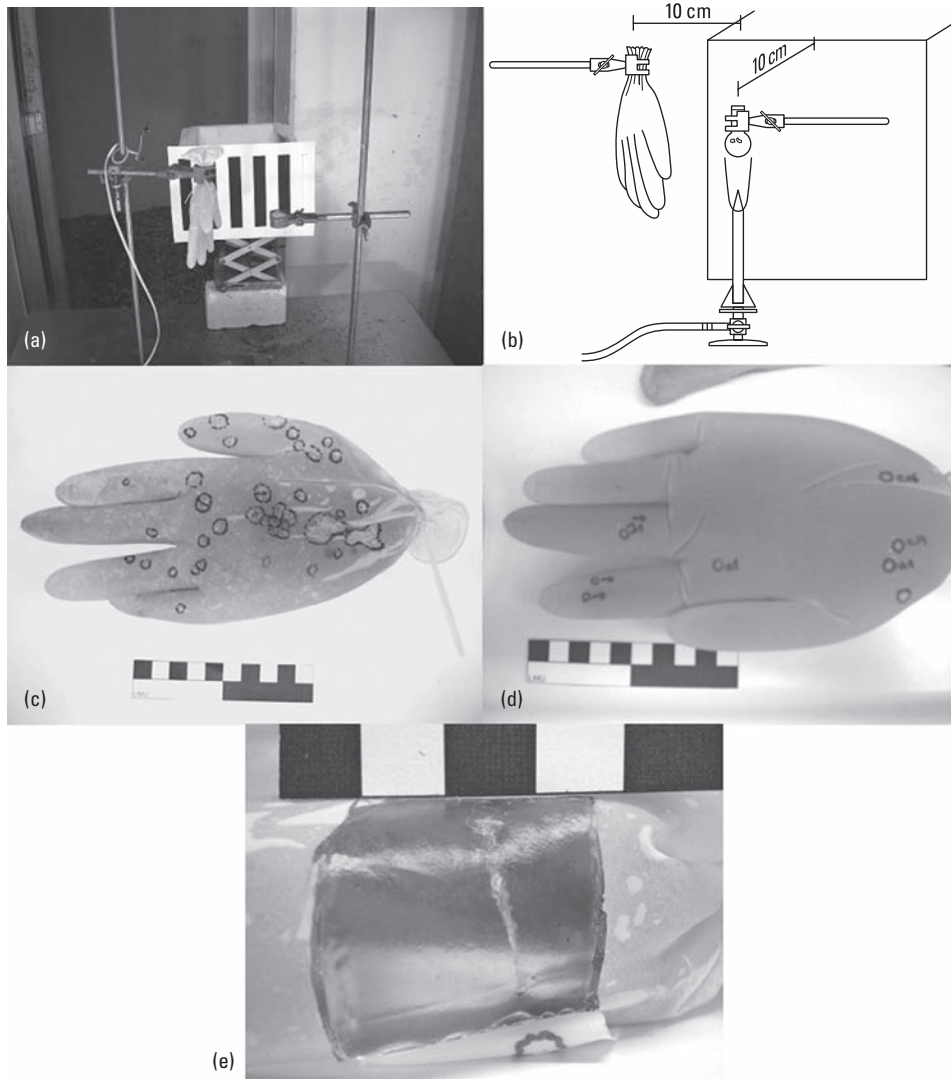
Fig. 11.2 Experimental set-up for investigating different protective gloves, scale unit 1 cm.

chemists prefer thick leather gloves (welding gloves), while others prefer Kevlar gloves. According to the DIN EN 388 (mechanical risks), protective gloves have been classified into three groups based on their cut resistance (I = low, II = medium, III = high). Gloves from class III should always be chosen. Relatively good protection is offered by the combination of two pairs of gloves: a tight-fitting pair made from Kevlar® ARMOR (a fiber developed by DuPont) or Kevlar® ES gloves and a second pair worn over the top made from Kevlar® with a woven steel core and a rubber or PVC coated palm side.

Tab. 11.1 Number of splinters and penetration depth using different gloves (exptl. set-up see Fig. 11.2 a and b)

		unprotected hand	Kevlar® glove		Kevlar®-glove with steel core		Kevlar®-glove with steel reinforcement		leather welding gloves	
		Exp. I	Exp. I	Exp. II	Exp. I	Exp. II	Exp. I	Exp. II	Exp. I	Exp. II
number of splinters										
in glove	≥ 1 mm	0	10	13	17	18	10	14	5	4
	< 1 mm	4	45	12	38	16	8	21	18	13
	total	4	55	25	55	32	18	35	23	17
in hand	≥ 1 mm	30[a]	14[b]	13	3	2	0	1	1[c]	0
	< 1 mm	20	0	5	3	0	2	1	1	0
	total	50	14	18	6	2	2	2	2	0
fragment distribution										
in glove	≥ 1 mm	0%	5%	9%	7%	9%	5%	6%	3%	2%
	< 1 mm	0%	4%	1%	3%	1%	1%	2%	1%	1%
	total	0%	2%	2%	4%	2%	1%	2%	1%	2%
in hand	≥ 1 mm	13%	9%	9%	1%	1%	0%	0%	1%	0%
	< 1 mm	1%	0%	0%	0%	0%	0%	0%	0%	0%
	total	3%	1%	1%	0%	0%	0%	0%	0%	0%
penetration depth (mm)	deepest	15.0	7.0	8.6	5.0	6.0	1.0	6.0	5.0	–
	average value	4.9	2.5	2.8	1.8	3.8	0.8	4.5	4.0	–

[a] 5 splinters > 5 mm; [b] 1 splinter penetrated the whole palm; [c] 1 splinter > 5 mm

Different tests have been suggested to estimate the protection in an explosion. [66] For example, the explosion of 1 g of lead azide in a 10 ml glass vessel has been investigated. The results of the fragment distribution (size and direction dependent) are shown in Figure 11.1.

Figure 11.2 shows a typical experimental set-up to investigate the protective effect of different gloves. Pictures a and b show the experimental set-up with a hand (gelatine in one-way gloves) at a distance of 10 cm from a 10 ml glass vessel containing 1 g $Pb(N_3)_2$. Figure 11.2 c shows the perforations in an unprotected glove and Figure 11.2 d shows the fragment impact on a hand protected with a Kevlar® glove. In Figure 11.2 e, the penetration depth of a glass splinter is enlarged, despite the protection offered by the Kevlar glove (from Figure 11.2 d, below right).

Table 11.1 shows the penetration depths of glass splinters with different types of gloves and an unprotected hand for comparison.

11.3 Laboratory Equipment

In addition to the personal protective equipment discussed above, one can/must equip the laboratory according to the current safety standards. Apart from the

standards that every chemical laboratory must correspond to anyway, particular attention must be paid to the following:

- conducting floor covering which is earthened,
- humidity over 60%, better 70% (using a humidifier, in particular during winter in rooms with central heating),
- short-term "intermediate storage" of small quantities of energetic materials in appropriate protective containers,
- storing of larger quantities of energetic materials in a specially designated store-room and not in the laboratory,
- separate fridges/cold rooms for oxidizers (HNO_3, NTO, H_2O_2, MON) and fuels (MMH, UDMH),
- mechanical manipulators for the handling of larger quantities of energetic materials,
- autoclave rooms or bunkers for performing different tests (Koenen test, detonation velocity, …).

12 Energetic Materials of the Future

Since the introduction of nitroglycerine as an explosive by Alfred Nobel in 1867 in the form of Dynamite, large advances have been made in the performance and reduction of sensitivities of highly energetic materials (Fig. 12.1). However, most of the formulations currently used are over 50 years old and do not fulfill all of today's requirements, in particular with regard to their performance, collateral damage, insensitivity, toxicity, compatibility with the environment and use in special operations.

Energetic materials are used mainly in explosives or propellant formulations. As we have already discussed, there are different parameters that characterize the performance of explosives and propellants and which are important in the development of new energetic materials. These include high densities (ρ, more important for explosives than for propellant charges), good oxygen balance (Ω) and high detonation and combustion temperatures (not for propellant charges). However, substances which are suitable for use as secondary explosives are not always suitable for use as propellants and vice versa. While the performance of explosives is particularly influenced by the heat of explosion ($Q_{C\text{-}J}$), the detonation pressure ($p_{C\text{-}J}$) and the detonation velocity (D), good rocket propellants possess a large specific impulse (I_{sp}) and thrust (F). For propellant charges, in addition to a high specific impulse, a high force (f), a low combustion temperature and the highest possible N_2/CO ratio in the products of the reaction are desirable.

When we consider the heat of explosion ($Q_{C\text{-}J}$), the detonation pressure ($p_{C\text{-}J}$) and the detonation velocity (D) as a measure that determines the performance of
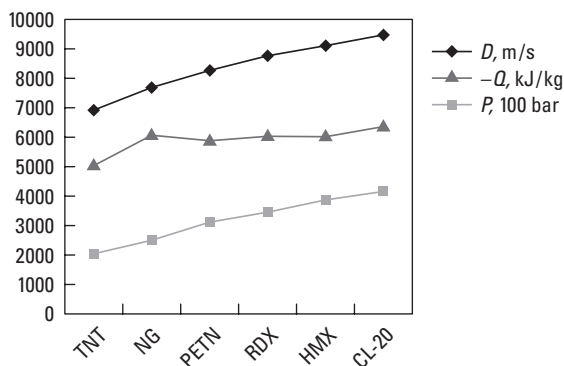
Fig. 12.1 Performance of explosives (Q, heat of explosion; D, detonation velocity; p, C-J detonation pressure).

Tab. 12.1   Nitrogen content and oxygen balance of some conventional explosives.

	nitrogen content/%	oxygen balance/%
TNT	18.5	−73.9
PETN	17.7	−10.1
RDX	37.8	−21.6
HMX	37.8	−21.6
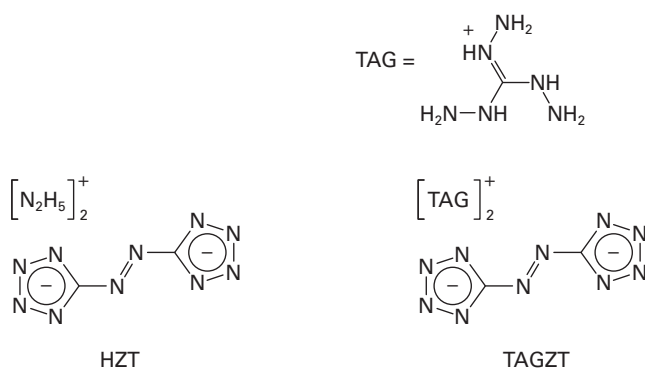
Fig. 12.2   Structures of hydrazinium azotetrazolate (HZT) and triaminoguanidinium azotetrazolate (TAGzT).

explosives, then Figure 12.1 shows that large advances have been made since the development of nitroglycerine.

Despite these advances, it appears to be difficult to make significant improvements to the performance with conventional C/H/N/O explosives based on nitro and nitrato compounds. This is partly due to, the fact that classic explosives suffer from the following three limitations (Tab. 12.1):

1. they are not nitrogen-rich enough (N rich > 60 % N),
2. the oxygen balance is often too negative,
3. to reach a good oxygen balance, different explosives have to be mixed.

More recent research on nitrogen-rich molecules (N > 60 %) has shown, that these compounds often have a higher energy content because of a much more positive enthalpy of formation in comparison with their C analogues. The first generation of nitrogen-rich compounds such as hydrazinium azotetrazolate (HZT) and triaminoguanidinium azotetrazolate (TAGzT) (Fig. 12.2) have already generated interest as components of propellant charges because of their low erosion properties. However, due to their poor oxygen balance, they are unsuitable for use as high-performance explosives (Tab. 12.2).

This could change with the introduction of the second generation of nitrogen-rich explosives which possess strongly oxidizing groups, and a (nearly) neutral

Tab. 12.2 Nitrogen content and oxygen balance of first and second generation N-rich compounds.

	nitrogen content/%	oxygen balance/%
1st generation		
HZT	85	−63
TAGZT	82	−73
2nd generation		
TAG-DN	57	−18
HAT-DN	58	0
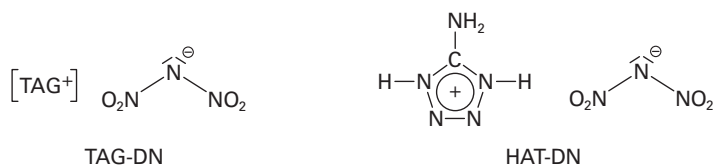
Fig. 12.3 Structures of triaminoguanidinium dinitramide (TAG-DN) and aminotetrazolium dinitramide (HAT-DN).
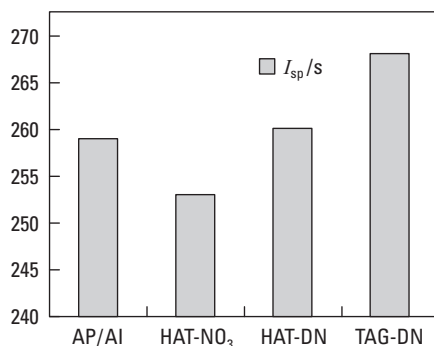
Fig. 12.4 Calculated specific impulses (I_{sp}^*/s) for AP/Al (70:30), HAT-NO$_3$, HAT-DN and TAG-DN (isobaric combustion at p = 70 bar).

oxygen balance. Examples of these are the compounds triaminoguanidinium dinitramide (TAG-DN) and aminotetrazolium dinitramide (HAT-DN) (Fig. 12.3, Tab. 10.3) [64, 65].

TAG-DN and HAT-DN are therefore potentially good candidates for use as explosives. But compounds with good oxygen balances are also suitable as components in rocket propellants. An increase in the specific impulse I_{sp}^* of only 20 s should be enough to allow almost a doubling of the payload. Figure 12.4 shows the calculated specific impulse (isobaric, p = 70 bar) for AP/Al (AP/Al) (70:30), HAT-NO$_3$, HAT-DN and TAG-DN.

Fig. 12.5 Detonation velocities (*D*) of classic CHNO and nitrogen-rich explosives.

The calculated detonation velocities for the second generation of nitrogen-rich compounds (which are one of the criteria for the performance of explosives) are not only better than those of the first generation, but in the case of HAT-DN it is even better than the values for RDX and HMX (Fig. 12.5).

Possible directions for future research are (see also Tab. 12.3):

1. metallized nitrogen-rich compounds with positive oxygen balances,
2. metastable poly-nitrogen element modifications,
3. organometallic compounds with nitrogen-rich or poly-N-ligands,
4. boron-nitrogen compounds with good oxygen balances,
5. substitution of oxygen (in —NO$_2$ groups) by fluorine (—NF$_2$ groups),
6. new, better and perchlorate free oxidizers,

Fig. 12.6 Energetic compounds (synthons) for "advanced oxidizers".

7. new synthetic, energy-rich polymers as nitrocellulose replacements,
8. more effective, F, Cl and peroxide containing agent-defeat substances,
9. nano-materials (carbon nanotubes),
10. N_4, N_8 fixation in SWCNTs,
11. new high energy oxidizers (HEDO) (Fig. 12.6)

Tab. 12.3 Future areas of research.

need	possible solution	research
downsizing of warheads: $4 \rightarrow 1$	increase of ΔU_{ex}: today: $5-6\,kJ\,g^{-1}$ future: $10-20\,kJ\,g^{-1}$; up to 75% of the mass of a warhead gets "wasted" (non-reactive structure material)	super high explosives, novel HEDMs: poly-N, poly-N_2O; reactive fragments: thermites, Al-PTFE composites, Al-Zn-Zr, Al-W and Al-U alloys
UxV's	increase of ΔU_{ex}: today: $5-6\,kJ\,g^{-1}$ future: $10-20\,kJ\,g^{-1}$; amalgamation of warhead and weapon into one no-return system	super high explosives, novel HEDMs: poly-N, poly-N_2O; reactive structures: novel materials
countermeasures against chemical WMDs	ADWs	peroxides, ozone, Cl-containing compounds, hypochlorites
countermeasures against biological WMDs	ADWs	peroxides, ozone, Cl-containing compounds, hypochlorites, F-containing compounds (HF formation)
more efficient fuels	nano	research concerning ageing problems, coating with strongly oxidizing groups (e.g. pernitro alcohols)
perchlorate-free oxidizers	new HEDOs	high-nitro compounds, compounds with peroxo groups
specialized GWT missions	thermobaric systems; Fuel Air Explosives (FAE)	coated nano-Al particles; strongly endothermic liquids

13 Related Topics

13.1 Thermobaric Weapons

There are two related weapon systems in this category: the thermobaric weapons and the Fuel Air Systems, also known in German as aerosol bombs (**FAE, Fuel Air Explosive**). Both function according to the same principle.

An **aerosol bomb**, Fuel Air Explosive (FAE) or Fuel Air Bomb, is a weapon whose effect on the detonation of an aerosol or substance distributed as a dust cloud does not depend on an oxidizer being present in the molecule. A FAE bomb consists of a container with a flammable substance (e.g. ethylene oxide). Two explosive charges are used as detonators: the first explosion causes the fuel to be distributed as fine particles into the air as an aerosol. Following this, microseconds − milliseconds later the aerosol is detonated, which results in the release of high pressure.

The pressure wave which results from the explosive deflagration is considerably weaker than that of a comparable explosive such as RDX. However, the explosive deflagration occurs almost simultaneously in a large volume of 10−50 m diameter. The fuel can penetrate caves, tunnels or bunkers, which makes this weapon effective when used on targets in the global war against terror (GWT), unlike conventional explosive charges which only have a limited effect due to their poor pressure effect.

Furthermore, aerosol bombs have a considerably larger heat effect than conventional explosive charges. Therefore these bombs are more effective at killing people and at the destruction of other soft targets such as unarmed vehicles and other targets.

The explosion removes the oxygen from the air, because the explosive composition does not contain its own oxidizer and uses the oxygen present in the air instead. This is however not the deadly mechanism of the aerosol bombs. Much more significant is death by suffocation which is observed as the result of an aerosol bomb. The reason for this is not the lack of oxygen, but the damage which is done to the lungs through a so-called barotrauma. The negative pressure phase which occurs after the positive pressure phase (see Ch. 2.2) causes an expansion of the air in the lungs; resulting in damage. The properties of an aerosol bomb − long, relatively flat pressure wave with a corresponding distinct "partial vacuum" as well as the use of atmospheric oxygen are beneficial effects.

For **thermobaric weapons** (also known as **EBX** = enhanced blast explosives), in addition to a conventional explosion, a flammable substance (usually Al), with

little or no oxidizer (e.g. oxygen) distributed in the air detonates immediately as a result of the explosion. This post-detonative reaction ("fireball" of Al with air) usually occurs within μs after the detonation of the high explosive. This causes the effect of the original explosion to be magnified which results in an even larger heat and pressure effect. It is interesting to note that when an EBX is detonated under anaerobic (experimental) conditions, the Al does not react and therefore does not contribute to the reaction enthalpy ($\Delta H_{comb.}$ or $\Delta H_{expl.}$).

The initial pressure wave and the subsequent underpressure, follow a phase in which the underpressure resulting from the explosion causes a flux of surrounding air to the centre of the explosion. The released, non-exploded, burning substance is as a result of the underpressure sucked into where the explosion occurred, and therefore enters all non air-tight objects (caves, bunker, tunnels) and burns these. Suffocation and internal damage can result to both humans and animals that are located out of the immediate vicinity: e.g. in deeper tunnels as a result of the pressure wave, the burning of oxygen, or the subsequent underpressure.

As discussed above, thermobaric weapons contain monopropellants or secondary explosives and energetic particles. Boron, aluminum, silicon, titanium, magnesium, zirconium and carbon can be considered to be energetic particles. The main advantage of thermobaric systems is that they release large quantities of heat and pressure, often in amounts larger than for only secondary explosives.

In thermobaric weapons, highly aluminized secondary explosives can be used instead of monopropellants. For example, RDX in combination with a binder and a large quantity of aluminum (fuel rich) can be used. Research is currently being undertaken to investigate energetic polymers which could possibly be metallized for possible applications.

In thermobaric weapons, first anaerobic detonation occurs within the microsecond time-frame, followed by a post-detonative combustion which is also anaerobic and occurs in the hundredth of a microsecond time-frame. Only then, the post detonative burning occurs, which lasts several milliseconds and generates strong heat radiation even at small shock-wave pressures (approx. 10 bar)

The following relationship gives a conservative approximation for the distance from the detonation of a thermobaric weapon, which can still experience large damage as a result of the heat and pressure-wave generated. D is the distance (in meters), C is a constant (0.15 for an assumed overpressure of 70 mbar), n is the so-called yield factor from the burning (normally 0.1) and E is the energy (in J) released on the explosion and combustion.

$$D = C(n\,E)^{0.33}$$

If the energy E is replaced by "$m\,Q$" in which m is the mass (in kg) of energetic material used and Q is the heat of combustion (in J kg^{-1}), the critical distance can be represented by:

$$D = 0.15\,\text{kg}^{-0.33}\,\text{s}^{0.66}\,\text{m}^{0.33}\,(0.1\,m\,Q)^{0.33}$$

Thermobaric weapons can be used as bombs or as shoulder-launch mobile systems. There are two fields of operation for which the thermobaric weapons are superior to other systems:

(i) Areas of conflict involving caves, tunnels or other difficult to access areas and deep, confined targets (HDBTs, hard and/or deeply buried targets).
(ii) Combat and destruction of chemical and biological (CB) weapons through the strong heat effect (see also Ch. 13.2).

13.2 Agent Defeat Weapons

Agent defeat weapons (also known as agent defeat warheads, ADW) are airborne warheads, which can be used in the fight against chemical and biological (CB) weapons of mass destruction (WMD) to minimize the amount of collateral damage that occurs. Collateral damage can largely be minimized when the active agents in the chemical or biological weapons are destroyed or neutralized upon being attacked, before they can be spread into the environment.

An ADW is constructed similarly to a multiprojectile warhead (see Ch. 7.1), but is additionally combined with a thermobaric weapon (see Ch. 13.1). After penetration of the chemical or biological weapon system, the active substances are destroyed as a result of the large heat effect of the thermobaric explosion. In addition, some ADWs also contain Cl-releasing systems, which also provide further destruction through oxidation in particular of the biological warfare agents. Other chemical compounds which are suitable for fighting biological agents contain peroxide and hypochlorite groups as well as chlorine.

It has been shown that although Cl_2 is a better biocide than HCl, the biocidal activity of HF exceeds both Cl_2 and HCl. Only 200 ppm HF destroy most bacteria, including Anthrax spores. The most recent research in particular by Bob Chapman (NAWC, China Lake) has shown that ADW containing fluorinated payloads
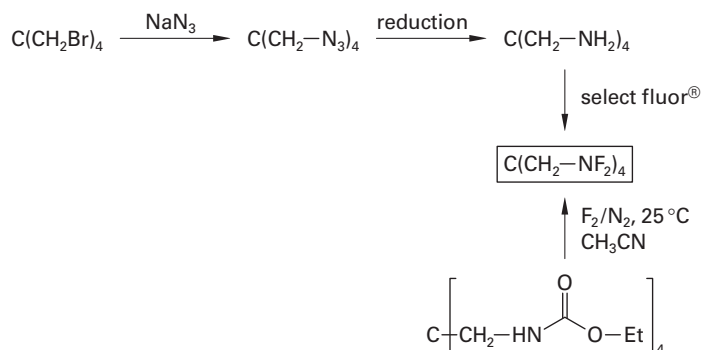
Fig. 13.1 Possible synthesis for octa-F-PETA.

(—NF$_2$ groups) are effective in destroying biological threats. For example, tetrakis-(difluoramino)octahydro-dinitro-diazocine, HNFX (see Fig. 10.1) [67] can very quickly remove the dangers of Anthrax spores. The biocidal activity of HNFX is not due to heat or pressure, but due to the harsh conditions of exposure to biocidal detonation products (i.e. HF). A control experiment using HMX as the explosive showed an order of magnitude lower killing of spores (86 % spore survival). Also octa-F-PETA, i.e. C(—CH$_2$—NF$_2$)$_4$ has successfully been tested against Anthrax spores. A possible synthesis for octa-F-PETA is shown in Figure 13.1.

Alternatively, octa-F-PETA can also be prepared according to the procedure shown in Fig. 13.2. Unfortunately, due to its high volatility (m.p. 40−42 °C; sublimes at ca. 30 °C) octa-F-PETA will not be employed as a main charge in ADWs.
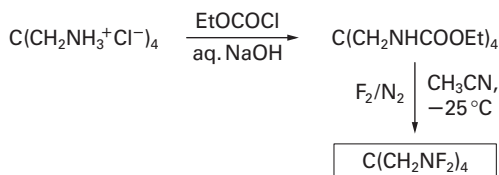
Fig. 13.2 Alternative synthesis for octa-F-PETA.

A chlorine containing energetic material which also shows use as a potential agent defeat explosive is hexachloromelamine, [—N=C(NCl$_2$)—]$_3$.

This compound is known to be biocidal and can be prepared by direct chlorination of melamine (Fig. 13.1).

hexachloromelamine
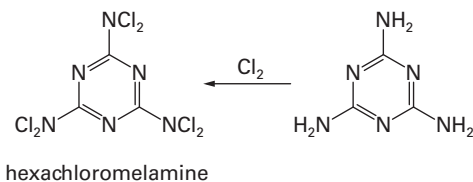
Fig. 13.3 Synthesis of hexachloromelamine.

The killing efficiency R is usually defined as

$$R = \log (N_0 + 1) - \log (N_E + 1)$$

Where N_0 is the bacterial count fort he inoculated control and N_E the bacterial count after exposure to the detonation products. In control experiments it could be shown that the killing efficiency R for HMX is ca 0.06 whereas using HNFX it is ca. 3 for wet and up to 9 for dry spores.

In a more recent study it could be shown that the combination of an explosive (diazidoglyoxime, **2**, Fig. 13.4) with a strongly biocidal agent defeat ingredient (guanidinium difluoroiodate, **1b** generates I$_2$, I and HF), could also result in very high the killing efficiencies of $R = 6$–8 [68].
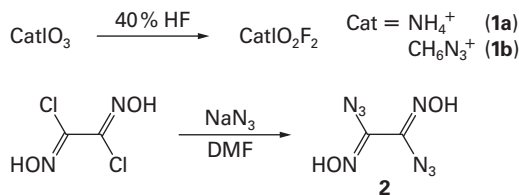
Fig. 13.4 Synthesis of difluoroiodate salts (**1a, b**) and diazidoglyoxime, **2**.

13.3 Nanothermites

Research into nanothermites is currently a hot topic in the field of energetic materials. For thermite-type reactions, a metal oxide is the oxidizer, and aluminum is the fuel. Thermite-type reactions on the nanoscale have been called many names including nanothermites, metastable intermolecular composites (MICs) or superthermites. The phrase "nanothermites" comes from the particle sizes used in these energetic mixtures, in contrast to the more familiar thermite type reaction in which the particle sizes are in the micron region. The term "metastable intermolecular composites" comes from the fact that the mixtures of metal oxide and aluminum are stable up to their ignition temperature, at which point self-propagating high-temperature synthesis (SHS) occurs and the thermodynamic products of a metal and aluminum oxide are produced. Finally, the term "superthermite" comes from the fact that thermites composed of nano-sized materials exhibit very different combustion characteristics when compared to those mixed with micron-sized precursors. Superior combustion velocites and explosive behavior compared to the usually observed deflagration often characterize thermites made with nanoscale precursors.

$$M_xO_y + Al \rightarrow M + Al_2O_3. \tag{1}$$

While most metal oxides can be reduced with aluminum in an exothermic thermite reaction, and many have had their reactivity studied on the nanoscale (including Fe_2O_3, MnO_2, CuO, WO_3, MoO_3, and Bi_2O_3), discussion of all nanoscale thermite reactions performed in the literature would be too broad. Discussion will focus on iron[III] oxide, molybdenum[VI] oxide, and copper[II] oxide as they provide good examples of either differing synthetic methodologies tailoring properties, exemplary final product properties, or of a material that has a high potential for practical use. We will limit the discussion of thermite examples to those where aluminum is the fuel because of the practical uses of such mixtures. However other fuels such as Zr, Hf, Mg etc. have been used.

An energetic material's particle size traditionally ranges from $1-100\,\mu m$. As is known, generally smaller particles give higher reaction rates and nanothermites are not an exeption. The reaction rate of a nanoscale thermite is generally several

orders of magnitude larger than those on micron scales, and the much larger surface area can significantly change combustion behavior, as well as ignition behavior by increasing sensitivity. The changes in properties are all associated with reduced diffusion distances since the associated surface area increases.

The initial reactions in a binary fuel-oxidizer system such as a thermite reaction are assumed to be diffusion-limited solid-solid reactions. As a result, the rate of reaction and therefore the combustion velocity can be increased dramatically as the particle size decreases and particle contacts increase. A mathematical study done by Brown et al. compared observed combustion rates for a Si/Pb_3O_4 pyrotechnic mixture with the calculated fuel-oxidizer contact points for silicon particles of given sizes mixed with 5 μm Pb_3O_4. Contact points were calculated assuming the approximation that the fuel and oxidizer are hard spheres. Results from this study are presented in Table 13.1, and show that a small change in particle size has a very strong effect on fuel-oxidizer contact points, and a correspondingly large effect on the combustion velocity.

Tab. 13.1 Combustion rate as a function of contact points in an Si/Pb_3O_4 composite.

Si particle diameter (μm)	contact points ($\times 10^9$)	combustion rate (mm/s)
2	30.2	257.4
4	8.7	100.6
5	6.1	71.5

Despite this study not being on the nanoscale, it does show the dramatic effect particle size has on combustion rate, since doubling the particle size causes the combustion rate to be more than halved. The Si/Pb_3O_4 mixture has found use as a pyrotechnic delay mixture (slow burning mixture used for timing in pyrotechnics) as its combustion rate is easily tailored.

As particle sizes decrease, the sensitivity of the thermite mixture to impact and friction increases. The micron scale thermites are usually quite insensitive to impact and shock, but thermites on the nanoscale can be quite sensitive to both or one of the two depending on the metal oxide. This is exemplified in the work of Spitzer, where a tungsten(VI) oxide and aluminum thermite was prepared by mixing nano and micron aluminum with nano and micron WO_3. The results of this are presented in Table 13.2.

Tab. 13.2 Sensitivities for nano vs. micron Al/WO_3 thermite.

Al diameter (nm)	WO$_3$ diameter (nm)	impact (J)	friction (N)	combustion rate (m/s)
1912	724	> 49 (insensitive)	> 353 (insensitive)	< 0.08
51	50	42 (insensitive)	< 4.9 (very sensitive)	7.3

Tab. 13.3 Active aluminum content of aluminum nanoparticles.

average Al nanoparticle size (nm)	active aluminum content (%)
30	30
45	64
50	43
50	68
79	81
80	80
80	88

While increased sensitivity can make nano-thermites more dangerous to handle, the increased friction or impact sensitivity is also beneficial in some practical applications such as percussion primers. However some nano-thermites have increased ESD sensitivity, which has no current practical application and is only a safety hazard. For example, a Bi_2O_3/Al nano-thermite has sufficient impact and friction sensitivity to be considered for use in ammunition primers, however it has an ESD sensitivity of 0.125 µJ (40 nm Bi_2O_3, 41 nm Al). This is a static potential, which is easily achieved by the human body. This makes handling hazardous, especially since the Bi_2O_3/Al thermite has a combustion velocity of over 750 m/s which means that this thermite explodes rather than burns. The increased ESD sensitivity of nano vs. micron composites is believed to be the result of the increased ability of high surface areas to develop charges.

A final property affected by the reduction in particle size from micron to nano scale is the ignition temperature of the thermites. For example, a thermite composed of 100 nm MoO_3 and 40 nm aluminum exhibits an ignition temperature of 458 °C whereas the same MoO_3 with 10−14 µm Al exhibits an ignition temperature of 955 °C. This indicates a change in mechanism between the two as the micron composite exhibits melting and volatilization of Al and MoO_3 (from DSC) before the thermite reaction occurs, while the nano-thermite reaction occurs before the Al melting could take place. This indicates that the reaction for the nano-composite is based on solid state diffusion, while for the micron composite the reaction is a gas (MoO_3)-liquid(Al) reaction. This change in mechanism may apply to other thermite systems as well, however detailed DSC data for many other systems has not been published so far.

In thermites using aluminum metal as the fuel, the passivation of the metal surface with oxide must be taken into account. For micrometer sized particles of aluminum, the oxide passivation layer is negligible, but on the nano-scale this passivation layer of alumina begins to account for a significant mass portion of the nanoparticles. In addition, the precise nature of the oxide layer is not the same for all manufacturers of aluminum nanoparticles, so the researcher must use TEM to measure oxide thickness to allow calculation of active aluminum content before stoichiometric calculations are carried out for the mixing of thermites. Table 13.3

Tab. 13.4   CuO/Al thermites with highly oxidized (49 % Al) aluminum nanoparticles.

CuO	Al	combustion velocity (m/s)	mass burning rate (g/s)
micron	micron	220	2700
micron	nano (49 % Al)	200	1100
nano	micron	630	4850
nano	nano (49 % Al)	900	4000

shows details of some of the percentages of aluminum in aluminum nanoparticles and shows just how significant and inconsistent the oxide layer can be.

The effect of the aluminum oxide layer is also known to reduce the propagation of thermite reactions since alumina is an effective absorber of thermal energy. A study by Weismiller et al. of a 49 % active aluminum nanopowder in a thermite with copper oxide supports the idea that too much oxide can actually reduce thermite performance. Table 13.4 shows Weismiller's data which indicates the negative effect of a thick oxide layer on aluminum nanoparticles.

The combustion velocities given in Table 13.4 show that the use of nano CuO is more of a factor towards high velocities than the Al when the Al is highly oxidized, and even slightly decreases performance when the velocity of μm-CuO/μm-Al is compared to μm-CuO/nm-Al. The mass burning rate shows this even more starkly, as with a given particle size of CuO, the switch from micron to heavily oxidized nano aluminum decreases the mass burning rate.

In general, there are three common ways of preparing nano-thermites; these include arrested reactive milling, physical mixing, and sol-gel methodology. Changing from the microscale to the nano, these methods provide accessibility and use of different particle sizes, as well as materials with different degrees of contact between oxidizer and fuel.

Arrested reactive milling (ARM) is a technique for the preparation of nano-energetic materials by milling the metal oxide and aluminum in a ball or shaker mill. While it may or may not involve particle sizes on the nanoscale, the energetic composites prepared through this method have properties more similar to those of the nano-thermites as mixing is on the nanoscale; fuel and oxidizer may be contained in the same particle after milling. The particles produced by arrested reactive milling are in the range of 1−50 μm, and are composed of layers of aluminum and oxidizer on the scale of 10−100 nm. The size of the particles obtained is a function of the milling time, however due to the reactivity of the mixture, after a certain milling time (a function of initial particle sizes, milling media used, and type of metal oxide) when the particle size is reduced below a certain value, the milling causes ignition of the thermite mix. A liquid such as hexane is usually added to the mill to reduce static build up. The term arrested reactive milling comes from the fact that milling is stopped before the mix ignites, resulting in a useable thermite mixture. Advantages of this method are that the particles produced approach their maximum density. Aluminum is hidden within the particle matrix which reduces

the presence of nonreactive alumina, the ability to start with non-nanoscale precursors, and milling time offers convenient control of the degree of intermixing and therefore the reactivity. Disadvantages include the fact that only few thermite mixtures can be prepared by this method as many other mixtures are too sensitive and ignite before sufficient intermixing can occur.

Physical mixing is the simplest and most common method for the preparation of nano-thermites. Nano-powders of metal oxide and aluminum are mixed in a volatile, inert liquid (to reduce static charge) and they are then sonicated to ensure good fuel-oxidizer mixing and to break up macroscale agglomerates. The liquid then evaporates and the thermite is ready to be used. Advantages of the physical mixing method is the simplicity and its wide range of applicability to many thermite systems. The only major disadvantage is the necessity of starting with nanoscale powders which may or may not be commercially available.

Sol-gel nanothermite preparations take advantage of the unique structural and mixing properties available from sol-gel chemistry. In these nanothermite mixtures, the aluminum nanoparticles reside in the pores of the metal oxide matrix, which is widely assumed to increase thermite power in comparison to physical mixing by huge reduction in diffusion distances between the fuel and oxidizer, and by increasing the contact area. The synthesis of energetic sol-gel thermites involves the addition of a suspension of aluminum nanopowder in a solvent to a metal oxide sol just prior to gellation. After gellation, the gel can be processed to an energetic xero or aero gel. Through the sol-gel methodology, interfacial area, pore size, and matrix geometry can be controlled which results in different, tunable energetic properties. In addition, the sol-gel methodology allows the molecular incorporation of organic agents to the matrix which further tune the thermite's properties by acting as a gas generating agent. Other than the ability to incorporate organics, advantages of the sol-gel method include its ability to form low density aero or xero gels, which brings with it the ability to form energetic surface coatings. Disadvantages include potential oxidation of the aluminum nanoparticles by water in the metal oxide gel before the solvent can be removed. This disadvantage can be overcome by using sol-gel chemistry to only prepare aero or xero-gel oxide precursors, which can then be followed by physical mixing with aluminum. But this option comes at the cost of reducing the high-level of interfacial contact achievable by sol-gel chemistry.

Due to the range of properties that nanothermites can be tailored to have, nanothermites find applications in a correspondingly large field. As research on nanothermites is a relatively new topic, many applications have only been proposed so far and testing in such areas has not yet been done. Many of the potential applications of nano-thermites are a direct result of their high energy densities, which are comparable to those of lithium batteries leading to applications of the power-generating variety such as microscale propulsion, energetic surface coatings and nano-scale welding. Other applications are a direct result of the pyrotechnic behavior of nano-thermites, and such materials may find use as gas generating agents for automobile air bags, exploding-on-contact missiles, environmentally

Fig. 13.5   Shotgun shell primer.

friendly ammunition primers and electric igniters. The fastest thermites even have potential application as primary explosives. Their application in microscale propulsion, ammunition primers, and electric igniters has had more experimental work conducted with them than other potential applications for nano-thermites, and show very promising results.

Microscale propulsion involves the production of thrust on the microscale (< 1 mm). This is referred to as micropyrotechnics or microenergetics, and applications include rapid switching and propulsion for small spacecrafts. Performance energetic materials used for propulsion on the macroscale including RDX (hexahydro-1,3,5-trinitro-1,3,5-triazine, hexogen) or HMX (1,3,5,7-tetranitro-1,3,5,7-tetrazocane, octogen) are unable to function on the microscale, as they cannot sustain combustion in such small diameters since too much energy is lost to the combustion chamber which inhibits propagation through the energetic material. Nanothermites have no such problem as they have a much higher energy density, so energy lost to the chamber becomes insignificant.

An ammunition primer is the part of a round of ammunition that is impacted by the firing pin of the firearm. Traditional primers contain lead containing compounds including lead azide and lead styphnate, as these sensitive explosives detonate from the impact of the firing pin, and the resultant flame ignites the propellant in the cartridge, firing the bullet. Figure 13.5 shows a shotgun shell primer. The toxicity of lead means the use of such primers is both an environmental and personal hazard to the user. Nanothermites have been shown to be an effective replacement for the lead salts, as they have been tailored to have properties similar to the currently used lead azide/styphnate mixture.

Electric igniters find use throughout the energetic material industry in all areas of propellants, explosives and pyrotechnics; they are used wherever an electric cur-
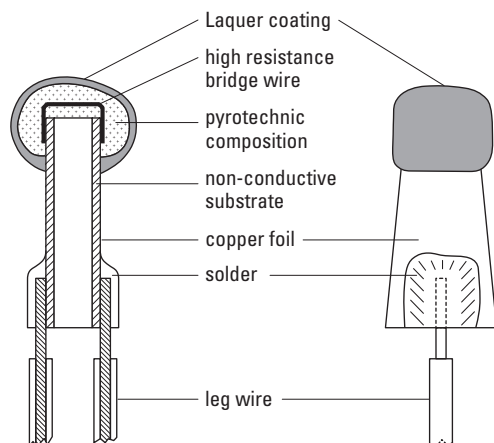
Fig.13.6 Electric igniter/match diagram.

rent is required to initiate an energetic material. As a result of the precise timing they afford, they can be used for igniting everything from rockets to blasting caps, to fireworks displays. Electric igniters are also known as electric matches, and they consist of a flammable head of material around a resistive bridgewire, igniting when a certain electrical current is passed through the match. Figure 13.6 shows a general diagram of an electric match. Like primers, commonly used electric matches contain toxic lead compounds including the dioxide, thiocyanate and nitroresorcinate. Therefore finding nontoxic replacements is desirable. Again, the use of nano-thermites has shown significant promise as non-toxic, green replacements for the lead compounds.

13.3.1 Example: Iron Oxide/Aluminum Thermite

On the macroscale, the iron oxide/aluminum thermite is used for the high temperature welding of iron railway rails. This is made possible through its slow rate of energy release and high combustion temperature. On the nanoscale, however, the iron oxide/aluminum thermite behaves very differently. In the literature, this thermite system is often synthesized by sol-gel methods as iron oxide sol-gel chemistry is well known, however, it has also been made by arrested reactive milling and physical mixing as well.

The iron oxide thermite is a very good example of the versatility of the sol-gel thermite methodology. Table 13.5 shows the huge effect the synthetic strategy used can have on the properties of the thermite.

From these numbers, the wide range of thermite properties that become available is apparent. The ease of tuning energetic properties is also apparent from the high velocity (320 and 895 m / s) xero and aerogels show as the xero and aerogel have

Tab. 13.5 Effect of the synthetic methodology used to prepare the Fe_2O_3/Al thermite on the combustion velocity.

synthetic methodology	velocity (m/s)
arrested reactive milling (max mill time before ignition)	0.5
physical mixing (80 nm Al, oxidizer size unmentioned)	9
sol gel (aerogel oxide physically mixed with 80 nm Al)	80
sol gel (xerogel, 70 nm Al added before gellation)	320
sol gel (aerogel, 70 nm Al added before gellation)	895

Tab. 13.6 Impact and ESD sensitivities of aero- and xerogel Fe_2O_3/Al thermite.

type	impact (J)	ESD (mJ)
xerogel	36.6	> 1000
aerogel	21.9	30

different sensitivities to ESD and to impact. These differences are shown in Table 13.6.

The impact sensitivity of the aerogel thermite may make it suitable for use in primers, because all of the other preparatory methods for the iron oxide thermite produce thermites which are unsuitable for this application. The especially sensitive nature of aerogel thermites stems from the inability of the aerogel matrix to conduct heat, a characteristic which is only applicable to aerogels, due to their insulating property.

A further development on the synthesis-dependent application of the iron oxide thermite is that of Clapsaddle et al. Tailoring of energetic properties was obtained by the addition of organo-silicon precursors to the sol leading to aerogel oxidizers containing any desired percentage of organic-functionalized silica. The silica functioned to reduce the combustion velocity, and the organic addition to increase the amount of gas released upon combustion. Research in this field is still in the initial stages, but the thermites may have application in the propulsive and gas-generating fields.

13.3.2 Example: Copper Oxide/Aluminum Thermite

Copper oxide and aluminum thermite is well known for its high combustion velocity even on the micron scale. This high combustion velocity is even more pronounced on the nano-scale where the thermites reach the highest combustion velocities known for a mixture of a metal oxide and aluminum.

Although in the literature CuO/Al thermites have not been prepared by reactive milling or sol-gel methods, unique to CuO/Al thermite is a new synthesis methodology by Gangopadhyay et al. called self-assembly. In this method, the authors coated copper nanorods (20 × 100 nm) with a coordinating polymer (P4VP) fol-

Tab. 13.7 Combustion velocities of the CuO/Al thermite (80 nm Al, 2.2 nm oxide layer).

synthetic method	CuO morphology	combustion velocity (m/s)
physical mixing	micron	675
physical mixing	nanorods	1650
self assembly	nanorods	2400

lowed by coating the coated rods with 80 nm aluminum powder. The result of this self-assembly process is the formation of the thermite with the highest combustion velocity known of 2400 m/s. Table 13.7 gives the combustion velocity of the self-assembled thermite compared with physically mixed thermites.

Gangopadhyay et al. state that the reason for the increased combustion velocity is the highly improved interfacial contact between fuel and oxidizer. However the presence of an organic material binding the fuel and oxidizer will increase the combustion pressure which has been shown by Weismiller and Bulian to result in an increase in the combustion rates. The dependence of the combustion velocity on pressure has been thought of as resulting from the of decomposition of CuO to gaseous oxygen at 1000 °C which may be the active oxidizer.

Despite the reason for the high combustion velocity being under debate, the high combustion velocity is in the range of explosive velocities, so the CuO/Al thermite may have application as a primary explosive. The more easily prepared, physically mixed CuO nanothermite has been patented for use in ammunition primers. Sensitivity data for the CuO/Al thermite is unavailable, but it is expected to be relatively high. High impact sensitivity may be the reason why there are no literature reports of its preparation by arrested reactive milling.

13.3.3 Example: Molybdenum Trioxide/Aluminum Thermite

MoO_3/Al has been prepared exclusively by physical mixing and arrested reactive milling. Due to the availability of both MoO_3 and aluminum nanopowders, the preparation used exclusively for practical applications of these thermites is physical mixing. With combustion velocities ranging from 150−450 m/s MoO_3/Al thermites are perhaps some of the most widely studied nano-thermites, and extensive work has been reported on their practical applications in electric igniters, primers (patented), and microscale propulsion.

A study reported by Son et al. on the feasibility of the use of a MoO_3/Al nanothermite (79 nm spherical Al, 30 × 200 nm sheet MoO_3) for microscale propulsion and microscale pyrotechnics shows great promise for the application of these materials. It was found that when confined in tubes with a diameter of 0.5 mm, the MoO_3/Al thermite would combust at rates as high as 790 m/s. This is an advantage over conventional energetic materials such as HMX which cannot propagate even in tubes under 1 mm.

Naud et al. have preformed extensive work on the use of the MoO_3/Al nanothermite for application in electric matches. Electric matches prepared from this thermite mixture have been shown to have lower friction, impact, thermal and ESD sensitivities than the currently used matches, which contain toxic lead compounds making them both safer and more environmentally friendly to use.

13.4 Homemade Explosives

Usually explosives can be categorized as military, commercial and homemade (HME) explosives. HMEs are energetic formulations that can be created "at home". The term HME has been used to cover a wide range of materials from pure explosive compounds, such as triacetone triperoxide (TATP), that can be synthesized from readily available articles of commerce or pentaerythritol tetranitrate (PETN), as pentaerythritol can be purchased in bulk for paint use to home-made variants of explosive formulations, such as ammonium nitrate fuel oil (ANFO), that are used in very large commercial blasting operations.

A major difference between military and commercial explosives on the one hand and HMEs on the other hand is that we do look at "made in a factory with rigorous reproducibility" (military/commercial) vs. "made anywhere else" (HME).

HMEs such as black powder, triacetonetriperoxide (TATP), hexamethylene-triperoxidediamine (HMTD), chlorates, and perchlorates mixed with sugar or other fuels have come to be used by terrorists instead of commercial explosives.

14 Study Questions

Answers can be found online under: www.degruyter.com/klapoetke-answers

1. Please write suitable Lewis-type structures for the following molecules,
   FOX-7:
   PETN:
   RDX:

2. If 10 kg of a common high explosive is detonated, the minimum distance from the explosion which gives a chance of survival is
   ○   2.2 m   ○   4.3 m   ○   8.6 m

3. Give examples for the following:
   – single base gun propellant:
   – double base gun propellant:
   – triple base gun propellant:

4. Why does Mg nowadays get replaced with Zr in smoke munition?

5. Name one commercially available computer code to calculate
   – enthalpies of formation:
   – detonation parameters:

6. Calculate the oxygen balance with respect to CO_2 of ethylene glycol dinitrate, $O_2N-O-CH_2-CH_2-O-NO_2$.

7. If a high explosive has a VoD of 9.000 m s^{-1}. What is its approximate Gurney velocity?

8. Which of the following materials is more suitable for a kinetic energy penetrator, and why?
   ○   SS-316   ○   DU

   reason:

9. In order to reduce the erosive effects of a gun propellant
   – the N_2/CO ratio should be   ○   high   ○   low
   – T_c should be   ○   high   ○   low

10. In a drophammer experiment, a mass of 5 kg hits the sample from a height of 50 cm. Calculate the impact energy.

11. Give five different nitrating agents.

12. For which application would hypergolic behaviour be desirable (give two applications)?

13. Name a possible replacement for TNT.

14. Name a possible replacement for Composition B.

15. How does the specific impulse I_{sp}^* depend on the combustion temperature (T_c) and the average molecular weight (M) of the combustion gases formed?

16. What is the relationship between the average thrust ($\overline{F}$) of a rocket and its specific impulse (I_{sp})?

17. Give one example each of a solid rocket propellant which belongs to the following classes and state whether the material is homogeneous or heterogeneous:
    − double-base:
    − composite:

18. As a "rule of thumb" by how much would one need to increase the specific impulse I_{sp}^* of a rocket in order to double its payload?

19. Which metals are clandestine signalling and illuminating formulations in this range $700-1000$ nm usually based on?

20. How does the detonation pressure (p_{C-J}) scales with the loading density?

21. How can the enthalpies of sublimation ($\Delta H_{sub.}$) and vaporization ($\Delta H_{vap.}$) be estimated from the melting and boiling points of a substance?

22. How does the penetration depth of kinetic energy munition depend on the material of the penetrator?

23. How does the Gurney velocity $\left(\sqrt{2E}\right)$ of an explosive depend on the detonation velocity ($D = $ VoD)?

24. Describe three different methods suitable for the synthesis of N_2O_5.

25. Describe the laboratory scale synthesis of ADN starting from ammonia.

26. Which detonation product seems to be most effective for biological agent defeat explosives (e.g. against anthrax spores)?

27. Which general reaction describes the combustion of Al based nanothermites?

28. Name one lead-free tetrazolate based primary explosive.

29. Name one high explosive which has the same chemical composition ($C_aH_bN_cO_d$) as CL-20.

30. What are the environmental/health concerns of AP?

31. For which type of rocket/missile propulsion could chemical thermal propulsion (CTP) be very valuable?

32. In which pressure range do the combustion chambers of a solid rocket motor and a large calibre gun operate?

33. What are the most important performance parameters for
    a) high explosives (secondary explosives),
    b) gun propellants,
    c) rocket propellants?

34. Which two parameters influence the erosion problems in gun barrels the most?

35. Compare the perforation of a shaped charge device (SC) with that of an explosively formed projectile (EFP) for ideal standoff distances.

36. Which experimental test is suitable to assess the shockwave sensitivity of an explosive?

37. Which experimental test (IM test) would be suitable to assess the behaviour of an explosive when subjected to a fuel fire?

38. Compare the high explosives RDX and HNS. What are the most important advantages and disadvantages of the two compounds?

39. What prevents TATP from having any application in the defense world (two reasons)?

40. Which condition is a good/reasonable approximation (e.g. isochoric, isobaric) for the following:
    a) gun propellants,
    b) rocket propellants,
    c) secondary explosives?

41. What are the main light emitting species in visible signal flare formulations which emit in the following regions:
    a) red,
    b) green?

42. How does the maximum wavelength of a blackbody radiator (λ_{max}) depend on/change with the temperature? Which law describes this phenomenon?

43. How does the linear burn rate generally depend on the pressure?

44. How does the electrostatic discharge sensitivity (ESD) usually depend on the particle (grain) size?

45. Are shaped charges (SC) or explosively formed projectiles (EFP) more sensitive to the standoff distance?

46. Why do detonations or combustions often produce CO and not exclusively CO_2 despite a positive oxygen balance?

47. What are the three main "strategies" of designing CHNO based high explosives?

48. For each of the following, give one example of an explosive that only contains the following energetic groups,
    – nitro:
    – nitrate (nitrate ester):
    – nitramino:
    – nitrimino:
    – azide:
    – peroxo:

49. What are the disadvantages of using nitroglycerine for military applications?

50. According to Kamlet and Jacobs the detonation velocity (D) and the detonation pressure (p_{C-J}) can be estimated. Give the relevant equations.

15 Literature

Additional Reading

General

Agrawal, J. P., *High Energy Materials*, Wiley-VCH, Weinheim, **2010**.

Agrawal, J. P., Hodgson, R. D., *Organic Chemistry of Explosives*, Wiley-VCH, Weinheim, **2007**.

Akhavan, J., *The Chemistry of Explosives*, 2nd edn., The Royal Society of Chemistry, Cambridge, **2004**.

Bailey, A., Murray, S. G., *Explosives, Propellants & Pyrotechnics*, Brassey's, London, **1989**.

Cook, J. R., *The Chemistry and Characteristics of Explosive Materials*, 1st edn., Vantage Press, New York, **2001**.

Dolan, J. E., Langer, S. S., (ed.), *Explosives in the Service of Man*, The Royal Society of Chemistry, Cambridge, **1997**.

Fair, H. D., Walker, R. F., *Energetic Materials*, Vol. 1 & 2, Plenum Press, New York, **1977**.

Fedoroff, B. T., Aaronson, H. A., Reese, E. F., Sheffield, O. E., Clift, G. D., *Encyclopedia of Explosives*, U.S. Army Research and Development Command (TACOM, ARDEC) Warheads, Energetics and Combat Support Center, Picatinny Arsenal, New Jersey, **1960**.

Fordham, S., *High Explosives and Propellants*, 2nd edn., Pergamon Press, Oxford, **1980**.

Jonas, J. A., Walters, W. P., *Explosive Effects and Applications*, Springer, New York, **1998**.

Klapötke, T. M., (ed.), *High Energy Density Materials*, Structure and Bonding, Vol. 125, Springer, Berlin, **2007**.

Klapötke, T. M., in E. Riedel (ed.), *Moderne Anorganische Chemie*, 3. edn., ch. 1, Nichtmetallchemie, Walter de Gruyter, Berlin, **2007**.

Köhler, J., Meyer, R., Homburg, A., *Explosivstoffe*, 10. Auflage, Wiley-VCH, Weinheim, **2008**.

Kubota, N., *Propellants and Explosives*, Wiley-VCH, Weinheim, **2002**.

Olah, G. A., Squire, D. R., *Chemistry of Energetic Materials*, Academic Press, San Diego, **1991**.

Urbanski, T., *Chemistry and Technology of Explosives*, Vol. 1−4, Pergamon Press, Oxford, **1964/1984**.

Synthetic Chemistry

Agrawal, J. P., Hodgson, R. D., *Organic Chemistry of Explosives*, Wiley, Hoboken, NJ, **2007**.

Ang, H. G., Santhosh, G., *Advances in Energetic Dinitramides*, World Scientific, New Jersey, London, Singapore, **2007**.

Bailey, P. D., Morgan, K. M., *Organonitrogen Chemistry*, Oxford Science Publications, Oxford, **1996**.

Boyer, J. H., *Nitroazoles*, VCH, Weinheim, **1986**.

Feuer, H., Nielsen, A. T., *Nitro Compounds*, VCH, Weinheim, **1990**.

Feuer, H., *Nitrile Oxides, Nitrones, and Nitronates in Organic Synthesis*, Wiley, Hoboken, NJ, **2008**.

Hammerl, A., Klapötke, T. M., *Pentazoles*. In: *Comprehensive Heterocyclic Chemistry III*, A.R. Katritzky, C. A. Ramsden, Scriven, E. F.V., Taylor, R. J. K., (ed.); Elsevier, Oxford, **2008**; Vol. 6, p. 739−758.

Ledgard, J., *The Preparatory Manual of Explosives*, 3rd edn., J. B. Ledgard, **2007**.

Nielsen, A. T., *Nitrocarbons*, VCH, Weinheim, **1995**.

Ono, N., *The Nitro Group in Organic Synthesis*, Wiley-VCH, New York, **2001**.

Torssell, K. B. G., *Nitrile Oxides, Nitrones, and Nitronates in Organic Synthesis*, VCH, Weinheim, **1988**.

Gao, H., Shreeve, J. M., *Chem. Rev.*, 2011, 111, 7377−7436.

Detonation Physics
Dremin, A. N., *Toward Detonation Theory*, Springer, Berlin, New York, **1999**.

Fickett, W., Davis, W. C., *Detonation Theory and Experiment*, Dover Publications, Mineola, New York, **1979**.

Hidding, B., *Untersuchung der Eignung von Silanen als Treibstoffe in der Luft- und Raumfahrt* (Diplomarbeit), UniBW München, **2004**.

Holian, B. L., Baer, M. R., Brenner, D., Dlott, D. D., Redondo, A., Rice, B. M., Sewell, T., Wight, C. A., *Molecular Dynamics Simulations of Detonation Phenomena*, ITRI Press, Laurel, MD, **2004**.

Liberman, M. A., *Introduction to Physics and Chemistry of Combustion*, Springer, Berlin, **2008**.

Penney, W. G., Taylor, G., Jones, H., Evans, W. M., Davies, R. M., Owen, J. D., Edwards, D. H., Thomas, D. E., Adams, C. A., Bowden, F. P., Ubbelohde, A. R., Courtnev-Pratt, J. S., Paterson, S., Taylor, J., Gurton, O. A., *Proc. Royal Soc.* **1950**, *204 A*, 3.

Zel'dovich, Y. B., Raizer, Y. P., *Physics of Shock Waves and High-Temperature Hydrodynamic Phenomena*, Dover, Mineola, New York, **2002**.

Pyrotechnics
Conkling, J. A., *Chemistry of Fireworks*, Marcel Dekker, New York, **1985**.

Hardt, A. P., *Pyrotechnics*, Pyrotechnica Publications, Post Falls, **2001**.

Koch, E.-C., *Journal of Pyrotechnics* **2002**, *15*, 9−23.

Koch, E.-C., *Journal of Pyrotechnics* **2005**, *21*, 39−50.

Koch, E.-C., *Propellants, Explosives, Pyrotechnics* **2001**, *26(1)*, 3−11.

Koch, E.-C., *Propellants, Explosives, Pyrotechnics* **2002**, *27(5)*, 262−266.

Koch, E.-C., *Propellants, Explosives, Pyrotechnics* **2002**, *27*, 340.

Koch, E.-C., *Propellants, Explosives, Pyrotechnics* **2004**, *29(2)*, 67−80.

Koch, E.-C., *Propellants, Explosives, Pyrotechnics* **2006**, *31(1)*, 3−19.

Koch, E.-C., *Propellants, Explosives, Pyrotechnics* **2008**, *33(3)*, 165−176.

Koch, E.-C., *Propellants, Explosives, Pyrotechnics* **2008**, *33(5)*, 333−335.

Koch, E.-C., *Propellants, Explosives, Pyrotechnics* **2009**, *34*, 6−12.

Russell, M. S., *The Chemistry of Fireworks*, The Royal Society of Chemistry, Cambridge, **2000**.

Steinhauser, G., Klapötke, T. M., *Angew. Chem.* **2008**, *120*, 2−21; *Intl. Ed.* **2008**, *47*, 2−20.

Steinhauser, G., Klapötke, T. M., *J. Chem. Educ.* **2010**, *87*(2), 150−156.

Koch, E.-C., *Metal-Fluorocarbon Based Energ. Materials*, Wiley-VCH, Weinheim, **2012**.

Crow, J. M., *Chem. World* **2012**, 46−49.

Material Sciences
Teipel, U., (ed.), *Energetic Materials*, Wiley-VCH, Weinheim, **2005**.

Engineering and Technology
Cooper, P. W., Kurowski, S. R., *Technology of Explosives*, Wiley-VCH, New York, **1996**.

Cooper, P. W., *Explosives Engineering*, Wiley-VCH, New York, **1996**.

Rocket Propulsion
Kubota, N., *Propellants and Explosives*, Wiley, VCH, Weinheim, **2002**.
Jacobs, P. W. M., Whitehead, H. M., *Chem. Rev.* **1969**, *69(4)*, 551−590.
Schmidt, E. W., *Hydrazine and its Derivatives*, 2. Aufl., Band 1 und 2, Wiley, New York, **2001**.
Yang, V., Brill, T. B., Ren, W.-Z., (ed.), *Solid Propellant Chemistry, Combustion, and Motor Interior Ballistics*, Vol. 185, AAIA, Reston, VA, **2000**.
Ulas, A., Kuo, K. K., *Comb. Flame*, **2001**, *127*, 1935−1957.

Gun Propulsion
Jahnuk, H., *Prop. Expl. Pyrotech.* **1976**, *1*, 47−50.
Dürschner, M. G., *Prop. Expl. Pyrotech.* **1976**, *1*, 81−85.
Zentner, B. A., Reed, R., *Calculated Performance of Gun Propellant Compositions Containing High Nitrogen Ingredients*, 5th Intl. Gun Propellant Symp., Picatinny Arsenal, NJ, November 19−21, **1991**, IV−278.

Weapons
Carlucci, D. E., Jacobson, S. S., *Ballistics − Theory and Design of Guns and Ammunition*, CRC Press, Boca Raton, Fl., **2008**.
Dathan, H., *Waffenlehre für die Bundeswehr*, 4th edition, Mittler, Herford, Bonn, **1980**.
Heard, B. J., *Handbook of Firearms and Ballistics*, 2nd edition, Wiley-Blackwell, Chichester, **2008**.

Testing Methods
Kneisl, P., *13th NTREM*, **2010,** 184−193.
Sućeska, M., *Test Methods for Explosives*, Springer, New York, **1995**.

Gurney Velocity
Backofen, J. E., *New Trends in Research of Energetic Materials*, **2006**, 9th Seminar, 76−89.
Backofen, J. E., Weickert, C. A., in: *Shock Compression of Condensed Matter*, **2001** (eds.: M. D. Furnish, N. N. Thadhani, Y. Horie) Amer. Inst. Phys. **2002**, 954−957.
Cooper, P. W., *Explosives Engineering*, Wiley-VCH, New York, Chichester, Weinheim, Kap. 27, **1996**, 385−403.
Gurney, R. W., *Internal Report BRL-405*, **1943**, Ballistic Research Laboratory, Aberdeen, MD.
Hardesty, D. R., Kennedy, J. E., *Combust. Flame* **1977**, *28*, 45.
Jaansalu, K. M., Dunning, M. R., Andrews, W. S., *Prop. Expl. Pyrotech.* **2007**, *32*, 80.
Kamlet, M. J., Finger, M., *Combust. Flame* **1979**, *34*, 213.
Keshavarz, M. H., *Prop. Expl. Pyrotech.* **2008**, *33*, 316.
Koch, A., Arnold, N., Estermann, M., *Prop. Expl. Pyrotech.* **2002**, *27*, 365.
Reaugh, J. E. , Souers, P. C., *Prop. Expl. Pyrotech.* **2004**, *29*, 124.
Stronge, W. J., Xiaoqing, M., Lanting, Z., *Int J. Mech. Sci.* **1989**, *31*, 811.

Computational Chemistry (quantum mechanics)
Politzer, P., Murray, J. S. N., Energetic Materials, Part 1: Decomposition, Crystal and Molecular Properties, in: *Theor. Comput. Chem.*, Vol. 12, Elsevier, Amsterdam, **2003**.
Politzer, P., Murray, J. S. N., *E*nergetic Materials, Part 2, Energetic Materials, Part 2: Detonation, Combustion, in: *Theor. Comput. Chem.*, Vol. 13, Elsevier, Amsterdam, **2003**.
Seminario, J. M., Politzer, P., Modern Density Functional Theory: A Tool for Chemistry, in: *Theor. Comput. Chem.*, Vol. 2, Elsevier, Amsterdam, **1995**.
Politzer, P. A., Murray, J. S., *Energetic Materials*, Part 1 & 2, Elsevier, Amsterdam, **2003**.

Nanothermites

Brown, M. E., Taylor, S. J., Tribelhorn, M. J., *Propellants, Explosives, Pyrotechnics.* **1998**, *23*, 320−327.

Bulian, C. J., Kerr, T. T., Puszynski, J. A., *Proceedings of the International Pyrotechnics Seminar* **2004**, 31st 327−338.

Clapsaddle, B. J., Zhao, L., Gash, A. E., Satcher, J. H., Shea, K. J., Pantoya, M. L., Simpson, R. L., *Res. Soc. Symp. Proc. Vol. 800.* **2004**, AA2.7.1—AA2.7.6.

Clapsaddle, B. J., Zhao, L., Prentice, D., Pantoya, M. L., Gash, A. E., Satcher, J. H., Shea, K. J., Simpson, R. L., *International Annual Conference of ICT* **2005**, 36th (Energetic Materials), 39/1−39/10.

Comet, M., Pichot, V., Spitzer, D., Siegert, B., Ciszek, F., Piazzon, N., Gibot, P., Pierre, *International Annual Conference of ICT* **2008**, 39th, V38/1−V38/8.

Gash, A. E., Satcher, J. H., Simpson, R. L., Clapsaddle, B. J., *Mat. Res. Soc. Symp. Proc. Vol. 800.* **2004**, AA2.2.1—AA2.2.12.

Naud, D. L., Hiskey, M., Son, S. F., Busse, J. R., Kosanke, K., *Journal of Pyrotechnics* **2003**, *17*, 65−75.

Pantoya, M. L., Granier, J. J., *Propellants, Explosives, Pyrotechnics,* **2005**, *30(1)*, 53−62.

Perry, W. L., Smith, B. L., Bulian, C. J., Busse, J. R., Macomber, C. S., Dye, R. C., Son, S. F., *Propellants, Explosives, Pyrotechnics,* **2004**, *29*, 99−105.

Piercey, D. G., Klapötke, T. M., *Central Europ. J. Energ. Mat.* **2010**, in press.

Prakash, A., McCormick, A. V., Zachariah, M. R., *Chem. Mater.* **2004**, *16(8)*, 1466−1471.

Puszynski, J. A., Bichay, M. M., Swiatkiewicz, J. J., United States Patent Application Number *20060113014.* June 1, 2006.

Puszynski, J. A., Bulian, C. J., Swiatkiewicz, J. J., *Journal of Propulsion and Power* **2007**, *23(4)*, 698−706.

Puszynski, J. A., *Mat. Res. Soc. Symp. Proc. Vol. 800.* **2004** AA6.4.1—AA6.4.10.

Sanders, V. E., Asay, B. W., Foley, T. J., Tappan, B. C., Pacheco, A. N., Son, S. F., *Propulsion and Power.* **2007**, *23(4)*, 707−714

Schoenitz, M., Ward, T., Dreizin, E. L., *Res. Soc. Symp. Proc. Vol. 800.* **2004**, AA2.6.1—AA2.6.6.

Shende, R., Subramanian, S., Hasan, S., Apperson, S., Thiruvengadathan, R., Gangopadhyay, K., Gangopadhyay, S., Redner, S., Kapoor, D., Nicolich, S., Balas, W., *Propellants, Explosives, Pyrotechnics.* **2008**, *33(2)*, 122−130.

Son, S. F., *Mat. Res. Soc. Symp. Proc. Vol. 800.* **2004**, AA5.2.1—AA5.2.12.

Son, S. F., Yetter, R. A., Yang, Y., *Journal of Propulsion and Power* **2007**, *23(4)*, 643−644.

Son, S. F., Asay, B. W., Foley, T. J., Yetter, R. A., Wu, M. H., Risha, G. A., *Propulsion and Power.* **2007**, *23(4)*, 714−721.

Spitzer, D., Comet, M., Moeglin, J.-P., Stechele, E., Werner, U., Suma, A., Yves, *International Annual Conference of ICT* **2006**, 37th (Energetic Materials), 117/1−117/10.

Tillotson, T. M., Gash, A. E., Simpson, R. L., Hrubesh, L. W., Satcher, J. H., Poco, J. F., *Journal of Non-Crystalline Solids,* **2001**, *285*, 338−345.

Umbrajkar, S. M., Schoenitz, M., Dreizin, E. L., *Propellants, Explosives, Pyrotechnics.* **2006**, *31(5)*, 382−389.

Walker, J., Tannenbaum, R., *Res. Soc. Symp. Proc. Vol. 800.* **2004**, AA7.8.1—AA7.8.10.

Walter, K. C., Pesiri, D. R., Wilson, D. E., *Propulsion and Power* **2007**, *23(4)*, 645−650.

Weismiller, M. R., Malchi, J. Y., Yetter, R. A., Foley, T. J., *Chemical and Physical Processes in Combustion*, **2007**, 595, 600.

Primary Explosives

Cartwright, M., Wilkinson, J., *Propellants, Explosives, Pyrotechnics* **2011**, *36*, 530−540.

Cartwright, M., Wilkinson, J., *Propellants, Explosives, Pyrotechnics* **2010**, *35*, 326−332.

Fronabarger, J. W., Williams, M. D., Sanborn, W. B., Bragg, J. G., Parrish, D. A., Bichay, M., *Propellants, Explosives, Pyrotechnics* **2011**, *36*, 541−550.

Ugryumov, I A., Ilyushin, M. A., Tselinskii, I. V., Kozlov, A. S., *Russian Journal of Applied Chemistry* **2003**, *76*, 439−441.

Fronabarger, J. W., Williams, M. D., Sanborn, W. B., Parrish, D. A., Bichay, M. *Propellants, Explosives, Pyrotechnics* **2011**, *36*, 459−470.

Fischer, D., Klapötke, T. M., Piercey, D. G., Stierstorfer, J., J. *Energ. Mat.* **2012**, *30*, 40−54.

Mehta, N., Damavarapu, R., Cheng, G., Dolch, T., Rivera, J., Duddu, R., Yang, K. *Proceedings of the International Pyrotechnics Seminar* **2009**, *36*, 175−180.

Matyáš, R., Pachman, J. *Primary Explosives*, Springer, Berlin, **2012**.

Cited Literature

[1] (a) W. Beck, J. Evers, M. Göbel, G. Oehlinger, T. M. Klapötke, *Z. Anorg. Allg. Chem.* **2007**, *633*, 1417−1422.

(b) W. Beck, T. M. Klapötke, *J. Mol. Struct.* (THEOCHEM) **2008**, *848*, 94−97.

(c) K. Karaghiosoff, T. M. Klapötke, A. Michailovski, G. Holl, *Acta Cryst. C* **2002**, *C 58*, o580−o581.

(d) E. Gökçınar, T. M. Klapötke, A. J. Bellamy, *J. Mol. Struct.* (THEOCHEM), **2010**, *953*, 18−23.

(e) G: Majano, S. Mintova, T. Bein, T. M. Klapötke, *Advanced Materials* **2006**, *18*, 2240−2243.

(f) G. Majano, S. Mintova, T. Bein, T. M. Klapötke, *J. Phys. Chem. C*, **2007**, *111*, 6694−6699.

[2] (a) J. Evers, T. M. Klapötke, P. Mayer, G. Oehlinger, J. Welch, *Inorg. Chem.* **2006**, *45*, 4996−5007.

(b) M.-J. Crawford, J. Evers, M. Göbel, T. M. Klapötke, P. Mayer, G. Oehlinger, J. M. Welch, *Propellants Explosives and Pyrotechnics* **2007**, *32*, 478−495.

[3] M. H. V. Huynh, M. A. Hiskey, T. J. Meyer, M. Wetzler, *PNAS*, **2006**, *103*, 5409−5412. See also: T. M. Klapötke, C. Miro Sabate, J. M. Welch, *J. Chem. Soc., Dalton Trans.*, **2008**, 6372−6380.

[4] G. Geisberger, T. M. Klapötke, J. Stierstorfer, *Eur. J. Inorg. Chem.* **2007**, 4743−4750.

[5] SERDP information: Cleanup CU-1164: http://www.p2pays.org/ref/19/18164.pdf (2/21/03).

[6] The official SERDP source for perchlorate information: http://www.serdp.org/research/er-perchlorate.cfm

[7] SERDP & ESTCP Annual Symposium **2007**: http://www.serdp.org/Symposium/.

[8] M. Göbel, T. M. Klapötke, *Z. Anorg. Allg. Chem.* **2007**, *633*, 1006−1017.

[9] T. M. Klapötke, A. Penger, S. Scheutzow, L. Vejs, *Z. Anorg. Allg. Chem.*, **2008**.

[10] K. Karaghiosoff, T. M. Klapötke, C. Miro Sabate, *Chemistry Europ. J.*, **2008**.

[11] R. M. Doherty, Novel Energetic Materials for Emerging Needs, 9th-IWCP on Novel Energetic Materials and Applications, Lerici (Pisa), Italy, September 14−18, **2003**.

[12] N. Fischer, T. M. Klapötke, S. Scheutzow, J. Stierstorfer, Centr. Europ. J. Energ. Mat. **2008**, *5*, 3−18.

[13] G. Steinhauser, T. M. Klapötke, *Angew. Chem.* **2008**, *120*, 2−21; *Intl. Ed.* **2008**, *47*, 2−20.

[14] Tetrazoles for the safe detonation, T. M. Klapötke, *Nachrichten aus der Chemie*, **2008**, *56(6)*, 645−648.

[15] T. M. Klapötke, J. Stierstorfer, K. R. Tarantik, Neue, umweltverträglichere Formulierungen für Pyrotechnika, *Die aktuelle Wochenschau, GDCh*, 15.09.**2008**, Woche 37: http://www.aktuelle-wochenschau.de/woche37/woche37.html.

[16] (a) B. Halford, *Chem. Eng. News*, **2008**, June 30, 14−18.
     (b) J. J. Sabatini, J. C. Poret, R. N. Broad, *Angew. Chem. Int. Ed.*, **2011**, *50*, 4624−4626.
[17] M. J. Kamlet, S. J. Jacobs, *J. Chem. Phys*. **1968**, *48*, 23.
[18] M. J. Kamlet, J. E. Ablard, *J. Chem. Phys*. **1968**, *48*, 36.
[19] M. J. Kamlet, C. Dickinson, *J. Chem. Phys*. **1968**, *48*, 43.
[20] M. Sućeska, Proceedings of 32nd Int. Annual Conference of ICT, July 3−6, Karlsruhe, **2001**, S. 110/1−110/11.
[21] L. A. Curtiss, K. Raghavachari, P. C. Redfern, J. A. Pople, *J. Chem. Phys*. **1997**, *106*, 1063.
[22] E. F. C. Byrd, B. M. Rice, *J. Phys. Chem. A*. **2006**, *110*, 1005.
[23] B. M. Rice, S. V. Pai, J. Hare, *Combustion and Flame* **1999**, *118*, 445.
[24] P. J. Linstrom, W. G. Mallard, Eds., NIST Chemistry WebBook, NIST Standard Reference Database Number 69, June **2005,** National Institute of Standards and Technology, Gaithersburg MD, 20899 (http://webbook.nist.gov).
[25] M. S. Westwell, M. S. Searle, D. J. Wales, D. H. Williams, *J. Am. Chem. Soc*. **1995**, *117*, 5013.
[26] H. D. B. Jenkins, H. K. Roobottom, J. Passmore, L. Glasser, *Inorg. Chem*. **1999**, *38(16)*, 3609−3620.
[27] H. D. B. Jenkins, D. Tudela, L. Glasser, *Inorg. Chem*. **2002**, *41(9)*, 2364−2367.
[28] H. D. B. Jenkins, L. Glasser, *Inorg. Chem*. **2002**, *41(17)*, 4378−88.
[29] H. D. B. Jenkins, Chemical Thermodynamics at a Glance, Blackwell, Oxford, **2008**.
[30] J. P. Ritchie, E. A. Zhurova, A. Martin, A. A. Pinkerton, *J. Phys. Chem. B*, **2003**, *107*, 14576−14589.
[31] M. Sućeska, Calculation of Detonation Parameters by EXPLO5 Computer Program, Materials Science Forum, **2004**, 465−466, 325−330.
[32] M. Sućeska, *Propellants, Explos., Pyrotech*. **1991**, *16*, 197.
[33] M. Sućeska, *Propellants Explos., Pyrotech*. **1999**, *24*, 280.
[34] M. L. Hobbs, M. R. Baer: Calibration of the BKW-EOS with a Large Product Species Data Base and Measured C-J Properties, Proc. of the 10th Symp. (International) on Detonation, ONR 33395−12, Boston, MA, July 12−16, **1993**, p. 409.
[35] (a) N. Fischer, T. M. Klapötke, S. Scheutzow, J. Stierstorfer, *Central Europ. J. of Energ. Mat.*, **2008**, *5(3−4)*, 3−18;
     (b) E. Gökçınar, T. M. Klapötke, M. P. Kramer, *J. Phys. Chem.*, **2010**, *114*, 8680−8686.
[36] F. Trimborn, *Propellants Explos., Pyrotech*. **1980**, *5*, 40.
[37] M. Held, *NOBEL-Hefte*, **1991**, *57*, 14.
[38] M. Sućeska, Intl. J. Blasting and Fragmentation, 1997, 1, 261.
[39] (a) Politzer, P.; Murray, J. S. *Computational Characterization of Energetic Materials*, in: Pauling's Legacy: Modern Modelling of the Chemical Bond, Maksic, Z. B. Orville-Thomas, W. J. (eds.), Theoretical and Computational Chemistry, Vol. 6, **1999**, pp 347−363;
     (b) Politzer, P., Murray, J. S.; Seminario, J. M.; Lane, P.; Grice, M. E.; Concha, M. C. *J. Mol. Struct*. **2001**, *573*, 1.
     (c) Murray, J. S.; Lane, P.; Politzer, P. *Molec. Phys*. **1998**, *93*, 187;
     (d) Murray, J. S.; Lane, P.; Politzer, P. *Mol. Phys*. **1995**, *85*, 1.
     (e) Murray, J. S.; Concha, M. C.; Politzer, P. *Molec. Phys*. **2009**, *107(1)*, 89;
     (f) P. Politzer, J. Martinez, J. S. Murray, M. C. Concha, A. Toro-Labbe, *Mol. Phys*. **2009**, *107 (19)*, 2095−2101;
     (g) M. Pospisil, P. Vavra, M. C. Concha, J. S. Murray, P. Politzer, *J. Mol. Model*. **2010**, *16*, 985−901.
[40] (a) B. M. Rice, J. J. Hare, E. F. Byrd, *J. Phys. Chem. A*, **2007**, *111(42)*, 10874.
     (b) B. M. Rice, E. F. C. Byrd, *J. Mater. Res.*, **2006**, *21(10)*, 2444.
[41] E. F. Byrd, B. M. Rice, *J. Phys. Chem. A*, **2006**, *110(3)*, 1005.

[42] B. M. Rice, J. Hare, *Thermochimica Acta,* **2002**, *384(1−2)*, 377.

[43] B. M. Rice, S. V. Pai, J. Hare, *Combustion and Flame*, **1999**, *118(3)*, 445.

[44] B. M. Rice, J. J. Hare, *J. Phys. Chem. A*, **2002**, *106(9)*, 1770.

[45] R. Engelke, *J. Phys. Chem.,* **1992**, *96*, 10789.

[46] M. N. Glukhovtsev, P. v. R. Schleyer, *Chem. Phys. Lett.,* **1992**, *198*, 547.

[47] M. I. Eremets, A. G. Gavriliuk, N. R. Serebryanaya, I. A. Trojan, D. A. Dzivenko, R. Boehler, H. K. Mao, R. J. Hemley, *J. Chem. Phys*. **2004**, *121*, 11296.

[48] M. I. Eremets, A. G. Gavriliuk, I. A. Trojan, D. A. Dzivenko, R. Boehler, *Nature Materials* **2004**, *3*, 558.

[49] M. I. Eremets, M. Y. Popov, I. A. Trojan, V. N. Denisov, R. Boehler, R. J. Hemley, *J. Chem. Phys*. **2004**, *120*, 10618.

[50] T. M. Klapötke, G. Holl, *Green Chemistry*, **2001**, G75.

[51] T. M. Klapötke, G. Holl, *Chemistry in Australia*, **2002**, 11.

[52] T. M. Klapötke, J. Stierstorfer, *Central Europ. J. of Energ. Mat.*, **2008**, *5(1)*, 13.

[53] T. M. Klapötke, J. Stierstorfer, *J. Chem. Soc., Dalton Trans.*, **2008**, 643−653.

[54] M. Göbel, T. M. Klapötke, *Adv. Funct. Mat.*, **2009**, *19*, 347−365.

[55] (a) R. P. Singh, R. D. Verma, D. T. Meshri, J. M. Shreeve, *Angew. Chem. Int. Ed*., **2006**, *45*, 3584.
(b) A. K. Sikder, N. Sikder, *J. Haz. Mater.*, **2004**, *A112*, 1.

[56] (a) Y.-H. Joo, B. Twamley, S. Grag, J. M. Shreeve, *Angew. Chem*. **2008**, *120*, 6332; *Angew. Chem. Int. Ed*. **2008**, *47*, 6236;
(b) Y.-H. Yoo, J. M. Shreeve, *Angew. Chem*. **2009**, *48(3)*, 564− 567.
(c) T. M. Klapötke, P. Mayer, J. Stierstorfer, J. Weigand, J. J. *J. Mat. Chem*. **2008**, *18*, 5248−5258.
(d) M. J. Saly, M. J. Heeg, C. H. Winter, *Inorganic Chemistry* **2009**, *48(12)*, 5303−5312.

[57] (a) S. D. Chambreau, S. Schneider, M. Rosander, T. Hawkins, C. J. Gallegos, M. F. Pastewait, G. L. Vaghjiani, *J. Phys. Chem. A*, **2008**, *112*, 7816.
(b) S. Schneider, T. Hawkins, Y. Ahmed, M. Rosander, L. Hudgens, J. Mills, *Angew. Chem. Int. Ed.*, **2011**, *50*, 5886−5888.

[58] (a) D. Amariei, L. Courthéoux, S. Rossignol, C. Kappenstein, *Chem. Engeneering and Processing*, 2007, *46*, 165.
(b) R. R. Singh, R. D. Verma, D. T. Meshri, J. M. Shreeve, *Angew Chem*. 2006, *118(22)*, 3664−3682;
(c) H. Gao, Y.-H. Joo, B. Twamley, Z. Zhou, J. M. Shreeve, *Angew. Chem*. 2009, *121 (15)*, 2830−2833.
(d) Y. Zhang, H. Gao, Y.-H. Joo, J. M. Shreeve, *Angew. Chem. Int. Ed.*, **2011**, *50*, 9554−9562.

[59] (a) T. Altenburg, A. Penger, T. M. Klapötke, J. Stierstorfer, *Z. Anorg. Allg. Chem*. 2010, *636*, 463−471.
(b) T. M. Klapötke, J. Stierstorfer, *Helv. Chim. Acta*, **2007**, *90*, 2132−2150.
(c) O. Bolton, A. J. Matzger, *Angew. Chem. Int. Ed.*, **2011**, in press.

[60] R. W. Millar, M. E. Colclough, P. Golding, P. J. Honey, N. C. Paul, A. J. Sanderson, M. J. Stewart, *Phil. Trans. R. Soc. Lond. A*, **1992**, *339*, 305.

[61] A. D. Harris, J. C. Trebellas, H. B. Jonassen, *Inorg. Synth.,* **1967**, *9*, 83.

[62] S. Borman, *Chem. Eng. News*, **1994**, *Jan. 17*, 18.

[63] K. O. Christe, W. W. Wilson, M. A. Petrie, H. H. Michels, J. C. Bottaro, R. Gilardi, *Inorg. Chem.,* **1996**, *35*, 5068.

[64] T. M. Klapötke, J. Stierstorfer, *Phys. Chem. Chem. Phys*., **2008**, *10*, 4340.

[65] T. M. Klapötke, J. Stierstorfer, A. U. Wallek, *Chem. Mater.*, **2008**, *20*, 4519.

[66] T. M. Klapötke, B. Krumm, N. Mayr, F. X. Steemann, G. Steinhauser, *Safety Science*, **2010**, 48, 28−34.

[67] R. D. Chapman, R. D. Gilardi, M. F. Welker, C. B. Kreutzberger, *J. Org. Chem.* **1999**, *64*, 960−965.

[68] D. Fischer, T. M. Klapötke, J. Stierstorfer, *Z. Anorg. Allg. Chem.* **2011**, *637*, 660−665.

Computer Codes

Sućeska, M., *EXPLO5* program, version 5.04, Zagreb, Croatia, **2010**.

Fraunhofer Institut Chemische Technologie, ICT, ICT Thermodynamic Code, Version 1.00, **1998−2000**.

Frisch, M. J., et al., Gaussian 03, Revision B04, Gaussian Inc., Wallingford, CT, **2004.**

Fried, L. E., Glaesemann, K. R., Howard, W. M., Souers, P. C., CHEETAH 4.0 User's Manual, Lawrence Livermore National Laboratory, **2004**.

Lu, J. P., Evaluation of the Thermochemical Code−CHEETAH 2.0 for Modelling Explosives Performance, DSTO-DR-1199, Defence Science and Technology Organization (Australian Government), Edinburgh, **2001**.

HyperChem, Release 7.0, Molecular Modeling System for Windows, Hypercube Inc., **2002**.

CHEMKIN, Release 3.5, R. J. Kee, F. M. Rupley, J. A. Miller, M. E. Coltrin, J. F. Grcar, E. Meeks, H. K. Moffat, A. E. Lutz, G. Dixon-Lewis, M. D. Smooke, J. Warnatz, G. H. Evans, R. S. Larson, R. E. Mitchell, L. R. Petzold, W. C. Reynolds, M. Caracotsios, W. E. Stewart, and P. Glarborg, CHEMKIN Collection, Release 3.5, Reaction Design, Inc., San Diego, CA, **1999**.

NASA-Glenn Chemical Equilibrium Program CEA, B. McBride, S. Gordon, **1999**.

WEB Pages

ARL:	http://www.arl.army.mil/www/default.htm
SERDP:	http://www.serdp.org/
ESTCP:	http://www.estcp.org/
WIWEB:	http://wiweb-erding.de/
ARDEC:	http://www.pica.army.mil/PicatinnyPublic/organizations/ardec/index.asp
NAWCWD:	http://www.navair.navy.mil/nawcwd/
NSWC:	http://www.ih.navy.mil/
ICT:	http://www.ict.fraunhofer.de/
DTRA:	http://www.dtra.mil/index.cfm
DTIC:	http://www.dtic.mil/dtic/
EPA:	http://www.epa.gov/
HEMSI:	http://www.hemsichd.org
RTO:	http://www.rta.nato.int
NIOSH:	http://www.cdc.gov/NIOSH/
NIST:	http://webbook.nist.gov/chemistry/
IMEMG	http://www.imemg.org/imemg-home.html
MSIAC	http://www.msiac.nato.int/
FHG	http://www.ict.fraunhofer.de/
SYSTAG	http://www.systag.ch/A4d_TAV_1m24.pdf
OZM	http://www.ozm.cz/en/

Journals

Propellants, Explosives, Pyrotechnics: http://www3.interscience.wiley.com/journal/26213/home

Central European Journal of Energetic Materials: http://www.ipo.waw.pl/wydawnictwa/cejem-glowna.html

Journal of Energetic Materials: http://www.marinkas.com/

Journal of Pyrotechnics: http://www.jpyro.com/

The American Institute of Aeronautics and Astronautics: http://www.aiaa.org/content.cfm?pageid=318&pubid=2

Journal of Hazardous Materials: http://www.sciencedirect.com/science/journal/03043894

Journal of Energetic Materials: http://www.tandf.co.uk/journals/titles/07370652.html

International Journal of Energetic Materials and Chemical Propulsion (IJEMCP): http://www.begellhouse.com/journals/17bbb47e377ce023.html

Conferences

Gordon Research Conference: Energetic Materials, every other year (2008, 2010, …), usually June, in New Hampshire (USA): http://www.grc.org/conferences.aspx?id=0000071

ICT International Annual Conference, annualy, June/July, in Karlsruhe (Germany): http://www.ict.fraunhofer.de/ http://www.ict.fraunhofer.de/EN/VuM/ICT_Jahrestagung/index.jsp

New Trends in Research of Energetic Materials (NTREM), annualy, April, in Pardubice (Czech Republic): http://www.ntrem.com/

PARARI − Australian Ordnance Symposium, every other year (2007, 2009, …), usually November, (Australia): http://www.adi-limited.com/

International Pyrotechnics Seminar, every other year (2008, 2010,…), July, CO (USA): http://www.ipsusa.org/

High Energy Materials Society of India (HEMSI), biannually (2011, 2013, …), usually November (India): http://www.hemsichd.org/index.html

16 Appendix

> I am one of those who think like Nobel,
> that humanity will draw more good
> than evil from new discoveries.
>
> *Marie Curie*

Important reaction types in organic nitrogen chemistry

$$R{-}NH_2 \xrightarrow{HNO_2,\,aq.} [R{-}N_2]^+ \xrightarrow{H_2O} R{-}OH$$

$$R{-}NH_2 \xrightarrow{HNO_2,\,aq.} [R{-}N_2]^+ \xrightarrow{NaN_3} R{-}N_3$$

$$R_2NH \xrightarrow{HNO_2,\,aq.} R_2N{-}N{=}O$$

$$Ph{-}NH_2 \xrightarrow{HNO_2,\,aq.} [Ph{-}N_2]^+ \xrightarrow{PhH,\,-H^+} Ph{-}N{=}N{-}Ph$$

$$Ph{-}NH_2 \xrightarrow{HNO_2,\,aq.} [Ph{-}N_2]^+ \xrightarrow{NaN_3} Ph{-}N_3$$

$$Ph{-}NH_2 \xrightarrow{HNO_2,\,aq.} [Ph{-}N_2]^+ \xrightarrow{NaBF_4} [Ph{-}N_2]^+[BF_4]^- \xrightarrow{NaN_3} Ph{-}N_5$$
$$\xrightarrow{-N_2} PhN_3$$

$$Ph{-}NH{-}NH{-}Ph \xrightarrow{HgO,\,-H_2O,\,-Hg} Ph{-}N{=}N{-}Ph$$

$$Ph{-}NH_2 \xrightarrow[\text{diazotation}]{HNO_2,\,aq.} [Ph{-}N_2]^+ \xrightarrow[\text{Sandmeyer}]{Cu^I X} Ph{-}X$$

$$NaN_3 + R{-}Br \longrightarrow R{-}N_3 \xrightarrow{H_2/Pd{-}C} R{-}NH_2$$

$$Ph{-}CH_2{-}Br + NaN_3 \longrightarrow Ph{-}CH_2{-}N_3$$

$$Ph{-}CH_2{-}N_3 \xrightarrow{H_2/Pd{-}C} Ph{-}CH_2{-}NH_2 + N_2$$

$$Ph{-}C(O){-}Cl + NaN_3 \longrightarrow Ph{-}C(O){-}N_3$$

$$Ph{-}CH_2{-}CN \xrightarrow{H_2/cat.\ or\ LiAlH_4} Ph{-}CH_2{-}CH_2{-}NH_2$$

$$R{-}CN \xrightarrow{H_2/cat.\ or\ LiAlH_4} R{-}CH_2{-}NH_2$$

$$R_1R_2HC{-}NO_2 \xrightarrow{H_2/cat.\ or\ LiAlH_4} R_1R_2HC{-}NH_2$$

$R_1R_2HC-CN \xrightarrow{H_2/cat.\ or\ LiAlH_4} R_1R_2HC-CH_2-NH_2$

$R-NO_2 \xrightarrow{H_2/cat.\ or\ LiAlH_4} R-NH_2$

$R-C(O)-NH_2 \xrightarrow{PCl_5} R-CN$

$R-C(O)-NH_2 \xrightarrow{LiAlH_4} R-CH_2-NH_2$

$HMTA \xrightarrow{HNO_3} RDX \quad (+\ HMX)$

$C(-CH_2-OH)_4 \xrightarrow{HNO_3} PETN$

$R-C(O)-R \xrightarrow{N_2H_4} R_2C=N-NH_2$

$R-X \xrightarrow{N_2H_4} R-NH-NH_2 \quad (X = Hal,\ OMe)$

$RC(O)R + H_2NR' \longrightarrow RC(=NR')R$

$R_2NH + CH_2O \xrightarrow{H^+} [R_2N=CH_2]^+ \longleftrightarrow [R_2N-CH_2]^+$
$\qquad\qquad\qquad$ Mannich $\qquad\qquad$ iminium ion (reacts with C nucleophiles)

$R_2N-C(O)H + POCl_3 \longrightarrow [R_2N=CHCl]^+ \longleftrightarrow [R_2N-CHCl]^+$
$\qquad\qquad\qquad\qquad$ Vilsmeyer iminium ion

$R-COOH \xrightarrow{SOCl_2} R-C(O)-Cl$

$R-C(O)-NH-R' \xrightarrow{N_2H_4} R-C(O)-NH-NH_2 + R'-NH_2$
$\qquad\qquad\qquad$ hydrazinolysis

$R-C(O)-OR \xrightarrow{N_2H_4} R-C(O)-NH-NH_2 \xrightarrow{HNO_2} R-C(O)-N_3$

$R-X + KCN \longrightarrow R-CN \quad (X = Cl,\ Br,\ I,\ OTs,\ ...)$

$Ph-C(O)-NH_2 \xrightarrow{PCl_5} Ph-CN$

$Ph-Cl \xrightarrow{N_2H_4} Ph-NH-NH_2$

$R-C(O)-Cl \xrightarrow{N_2H_4} R-C(O)-NH-NH_2$

$R-C(O)-NH-NH_2 + NO^+ \xrightarrow{-H^+} R-C(O)-NH-NH-N=O$
$\qquad\qquad\qquad \longrightarrow R-C(O)-NH-N=N-OH \longrightarrow R-C(O)-N_3 + H_2O$

$R-C(O)-N_3 \xrightarrow{T,\ -N_2} R-N=C=O$

$$R-C(O)-R \xrightarrow{N_2H_4} R_2C=N-NH_2$$

$$R_3N \xrightarrow{PhCO_3H \text{ or } H_2O_2/AcOH} R_3N^+-O^- \quad \text{(also with pyridines instead of } R_3N)$$

$$R_2N-H \xrightarrow{MSH \text{ or } DPA, \text{ Base}} R_2N-NH_2$$

MSH = mesitylsulfonylhydroxylamine
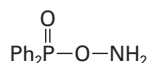
DPA = diphenylphosphenylhydroxylamine

TOAH
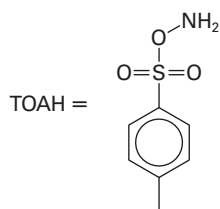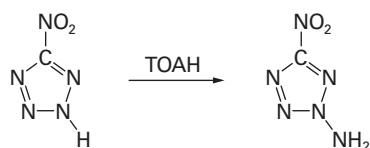
Curing of a diol (HTPB) with isocyanate binder
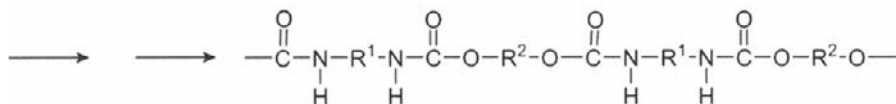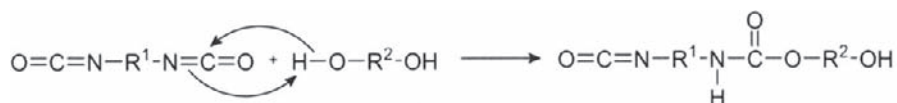
Important reaction types in inorganic nitrogen chemistry

azide transfer reagents: NaN_3
$\qquad\qquad\qquad\qquad\quad AgN_3$
$\qquad\qquad\qquad\qquad\quad Me_3SiN_3$

HN$_3$ synthesis:

$$RCO_2H + NaN_3 \xrightarrow[\text{melt}]{\sim 140\,°C} RCO_2Na + HN_3\uparrow$$
stearic acid

$$HBF_4 + NaN_3 \xrightarrow{Et_2O} NaBF_4\downarrow + HN_3\uparrow$$

$$H_2SO_4 + NaN_3 \longrightarrow HN_3 + NaHSO_4$$

NaN$_3$ synthesis:

$$NaNO_3 + 3\,NaNH_2 \xrightarrow{100\,°C,\ NH_3\,(l)} NaN_3 + 3\,NaOH + NH_3$$

$$N_2O + 2\,NaNH_2 \xrightarrow{190\,°C} NaN_3 + NaOH + NH_3$$

$$R'\!-\!NH_2 \xrightarrow{HC(OR)_3,\ NaN_3\ H^+} R'\!-\!N_4CH$$
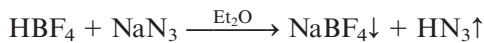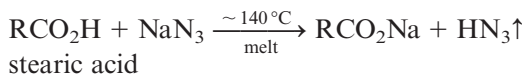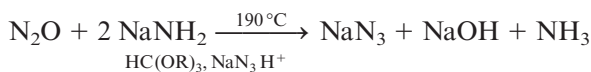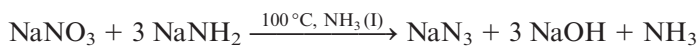
hydrazine synthesis:

Raschig process (SNPE):

$$NaOCl_{aq.} + NH_{3\,aq.} \xrightarrow{0\,°C} NH_2Cl_{aq.} + NaOH$$

$$NH_2Cl_{aq.} + NaOH + NH_3 \xrightarrow{130\,°C} N_2H_4 + H_2O + NaCl$$

$$NH_2Cl + H_2N\,(CH_3) \xrightarrow[-NaCl/-H_2O]{NaOH} H_2N\!-\!NH(CH_3)$$
$$\text{MMH}$$
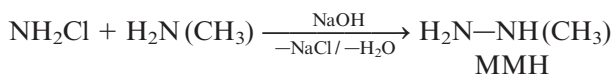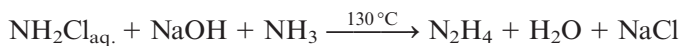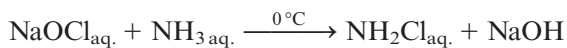
laboratory-scale preparation of anhydrous hydrazine:

$$N_2H_4 \cdot H_2O \xrightarrow{BaO} N_2H_4 \xrightarrow{Na} N_2H_4 \text{ anh.}$$

$$(HOCN)_3 + N_2H_4/H_2O \longrightarrow (HOCN)_3 \cdot N_2H_4 \xrightarrow{200\,°C} (HOCN)_3 + N_2H_4$$

ammonium perchlorate (AP):

$$NH_3 + HClO_4 \longrightarrow AP$$

ammonium nitrate (AN):

$$NH_3 + HNO_3 \longrightarrow AN$$

N-oxide formation:
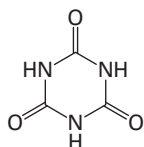
OR e.g. Oxone
         MCP BA
         H_2O_2/H_2SO_4
         $H_2O_2/F_3C\text{-}COOH$
         Ozone
         HO-F*CH_3CN ($F_2+H_2O+CH_3CN$)
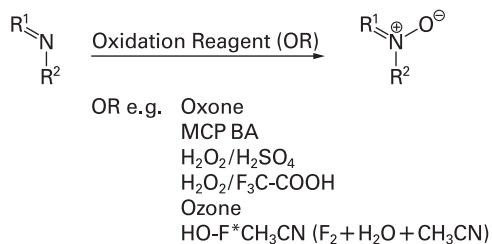
For organic azides the following rule of thumb applies: organic, covalently bound azide compounds can be handled and are not expected to be explosive if the number (#) of N atoms is smaller than the number of C atoms and if the ratio of (C atoms + O atoms) divided by the number of N atoms is greater than three:

$\#(N) < \#(C)$

$[\#(C) + \#(O)] / \#(N) > 3$

a) P. A. S. Smith, Open-Chain Nitrogen Compounds, Bd. 2, Benjamin, New York, **1966**, 211−256;
b) J. H. Boyer, R. Moriarty, B. de Darwent, P. A. S. Smith, *Chem. Eng. News* **1964**, *42*, 6.

Tab. I   Technical terms in German and English language

German	English
Abbrandgeschwindigkeit	burn rate
Abgaswolke (Flugzeug, Rakete)	plume
Aufschlagzünder oder Perkussionszünder	percussion primer
Binder	binder
Brandwaffe	incendiary device
Brennkammer	combustion chamber
Brennstoff, Treibstoff	fuel
Detonationsgeschwindigkeit	velocity of detonation, detonation velocity
Dreibasig	triple-base
Einbasig	single-base
Elektrostatische Empfindlichkeit	electrostatic sensitivity
Elektrostatisches Potential	electrostatic potential
Energetischer Stoff	energetic material
Expansionsdüse	(expansion) nozzle
Fallhammer	drophammer
Flachladung	flat cone charge
Gasgenerator	gas generator
Hohlladung	shaped charge
Ionische Flüssigkeit	ionic liquid
Köder-Munition oder Täuschkörper	decoy flares / countermeasure munition
Leuchtsatz	illuminating device
Mündungsfeuer	muzzle flash
Oxidator	oxidizer
Plastifizierungsmittel	plasticizer
Primärer Explosivstoff	primary explosive
Projektilbildende Ladung	explosively formed projectile
Pyrotechnische Mischung	pyrotechnic composition
Raketentreibstoff	rocket propellant
Raucherzeuger	smoke generator
Reibeapparat	friction tester
Reibeempfindlichkeit	friction sensitivity
Schlagempfindlichkeit	impact sensitivity
Schmelzgießen	melt cast
Schwarzpulver	blackpowder
Sekundärer Explosivstoff	secondary explosive, high explosive
Signalfackel	signal flare
Spezifische Energie	force
Sprenggelatine	blasting gelatine
Sprengkapsel (Schockwelle)	blasting cap / detonator / primer
Stahlhülsentest	steel shell test
Täuschkörper	decoy flare
Treibladungspulver	gun propellant
Universalbombe	general purpose bomb
Verdämmung	confinement
Verzögerungssatz	delay composition
Zünder (durch Hitze)	initiator
Zweibasig	double-base

Tab. II   Abbreviations

AA	ammonium azide
ADN	ammonium dinitramide
ADW	agent defeat warhead
AF	azidoformamidinium
AF-N	azidoformamidinium nitrate
AG	aminoguanidinium
AG-N	aminoguanidinium nitrate
ALEX	electrically exploded aluminum, nano material (20−60 nm)
AN	ammonium nitrate
ANFO	ammonium nitrate fuel oil
AT, 5-AT	aminotetrazole, 5-aminotetrazole
BI	bullet impact
BP	black powder (gun powder)
BTA	bis(tetrazolyl)amine
BTAT	bis(trinitroethyl)-1,2,4,5-tetrazine-3,6-diamine
BTH	bistetrazolylhydrazine
BTTD	bis(trinitroethyl)-tetrazole-1,5-diamine
C-J point	Chapman-Jouguet point
CL-20	HNIW, hexanitrohexaazaisowurtzitane
CTP	chemical thermal propulsion
DADNE	1,1-diamino-2,2-dinitro-ethene
DADP	diacetone diperoxide
DAG	diaminoguanidinium
DAG-Cl	diaminoguanidinium chloride
DAT	diaminotetrazole
DDNP	diazodinitrophenole
DDT	deflagration to detonation transition
DINGU	dinitroglycoluril
DNAN	2,4-dinitroanisole
EDD	explosive detection dog
EFP	explosively formed projectile
EPA	environmental protection agency
ESD	electrostatic discharge sensitivity
ESP	electrostatic potential
FAE	fuel-air explosives
FCO	fast cook-off
FI	fragment impact
FLOX	fluorine − liquid oxygen
FOX-12	guanylurea dinitramide
FOX-7	DADNE, diaminodinitroethene
FOX-7	1,1-diamino-2,2-dinitro-ethene
GUDN	guanylurea dinitramide
GWT	global war on terror
H_2BTA	bis(tetrazolyl)amine
HA	hydrazinium azide
HAA	hydroxylammonium azide
HAN	hydroxylammonium nitrate
HAT-DN	aminotetrazolium dinitramide
HME	homemade explosive
HMTA	hexamethylenetetramine
HMTD	hexamethylene triperoxide diamine
HMX	octogen, high melting explosive, her / his Majesty's explosive

Tab. II   (continuation)

HN	hydrazinium nitrate
HNFX-1	tetrakis(difluoramino)octahydro dinitro diazocine
HNS	hexanitrostilbene
HTPB	hydroxy-terminated polybutadiene
HyAt	hydrazinium 5-aminotetrazolate
Hy-At	hydrazinium aminotetrazolate
HZT	hydrazinium azotetrazolate
IED	improvised explosive device
IM	insensitive munition
IRFNA	inhibited red fuming nitric acid
LOVA	low-vulnerability ammunition
LOX	liquid oxygen
MEKP	methylethylketone-peroxide
MF	mercury fulminate
MMH	monomethylhydrazine
MOAB	massive ordnance air blast bomb
MON-XX	mixture of dinitrogen tetroxide (NTO) with XX % NO
MTV	magnesium-Teflon-Viton
Na_2ZT	sodium azotetrazolate
NC	nitrocellulose
NG	nitroglycerine
NIOSH	National Institute for Occupational Safety and Health
NQ	nitroguanidine
NT	nitrotetrazole
NTO	5-nitro-1,2,4-triazol-3-one
NTP	nuclear thermal propulsion
ONC	octanitrocubane
PA	picric acid
PBX	polymer bonded explosive
PETN	nitropenta, pentaerythritoltetranitrate
RDX	hexogen, research department explosive, Royal demolition explosive
RFNA	red fuming nitric acid
SC	shaped charge
SCI	shaped charge impact
SCJ	shaped charge jet
SCO	slow cook-off
SCRAM-Jet	supersonic combustion RAM jet
SR	sympathetic reaction
STP	solar thermal propulsion
TAG	triaminoguanidine
TAG-Cl	triaminoguanidinium chloride
TAG-DN	triamonoguanidinium dinitramide
TAGzT	triaminoguanidinium azotetrazolate
TART	triacetyltriazine
TATB	triaminotrinitrobenzene
TATP	triacetone triperoxide
TMD	theoretical maximum density (in the crystal)
TNAZ	1,3,3-trinitroazetidine
TNT	trinitrotoluene
TO	triazol-5-one
TTD	trinitroethyl-tetrazol-1,5-diamine
TTD	trinitroethyl-1*H*-tetrazole-1,5-diamine

Tab. II   (continuation)

UDMD	unsymmetrically substituted dimethylhydrazine
UXO	unexploded ordnance
VOD	velocity of detonation
WFNA	white fuming nitric acid
WMD	weapon of mass distruction
ZT	azotetrazole

Tab. III   CBS-4M calculated gas-phase enthalpies of formation

M	M	$\Delta_f H°$(g, M)/ kcal mol^{-1}	$\Delta_f H°$(g, M)/ kcal mol^{-1}, lit. value
1-H-nitrotetrazole, 1-H-NT	CHN_5O_2	+ 87.1	
1-Me-aminotetrazolium, 1-MeHAT$^+$	$C_2H_6N_5^+$	+224.0	
1-Me-nitriminotetrazole, 1-MeHAtNO$_2$	$C_2H_4N_6O_2$	+ 86.5	
1-Me-nitrotetrazole, 1-Me-NT	$C_2H_3N_5O_2$	+ 80.7	
2-H-nitrotetrazole, 2-H-NT	CHN_5O_2	+ 84.0	
2-Me-nitrotetrazole, 2-Me-NT	$C_2H_3N_5O_2$	+ 74.5	
aminoguanidinium, AG$^+$	$CH_7N_4^+$	+161.0	
aminotetrazolium, HAT$^+$	$CH_4N_5^+$	+235.0	
ammonium, NH$_4^+$	NH_4^+	+151.9	+147.9[a]
azidoformidinium, AF$^+$	$(H_2N)_2CN_3^+$, $CH_4N_5^+$	+235.4	
azidotetrazolate, CN$_7^-$	CN_7^-	+114.1	
bistetrazolylamine, BTA	$C_2H_3N_9$	+178.2	
diaminotetrazolium, HDAT$^+$	$CH_5N_6^+$	+252.2	
dinitramide, DN$^-$	$N(NO_2)_2^-$, $N_3O_4^-$	− 29.6	
guanizinium, Gz$^+$	$C_2H_7N_6$	+207.7	
hydrazinium, N$_2$H$_5^+$	$N_2H_5^+$	+185.1	+184.6[b]
NG-A	$C_3H_7N_5O_7$	− 13.1	
nitrate, NO$_3^-$	NO_3^-	− 74.9	− 71.7[c,d]
nitriminotetrazole, H$_2$AtNO$_2$	$CH_2N_6O_2$	+ 95.0	
nitroglycerine, NG	$C_3H_5N_3O_9$	− 67.2	
perchlorate, ClO$_4^-$	ClO_4^-	− 66.1	
triaminoguanidinium, TAG$^+$	$C(NH-NH_2)_3^+$, $CH_9N_6^+$	+208.8	

[a] D. A. Johnson, *Some thermodynamic aspects of inorganic chemistry*, Cambridge Univ. Press, 2nd edn., Cambridge, **1982**, appendix 5.

[b] P. J. Linstrom and W. G. Mallard, Eds., *NIST Chemistry WebBook*, NIST Standard Reference Database Number 69, June **2005**, National Institute of Standards and Technology, Gaithersburg MD, 20899 (http://webbook.nist.gov).

[c] J. A. Davidson, F. C. Fehsenfeld, C. J. Howard, *Int. J. Chem. Kinet.*, **1977**, *9*, 17.

[d] D. A. Dixon, D. Feller, C.-G. Zhan, J. S. Francisco, *International Journal of Mass Spectrometry,* **2003**, *227(3)*, 421.

Tab. IV   Molecular volumes[e,f,g]

	$V_M/\text{Å}^3$	V_M/nm^3
aminotetrazolium cation, $[\text{HAT}]^+$	69	0.069
ammonium, NH_4^+	21	0.021
azide, N_3^-	58	0.058
Ba^{2+}	12.3	0.0123
chloride, Cl^-	47	0.047
diaminotetrazolium cation, $[\text{HDAT}]^+$	93	0.093
dinitramide, DN^-	89	0.089
guanizinium, $[\text{Gz}]^+$	117.6	0.118
H_2O, hydrate water	25	0.025
H_2O, structural water	14	0.014
hydrazinium, N_2H_5^+	28	0.028
Mg^{2+}	2.0	0.00199
nitrate, NO_3^-	64	0.064
nitriminotetrazolate anion, $[\text{HAtNO}_2]^-$	136	0.136
nitriminotetrazolate diianion, $[\text{AtNO}_2]^{2-}$	136	0.136
perchlorate, $[\text{ClO}_4]^-$	89.0	0.089
Sr^{2+}	8.6	0.00858
triaminoguanidinium, $[\text{TAG}]^+$	108	0.108
$[\text{1-MeHAT}][\text{NO}_3]$	208	0.208
$[\text{2-MeHAt}][\text{DN}]$	206.4	0.206
$[\text{2-MeHAt}]^+$	117.4	0.117
$[\text{AF}][\text{DN}]$	174	0.174
$[\text{AF}][\text{DN}] \cdot \text{H}_2\text{O}$	199	0.199
$[\text{AG}][\text{CN}_7]$	201.8	0.202
$[\text{CH}_3\text{N}_4][\text{DN}]$	161.3	0.161
$[\text{Gz}][\text{DN}]$	206.6	0.206
$[\text{HAT}][\text{DN}]$	172	0.172
$[\text{HAT}][\text{NO}_3]$	133	0.133
$[\text{HDAT}][\text{DN}]$	182	0.182
$[\text{N}_2\text{H}_5][\text{CN}_7]$	151.6	0.152
$[\text{N}_2\text{H}_5][\text{CH}_2\text{N}_5]$	125.7	0.126
$[\text{N}_2\text{H}_5]_2[\text{OD}]$	224.4	0.224
$[\text{NH}_4][\text{1,5-BT}]$	164	0.164
$[\text{NH}_4][\text{CN}_7]$	132.3	0.132
$[\text{NH}_4][\text{DN}]$, ADN	110	0.110
$[\text{NH}_4][\text{NO}_3]$, AN	77	0.077
$[\text{NH}_4]_2[\text{OD}]$	195.0	0.195
$[\text{Sr}][\text{AtNO}_2] \cdot 2\text{H}_2\text{O}$	172.5	0.173
$[\text{TAG}][\text{1-Me-AtNO}_2]$	262	0.262
$[\text{TAG}][\text{Cl}]$	153.5	0.154
$[\text{TAG}][\text{DN}]$	215	0.215
$[\text{TAG}][\text{HAtNO}_2]$	244	0.244
$[\text{TAG}][\text{NO}_3]$	174.1	0.174
$[\text{TAG}]_2[\text{AtNO}_2]$	352	0.352

[e] H. D. B. Jenkins, H. K. Roobottom, J. Passmore, L. Glasser, *Inorg. Chem.*, **1999**, *38(16)*, 3609.
[f] H. D. B. Jenkins, D. Tudela, L. Glasser, *Inorg. Chem.*, **2002**, *41(9)*, 2364.
[g] H. D. B. Jenkins, L. Glasser, *Inorg. Chem.*, **2002**, *41(17)*, 4378.

Tab. V   Classification of some weapon systems and war-heads

weapon	description	example
bomb	war-head respectively HE in a shell, solely ballistic	MK 80 series
rocket	bomb + propulsion system, solid rocket motor	Hydra 70 (70 mm)
missile	guided rocket, guidance: sensor, IR seeker, radar, GPS	AIM (air intercept missile), e.g. AIM-9-Sidewinder
strategic missile	missile for larger targets, target: military base or city; large often intercontinental; war-head often nuclear; propulsion: AP/Al = high I_{sp}	Peacekeeper
tactical missile	missile for tactical use, target: localized in battlefield; often conventional war-head with HE; only occasionally nuclear, relatively small system; 3 types: 1. high I_{sp}: AP/Al 2. smoke-reduced: AP only 3. minimum signature (smoke): NG/NC or NG/NC/NQ	Cruise Missile
ballistic missile	no propulsion system for most of the flight (except launch), free fall (ballistic) to target, leaves atmosphere during flight, liquid or solid boosters	SCUD (Russian)
cruise missile	remains in atmosphere, own propulsion system during entire flight, smaller than ballistic missile, for tactical purpose	Tomahawk

Tab. VI   Classification of low- and high-explosives

	low-explosive	high-explosive
example	black powder, gun powder	RDX, HMX
initiation	flame, spark	detonation, shock-wave
confinment	necessary	not necessary
propagation	particle-to-particle burning (thermal)	shock-wave
velocity	subsonic	supersonic
effect	bursting, deformation, cracking	shattering
chemical analysis after reaction	uncombusted particles	traces $(25-100$ ppb$)$, MS, LC/MSMS (electrospray)

Author

Thomas M. Klapötke, born in 1961, studied chemistry at TU Berlin and received his PhD in 1986 under the supervision of Hartmut Köpf. After his postdoctoral studies in Fredericton, New Brunswick with Jack Passmore he finished his habilitation at TU Berlin in 1990. From 1995 until 1997 Klapötke was Ramsay Professor of Chemistry at the University of Glasgow in Scotland. Since 1997 he is Professor and holds the Chair of Inorganic Chemistry at LMU Munich. In 2009 Klapötke was appointed a visiting Professor for Mechanical Engineering and Chemistry at the Center of Energetic Concepts Development (CECD) in the University of Maryland (UM), College Park and was also appointed a Senior visiting scientist at the Energetics Technology Center (ETC) in La Plata, MD. In 2011 Klapötke was appointed a Honorary Fellow of the High Energy Materials Society of India (HEMSI). Klapötke is a Fellow of the Royal Sociate of Chemistry (C.Sci., C.Chem. F.R.S.C., U.K.), a member of the American Chemical Society (ACS) and the Fluorine Division of the ACS, a member of the Gesellschaft Deutscher Chemiker (GDCh), a Life Member of the International Pyrotechnics Sociaty (IPS) and a Life Member of the National Defense Industrial Association (NDIA, USA). Most of Klapötke's scientific collaborations are between LMU and the US Army Research Laboratory (ARL) in Aberdeen, MD and the US Army Armament Research, Development and Engineering Center (ARDEC) in Picatinny, NJ. Klapötke also collaborates with the US Army Engineer Research and Development Center (ERDC) in Champaign, IL and several industrial partners in Germany and the USA. He is the executive editor of Zeitschrift für Anorganische and Allgemeine Chemie (ZAAC) and an editorial board member of Propellants, Explosives and Pyrotechnics (PEP), Journal of Energetic Materials and Central European Journal of Energetic Materials (CEJEM) and the International Journal of Energetic Materials and Chemical Propulsion (IJEMCP). Klapötke has published over 500 scientific papers in international peer reviewed journals, 23 book chapters and five books.

Index